

Thermal and Catalytic Conversion of
Inedible Vegetable Oils to Higher
Value Products or Aromatics

Sarah Louise Asplin

Doctor of Philosophy

Aston University

November 2021

© Sarah Louise Asplin, 2021

Sarah Louise Asplin asserts her moral right to be identified as the author of this
thesis

This copy of the thesis has been supplied on condition that anyone who consults it is
understood to recognise that its copyright rests with its author and that no quotation
from the thesis and no information derived from it may be published without
appropriate permission or acknowledgement.

Aston University (Energy and Bio-products Research Institute-EBRI)

Thermal and Catalytic Conversion of Inedible Vegetable Oils to Higher Value
Products or Aromatics

Sarah Louise Aspin

Doctor of Philosophy

November 2021

THESIS SUMMARY

Jatropha oil is an inedible vegetable oil obtained from the *Jatropha Curcas* plant. It comprises triglyceride molecules consisting of glycerol and fatty acids, including oleic acid, which makes up 46 wt.% of jatropha oil. When subjected to pyrolysis, Jatropha oil components can yield high-value products such as biofuels and aromatic compounds such as benzene, toluene, or xylenes (BTX). BTX are used to manufacture a range of everyday products (i.e., paints, solvents, etc.), and its current production relies on processing finite fossil fuel-based feedstocks. Therefore, a renewable and sustainable feedstock to produce these chemicals is required in the near future.

This work considers the non-catalytic and catalytic pyrolysis of the inedible feedstock jatropha oil to high-value products or aromatics, particularly BTX. Oleic acid was also used as a feedstock and a fatty acid model compound to better understand the jatropha oil decomposition pathways. Two reaction systems were used for the pyrolysis tests, including a small-scale batch Pyroprobe-GCMS system and a continuous fluidised bed system (90 g h^{-1}).

The non-catalytic pyrolysis of oleic acid and jatropha oil was undertaken in the Pyroprobe system at 400°C , 500°C and 600°C . The influence of temperature on the yield and distribution of products was studied, focusing on the proportion of aromatics (including BTX). At all the temperatures and for both feedstocks, high proportions of acid compounds were observed in the products, attributed to unconverted fatty acids from the feedstocks. The lowest proportions of acids were obtained at 600°C and accounted for 82.0% and 39.3% of the total peak area for oleic acid and jatropha oil. Aliphatics such as alkenes and alkanes were the second-largest group of compounds produced and were identified at all three temperatures. Aliphatics were identified as the main decomposition product in the absence of a catalyst and have been reported as aromatics precursors in the triglycerides decomposition pathway. Therefore, their identification in the product distribution is relevant when looking at aromatics production.

A commercial ZSM-5 catalyst, alongside a range of Ni/ZSM-5 catalysts (1 wt.%, 2 wt.%, 5 wt.% and 10 wt. %), were used for the catalytic tests in the Pyroprobe. Oleic acid and jatropha oil were used as feedstocks at 400°C , 500°C and 600°C . At 500°C , it was observed that the aromatics yield was increased from 70.6% using ZSM-5 catalyst up to the maximum proportion of aromatics achieved at 76.1% when a small amount of nickel was added to the catalyst (1wt.% Ni/ZSM-5). This was attributed to a slight increase in pore diameter (1.505 nm for ZSM-5 and 1.528 nm for 1Ni/ZSM-5) as no significant changes were observed on the catalyst surface area ($383.0 \text{ m}^2/\text{g}$ for ZSM-5 and $370.0 \text{ m}^2/\text{g}$ for 1Ni/ZSM-5). Other major groups of products identified in the catalytic decomposition of jatropha oil included aliphatics and polyaromatics. These aliphatics were highlighted earlier as precursors to aromatics, whilst the evolution of polyaromatics has likely come from further reactions between some of the aromatic compounds present.

Finally, the non-catalytic fast pyrolysis of jatropha oil was carried out in the fluidised bed system at 450°C . The reactor type selection was novel as no prior literature reported a continuous reactor used to process this feedstock. The conversion of the

jatropha oil yielded on average 88.21 wt.% \pm 0.77 liquid products, with a small proportion of gases (3.12 wt.% \pm 0.78), and near to negligible solids (0.72 wt.% \pm 0.27). This system showed a preference for the decomposition of jatropha oil to ester compounds which made up on average 70.3% of the liquid products with just 4.2% acids. It has been reported that esters can be converted to aromatics in the presence of a catalyst, which has been suggested as part of future work.

For the jatropha oil non-catalytic tests, the fluidised bed system showed a preference to yield esters, whilst the Pyroprobe showed a preference towards aliphatic compounds and small amounts of aromatics. The differences in the decomposition pathways were attributed to the different reactor type configurations. Nevertheless, the main functional groups identified (esters and aliphatics) can yield aromatics, including BTX via catalyst addition.

For the Pyroprobe system, it was concluded that aromatics including BTX can be obtained from the catalytic pyrolysis of jatropha oil at 500 °C. The 1Ni/ZSM-5 catalyst is preferable to maximise the yield and distribution of these compounds. The two pyrolysis systems showed different decomposition pathways and product distribution; however, it could be feasible for aromatics to be produced in the fluidised bed reactor using ZSM-5 catalysts.

Keywords: Pyrolysis, Zeolites, ZSM-5, Aromatics, BTX, Jatropha Oil, Inedible Oil

ACKNOWLEDGEMENTS

Firstly, I would like to express my appreciation to my supervisor Dr Paula Blanco-Sánchez for her ongoing guidance and masses of encouragement throughout my PhD studies here at the Energy and Bio-products Research Institute at Aston University.

I would also like to thank my co-supervisors Dr Katie Chong and Professor Tony Bridgwater for their support and instruction throughout my research.

I would also like to thank past and present fellow colleagues in EBRI whom have supported me with my work with particular thanks to Dr Stylianos Stefanidis, Dr Scott Banks, Dr Jinesh C. Manayil and Dr Daniel J. Nowakowski for their time, advice, and assistance with training in the laboratories helping me to complete my experimental work.

In addition, I would like to thank the College of Engineering and Applied Sciences at Aston University for my studentship, allowing me to undertake this work within the Energy and Bio-products Research Institute (EBRI) and offering further support from the COVID-19 Hardship Fund to support fund following delays due the University closure and fluctuating restrictions these last 18 months.

Finally, a big thanks to my parents Karl and Karen, fiancé Tom and sister Chrissy for their support and constantly reminding me that I can do this! I know I wouldn't have got here if it wasn't for all of you too.

CONTENTS

Thesis Summary	ii
Acknowledgements	iv
Contents	v
List of Tables	ix
List of Figures	xi
List of Equations	xv
Abbreviations	xvi
Chapter 1.0 Introduction.....	1
1.1. Research outline.....	1
1.2. Research goals and objectives	3
Chapter 2.0 Literature Review.....	4
2.1. Biomass feedstocks.....	4
2.1.1. Introduction to biomass	4
2.1.2. Lignocellulosic biomass.....	6
2.1.3. Triglyceride biomass	7
2.2. Biomass conversion processes	18
2.2.1. Pyrolysis	19
2.2.2. Types of pyrolysis	20
2.2.3. Fast pyrolysis systems	21
2.3. Conversion of triglyceride feedstocks to yield aromatics	24
2.3.1. Aromatic compounds from fossil fuels	25
2.3.2. Conversion of triglycerides to aromatics	27
2.3.3. Triglyceride decomposition pathways.....	30
2.3.4. Catalytic conversion of triglyceride feedstocks	36
2.4. Summary and research objectives.....	49
Chapter 3.0 Experimental Methodology	50
3.1. Introduction.....	50

3.2. Pyroprobe Experiments	50
3.2.1. Materials and Catalyst Preparation for Pyroprobe Experiments.....	50
3.2.2. Pyroprobe Experiment Methodology	52
3.2.3. Catalyst Characterisation	55
3.3. Fluidised Bed Reactor Experiments.....	60
3.3.1. Reactor Re-Commissioning	66
3.3.2. Experimental Procedure.....	69
3.3.3. Selection and Definition of Experimental Conditions	70
3.4. Characterisation methods.....	72
3.4.1. Characterisation of liquids	72
3.4.2. Characterisation of solid content on fluidised bed material	81
3.4.3. Characterisation of gases.....	82
3.5. Summary	83
Chapter 4.0 Pyrolysis of Oleic Acid and Jatropha Oil	84
4.1. Introduction and aims	84
4.2. Pyroprobe GC-MS	85
4.2.1. Pyrolysis of oleic acid at different temperatures.....	86
4.2.2. Pyrolysis of jatropha oil at different temperatures	96
4.3. Comparing decomposition pathways for oleic acid and jatropha oil	110
4.4. Conclusions	111
Chapter 5.0 Catalytic Decomposition Of Oleic Acid And Jatropha Oil	112
5.1. Introduction and aims	112
5.2. Catalyst characterisation	112
5.2.1. Thermogravimetric analysis (TGA).....	113
5.2.2. N ₂ porosimetry	113
5.2.3. X-ray diffraction (XRD)	117
5.3. Catalytic decomposition using a pyroprobe GCMS	119
5.3.1. Introduction and aims.....	119

5.3.2. Catalytic pyrolysis of oleic acid at different temperatures	120
5.3.3. Catalytic pyrolysis of jatropha oil at different temperatures	132
5.4. Comparing catalytic decomposition of oleic acid and jatropha oil.....	143
5.5. Conclusions.....	144
Chapter 6.0 Fluidised Bed Fast Pyrolysis Of Jatropha Oil	146
6.1. Introduction and aims	146
6.2. Feedstock characterisation	147
6.2.1. Heating value	147
6.2.2. Viscosity.....	147
6.2.3. Fatty acid composition via GCMS	148
6.2.4. Water content via Karl-Fischer titration.....	151
6.3. Non – catalytic fluidised bed fast pyrolysis.....	151
6.3.1. Fluidised bed fast pyrolysis products and characterisation	151
6.3.2. Mass balance.....	163
6.4. Comparison of fluidised bed and pyroprobe systems.....	164
6.5. Further recommendations.....	171
Chapter 7.0 Conclusions, Recommendations And Further Work.....	172
7.1. Conclusions.....	172
7.2. Recommendations and future work	174
7.2.1. Py-GCMS Studies	174
7.2.2. Fluidised bed studies	174
Chapter 8.0 - Appendices	175
8.1. Appendix One- Reaction descriptors for the thermal cracking of canola oil.....	175
8.2. Appendix Two- Estimation of nitrogen fluidisation velocity	176
8.2.1. Calculation of fluidisation velocity at room temperature	176
8.2.2. Calculations at reactor operating temperature	178
8.3. References	180

LIST OF TABLES

Table 2-1. Summary of popular triglyceride feedstocks	9
Table 2-2. Summary of physiochemical characteristics of jatropha, karanja, and neem oil..	15
Table 2-3. Typical fatty acid composition of jatropha, karanja and neem oil [3, 5-10]	16
Table 2-4. Parameters for slow and fast pyrolysis of different types of lignocellulosic feedstocks [37, 82, 85, 87-89]	20
Table 2-5. A summary of the typical fractions of products from different types of pyrolysis of a lignocellulosic feedstock [8].....	21
Table 2-6. Lignocellulosic feedstock pyrolysis reactor design selection parameter matrix [94]	23
Table 2-7. Summary of studies evaluating the catalytic conversion of triglyceride feedstocks into aromatic compounds	28
Table 2-8. A summary of common catalyst types used for the upgrading of pyrolysis oils [103]	36
Table 2-9. Key parameters from fixed bed studies by Than-An Ngo.....	46
Table 2-10. Example conditions used for impregnation of metals in ZSM-5 zeolite catalysts	48
Table 3-3. Calibration of fluidising nitrogen feeds and feeder nitrogen.	70
Table 3-1. Oil characteristics, standard test methods, and equipment (expanded from [3]).	72
Table 4-1. Functional group abbreviations for major products of pyroprobe GC-MS	85
Table 4-2. Notable peaks from pyrolysis of oleic acid at 400 °C,500 °C and 600°C.....	90
Table 4-3. Notable peaks from pyrolysis of jatropha Oil at 400 °C,500 °C and 600 °C	100
Table 5-1. Catalyst moisture content.....	113
Table 5-2. Properties of Ni/ZSM-5 catalysts	116
Table 6-1. Summary of fluidised bed fast pyrolysis reactor parameters.....	146
Table 6-2. Fatty acids identified in GCMS of jatropha oil	150
Table 6-3. Water content (%) of jatropha and neem oil by KF titration.....	151
Table 6-4. Characteristics of liquid fluidised bed fast pyrolysis product and jatropha oil feedstock	152

Table 6-5. Summary of key peaks from GCMS of liquid pyrolysis product.....	155
Table 6-6. Average gas products composition from the pyrolysis of jatropha oil.....	159
Table 8-1. Descriptors of reactions occurring in the proposed reaction scheme for the thermal cracking of canola oil.....	175

LIST OF FIGURES

Figure 2.1. Composition of lignocellulosic feedstocks [15].....	6
Figure 2.2. Structure of a typical triglyceride molecule	7
Figure 2.3. Van Krevelen plot for principal biomass constituents[21].....	7
Figure 2.4. Skeletal formulae of: (a) oleic; (b) linoleic; and (c) palmitic acid.....	17
Figure 2.5. Major types of products obtained from pyrolysis of biomass. (adapted from [82, 83])	19
Figure 2.6. Reaction systems for fast pyrolysis: (a) ablative, (b) bubbling fluidised bed (BFB), (c) circulating fluidised bed (CFB), (d) auger (screw), (e) vacuum, (f) rotating cone [93]	22
Figure 2.7. World biofuels production (MTOE: Million Tonnes of Oil Equivalent) from 2008 to 2018 [105].....	25
Figure 2.8. Schematic overview of aromatics production from naphtha via catalytic cracking [106].....	26
Figure 2.9. Worldwide applications of BTX compounds[108].....	27
Figure 2.10. Structures of benzene, toluene and xylenes.....	27
Figure 2.11. Reaction mechanism for the decomposition of unsaturated triglycerides[119] .	31
Figure 2.12. Decomposition of glycerol to aromatics in the presence of H-ZSM-5.....	32
Figure 2.13. Decomposition of saturated triglycerides: reaction mechanism for the Chang et al. 1947 [114]	33
Figure 2.14.Reaction mechanism for the decomposition of saturated triglycerides Alencar et al.,1983 [27]	34
Figure 2.15. Proposed reaction scheme for thermal cracking of a mixture of unsaturated and saturated triglycerides, Idem et al,1996 (canola oil) [123].....	35
Figure 2.16. Canola oil pyrolysis: Influence of pyrolysis temperature on aromatics yield [112]	38
Figure 2.17. Effect of temperature on aromatics yield and conversion in the catalytic processing of canola oil by Prasad et al. 1985 (data from [113])	39
Figure 2.18. A graph to show the effect of Silica Alumina ratio of H-ZSM-5 catalysts and temperature on conversion of soyabean oil feedstock (data from Thanh- An Ngo [110]....	40

Figure 2.19. Structures of four selected zeolites (a) Faujasite or zeolites X, Y (b) zeolite ZSM-12 (c) zeolite ZSM-5 or silicate-1 d) zeolite theta 1 or ZSM-22 and their microporous systems and dimensions [137]).....	41
Figure 2.20. A flowchart representing the different pore sizes of catalysts [3, 137, 145].....	43
Figure 2.21. A visual representation of the shape selectivity of zeolite catalysts[147]	44
Figure 3-12. Schematic of a Pyroprobe GC-MS (Not to Scale).....	52
Figure 3-13. Pyroprobe 5000 pyrolzer (CDS Analytical) system	53
Figure 3-14. Cross section of Py-GC-MS quartz tube.....	53
Figure 3-7. Mettler Toledo TGA/DSC 2 STA system	55
Figure 3-8. Schematic of X-ray diffraction	56
Figure 3-9. Bruker D8 advance diffractometer.....	57
Figure 3-10. Quantachrome NOVA 2200e series equipment.....	59
Figure 3-15. Descriptive photo of fast fluidised bed system.....	62
Figure 3-16. Process flow diagram fast fluidised bed reactor system process flow diagram initial set up.....	63
Figure 3-17. Process flow diagram fluidised bed fast pyrolysis reactor system- final	64
Figure 3-18. Initial reactor assembly major steps timeline	67
Figure 3-19. Reactor assembly modifications and improvements.....	68
Figure 3-20. Fast fluidised bed reactor experimental procedure flow chart.....	69
Figure 3-1. Mettler Toledo titration system [166]	74
Figure 3-2. Karl Fischer Titration equipment used for water content determination; (a) Mettler Toledo V20 Karl Fischer Titrator (b) Sartorius Analytical balance.....	75
Figure 3-3. Brookfield rotational viscometer schematic[168].....	76
Figure 3-4. Brookfield rotational viscometer model DV-II+ Pro	77
Figure 3-5. (a) Parr 6100 oxygen bomb calorimeter [170]; (b) sample holder and crucible ..	78
Figure 3-6. Bomb calorimeter vessel in-situ in Parr 6100 equipment.....	79
Figure 3-11. Varian CP 4900 Micro-GC, micro gas chromatograph with a thermal conductivity detector (TCD) with two columns (Varian CP-5A mol sieve and CP-PortaPLOT)	82
Figure 4-1. Pyrolysis of oleic acid at 400 °C in the absence of a catalyst	87

Figure 4-2. Pyrolysis of oleic acid at 500 °C in the absence of a catalyst	88
Figure 4-3. Pyrolysis of oleic acid at 600 °C in the absence of a catalyst	89
Figure 4-4. Products from the pyrolysis of oleic acid at different temperatures (average values from duplicated runs)	93
Figure 4-5. Yields of aromatics and aliphatics from the pyrolysis of oleic acid pyrolysis at different temperatures (average of duplicate runs, standard deviation given in error bars)..	95
Figure 4-6. Jatropha oil pyrolysis at 400 °C in the absence of a catalyst	97
Figure 4-7.Jatropha oil pyrolysis at 500 °C in the absence of a catalyst	98
Figure 4-8. Jatropha oil pyrolysis at 600 °C in the absence of a catalyst	99
Figure 4-9. Product composition of jatropha oil pyrolysis at different temperatures *average values from duplicate runs	103
Figure 4-10. Decomposition of linoleic acid (Frankel et al 1984)[195].....	105
Figure 4-11. Decomposition of linoleic acid (Shi et al 1994, *adapted from graphic by Jayasena et al 2013) [196](Shi et al 1994, *adapted from graphic by Jayasena et al 2013)	106
Figure 4-12. Decomposition of oleic and linoleic acid to aldehyde compounds[198].....	107
Figure 4-13. Degradation products of oleic acid from different parts of the fatty acid molecule [200].....	108
Figure 4-14. Glycerol decomposition products, Mitrea et al. 2017 [205]	109
Figure 5-1. N ₂ adsorption-desorption isotherms (a) ZSM-5, (b) 1Ni/ZSM-5, (c) 2Ni/ZSM-5, (d) 5Ni/ZSM-5, (e) 10Ni/ZSM-5.....	114
Figure 5-2. IUPAC adsorption-desorption isotherms[207]	114
Figure 5-3. Hysteresis loops in type IV and type V isotherms[207]	115
Figure 5-4. XRD Diffraction Pattern for a) ZSM-5 b) 1Ni/ZSM-5 c) 2Ni/ZSM-5 d) 5Ni/ZSM-5 e) 10Ni/ZSM-5.....	117
Figure 5-5. XRD NiO peaks at 2θ, a) 37.2° b) 43.3° c) 62.9° d) 75.2°	118
Figure 5-6. Py-GCMS chromatogram for the pyrolysis of oleic acid at 400 °C: without catalyst (red); and with ZSM-5 (blue).	121
Figure 5-7. Functional groups products from the pyrolysis of oleic acid with and without catalysts at: (a) 400 °C; (b) 500 °C; (c) 600 °C	123

Figure 5-8. Yield of major compound groups in the catalytic pyrolysis of oleic acid (average values from duplicate runs)	126
Figure 5-9. Decomposition of oleic acid to aromatics in the presence of H-ZSM-5 catalyst, Benson et al. 2008[217]	128
Figure 5-10. Proportions of aromatics from pyrolysis of oleic acid at 400 °C	129
Figure 5-11. Proportions of aromatics from pyrolysis of oleic acid at 500 °C	130
Figure 5-12. Proportions of aromatics from pyrolysis of oleic acid at 600 °C	130
Figure 5-13. Py-GCMS Chromatogram showing decomposition of jatropha oil in absence of catalyst at 400 °C (red) & decomposition of jatropha oil in the presence of a ZSM-5 catalyst at 400 °C (blue).....	133
Figure 5-14. Functional groups products from the pyrolysis of jatropha oil with and without catalysts at: (a) 400 °C; (b) 500 °C; (c) 600 °C	135
Figure 5-15. Decomposition of glycerol, Corma et al. 2008 [202]	137
Figure 5-16. Decomposition of palmitic acid to aromatic compounds, (1A) decarboxylation, (1B) decarbonylation, (1C) ammonia substitution, (2A) thermal cracking, (2B) amine pyrolysis, (3) catalytic cracking, (4) oligomerization, cyclization, and aromatization, Fisher et al. 2015[219].....	138
Figure 5-17.Yield of major compound groups in the catalytic pyrolysis of jatropha oil (average values from duplicate runs)	140
Figure 5-18. Proportions of aromatics from pyrolysis of jatropha oil at 400 °C.....	141
Figure 5-19. Proportions of aromatics from pyrolysis of jatropha oil at 500 °C.....	141
Figure 5-20. Proportions of aromatics from pyrolysis of jatropha oil at 600 °C.....	142
Figure 6-1. GCMS chromatogram of acetone with jatropha oil and peak identification (2:1)	149
Figure 6-2. Visual comparison of fresh jatropha oil (left) and fluidised bed fast pyrolysis liquid product (right)	152
Figure 6-3. Relationship between water content and viscosity of pyrolysis bio-oils, Nolte et al. 2010 [225].....	153
Figure 6-4. GCMS chromatogram acetone: liquid pyrolysis product (3:1) from run 1	154
Figure 6-5. GCMS chromatogram acetone: liquid pyrolysis product (3:1) from run 2.....	154
Figure 6-6. GCMS chromatogram acetone: liquid pyrolysis product (3:1) from run 3.....	155

Figure 6-7. Pyrolysis liquid products from jatropha oil in a fluidised bed reactor at 450 °C	156
Figure 6-8. Decomposition scheme for oleic acid to alcohols and ethers, Wang et al. [227]	
.....	157
Figure 6-9. Comparison of the composition of gaseous products from the pyrolysis of jatropha oil	160
Figure 6-10. Beims et al., 2018, Composition of gaseous fractions produced in thermal cracking of soybean oil(SO) and soybean oil:hydrogenated fat mixtures (SH)[2].....	161
Figure 6-11. Mass balance, composition of products for fluidised fast bed pyrolysis of jatropha oil	163
Figure 6-12. Product distribution from non-catalytic pyrolysis of jatropha oil: a) Py-GCMS at 400 °C, b) Py-GCMS at 500 °C; and c) fluidised bed at 450 °C.....	165
Figure 6-13. Part one- conversion of esters to aromatics in the presence of a ZSM-5 catalyst, Habibi et al., 2018 [22]	167
Figure 6-14. Part two- conversion of esters to aromatics in the presence of a ZSM-5 catalyst, Habibi et al., 2018 [229]	168
Figure 6-15. Decomposition of esters BTX aromatics, Singh et al., 2021[230]	169

LIST OF EQUATIONS

Equation 3-5. Bragg's law	57
Equation 3-6. BET specific surface area	58
Equation 3-7. BJH pore size.....	58
Equation 3-8. Archimedes number for estimation of minimum fluidisation velocity[188]	60
Equation 3-9. Wen and Yu correlation for minimum fluidisation[188].....	60
Equation 3-10. Reynolds number at minimum fluidisation[188]	60
Equation 3-1. Redox reaction for Karl-Fischer titration	74

ABBREVIATIONS

AC	Acids
AR	Aromatics
AL	Alcohols
ALI	Aliphatics
ASTM	American Society for Testing and Materials
BET	Brauner- Emmet-Teller
BFB	Bubbling Fluidised Bed
BJH	Barret-Joyner-Halenda
BTX	Benzene, Toluene and Xylenes
CFB	Circulating Fluidised Bed
COLO	Coal Liquids from Coke Ovens
ESP	Electrostatic Precipitator
EST	Esters
EM	Electron Microscopy
D _p	Pore Diameter (nm)
FAME	Fatty Acid Methyl Ester
FAEE	Fatty Acid Ethyl Ester
FID	Flame Ionisation Detector
GC	Gas Chromatography
GC-MS	Gas Chromatography-Mass Spectrometry
H/C	Hydrogen to Carbon ratio

HHV	Higher Heating Value (MJ/kg)
HVRT	Hot Vapour Residence Time
ICP-OES	Inductively Coupled Plasma Optical Emission Spectroscopy
IUPAC	International Union of Pure and Applied Chemistry
KF	Karl-Fischer
KFT	Karl Fischer Titration
L	Length (cm)
LHV	Lower Heating Value (MJ/kg)
MCM	Mobil Composition of Matter
M_r	Relative Molecular Mass
MS	Mass Spectrometry
MZ	Microcrystalline
m/z	Mass to charge ratio
NIST	National Institute of Standards and Technology
NZ	Nanocrystalline
PAH	Polyaromatic Hydrocarbons
PFD	Process Flow Diagram
PTA	Phosotungstic acid
PTFE	Polytetrafluoroethylene
PS	Particle Size (mm)
Py-GCMS	Pyroprobe- Gas Chromatography Mass Spectrometry
REY	Rare Earth Type Y Zeolite

S_{BET}	Surface Area (m ₂ /g)
SEM	Scanning Electron Microscopy
Si/Al	Silica Alumina ratio
TCD	Thermal Conductivity Detector
TEA	Tetraethylammonium
TEM	Transmission Electron Microscopy
TGA	Thermogravimetric Analysis
TPA	Tetrapropylammonium
UN	Unidentified
USA	United States of America
VGO	Vacuum Gas Oil
V_p	Pore Volume (cc/g)
WCO	Waste Cooking Oil
WHSV	Weight Hourly Space Velocity
XRD	X-ray Diffraction
ZSM-5	Zeolite Socony Mobil-5

CHAPTER 1.0 INTRODUCTION

1.1. Research outline

This research considers the pyrolysis of the inedible vegetable oil feedstock, jatropha oil and the triglyceride model compound oleic acid to produce higher-value compounds such as aromatics. The higher value compounds of interest include aromatics, which are staple chemical compounds used for a wide variety of products that we rely on a day-to-day basis. The aromatics known as benzene, toluene and xylene (BTX) are of particular interest, as they have many applications, including clothing, packaging, solvents and paints. Presently, BTX production depends on depleting fossil fuels[1]. Therefore, renewable and sustainable means to produce these high-value aromatics are desirable. Among these renewable resources are inedible oils, some of which have a very high proportion of unsaturated fatty acids, including the jatropha oil feedstock selected for this work. This is of significance as these types of fatty acids reportedly allow the production of aromatic compounds via thermal catalytic processes. Although lignocellulosic feedstocks are heavily utilised in thermal catalytic processes, the use of a triglyceride feedstock for the production of aromatics has additional benefits. The organic compounds from pyrolysis, including aromatics, are contained within the bio-oil product from pyrolysis of the feedstocks. It is known that bio-oils from lignocellulosic feedstocks have higher water content and oxygen content reducing their heating value and stability in comparison to triglyceride bio-oils where the water content is negligible, improving the quality of the bio-oil and removing the need for pre-treatment of the feedstock via methods such as torrefaction[2].

The jatropha oil feedstock used in this work comprises triglycerides, consisting of one glycerol molecule and three fatty acid chains of differing lengths [3] [4]. However, the most prevalent fatty acid chain in this feedstock is oleic acid making up around 46 wt.% of the oil [3, 5-10]. For this reason, oleic acid was selected as a jatropha oil model compound. Its application would allow a less complex analysis of the potential decomposition pathways of this feedstock to obtain higher-value compounds.

In this work, two pyrolysis systems have been utilised to convert the feedstocks, including a pyroprobe (CDS 5200 pyrolyzer) with gas chromatography and mass spectrometry (Py-GCMS) for the non-catalytic and catalytic conversion of oleic acid and jatropha oil. A 90 gh^{-1} fluidised bed fast pyrolysis reactor was utilised for the non-catalytic conversion of jatropha oil. The methodologies used for the experimental work can be reviewed in Chapter 3.0.

Firstly, the non-catalytic pyrolysis of oleic acid and jatropha oil is considered in the absence of catalyst in Chapter 4.0. The Py-GCMS was utilised to process oleic acid and jatropha oil samples at 400 °C, 500 °C and 600 °C in the absence of a catalyst.

The non-catalytic data from the Py-GCMS investigations was obtained to investigate jatropha oil's thermal decomposition pathways. In addition, the oleic acid compound was utilised to provide a less complex data set to make it easier to establish such pathways and ascertain if any aromatics were present in the absence of a catalyst.

Following this, the catalytic conversion of oleic acid and jatropha oil is considered in Chapter 5.0. The two feedstocks were processed using the same Py-GCMS system utilising a ZSM-5 and several Ni/ZSM-5 catalysts with varying nickel loadings (1 wt.%, 2 wt.%, 5 wt.% and 10 wt.%). The Ni/ZSM-5 catalysts were prepared by wet impregnation as per the methodology described in Chapter 3.0, section 3.2.2 and investigations were conducted using the temperatures 400 °C, 500 °C and 600 °C. The metal nickel was selected alongside ZSM-5 because literature suggested that it can improve the yields of aromatics. These investigations were conducted to ascertain the implication of adding a catalyst or change in reaction temperature on the aromatics yields. Furthermore, data obtained from the decomposition of jatropha oil in the absence of a catalyst could be compared to data obtained from the fluidised bed fast pyrolysis reactor system.

The fluidised bed fast pyrolysis reactor used is a bench-scale system commissioned to process liquids and undertake preliminary investigations using jatropha oil. The characteristics of jatropha oil, including viscosity, higher heating value, water content, and fatty acid composition, were initially established and compared against data from the literature. Pyrolysis tests were carried out for ~30 minutes, at a 450 °C, 90 g h⁻¹ flowrate, and using silica sand (250-355 µm) as bed material. The pyrolysis liquids were characterised by GC-MS, and major components identified were esters, together acids and small amounts of aldehydes. These preliminary results are relevant as the identified components in the pyrolysis liquid have the potential to yield aromatics via catalytic pyrolysis. Therefore, further studies using catalysts such as ZSM-5 with other metals are recommended within the future work.

1.2.Research goals and objectives

In this work the overall aim is to determine a route for the conversion of a triglyceride feedstock aiming to yield aromatic products, including BTX. This will involve the identification of pyrolysis conditions (temperature, catalyst: feedstock ratios) that favour decomposition pathways yielding higher proportions of aromatics and BTX, which may be achieved by considering the following:

- Utilise a fatty acid model compound prevalent in the selected feedstock to understand the decomposition pathways and contribution towards the formation of aromatics and BTX.
- Assess the effect of different temperatures on the selected triglyceride feedstock and model compound in the absence and presence of a ZSM-5 catalyst on the yield and distribution of aromatic compounds, with a focus on the evolution of BTX.
- Determine if the addition of nickel to the ZSM-5 catalysts (Ni-ZSM-5) implicates the yields and distribution of aromatics, in particular BTX in the selected conversion process or analytical pyrolysis system.
- Extrapolate the small-scale pyrolysis tests into a continuous fluidised bed pyrolysis system to compare the effects in aromatic and BTX yields.

CHAPTER 2.0 LITERATURE REVIEW

2.1.Biomass feedstocks

2.1.1.Introduction to biomass

Biomass is a readily available, renewable, and potentially sustainable alternative to fossil fuels such as natural gas, coal and oil, which are typically utilised to produce energy, fuels, and chemicals. Biomass like fossil fuels is a source of hydrocarbons, organic compounds made of carbon and hydrogen. A future alternative to these is necessary, owing to the finite nature of these resources. In addition, demand for these types of resources is only growing due to increasing populations worldwide. So, a renewable alternative could help provide security for future generations. Furthermore, it is of significance that they also produce less greenhouse gases than fossil fuel alternatives[3, 8]. Greenhouse gases include carbon dioxide (CO_2), methane (CH_4), and nitrous oxides (NO_x) that are released by the burning of fossil fuels. These greenhouse gases are released into the earth's atmosphere, stop solar heat from dissipating back into space, and heat the earth, contributing to globally rising temperatures. Further issues such as acid rain and ozone depletion are associated with the release of sulphur oxides, nitrous oxides, hydrocarbons and carbon monoxide [11]. Therefore, the application of biomass feedstocks will bring a multitude of benefits.

Although plant materials can be regrown once used, considerations must be made to utilise biomass sustainably. In recent years the utilisation of edible biomass to produce fuels, energy and chemicals has created what is known as the food versus fuel debate [12]. Using food sources to produce fuels or chemicals directly competes with the food supply chain, risks increasing food prices and reduces agricultural land availability for food production. Simply it is immoral and unethical to create competition between the food and fuel industries. Ideally, land utilised for energy crops should not be detrimental to the availability or cost of food products. Ultimately, a balance must be struck between producing more food in a world with an increasing population while increasing the availability of sustainable energy, fuels, and chemicals. The food versus fuel argument also considers that agricultural land is not just used for food or fuel; it is also used for flowers, plants, and pharmaceutical ingredients, to name a few. It highlights the importance of ensuring that land can be utilised without creating competition that could be detrimental to the environment, economy or people's health [12].

The above arguments need to be considered when selecting a sustainable feedstock. The selection of a biomass feedstock can be complex as it can also be influenced by but not limited to; its means and ease of production, cost, energy density, environmental impacts and other uses of the oil, e.g. food, cosmetics and medicinal benefits [3, 13].

All of these must be considered alongside the potential of the feedstock to yield the desired product, i.e., biofuels or higher value chemicals. There are multiple types of biomass feedstocks, but the two well-known types can be categorised as either lignocellulosic (solid biomass) or triglyceride (liquid biomass) feedstocks. Ideally, the selected biomass feedstock should be unsuitable for humans and animal consumption, which means being inedible. Inedible biomass feedstocks contain toxic compounds and typically grow on marginal land unsuitable for food crops [14].

Examples of lignocellulosic inedible biomass feedstocks include switch grass, forestry, and crop wastes. [13]. Triglycerides or inedible oils are extracted by pressing the seeds from inedible plants such as karanja, jatropha, neem, mahua and cottonseed. Further information about these two types of biomass feedstocks is discussed in more detail below.

2.1.2. Lignocellulosic biomass

There are several sources of biomass, but lignocellulosic biomass is prevalent when considering biomass conversion owing to its abundance in comparison to others such as algae[14]. This type of biomass includes solid materials such as forest residues, agricultural waste, industrial waste and energy crops [15, 16]. These feedstocks are composed of cellulose, hemicellulose, and lignin; the two former compounds are carbohydrate polymers, while lignin is an aromatic polymer. Alongside cellulose, hemicellulose and lignin, small amounts of extractives such as fats, resins and ash can also be found [17]. The chemical structures for hemicellulose, cellulose, and lignin can be found in Figure 2.1.

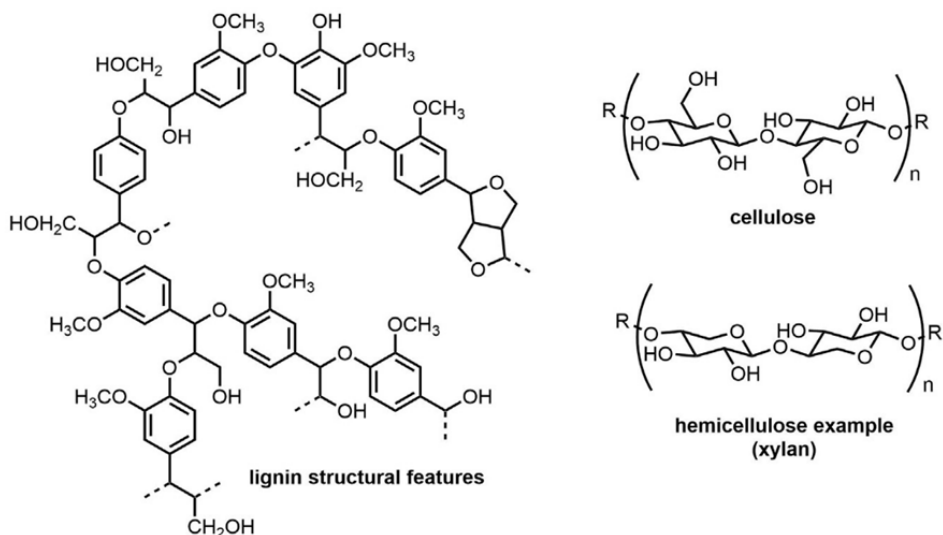


Figure 2.1. Composition of lignocellulosic feedstocks [15]

The proportions of cellulose, hemicellulose, and lignin within each type of biomass vary, but typically lignocellulosic materials are comprised of 40-50 wt.% cellulose, 10-25 wt.% lignin, and 25-40 wt.% hemicellulose. A significant challenge associated with this type of feedstock is its high oxygen content in the range of 37 wt.% to 50 wt.%. The oxygen content can be reduced via biomass conversion processes which can also increase the energy density[18, 19]. The feedstock energy density can also be influenced by other factors such as ash and water content. Lower ash content can be found in woody fuels[20]. As for the water content, this is significant as the water often has to be evaporated from the biomass before its use. This is very energy-intensive, making the process less economical [17].

2.1.3. Triglyceride biomass

Triglyceride based feedstocks are substantially different from lignocellulosic feedstocks. Firstly, most triglyceride feedstocks are typically liquids rather than solids. In addition to this, they are comprised of a glycerol molecule and three fatty acid molecules, as shown below in Figure 2.2 [3] [4]:

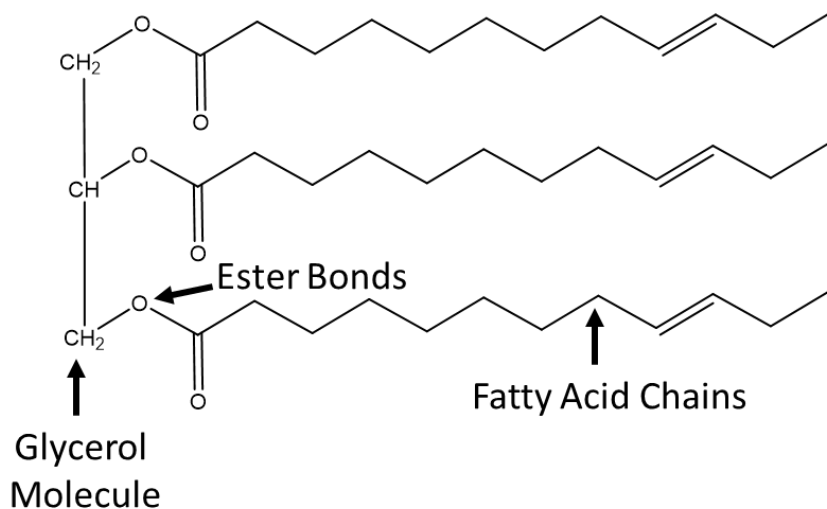


Figure 2.2. Structure of a typical triglyceride molecule

These three fatty acid chains are typically hydrocarbon chains twelve to twenty-four carbons in length, with some being the same and others different lengths, in different triglyceride molecules. This type of feedstock has a very high hydrogen to carbon ratio (H/C) combined with low oxygen content. This can be observed from the graph Figure 2.3 below.

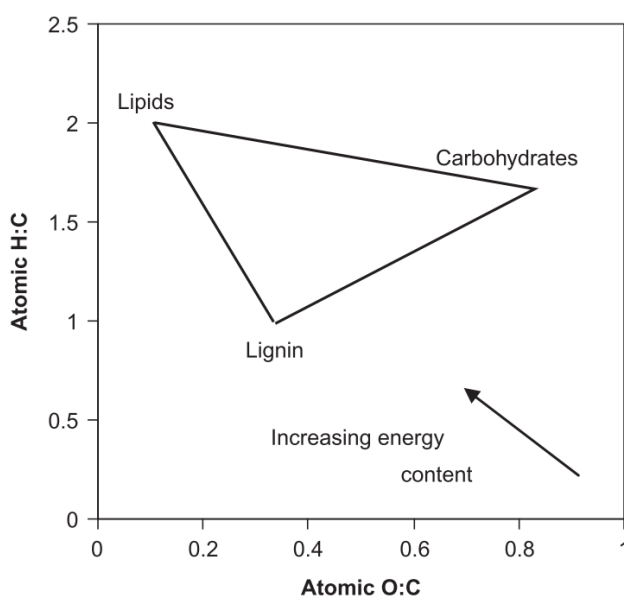


Figure 2.3. Van Krevelen plot for principal biomass constituents[21]

The graph Figure 2.3 above compares the hydrogen to carbon ratio as well as oxygen to carbon ratio of several different types of feedstocks. The lipids include triglycerides whereas the carbohydrates included the formerly discussed cellulose and hemicellulose compounds that are found in lignocellulosic feedstocks. This is desirable as the higher hydrogen to carbon ratio and lower oxygen content increases the energy density of the feedstock [18]. This is helped further because oil and water are immiscible. Therefore, this type of feedstock also benefits from negligible water content, unlike lignocellulosic feedstocks which can be subject to the previously mentioned energy intense process of evaporating the water before it can be utilised.

Triglycerides can be categorised into four categories: crude vegetable oils, used vegetable oils, animal fats, and inedible oils. A summary of several types of oil, both edible and inedible, that are popular in literature are summarised in Table 2-1 below. This offers insight into the diverse applications of differing oil feedstocks and the climate and region of the world where they are grown.

Table 2-1. Summary of popular triglyceride feedstocks

Oil	Applications	Region of Growth and Conditions	Alternative Names
Edible Oils			
Rapeseed	Widely utilised edible oil in Europe, America and Australia [3]. Major uses vegetable oil (human consumption), animal feed, and biofuels feedstock.	Rapeseed crop is grown in Europe, Western Asia, and Northern Africa (temperate climates) [22].	Brassica Campestris Oleifera [22]
Canola	Widely used for human consumption and promoted as being healthier as it contains less saturated fats and high amounts of mono-unsaturated fats than regular rapeseed [23].	Rapeseed crop, it is usually found growing in western Canada in semi-arid conditions [22]	Low Erucic Acid Rapeseed Oil
Palm	Cooking, food products (frying oil, margarine spreads, salad oils, fats for desserts-ice cream, sweets, infant formulae and noodles), oleochemicals industry (fatty acids and fatty esters for non-food products and biofuel) [3].[24, 25].	The crop is grown widely in South East Asia and Indonesia, it is the most popular oil of choice in Asia and Africa. Malaysia and Indonesia are the largest exporters of the oil [3, 26]	Elaeis guineensis[27]
Soybean	This oil has applications in food and non-food products [2, 3]. For non-food produce, soybean can be used to produce biofuel, it is only at a commercial scale in the USA[28]. Other non-food items include paints, cosmetics and plastics[23]. As for food produce the oil is used for cooking mostly in the USA but also in Australia and Europe to an extent but others are more popular[3].	Soybean is predominantly harvested in the USA, Brazil, Argentina, and China. The crop is highly sensitive to environmental fluctuations and grows best in temperature conditions [28]	Glycine Max L. Merrill[28]
Cottonseed	Although this oil is less commonplace, it still has a wide range of food and non-food applications. These include cooking oil, salad dressings and cake shortenings. A small amount is used in soaps and cosmetics.[29]	This crop requires a tropical or sub-tropical environment. It is widely cultivated in India, USA, China & Pakistan [28]	Gossypium Hirsutum L. [28]

Oil	Applications	Region of Growth and Conditions	Alternative Names
Inedible Oils			
Castor	The wide variety of applications include soaps, lubricants, paints, and minor pharmaceutical applications. The pharmaceutical applications are only minor owing to castor oils laxative properties[30].	The castor bean crop yields best in sub-tropical climates but can also prosper in semi-arid environments. The predominant country of production is India, particularly within the Gujarat region. Other areas of production include China, Brazil and areas of Africa [30].	<i>Ricinus Communis L.</i> [30]
Karanja	This oil has quite varied applications either as a biofuel or body care products including soaps, creams and hair care [7].	This tree grows best in tropical or sub-tropical climates and is particularly well established in India. It is a versatile plant as it can grow in most soil types.	<i>Pongamia Pinnata</i> [7]
Jatropha	This oil is mostly utilised for its potential biofuel applications. Other applications include remedies within traditional medicine and veterinary medicine [31, 32].	This plant grows well in tropical or sub-tropical environments on marginal land. The predominant areas of production include countries in sub-Saharan Africa, India, south east Asia and China [33].	<i>Jatropha Curcas</i> [7]
Neem	This oil has applications within the agricultural and cosmetics industry. In the agricultural industry it is used as a bio-pesticide to protect crops. As for cosmetics it is used in hair and skin care products. It also has uses in traditional medicine because of its antibacterial properties [28, 34, 35].	The Neem tree is native to eastern India and Burma. It grows in tropical climates in other areas including South East Asia, Western Africa, Central America and Mexico [36]	<i>Azadirachta Indica</i> or <i>A. Indica</i> [37]

2.1.3.1. Inedible Triglyceride Feedstocks

This work will focus on the conversion of inedible feedstocks via pyrolysis. The particulars of this process are discussed further in section 2.2.1 within this chapter. Firstly, discussion of the inedible crops mentioned in Table 2-1 above will be considered. These oils can mostly be grown on marginal land; this enables the production of renewable energy, income and employment from land that may have otherwise provided nothing. The use of inedible crops categorises these products as second-generation bioproducts (first generation are those from edible feedstocks). It is known that the technology for processing these types of feedstocks is less established, offering a greater window for development [8, 38, 39]. Inedible oils also provide an economic benefit as they are typically cheaper than edible oils [40].

The potential of castor, neem, karanja, and jatropha oil as triglyceride feedstocks, will be evaluated considering factors such as availability, cost, and present applications.

Castor oil contributes a mere 0.15 % to vegetable oil produced worldwide. It is considered a speciality chemical worldwide as it is the primary source of commercial hydroxylated fatty acids [30]. The fatty acid within castor oil is ricinoleic acid, which is not common in other edible or non-edible oils. This unique property is likely to increase its cost compared to the other potential oil feedstocks [3]. The cost of castor oil can fluctuate depending on the cost of other vegetable oils, and it can vary widely and be highly volatile [41]. For example, in 2002, its cost stood at 650 US\$ ton⁻¹ and rose to a maximum of 2700 US\$ ton⁻¹ by 2011; although in early 2017 the cost had dropped to 523 US\$ ton⁻¹ [41, 42]. In summary, this oil has limited applications outside of its specialist chemical industry applications. It has a volatile market price and little evidence from other studies or investigations to indicate its potential to produce aromatics or fuels.

Jatropha oil primary application is within sustainable fuels research. The oil is deemed promising due to its economic viability, which arises from its ease in cultivation because of its high oil yield and capacity to grow on marginal land that is less fertile [43, 44]. Multiple studies investigate and discuss its potential as a renewable fuel source [33, 43, 45-49]. Some biofuel related studies using jatropha and karanja oil have been carried out at Aston University within the Sustainable Environmental Research Group, so these oils are readily available to use in desired investigations as part of this research [50, 51].

However, some literature studies question the long-term viability and sustainability of using the jatropha crop. It can be a highly labour-intensive crop at a large scale and has uncertainty surrounding the crop and oil yields. Although it is an inedible oil, it can still create food insecurity issues due to its impact on soil quality, especially in rural areas [12, 52]. The potential implications of using jatropha oil for the production of biochemicals is complex due to various ecological, socioeconomic, legislative, and technological factors. Ecologically speaking, the Jatropha Curcas plant is drought resistant and grows well on marginal land, reducing its need for arable land that could be utilised for food crop cultivation. Furthermore, its shallow and expansive system of roots has proven to help with soil stabilization, which has helped with soil erosion and the prevention of landslides. Therefore particularly in rural areas of a tropical climate it is considered to be better in terms of its environmental and economic benefits compared with other biofuel crops that can be grown in the region. However, these benefits have been conflicted by studies which have shown less successful production of oil than anticipated, with suggestions that the agricultural characteristics of the jatropha plant are overrated due to low seed yield but this has largely been attributed to growing jatropha in areas in poor or infertile soil. This means that it's important to consider where the oil is grown in order to maximise its oil yield and therefore potential for biofuels or biochemicals production [53]. In order to maximise the yield of oil there are preferred methods of extraction which is where technological factors arise. The traditional extraction method starts with roasting seeds which are ground into a paste and soaked in boiling water with a mechanical stirrer. The oil is separated from the resulting paste via several simple filtration steps. This method can be carried out at low cost by a semi-skilled worker so it is fairly inexpensive to obtain the oil this way. Comparatively other more technical methods like mechanical extraction, solvent extraction and even enzymatic extraction are available and although they may produce a better-quality oil product and be more efficient, they also have larger capital costs and require more highly skilled workers to produce the oil. Ultimately the selection of the method of production has significant economic and socioeconomic implications. In areas where the traditional method can be used it could provide an additional or better source of income to those people and increase their standard of living but decrease the quality of the oil product making it less profitable. On the other hand, a better-quality product can be obtained using more highly skilled workers giving a better-quality product, but this is unlikely to offer a benefit to local people in terms of work opportunities and increasing their standard of living and could negatively implicate them in terms of how the change in land use around them implicates their access to

transport, water and housing if skilled workers are moved into the area. From literature, the estimated cost of jatropha oil in 2012 literature was 336 US\$ ton⁻¹. There was no extensive information on the change in market price, but as this is not a chemical speciality oil, it is likely cheaper than castor oil [54]. In summary, this oil has numerous potential applications in the bio-products industry, and the market cost is comparatively low compared to castor oil.

As for karanja oil, this is known to be used for body care products and biofuels [7]. Similarly, to jatropha oil, this oil has been explored in multiple studies for uses, including biofuel blends and alternative fuels. However, compared to jatropha oil, it is evident that it has not been investigated as widely [5, 7, 34, 55-57]. The estimated cost of karanja oil in 2016 ranged from 471 US\$ ton⁻¹ to 1620 US\$ ton⁻¹ [58]. Although this is more expensive than jatropha oil, there are other potential benefits of karanja. Unlike jatropha, the karanja plant is a member of the legume family, and these types of crops can be used to restore degraded land via the fixation of nitrogen in the soil, whilst providing the crop for oil production. The literature suggests that the karanja crop produces 4000 kg ha⁻¹ y⁻¹ compared to just 3000 kg ha⁻¹ y⁻¹ for the castor crop [59].

In summary, karanja oil is already being investigated for applications within the biofuels industry. The market cost of karanja oil is slightly more than that of jatropha but less so than castor oil. However, this additional cost does come with the added benefit of potentially improving soil quality and using a more sustainable crop.

The final oil of consideration is neem oil which has more widely known applications in body care. Although it has applications in the agricultural industry for fertilisation and pesticides, beyond that, it does not seem to be as prevalent in the bio-products domain or any other significant areas [28, 34-36]. The market price of neem oil was estimated by calculation from data in the literature to be around 108 US\$ ton⁻¹ in India and Australia in 2014 and 2001, respectively. However, in the USA in 2001, data suggested its market price was around 1746 US\$ ton⁻¹ [60-62]. Despite the large range, neem is the cheapest and, if not of similar cost to karanja oil.

Upon assessing the above information, it is apparent that neem has not been considered in past research studies as frequently as other inedible oils like jatropha and karanja. Its applications, particularly for skin care, mean that it is readily available online.

Despite potentially being the cheapest oil out of the four discussed, the market cost of the oil is only estimated, and present current cost could be quite different. Considering the above, castor oil was excluded from further consideration, primarily for its volatile and high market cost attributed to its chemical industry applications. In this discussion, it will be essential to identify what characteristics of triglyceride feedstock are of significance when considering their conversion to other products. The physicochemical properties of triglyceride feedstocks are major parameters to support their selection, as these can provide an idea of their potential conversion into other products, including biofuels and aromatics. The following section will compare both the physical and chemical properties of the oils.

2.1.3.2. Physical and Chemical Properties of Selected Non-Edible Oils

The variety of chemical and physical characteristics associated with the characterisation of triglyceride feedstocks such as jatropha, karanja, and neem oil have been selected based on those typically used to analyse conventional fuels. This is because products from thermal and catalytic conversion processes such as biofuels must have similar thermal, chemical and physical properties to conventional products [3]. A range of these parameters are stated in Table 2-2 below, which allows comparison of key parameters associated with the potential feedstocks jatropha, karanja, and neem oil:

Table 2-2. Summary of physiochemical characteristics of jatropha, karanja, and neem oil

Characteristic	Jatropha	Karanja	Neem
Kinematic Viscosity	36.5 cSt @40°C [63]	27.9 cSt @40°C [64]	22.6 cSt @40°C [64]
Pour Point, °C	1[65]	-4 [34]	12[66, 67]
Density, 15°C, kg/m³	917- 926 [47, 49, 65]	936-938 [34, 55]	890-911 [40, 60, 67]
Average Molecular Weight (kg/mol)	927.99 [44]	892.7 [68]	815 [69]
Iodine Value (gI₂/100g)	93-107 [7]	86.5-97.27 [34, 57]	65-80 [6, 60, 66]
Elemental Analysis (wt.%); C, H, N, S & O**	C (70.8), H (10.8), N (0), S (0), O (18.31) [48, 70, 71]	C (73.7), H (10.8), N (1.0) S (0), O (1.76) [57]	C (74.9), H (10.4), N (0), S (0), O (14.7) [67]
Boiling Point, (°C)	395.9[65]	330 [34]	*
Acid Value, mg KOH/g	3-38 [7]	0.4-16.8 [7, 34, 57]	10.2 [66]
Water Content, %	0.2 [72]	0.05 [34]	0.2 [66]
Oil Decomposition Temperature °C	168 in O₂ OR AIR? 225 in N₂ [73]	391 in N₂ [74]	*
Higher Heating Value, MJ/kg	37.46-46.91 [45, 47, 48, 65, 70, 71]	36.72-41.66 [34, 55]	39-40 [40, 66, 67]

* Unavailable data; ** Oxygen content obtained by difference

From Table 2-2, a very low water content (between 0.05 % and 0.2 %) and absent sulphur contents for all the oils can be observed. This is ideal as a higher water content could result in higher pre-treatment costs so that the feedstock can be processed. At the same time, the presence of sulphur could cause catalyst deactivation due to poisoning, as well as releasing sulphur compounds during the conversion process.

A significant characteristic that could be of concern is viscosity. To process the oil, it may need to be pumped, which will be more difficult with more a viscous oil. It is noticeable that neem oil appears to have the lowest viscosity (36.5 cSt) but with its higher temperature pour point (12 °C), it may be more viscous at lower temperatures.

The iodine value affects the level of unsaturation of the oil, which may influence how it decomposes. The acid value indicates oil acidity and, therefore, corrosivity, an essential factor to consider in long-term use. The final characteristic of significance from Table 2-2 is the fatty acid composition, as this is the most important in assessing how it may produce aromatic compounds.

The fatty acid composition of the oils jatropha, karanja and neem constitute varied proportions of different fatty acids; the typical amounts present in each oil are denoted in

Table 2-3 below.

Table 2-3. Typical fatty acid composition of jatropha, karanja and neem oil [3, 5-10]

Acid (wt. %)	Karanja Oil	Jatropha Oil	Neem Oil
Oleic Acid ($C_{18}H_{34}O_2$)	55.00	46.00	48.95
Linoleic Acid ($C_{18}H_{32}O_2$)	16.33	31.20	15.82
Palmitic Acid ($C_{16}H_{32}O_2$)	9.73	10.33	17.00
Stearic Acid ($C_{18}H_{36}O_2$)	7.33	6.25	13.21
Linolenic Acid ($C_{18}H_{32}O_2$)	1.73	0.32	3.11
Eicosenoic Acid ($C_{20}H_{38}O_2$)	2.30	0.00	0.00
Behenic Acid ($C_{22}H_{44}O_2$)	4.20	0.00	0.00
Lignoceric Acid ($C_{24}H_{48}O_2$)	0.67	0.00	0.00
Myristic acid ($C_{14}H_{28}O_2$)	0.00	0.33	0.01
Arachidic Acid ($C_{20}H_{40}O_2$)	0.57	0.00	0.53
Other	2.14	5.57	1.37

The information in Table 2-3 is of significance because different fatty acids can decompose into different products, and some may yield more aromatic compounds under given conditions than others. From Table 2-3, it is observed that the three most abundant fatty acids in jatropha, karanja and neem oil are oleic acid, linoleic acid and palmitic acid. Although similar, these three fatty acids have structural differences, which can be seen in Figure 2.4 below:

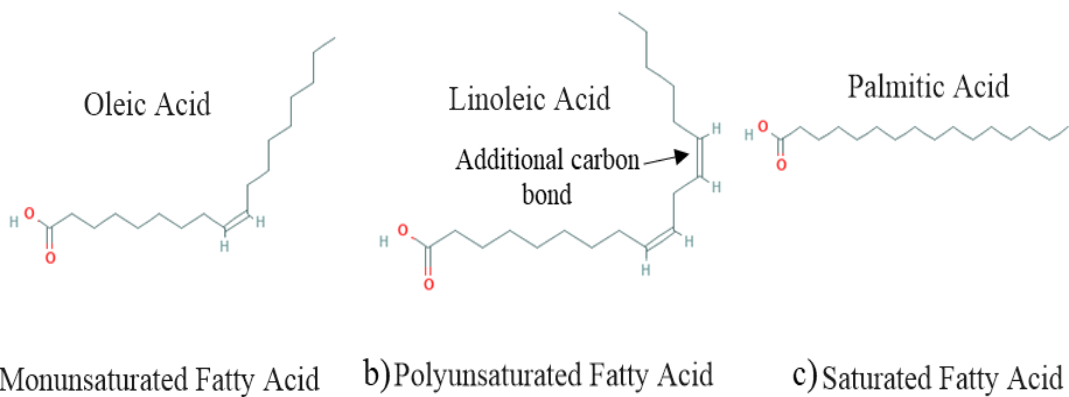


Figure 2.4. Skeletal formulae of: (a) oleic; (b) linoleic; and (c) palmitic acid

From Figure 2.4 above it can be observed that the compounds oleic acid ($C_{18}H_{34}O_2$) and linoleic acid ($C_{18}H_{32}O_2$) are structurally more similar. The main difference being an additional double carbon bond in the linoleic acid and, therefore, two less hydrogen atoms. This difference is what makes oleic acid a monounsaturated fatty acid and linoleic acid a polyunsaturated fatty acid. As for palmitic acid ($C_{16}H_{32}O_2$), this is defined as a saturated fatty acid with none of these double bonds present. These differences in structure are of significance as they could affect the products from their decomposition. The decomposition of these fatty acids and others are studied because they are common in other triglyceride feedstocks, so they are used as model compounds [75, 76]. Using a model compound allows a greater understanding of a particular component's decomposition and identification of key products from its conversion. Therefore, making it easier to deduce decomposition pathways of compounds within the feedstock. These potential pathways are discussed in section 2.3.3, focusing on triglyceride compounds' thermal and catalytic decomposition.

The conversion of triglyceride feedstocks is a topic of both value and interest owing to the potential to produce renewable bio-based products appropriate for utilisation in the fuels and chemicals sector [77]. As a result, various processes have been developed and refined, such as the transesterification of triglycerides, widely used in Brazil. This process produces a renewable fuel known as biodiesel, also called fatty acid methyl ester (FAME) or fatty acid ethyl ester (FAEE), which is presently used as an additive to diesel [78]. However, this process alone will not satisfy the entire global demand for liquid fuels, especially in areas where fuel distribution is difficult [79, 80]. A summary of the various processes typically utilised to convert lignocellulosic and triglyceride feedstocks is discussed further below in section 2.2.

2.2.Biomass conversion processes

Thermal or chemical conversion technologies can be utilised to convert biomass feedstock to biofuels or biochemicals, particularly higher-value chemical products [16, 20]. The application of renewable feedstocks is beneficial as it can reduce emissions of greenhouse gases, compared to when they are manufactured from fossil fuel sources, reducing the impact upon our environment [81]. Numerous processes are being researched and implemented with potential feedstocks to provide more sustainable and environmentally friendly methods of producing fuels and chemicals.

There are multiple conversion processes, with combustion, torrefaction, hydrolysis, gasification, transesterification, pyrolysis and hydrotreating being common choices. Each of these processes has specific conditions and different types of products due to the nature of the process. The products can be implied by the type of feedstock (i.e., lignocellulosic or triglyceride) utilised due to their different chemical composition and structure. This work focuses on the application of the fast pyrolysis process.

2.2.1.Pyrolysis

The pyrolysis process is an advanced thermal treatment method involving biomass degradation in the absence of oxygen [82]. The process requires an external heat source to maintain a temperature of 300 °C to 850 °C depending on the type used (fast or slow). The process requires a consistent biomass feedstock that is not contaminated with foreign objects; otherwise, it can damage or corrode the equipment [17, 83]. This conversion method has been noted as a convenient and valuable technology [84]. The three primary products from biomass pyrolysis are solids, liquids and gases, and their distribution varies depending on the biomass properties and pyrolysis conditions used. The main pyrolysis products and examples are shown below in Figure 2.5 below.

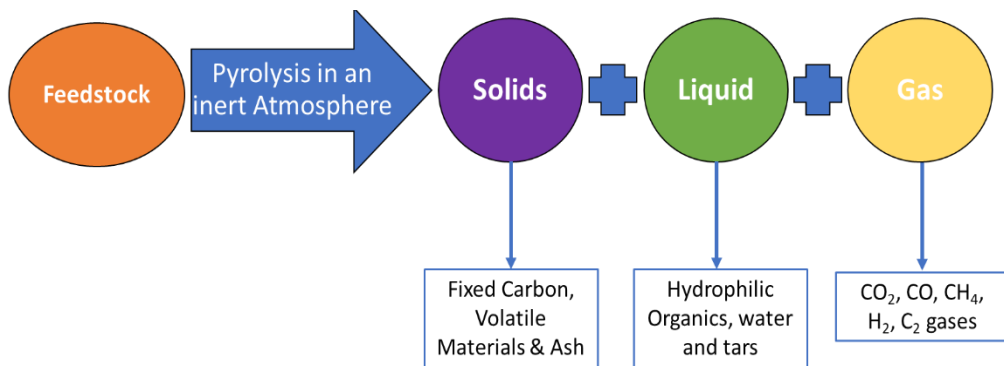


Figure 2.5. Major types of products obtained from pyrolysis of biomass. (adapted from [82, 83])

Biomass degradation can also be referred to as thermal cracking or catalytic cracking when carried out in the presence of a catalyst [3, 15]. The solid product from pyrolysis, also known as char, is a residue with a varying carbon content between 60 % and 90 %. Whilst some of this maybe fixed carbon, the remaining inorganic material is referred to as ash [82]. Almost all the feedstock's alkali metals, including potassium and sodium, can be found in the ash [85]. The presence of these metals can have catalytic effects on pyrolysis resulting in higher char yields, with the char itself potentially having a higher reactivity and ignition properties[82]. Although, the solid pyrolysis products have applications as biochar (i.e., soil amendment) in commercial process the char is typically burnt to provide process heat. The liquid product is an organic liquid known as bio-oil it is a homogenous mixture of organics, water- and water-soluble organics. This material is usually a single phase but can be phase-separated liquid if too much alkali metals crack too much water in the feed. Phase separation occurs when water from the feedstock or water produced in the pyrolysis reaction condenses with the products in the oil [82].

Finally, the gas product, which often comprises varying proportions of CO₂, CO, CH₄, and small chain hydrocarbon gases that can be burnt as a fuel.

The processing of biomass via pyrolysis benefits from the flexibility to produce varying proportions of liquid, gas, and solid products, each of them with varying applications. Pyrolysis conditions can be altered to maximise the desired product's yield. In some cases, the liquid pyrolysis products have reduced water and oxygen content compared to their parent biomass feedstocks, which improves the calorific value and stability of the liquid product, often known as bio-oil [2]. Following pyrolysis, bio-oil products may be upgraded using hydrotreating, which alters the oxygen content by using high temperature, pressure, and hydrogen in the presence of a catalyst. This improves the quality of the bio-oil product further and can allow it to be used within conventional transportation fuels[86].

2.2.2.Types of pyrolysis

There are two different types of pyrolysis, slow and fast. The difference between the types is based on the different residence times known as hot vapour residence time, temperature range, and heating rates as shown below in Table 2-4 alongside other additional parameters associated with each type of pyrolysis [37, 82, 85, 87-89]:

Table 2-4. Parameters for slow and fast pyrolysis of different types of lignocellulosic feedstocks [37, 82, 85, 87-89]

Parameter	Slow Pyrolysis	Fast Pyrolysis
Typical Operating Temperature (°C)	400	500
HVRT*	Hours to days	~1-2 s
Heating rate (K/min)	<10	>300
Ideal Feedstock Particle Size (PS) (mm), Length (L) (mm)	PS (5-50), L (<30)	PS-Less than 3 (diameter)
Moisture Content (%)	<40 but ideally <30	<10

* HVRT- Hot Vapour Residence Time

It can be observed from Table 2-4 that the feedstock's particle size and moisture content are important parameters that influence the yield of liquid and solid products in all three types of pyrolysis of lignocellulosic feedstocks. A higher moisture content

usually means less solid is produced, resulting in more water collecting within the liquid bio-oil [37, 82, 87-89]. This can make it more likely for a phase separated product to form. The proportion of the products is also influenced by the type of pyrolysis utilised, shown below in Table 2-5[17].

Table 2-5. A summary of the typical fractions of products from different types of pyrolysis of a lignocellulosic feedstock [8]

Pyrolysis Type	Products Distribution		
	Solid	Liquid	Gas
Slow	35 %	30 %	35 %
Fast	12 %	75 %	13 %

Furthermore, the composition of the lignocellulosic biomass feedstock affects the yield of the different products. An important consideration is the proportions of the three main biomass components, including hemicellulose, cellulose, and lignin. These undergo different reactions during this process, and these proportions vary in different feedstocks [90].

2.2.3. Fast pyrolysis systems

Typically, reactors are utilised for just one or two of the different types of pyrolysis as they all operate most effectively in different ways. It would be complex to design a system that would efficiently manage more than this [20]. Of the different types of pyrolysis and reactor types available, it is apparent from the literature that fast pyrolysis of biomass is often used when the desired products are high-quality bio-oil for liquid fuels or chemicals [20, 85, 87, 91, 92].

As the focus of this work concerns the conversion of a liquid feedstock to produce aromatic chemical compounds, the discussion of reactor types typically used for fast pyrolysis is of significance. Therefore, the main reactor types associated with fast pyrolysis are presented in Figure 2.6 below:

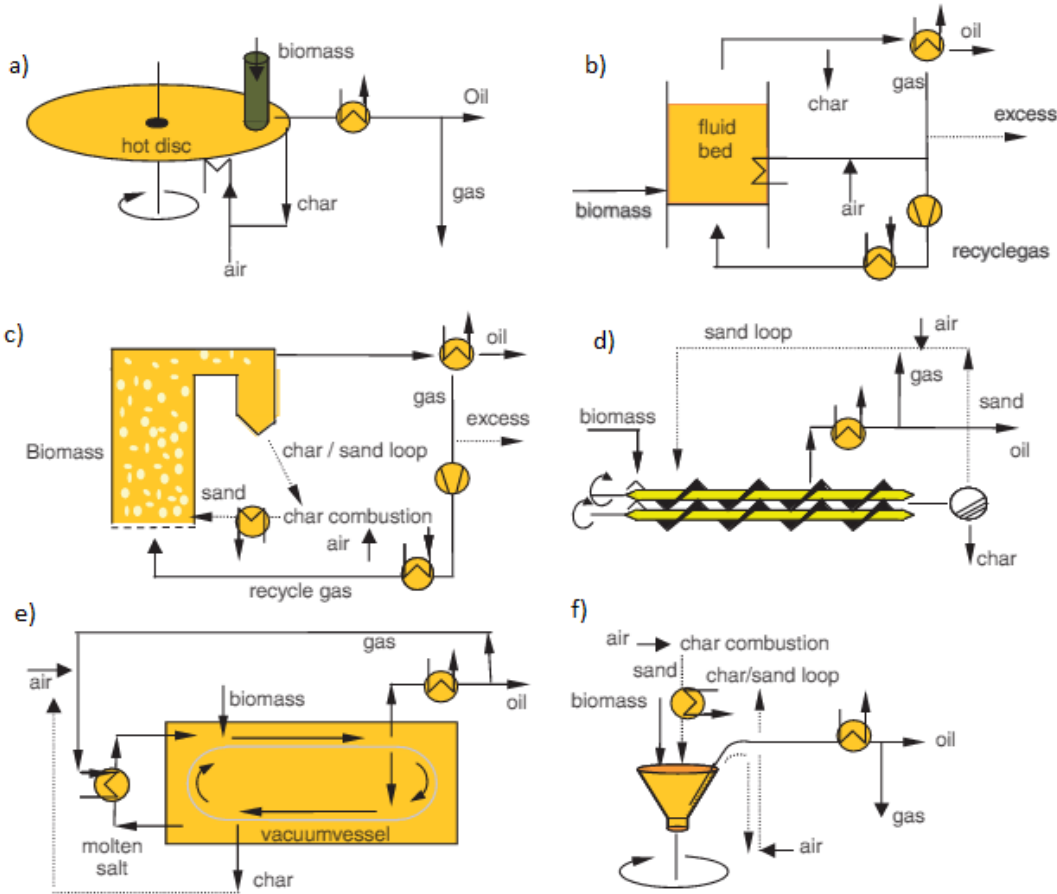


Figure 2.6. Reaction systems for fast pyrolysis: (a) ablative, (b) bubbling fluidised bed (BFB), (c) circulating fluidised bed (CFB), (d) auger (screw), (e) vacuum, (f) rotating cone [93]

Of these reactor types, the bubbling fluidised bed reactor is of most significance because these reactors are of simple design and operate with good temperature control and heat transfer. Moreover, their high liquid yields are desirable for the application to produce liquid fuels and chemicals and are more easily scalable to commercial capacities than other reactor types[20, 92]. The utilisation of this reactor type to process a liquid triglyceride feedstock using fast pyrolysis is further supported by additional information in Table 2-6 below.

Table 2-6. Lignocellulosic feedstock pyrolysis reactor design selection parameter matrix [94]

Reactor Type	Simplicity	Capital Expenditure	Low Temperature	Low Gas/Solid Ratio	Operating Cost	Scalability
Ablative	Fair	Very Good	Very Good	Excellent	Good	Very Poor
Bubbling Fluidised Bed	Very Good	Excellent	Very Good	Good	Very Good	Excellent
Circulating Fluidised Bed	Fair	Good	Very Good	Poor	Fair	Very Good
Auger	Very Good	Excellent	Very Good	Excellent	Good	Poor
Vacuum	Fair	Excellent	Excellent	Excellent	Poor	Good
Rotating Cone	Fair	Good	Very Good	Very Good	Fair	Poor

Out of the six reactor systems shown in Table 2-6, the bubbling fluidised bed (BFB) is the only system described as good or better in all six of the selection parameters considered. The high ratings are owed to its simple design, good temperature control and rapid heat transfer[20, 92, 94]. Combined with the BFB's high average bio-oil yield when processing lignocellulosic feedstocks, these factors make this reactor system desirable for fast pyrolysis of lignocellulosic feedstocks. Furthermore, a high yield of liquid products may make it easier to scale up if required in the future.

It is apparent across literature that there is a lack of information on the pyrolysis of liquid triglyceride feedstocks and within bubbling fluidised bed pyrolysis systems. Therefore, considering this reactor type for processing a triglyceride feedstock novel. This work focuses on producing aromatic products in liquid form, and there is the potential for high liquid yields from fast pyrolysis using a triglyceride feedstock. Examples of aromatic compounds in liquid products from pyrolysis of triglycerides are given in more detail in section 2.3.2 and 2.3.4.

This system's principles are discussed further, especially when prior studies demonstrate that high-value aromatic compounds are typically contained within the liquid products. Bubbling fluidised bed systems rely on fluidisation, and its operation can be influenced by several design parameters, including nitrogen velocity, the particle size of bed material, feed rate and reactor operating temperature [95, 96]. The feed rates of experimental systems can range from a couple of hundred grams an hour to kilograms per hour[95, 97, 98]. If a catalyst is utilised, additional consideration will also be given on how that may be incorporated and a catalyst to feed ratio. There are generally two given methods for adding a catalyst to a fluidised bed system known as *in-situ* or *ex-situ*. *In-situ* refers to the catalyst and feedstock mixed inside the reactor, mainly in the reactor's bed. In comparison, *ex-situ* involves utilising a second reactor

where the pyrolysis gases are passed through for further catalytic cracking [99]. Owing to the varied number of parameters discussed when investigating a range of catalysts and feedstocks, pyrolysis gas chromatography is often used.

2.2.3.1. Analytical Pyrolysis

In Pyrolysis- Gas Chromatography- Mass Spectrometry, known as Pyroprobe GC-MS (Py-GCMS) systems, they operate at smaller scales than those previously discussed, such as bubbling fluidised beds as these use samples typically less than a milligram. There are several advantages to utilising such systems, including a reduced time for analysis compared to larger bench scale systems. It only requires small sample sizes, reducing the time required for sample preparation(feedstock and catalyst) [100]. With the thermal and catalytic degradation of biomass being complex, this type of investigation can directly analyse the resulting pyrolysis products. The results from pyroprobe investigations are often considered adequately representative of what is produced when a given sample is pyrolyzed. The products are identified using GC retention times and mass spectra data allowing comparison with those obtained under different conditions such as a range of temperatures or catalysts [100, 101]. However, these small-scale systems do have their differences. Pyroprobe systems typically operate by heating a sample in an inert atmosphere with the products cleared towards an analytical system such as GC-MS using a carrier gas. The heating can be carried out using one of three modes: flash pyrolysis (pulse mode), slow gradient heating (continuous mode), or step pyrolysis. Typically, analytical flash pyrolysis uses a very rapid heating rate to ensure that isothermal conditions are achieved when the sample is pyrolyzed. Thus, the differences in scale and being a batch process rather than continuous like a bubbling fluidised bed reactor could explain differences in the products obtained.

2.3. Conversion of triglyceride feedstocks to yield aromatics

The thermal conversion and catalytic cracking of triglyceride feedstocks have been recorded in the literature as early as the mid-1980s [102]. Some processes have been used to produce liquid biofuels and highly valuable compounds, including aromatics compounds such as benzene, toluene, and xylenes. The significance of these high-value compounds is discussed further below[15, 103]. Furthermore, a summary of several studies converting triglyceride-based feedstocks predominately using the pyrolysis process, with an aromatics fraction is provided in Table 2-7 in section 2.3.2.

2.3.1. Aromatic compounds from fossil fuels

The studies presented in Table 2-7 in the following section demonstrate the varying proportion of aromatic compounds that have been reported in the literature. Aromatic compounds production is of significance as their global demand is growing at the same time as fossil fuel feedstocks are being depleted. Other commodities such as energy, transportation, fuels, and other chemicals also rely on fossil fuels. Thus, finding alternative sustainable sources for these commodities is ever more desirable [14, 92]. The energy demand is estimated to increase by 45 % between 2017 and 2040 worldwide, with the most significant growth in developing countries within Asia. An increasing proportion of this demand could be met using nuclear power or renewable power, including hydro, solar and wind power or modern bioenergy technologies [104]. As for transportation, there has been a steady growth in the application of biofuels. A biofuel is a liquid fuel source derived from renewable plant material, commonly called biomass [14].

In Figure 2.7, it is observed that in 2018 there was a significant increase in bio-fuel production. From the graph, the bio-fuels produced show a steeper incline between 2017 and 2018, as during this period production grew by 9.7 % worldwide [105].

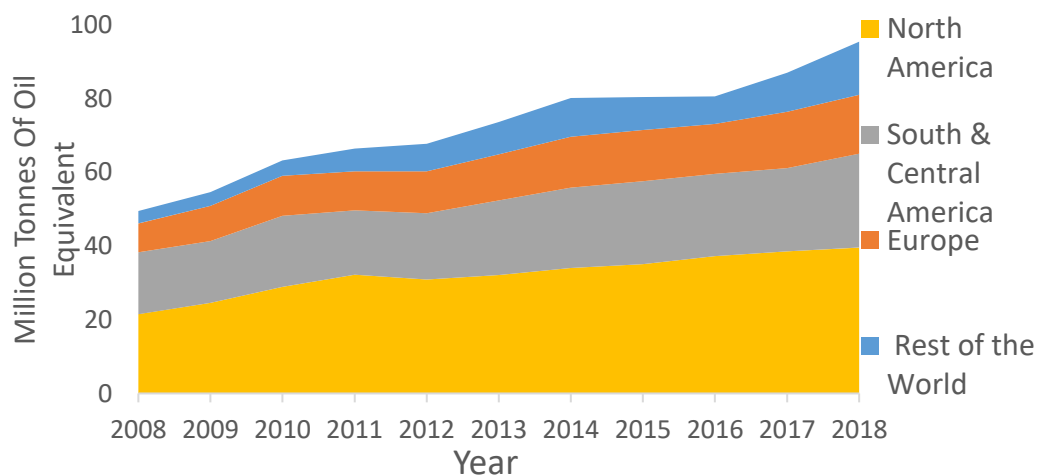


Figure 2.7. World biofuels production (MTOE: Million Tonnes of Oil Equivalent) from 2008 to 2018 [105]

However, biofuels do not play a major role in transport infrastructures yet. In 2014 biofuels just had a 4% share of the transport energy demand within the European Union. The major sources utilised were fossil-derived fuels, including diesel, kerosene, and gasoline, sharing 55 %, 14 % and 22 % of the transport energy demand.

Furthermore, this major industrial sector still has a high dependency on fossil fuel feedstocks when it comes to aromatics and chemicals. Around the world, millions of

tonnes of chemicals are produced per year for further processing into essential everyday products in this sector. An estimated 70 % of aromatic compounds, including benzene, toluene, and xylenes (BTX), originate from the catalytic reforming of naphtha, a fossil fuel derived feedstock. A simple schematic giving an overview of this process is shown in Figure 2.8:

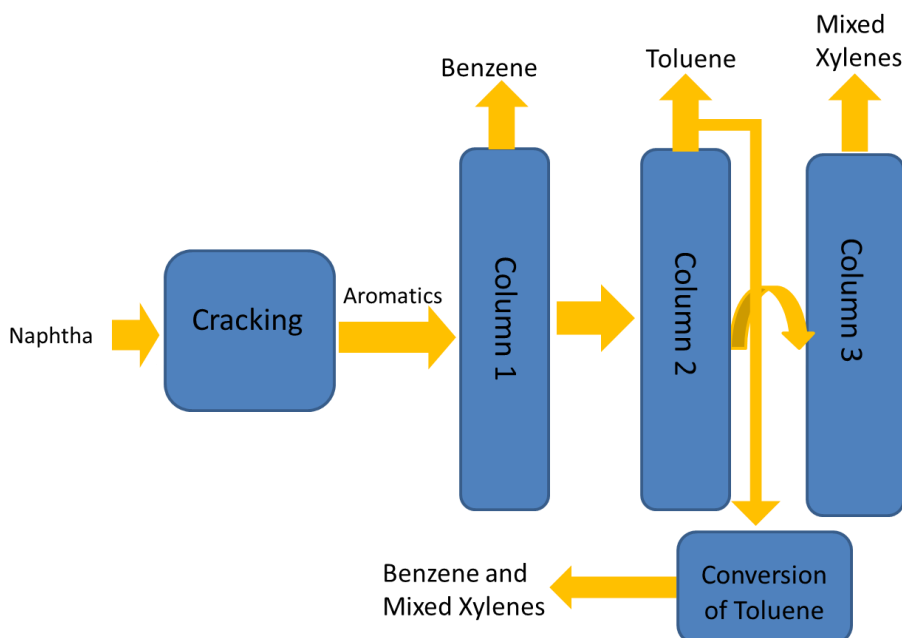


Figure 2.8. Schematic overview of aromatics production from naphtha via catalytic cracking [106]

The remaining 30 % of aromatic compounds is still obtained from other fossil fuel sources, including ethylene plant pygas and coal liquids from coke ovens (COLO) at 23 % and 7 % correspondingly worldwide [1]. This is important because as the world's population rises, the demand for energy, fuels, and chemicals to sustain a growing population will only increase. Some examples of high demand chemicals are ammonia, methyl alcohol, carbon black, ethylene, propylene, C₄ olefins and aromatics, including BTX, just to name a few. Of these chemicals, data that suggests olefins and aromatics sourced from the steam cracking account for around 57 %, more than half of the fossil fuels used within the chemical sector [107].

Within the aromatics group, the compounds benzene, toluene, and xylenes (BTX) are primary petrochemical intermediates considered building blocks in the petrochemical industry. They have a multitude of worldwide applications, as shown by the pie charts in Figure 2.9 below [1]:

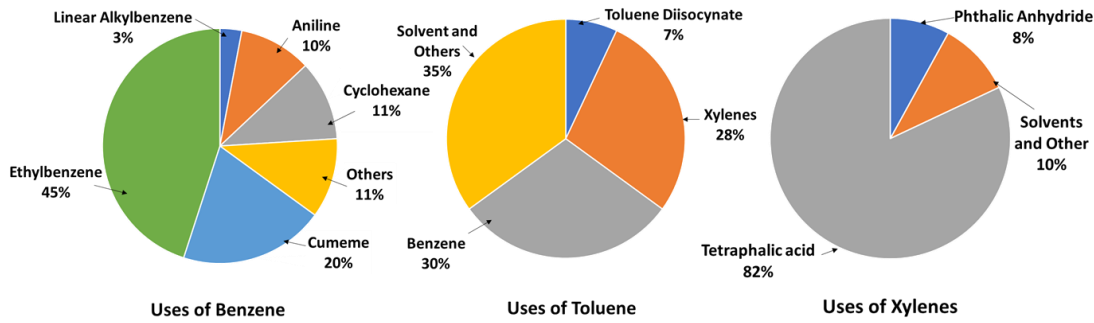


Figure 2.9. Worldwide applications of BTX compounds[108]

It is possible to derive many other compounds from BTX, such as adsorbents, paints, solvents and lubricants, to name a few [1, 103]. Therefore, finding an alternative source that is both renewable and sustainable for producing these aromatics is highly desirable. The BTX compounds are comprised of hydrocarbons, which means they contain the elements hydrogen and carbon. Their structure is shown in Figure 2.10 below:

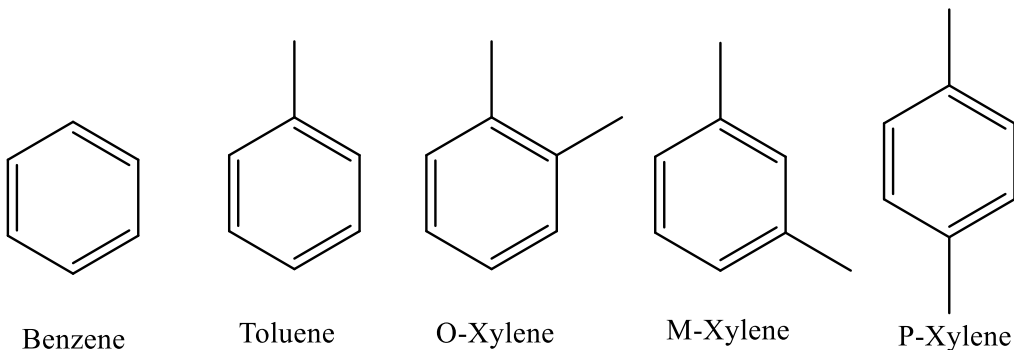


Figure 2.10. Structures of benzene, toluene, and xylenes

Since aromatic hydrocarbons are currently derived from naphtha, any new alternative feedstock must be of similar composition to fossil fuels. A potential feedstock is biomass, particularly triglyceride feedstocks, as they can be converted into either biofuels or biochemicals, with examples of this discussed in the following section 2.3.2.

2.3.2. Conversion of triglycerides to aromatics

This summary in Table 2-7 considers the use of different triglyceride feedstocks such as inedible jatropha oil and fatty acids such as oleic acid. Fatty acid compounds have been studied as model compounds because they can help understand the decomposition pathways of a proportion of a triglyceride feedstock. This information can then be used to ascertain how the whole feedstock may decompose under similar conditions, i.e., different catalysts, temperatures, or pressures [103].

Table 2-7. Summary of studies evaluating the catalytic conversion of triglyceride feedstocks into aromatic compounds

Oil Type	Reactor Type/ Additional Info	Process conditions (Temperature and Pressure)	Catalyst	Aromatics yields	Reference.
Jatropha Oil	Continuous flow fixed bed with hydrogen gas feed.	380°C; 3 MPa	PTA 20-NiMo/ZSM-5 (Si/Al 25)	Organic liquid products yield: 70%; out of which 59 wt.% was BTX, other major product was light oil.	Yang, 2017, [109]
	Fixed bed down flow micro-reactor with N ₂ carrier gas	550°C; atmospheric pressure.	ZSM-5(NZ) (Si/Al 30)	Aromatics yield: 45.4 wt. %	Viswanadham, 2014, [43]
	Tubular batch reactor with N ₂ carrier gas	375°C; atmospheric pressure.	ZSM-5(Si/Al 35), ZSM-5 +(Si/Al 45) and Ni-Mo/SiAl (4%Ni, 15% Mo loading on support)	Highest aromatics yield: 45.9 vol %; achieved using ZSM-5 (Si/Al 35) catalyst.	Biswas, 2014 [45]
Soybean Oil	Fixed-bed reactor under nitrogen flow.	420° C and 450° C. Unknown pressure.	ZSM-5 catalysts (Si/Al ratios 28, 40, and 180)	Si/Al (28) at 450° C. 79wt.% bio-oil yield with ~54wt.% of BTX. Overall yield of aromatics 42.7wt.%, also gave 25 wt.% gas and 1wt.% coke.	Thanh-An-Ngo,2010 [110]
			2 wt.% (Ga, Al, or Cu) impregnated MCM41 catalysts	Present but negligible and in a mixed of other hydrocarbons.	
	Fixed bed flow reactor under nitrogen Flow.	380° C 3 MPa	Ni-Mo/ ZSM-5 (0), Ni-Mo/ ZSM-5 (0.0005), Ni-Mo/ ZSM-5 (0.01) – Bracket number is [NH ₄] ⁺	Present but only in negligible amounts mostly diesel range hydrocarbons (C ₁₆ - C ₁₈)	Chena,2015[111]
			Ni-Mo/ZSM-5(1.0)	Aromatics were present but data only provided a selectivity of 64.7%.	
	Fixed Bed Micro Activity Unit	565°C	Repsol Industrial FCC Catalyst	80wt% aromatics	Melero,2010,[18]

Canola Oil	Continuous fixed bed Micro-reactor with argon carrier gas	375–500° C Atmospheric pressure.	HZSM-5, HY, aluminium-pill-clay, silica-aluminium, silicate, HMor	BTX yield of 40.2wt. % with HZSM-5 catalyst at 400°C, other notable products include water, coke, and residues.	Sadrameli, 2009,[112]
	Continuous flow fixed bed micro-reactor with argon carrier gas.	Range between 342°C and 398° Atmospheric pressure.	HZSM-5	41 wt. % within a liquid product yield of 78.1wt.% of aromatics at 383°C and 3.8g oil/g cat. H. Overall yield of aromatics calculated 32wt. %.	Bakhshi, 1986,[113]
Palm Oil	Transport riser reactor with Argon carrier gas.	450°C, residence time of 20 seconds, at Atmospheric pressure and catalyst/oil ratio of 5 g/g.	Rare earth Y(REY) Catalyst	40.6wt % Yield of Aromatics.	Bhatia, 2011,[3]
Tung Oil and Waste Cooking Oil	Fixed Bed reactor	300-500°C Atmospheric Pressure	Binary oxide solid superacid SO ₄ ²⁻ /TiO ₂ ZrO ₂ catalyst	Tung Oil, 66wt% Aromatic Compounds and Waste Cooking oil 18% Aromatic Compounds	Chu, 1947,[114]
Soyabean Oil and Soybean Hydrogenated Fats	Plug flow reactor	525°C Pressure not reported	None	Very small amounts 1.8 %.vol of BTX. It was observed that this was highest with pure soyabean oil and was reduced by presence of saturated fats (lower iodine value)	Beims, 2018,[2]
Cottonseed Oil	Fixed- Fluidised Bed Reactor	520°C	Shanghai Oil FCC Catalyst	Aromatics yields 32 vol.% without catalyst; 44 vol.% from catalytic pyrolysis,	Li, 2009,[115]
Triglyceride Model Compounds					
Palmitic Acid	Swagelok batch reactors, water or hydrogen added.	400°C 24 MPa	Ammonium form ZSM-5 (Si/Al 30)	Major liquid product was aromatic and alkenes, however this was only 12wt. %.	Savage, 2013,[116]
Oleic Acid	Fixed Bed Reactor (Pyroprobe CDS5200)	650°C	NiO or Silica and NiO or Alumina (10:1 catalyst to feed ratio)	21.5% of total area of deoxygenated products with a NiO Alumina catalyst- 7 times more than NiO/Silica	Fréty, 2014 [117]

From the studies presented in Table 2-7, it is clear there are similarities and differences in terms of reactor type, triglyceride feedstocks, and aromatics yields, including BTX. These include the type of catalyst used, reactor types and the varying yields of high-value aromatics. First and foremost, the most prevalent reactor types reported were batch and fixed bed reactors. A significant observation is that none of these studies from Table 2-7 appeared to utilise bubbling fluidised bed (BFB) reactors. Furthermore, to date, there is no evidence of triglyceride feedstocks being processed using this reactor type in the literature. This is important as aromatic products typically seem to be present within the bio-oil products. A known characteristic of bubbling fluidised beds is their high bio-oil yield.

2.3.3. Triglyceride decomposition pathways

In Table 2-7 discussed in the prior section 2.3.2, varied reactor types and feedstocks are used. An observation has been made those three studies denote that more aromatics may be obtained with a feedstock with a higher degree of unsaturation. For example, a more unsaturated triglyceride feedstock will have a higher iodine value [2, 18, 118]. The study by Beims et al. 2018, specifically investigated the effect of feedstock saturation on aromatics production. A varying proportion of soybean oil and hydrogenated fats were processed using a 320 gh^{-1} plug flow reactor at a temperature of 525 °C. It was found that the aromatics content decreased by 14 % when utilising the least unsaturated feedstock (80 wt.% soybean oil, 20 wt.% hydrogenated fats) [2]. Zhang et al. 2020, processed Tung Oil, rubber seed oil, Jatropha oil and waste cooking oil (WCO) using a lab-scale fixed bed reactor. Tung oil was the most unsaturated oil as it had the highest iodine number of 141.77 g I₂/100g, and it yielded 66% aromatic hydrocarbons. In comparison, the waste cooking oil with the lowest iodine number of 88.67 g I₂/100g yielded a significantly lower proportion of 18 % aromatic hydrocarbons under the same process conditions. Finally, Melero et al. 2010 processed vacuum gas oil (VGO) with a 30 % proportion of soybean oil, palm oil or waste cooking oil (WCO) in a fixed bed micro activity reactor at 565 °C. The product distribution of these different blends followed the same trend observed by Beimsa et al. and Zhang et al., with both seeing a reduction in the aromatic content using more saturated feedstocks.

It is important to understand how unsaturated fatty acids can decompose during pyrolysis to yield aromatic compounds. One route for the decomposition of unsaturated fatty acids into aromatics was suggested by Schwab et al. 1998, as shown in Figure 2.11 below [119]:

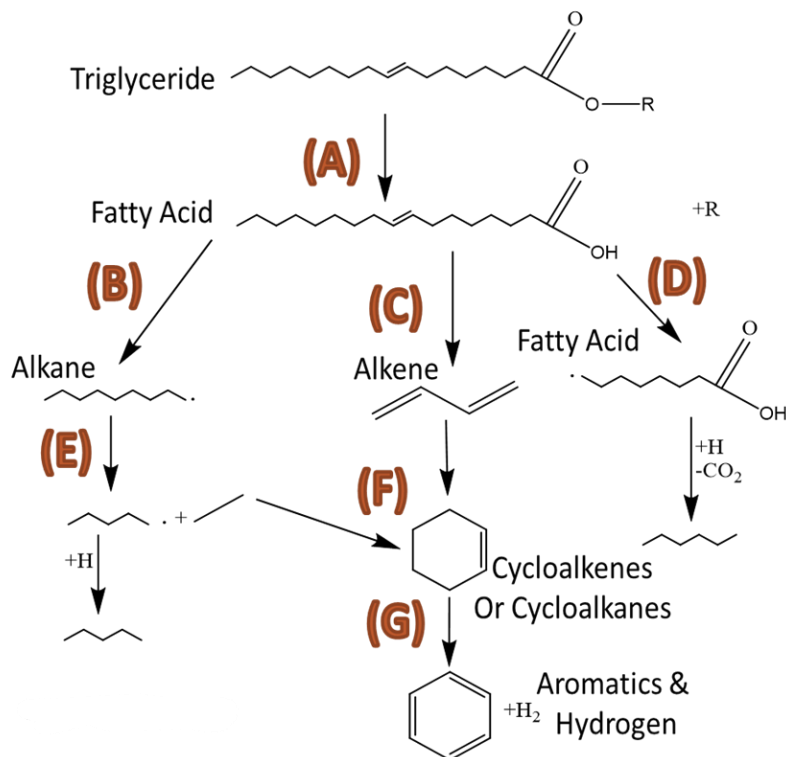


Figure 2.11. Reaction mechanism for the decomposition of unsaturated triglycerides[119]

From Figure 2.11, it was proposed that the ester bond between the fatty acid and glycerol molecule is broken in reaction “A”, resulting in the formation of a fatty acid chain. This fatty acid chain further decomposes into alkanes, alkenes, and shorter chain fatty acids via the pathways “B, C and D”, respectively. The alkenes from pathway “C” form cycloalkanes and cycloalkenes via the Diels-Alder reactions, which can consequently undergo dehydrogenation forming aromatics including BTX. In addition, the alkanes from pathway “E” also contribute to the formation of aromatics via pathway F.

Triglyceride feedstocks are a mixture of unsaturated and saturated fatty acids bonded to a glycerol molecule (see Figure 2.2, section 2.1.3), so other parts of the feedstocks may also yield aromatic compounds. In the mechanism proposed by Schwab et al. 1998, (Figure 2.11) the first step leaves the glycerol molecule “R”. This is of significance as it has been suggested in the literature by Zakaria et al. 2013, glycerol can decompose into aromatics in the presence of ZSM-5 catalyst shown by the mechanism in Figure 2.12 below [120] :

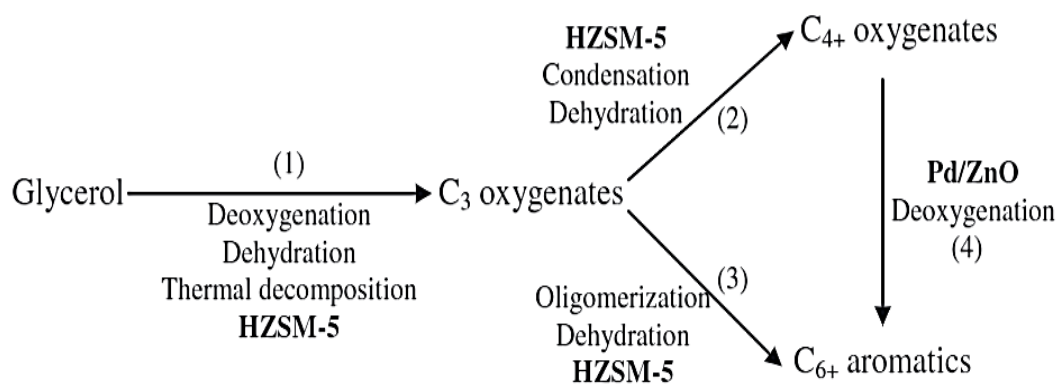
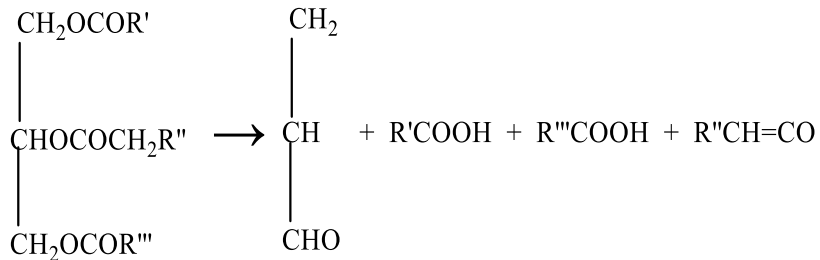


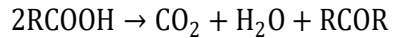
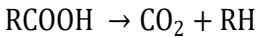
Figure 2.12. Decomposition of glycerol to aromatics in the presence of H-ZSM-5

The further literature explicitly relating to the cracking of triglycerides is not extensive due to the sporadic nature in which information on this topic appears over the last several decades [121]. The earliest decomposition pathways of saturated fatty acids were suggested by Chang et al. 1947, and Greensfelder et al. 1949, which were later modified by Alencar et al. 1983. The development of this pathway was highlighted more recently in a review by Maher et al. [27, 103, 114, 122]. The proposed reaction scheme by Chang et al. 1947 comprised of sixteen different suggested reactions as shown in Figure 2.13 below:

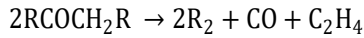
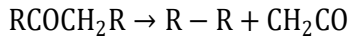
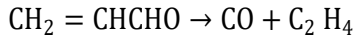
(1) Decomposition of the triglyceride.



(2) Decomposition of Fatty Acids.



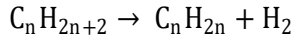
(3) Decomposition of Ketenes and Acrolein.



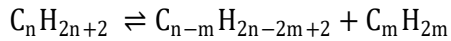
(4) Decomposition into Elements.



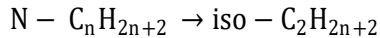
(5) Dehydration of Paraffins.



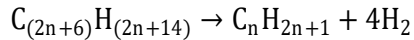
(6) Splitting Decomposition (forward reaction) and (7) Alkylation (reverse reaction) of Paraffins.



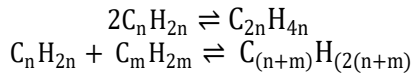
(8) Isomerisation of Paraffins



(9) Aromatic Cyclization of Paraffins.



(10) Polymerisation (forward reaction) and (11) Depolymerisation (reverse reaction) of Olefins.

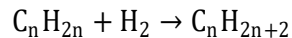


(12) Decomposition of Olefins to Diolefins.

(13) Decomposition of Olefins to Acetylenic Hydrocarbons.

(14) Aromatization or Cyclization of Olefins.

(15) Hydrogenation of Olefins.



(16) Isomerisation of Olefins.

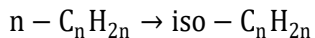


Figure 2.13. Decomposition of saturated triglycerides: reaction mechanism for the Chang et al. 1947

[114]

Of the reactions shown in Figure 2.13, it is suggested that a large proportion of the acids, acrolein, and ketenes formed in reaction (1) go on to decompose further in equations (2) and (3) with hydrocarbon products predominant in gasoline being produced from equations (6) and (11). From the pathway in Figure 2.13, Alencar et al., 1983; proposed a slightly different scheme, as shown in Figure 2.14.

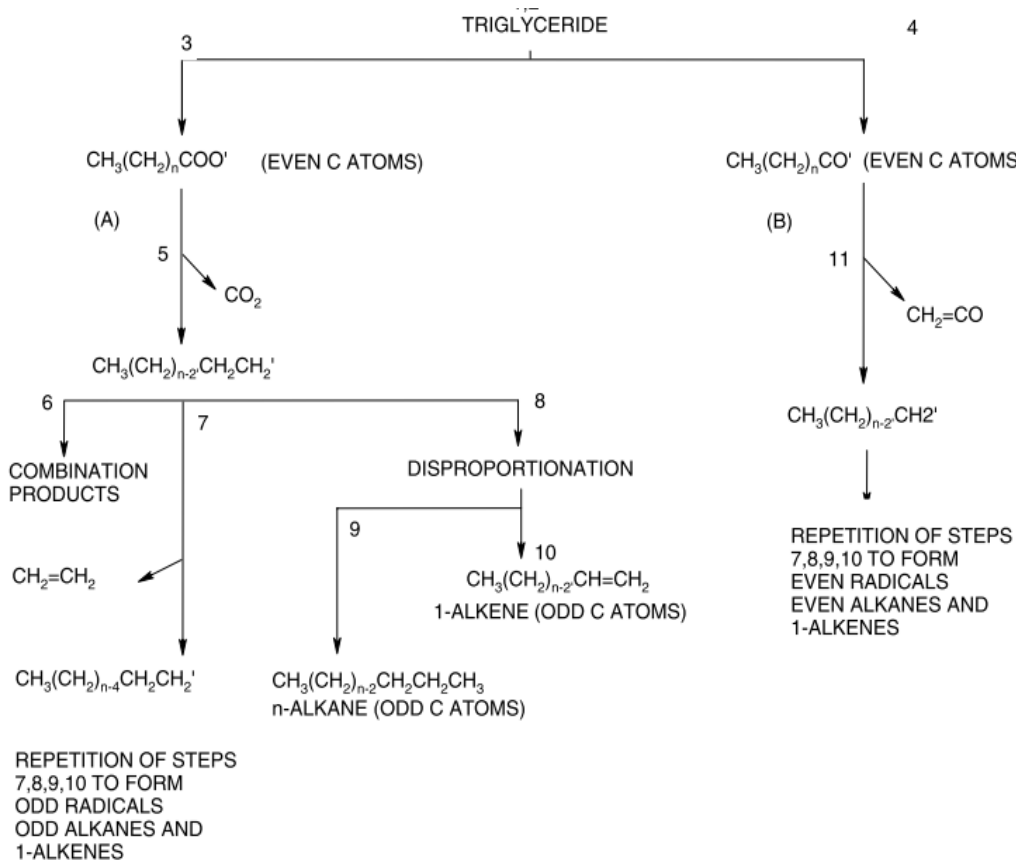


Figure 2.14. Reaction mechanism for the decomposition of saturated triglycerides Alencar et al., 1983 [27]

Alencar et al., 1983; proposed that the triglyceride initially decomposed into the radicals (A) and (B) as shown in Figure 2.14. This gives rise to two different paths producing a series of odd alkanes and 1-alkenes via decarboxylation of radical (A) followed by disproportionation and ethylene elimination. A similar process is applied to the even alkanes and alkenes formed by the loss of ketene from radical (B), then the same pathway of disproportion and ethylene elimination [27, 103]. However, the triglyceride feedstock utilised will have to consider the combined decomposition of both saturated and unsaturated fatty acids, which is a lot more complex, as discussed in work by Idem et al., 1996. Idem et al. studied the pyrolysis of canola oil in a fixed bed reactor over a temperature range of 300 °C to 500 °C and suggested the scheme shown in Figure 2.15, the detailed descriptors for the numbered reactions are available in Chapter 8.0, Appendix One.

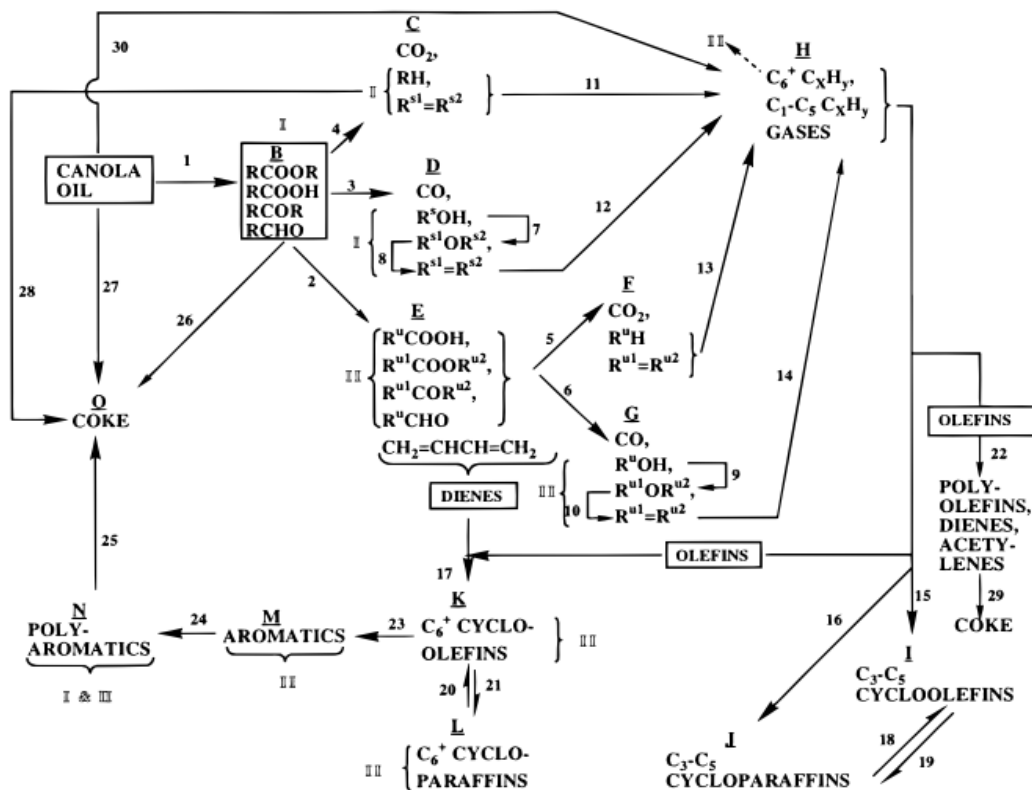


Figure 2.15. Proposed reaction scheme for thermal cracking of a mixture of unsaturated and saturated triglycerides, Idem et al,1996 (canola oil) [123]

This set of pathways presented in Figure 2.15 is one of the most complex schemes. However, it considers the triglyceride feedstock as a whole by representing the decomposition of both saturated and unsaturated fatty acids using 30 different pathways. Alongside the processing of canola oil, Idem et al., 1996; identified a wide variety of studies that concerned the production of hydrocarbons from plant-based oils or animal fats using catalysts including HZSM-5, Pt/HZSM-5, Silica-alumina, H-Y, Mordenite, Aluminium Pillared Clays, Alumina Silicate, and other variations of these catalysts. It was suggested from studies by Weisz et al. 1979, Prasad et al. 1985 and Katikaneni et al., 1995 that oil conversion and the products obtained were attributed to the acidity and shape selectivity of the catalysts [113, 124-127]. Furthermore, these authors, in addition to Milne et al., 1998 suggested that the formation of aromatics was related to the presence of high strength Brønsted sites on the catalysts [113, 125-128]. However, this finding contrasts with conclusions drawn from studies by Chang et al. 1947, Egloff et al. 1932, Lipinsky et al. 1985, Schwab et al. 1988, and Crossley et al. 1962, who suggested that formation of aromatics did not necessarily require the presence of acid centres on a catalyst [114, 119, 129-131].

There are numerous characteristics of catalysts that may affect the processing of triglyceride feedstocks discussed in section 2.3.4.1. It will be important to understand the catalyst's effect on producing different types of compounds, including aromatics.

2.3.4.Catalytic conversion of triglyceride feedstocks

Catalysts have been utilised in numerous studies concerning the conversion of triglyceride-based feedstocks. The purpose of using a catalyst may be to improve the yield or selectivity of the preferred product or sometimes both [6]. There are many variations in the definition of a catalyst, but simply it is a substance that changes the kinetics of a reaction but not the thermodynamics. A more detailed example would be a substance that can transform reactants into products via a series of interrupted and repeated steps in which the substance participates but is regenerated and is present in its original form at the end of each cycle throughout its catalyst's lifetime [132].

Prior literature suggests two major and two minor categories of catalysts that are associated with the cracking of edible and inedible triglyceride feedstocks, such as vegetable oils. These include transition metals catalysts and molecular sieve form catalysts, whilst others include activated alumina and sodium carbonate [103].

These catalyst types are explained in further detail in Table 2-8 below:

Table 2-8. A summary of common catalyst types used for the upgrading of pyrolysis oils [103]

Catalyst Type	Overview
Activated Alumina	Different forms of alumina are used to activate (acidic) the catalyst, which exhibits high catalytic activity. The common form, γ -alumina, has been utilised in a variety of studies. Key liquid products included hydrocarbon compounds such as alkenes, alkanes and in some cases, carboxylic acids [47, 103].
Sodium Carbonate	This catalyst has been used in pyrolysis reactions of vegetable oils in addition to pure forms of the fatty acids that these oils contain (i.e., linolenic, linoleic acid, oleic acid, palmitic acid, and stearic acid). In different studies, unsaturated fatty acids produced more aromatic compounds than saturated. Thus, although there is a presence of aromatics in other studies, there are less suggesting some inconsistency. Furthermore, a concern with using this type of catalyst is that the product can be contaminated with sodium[103].
Transition Metals	Widely in the hydro processing industry for the upgrading of heavy oils. The high-pressure conditions and temperature range of 350°C to 450°C give diesel-like fuels. Some studies using this catalyst to process vegetable oils provided products

Catalyst Type	Overview
	rich in alkanes and cycloalkanes but not aromatic compounds[103]. As a primary aim of this project concerns producing fuels with a higher aromatic content, this likely makes this catalyst type unsuitable for this application.
Zeolites	These catalysts can also be referred to as molecular sieve catalysts. The name arises from the size selectivity characteristic of zeolites, a highly desirable property as the pore size can be altered to produce the most desired products. Furthermore, they are also both crystalline and porous. [103]. These primary properties have made zeolite catalysts of great interest in bioenergy applications, especially the conversion of vegetable oils [3, 15]. The popularity of this type of catalyst is demonstrated However, a major issue associated with the catalytic cracking of vegetable oils has been coking. Although there are numerous investigations into how to improve this issue [85].

The four types of catalysts shown in Table 2-8 are all heterogeneous catalysts. The difference between heterogeneous catalysts and homogenous catalysts is in the phases that are present during the reaction. Homogenous catalysts are in the same phase as their reactants and products, which are typically liquids, whereas, for heterogeneous catalysts, they are in different phases. The catalyst is typically solid in these cases, and the reactants and products are either liquids or gases. A benefit of utilising heterogeneous catalysts is that they can be easily separated from the product stream, which is highly desirable for applications in continuous processing. Furthermore, heterogeneous catalysts are typically more resistant to extreme operating conditions than alternative homogenous catalysts [133].

Of these four major types of catalysts and the triglyceride conversion studies presented in Table 2-7, it is apparent that zeolite catalysts are highly prevalent in this area of research. Although transition metal catalysts and activated alumina catalysts may have been utilised in some cases, these do not seem to yield any aromatics. Although there is some evidence to suggest sodium carbonate catalysts may produce small proportions of aromatics, the information in the literature is inconsistent.

Moreover, most recent studies have focused on modifying zeolites catalysts, including ZSM-5 and MCM-41 [134]. In literature, the potential of zeolite catalysts for converting vegetable oils into biofuels is discussed because of their range of diverse properties [8]. Owing to this, the zeolite catalysts used in studies with triglyceride feedstocks, with a particular focus upon ZSM-5, are discussed further in the following sections.

2.3.4.1.Zeolite catalysts and production of aromatics

When it comes to the use of catalysts and zeolites for the conversion of triglyceride feedstocks, multiple examples were provided earlier in Table 2-7. This information has been utilised to provide a more detailed comparison of how different reaction parameters may influence product distribution and yield outcomes in studies utilising zeolite catalysts. The majority of the catalyst presented in Table 2-7 are different forms of ZSM-5, which have proved to be more successful in yielding aromatics than alternative catalysts such as MCM-41, Silicate, Silicate Alumina, Beta and Ultrastable Y [110, 112, 113].

The variation in the pyrolysis temperature between 375 °C and 500 °C, and its effect on aromatics yields via pyrolysis has been reported by Thanh-An Ngo et al. 2010, Sadrameli et al., 2009 and Prasad et al., 1985. Furthermore, Thanh-An Ngo et al., 2010; also considered the implications of the silica-alumina ratio of the HZSM-5 catalyst, which is discussed later in this section. The following graphs in Figure 2.16, Figure 2.17 and Figure 2.18 demonstrate the implications of altering these parameters on outcomes such as aromatics yield (wt.%) and conversion (wt.%). Firstly, considering Sadrameli et al., 2009 whom reported the catalytic pyrolysis of canola oil for the production of renewable aromatics. A canola oil feedstock was processed in a continuous fixed bed micro reactor in the presence of an HZSM-5 catalyst over a temperature range of 375 °C to 500 °C, at atmospheric pressure, with 1.8 h⁻¹ weight hourly space velocity (WHSV) [112]. The trend showing the change in aromatics yield (wt.%) with the temperature is shown below in Figure 2.16

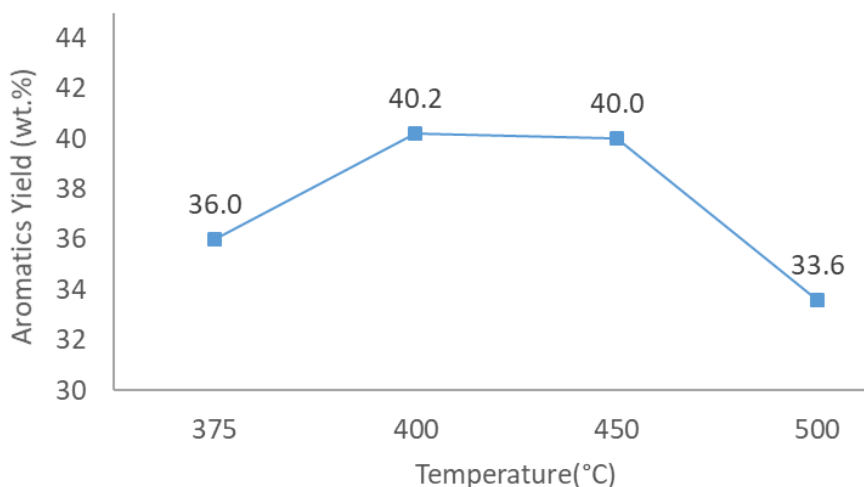


Figure 2.16. Canola oil pyrolysis: Influence of pyrolysis temperature on aromatics yield [112]

The highest aromatics yield was achieved at a temperature of 400 °C was 40.2 wt.%, decreasing significantly to 33.6 wt.% at higher temperatures of 500 °C. It is indicated that this trend is attributed to increased catalytic cracking around 450 °C followed by a reduction due to the catalyst losing effectiveness at the higher temperature of 500 °C [112].

As for the study by Prasad et al. 1985, this considered both the aromatics yield (wt.%) and conversion (wt.%) of the feedstock in relation to the reaction temperature. A fixed bed microreactor, HZSM-5 catalyst and canola oil feedstock within a temperature range of 342 °C to 401 °C. The aromatics yield and conversion of the oil at the temperatures where the WSHV are all similar (~3.8 g oil/ g cat. h) is displayed in the graph Figure 2.17 below.

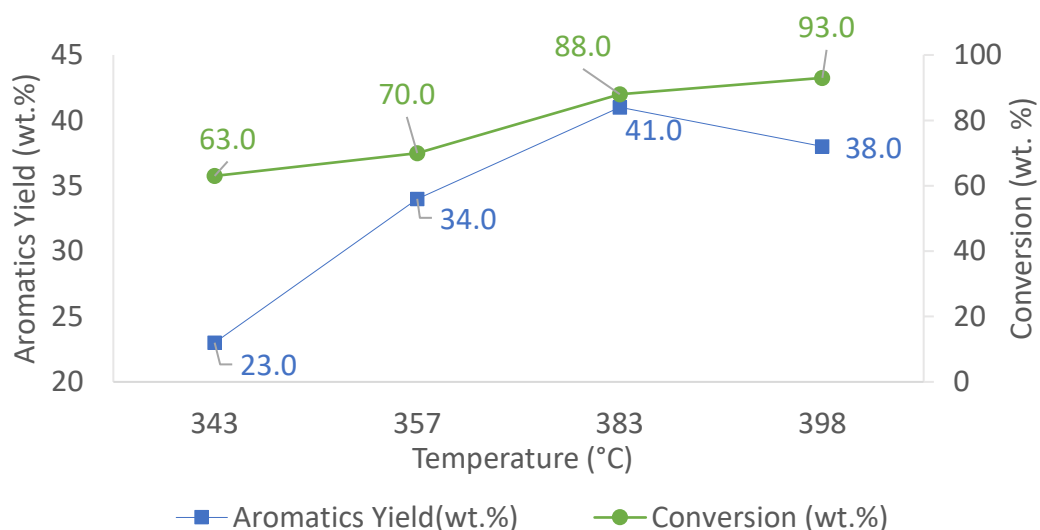


Figure 2.17. Effect of temperature on aromatics yield and conversion in the catalytic processing of canola oil by Prasad et al. 1985 (data from [113])

From work by Prasad et al. 1985 a similar observation to Sadrameli et al.,2009 work can be made with the aromatics yield increasing with temperature up to 383 °C to a value of 41.0 wt. % but then decreasing to 38.0 wt.% as the temperature rises further to 398 °C. However, a different trend is observed in the conversion (wt.%) of the feedstock, with a maximum conversion of 93.0 wt. % achieved at the highest temperature. This could be attributed to the fact that although fewer aromatics are formed at higher temperatures, more cracking reactions are forming other products [113].

The final study to highlight is that by Thanh-An Ngo. This study highlighted the trend between the silica-alumina ratio of the catalyst at different processing temperatures. A soybean oil feedstock was processed in a fixed bed reactor under an inert nitrogen atmosphere. Several investigations were completed with the reactor at 420 °C and 450 °C in the absence of a catalyst and presence of an H-ZSM-5 catalyst with varying silica-alumina ratios of 28, 40 and 180. In Figure 2.18, the effect of both temperature and Si/Al ratio of the HZSM-5 catalyst can be seen on the conversion of the feedstock:

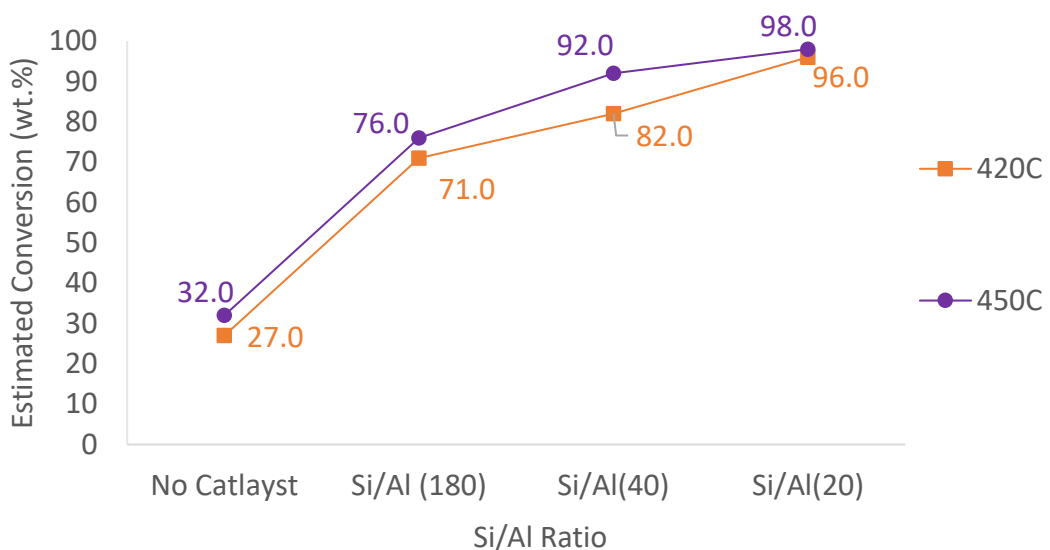


Figure 2.18. A graph to show the effect of Silica Alumina ratio of H-ZSM-5 catalysts and temperature on conversion of soyabean oil feedstock (data from Thanh- An Ngo [110]

It is observed that the conversion is consistently higher at 450 °C, and Thanh-An Ngo also noted that bio-oil and gas yields were simultaneously increasing with the decreasing silica-alumina ratio (Si/Al). This change is attributed to the fact that the lower the Si/Al ratio, the more acidic the catalyst is. A further observation by Thanh-An Ngo was that with the ZSM-5 catalyst, the liquid products were predominantly aromatics. In investigations using the MCM-41 catalyst, significant products included alkanes and alkenes alkadienes, aromatics and some fatty acids[110]. The characteristics of ZSM-5 catalysts such as acidity are discussed further in section 2.3.4.2 alongside a discussion of methods in which this type of catalyst may be prepared or modified to enhance given characteristics.

2.3.4.2. Zeolites and ZSM-5

Zeolites have numerous applications in the industrial processes and environmental pollution fields due to their versatile properties [103]. Some zeolites occur naturally; however, these are often tainted with minerals, metals, quartz, or other zeolites. Therefore, zeolites used in industry for commercial use or research are produced synthetically to ensure the purity and consistency of the material [135]. This also allows for the properties of the zeolite to be optimised for its intended application. Typically, zeolites consist of AlO_4 and SiO_4 three-dimensional tetrahedral units linked by oxygen atoms. This network of tetrahedral units can form channels and cages of different molecular sizes. Within these cages or voids, water molecules and small cations reside which negate the negative charge of the Silica Alumina network.

The graphic Figure 2.19 shows the structure of four zeolites and provides information about the microporous systems and their relevant dimensions [136, 137]:

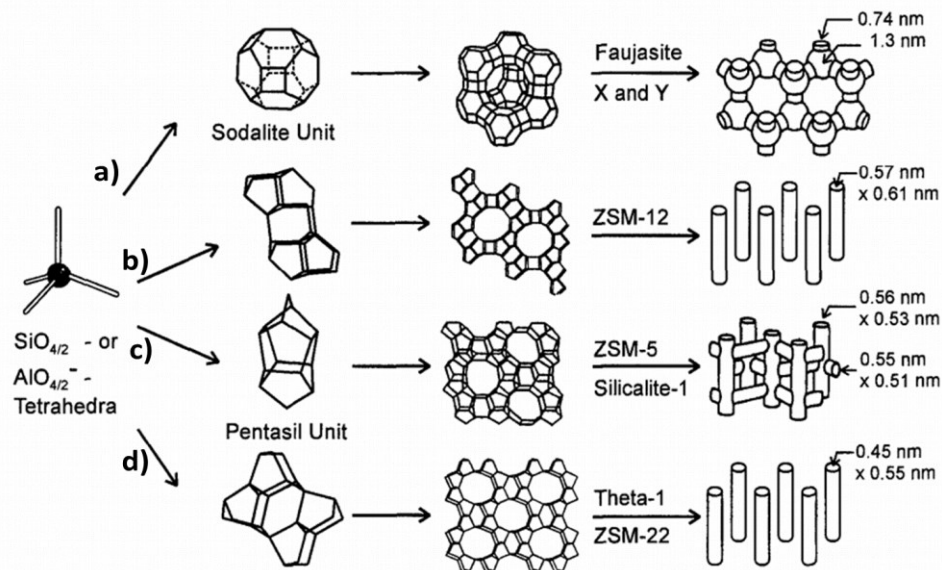


Figure 2.19. Structures of four selected zeolites (a) Faujasite or zeolites X, Y (b) zeolite ZSM-12 (c) zeolite ZSM-5 or silicate-1 d) zeolite theta 1 or ZSM-22 and their microporous systems and dimensions [137]

The zeolite ZSM-5 is a synthetic zeolite widely used in research and industry and is named so owing to its pore diameter of 5 Å. Zeolite catalysts such as ZSM-5 have applications predominantly in catalytic cracking of oil owing to their high thermal stability and microcrystalline structure alongside their ion-exchange capabilities and high adsorption capacity.

The properties of ZSM-5 can be influenced during its synthesis by parameters such as the sources of silica and alumina, template and crystallisation conditions [138]. The most popular methods for synthesising ZSM-5 can fall into one of the following three categories: organic amine and inorganic amine systems, load in systems and hydrothermal or non-hydrothermal systems. Each of these methods utilises different templates, raw materials (i.e., different sources of alumina and silica), but the raw materials are used to form the zeolite structure in a similar way. Each of these methods can alter preparation conditions which in turn alter the properties of the final catalyst [139]. During the synthesis of zeolites like ZSM-5, two of the most significant factors are the ratios of tetra propylammonium ions (TPA^+) and $\text{SiO}_2/\text{Al}_2\text{O}_3$ (or tetraethylammonium ions (TEA^+)). It appears that lower proportions of TPA^+ may result in the formation of large crystallites forming. If the zeolite crystals are larger, then the internal surface area of the catalyst will also be greater. This can increase the total surface area more substantially than having smaller crystallites resulting in higher selectivity to given compounds [140]. This is an example of the zeolite synthesis can affect the crystallinity of a catalyst. The crystallinity of catalysts is typically investigated using techniques such as electron microscopy (EM), either transition electron microscopy (TEM) or scanning electron microscopy (SEM). This can give additional information about the textural properties of the catalyst alongside the use of X-ray diffraction (XRD) studies [140, 141].

Several other characteristics of zeolites like ZSM-5 that are significant include acidity, pore size, surface area, shape selectivity, adsorption capacities and thermal stability. These characteristics have been discussed in more detail to explain how they may influence outcomes such as aromatics yield, conversion and catalyst suitability [135, 142].

The ZSM-5 zeolite catalyst typically has a relatively strong acidity owing to its high silica: alumina ratio [132]. The acidity can affect both the catalysts activity and selectivity because acid sites on the zeolite catalyse the reaction of the biomass feedstock[15, 103]. It is established that within zeolite, the acid sites are commonly Brønsted acid sites; the properties of these sites depend upon the zeolite structure [15, 137, 143]. Alternatively, Lewis acid sites can also be present if the zeolite is exposed to high temperatures as this causes dehydration of the zeolite framework [143].

However, a strong presence of these sites is not preferable as the literature suggests coke is preferably formed on strong Lewis acid sites. This is undesirable as the accumulation of coke can cause catalyst deactivation [3]. Fortunately, zeolites tend to have significantly weaker sites than other catalyst types such as silica-alumina [144].

The presence of these sites can be altered by the Si/Al ratio variation, as low Si/Al ratios are associated with a high density of Brønsted acid sites. Furthermore, the literature noted that zeolites with lower silica-alumina ratios (Si/Al) could yield greater aromatics proportions, as seen in Thanh-An Ngo's study [110]. This is because cracking reactions such as decarbonylation are promoted on more acidic catalysts[15]. Therefore, in selecting an appropriate zeolite catalyst, this influence of a low silica/alumina ration will have to be considered.

Further characteristics of zeolite catalysts include shape selectivity and pore size. It is the differences in the structure of the Silica- alumina network that can influence these factors. One of four categories can describe the pore size of any catalyst. These are presented with examples of the catalysts in this group and an indication of the pore dimensions where possible in the flowchart Figure 2.20 [3, 137, 145]:

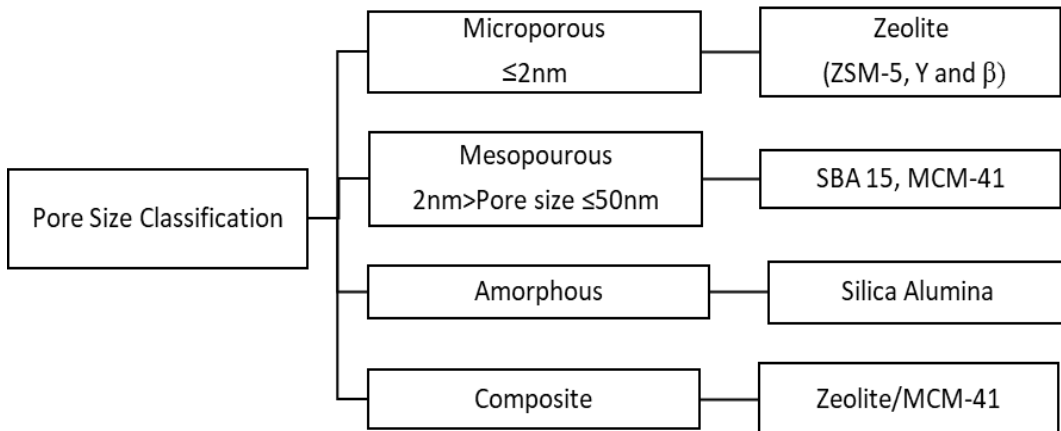


Figure 2.20. A flowchart representing the different pore sizes of catalysts [3, 137, 145]

For the first two categories indicated in the flow chart, it is possible to define the range of sizes for a consistent material easily. However, as for amorphous and composite catalysts, these are a little different. Those defined as amorphous lack consistency in the pore size and are unstructured[144]. As for composite catalysts, these are made of more than one type of material, so that an example could be a mixture of a microporous and mesoporous catalyst.

In terms of application, the small pore dimensions can cause mass transfer limitations if utilising microporous zeolites, resulting in pore blocking and catalyst deactivation. The creation of hierarchical porosity can overcome this undesirable effect. A hierarchical porous zeolite is defined as a zeolite with more than one type of porosity, i.e. two of micro-, meso- or macro[146]. This can enable the catalyst to upgrade larger molecules by allowing further reactions in larger mesopores, potentially improving product yield and distribution[143]. The most utilised process used to achieve this can be either dealumination or desilication. However, a side effect of this process is that it alters the silica-alumina ratio and, therefore, the zeolite's acidity, which may influence the yield of aromatics [15]. Furthermore, the alteration of the pore size will also influence pore volume and, in turn, surface area. This is because the larger the pores, the larger their volume and the larger the overall surface area of the catalyst. Therefore, a catalyst with a larger surface area is preferable as it will have a higher area where catalytic reactions occur. The pore diameter, pore-volume, and catalyst surface area are typically measured using gas physisorption and are typically used alongside other techniques such as electron microscopy to analyse the catalyst further [139].

The pore size of the catalyst can also attribute to another desirable property of zeolites called shape selectivity. The principle of shape selectivity is that the network of pores within the zeolite controls the entry of the reagents' molecules and determines the dimensions of the intermediates and the products[1]. The graphic in Figure 2.21 demonstrates these different types of selectivity.

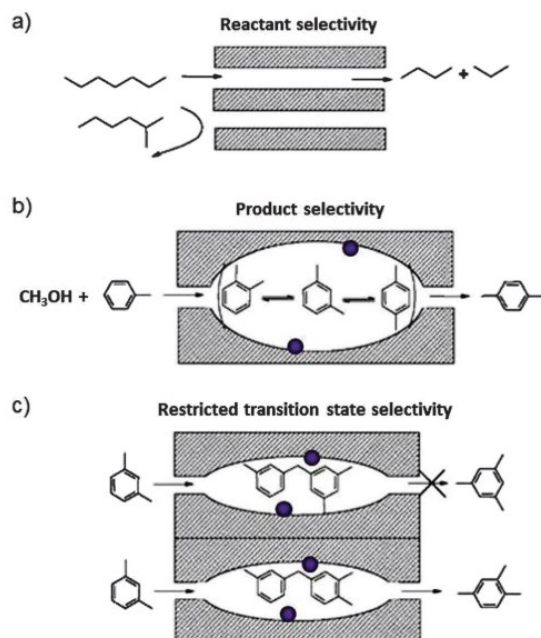


Figure 2.21. A visual representation of the shape selectivity of zeolite catalysts[147]

The bulkier reactant molecules cannot react in the same way as the narrow molecules in reactant selectivity shown by example (a). Only specific shaped reactants can fit into the pores. As for product selectivity, (b) only narrow products can exit the pores of the catalyst. Those that are not narrow enough can, however undergo further reactions. Finally, in restricted transition state selectivity, only the products of certain transition state intermediates will form products, this kind of selectivity can be applied when a certain stereoisomer is desired [1, 147].

This shape selectivity characteristic is the basis for zeolite catalysis application in molecular adsorption. The process is termed molecular sieving and relies upon the zeolite catalyst allowing specific molecules to diffuse through the channels of the catalyst whilst others cannot or do so much slower. An example of this is the purification of xylenes which have 3 different isomers (para-, ortho- and meta). Additional examples of the adsorption or separation capabilities include their use as desiccants, as they can either have a high affinity for water or conversely if hydrophobic zeolites can absorb organic solvents. These properties allow zeolite catalysts to separate molecules based on varying size, shape or polarity[148].

A further characteristic of zeolite catalysts for discussion is thermal stability. The thermal decomposition of a catalyst occurs during different stages. During synthesis, it may be subject to calcination, which is the process of heating the catalyst in air or oxygen[145]. This process removes their adsorbed water from the catalyst. However, if dried too quickly, it can disrupt the uniformity of the catalyst and where a compound has not sufficiently attached itself to the solid catalyst, it can be expelled from the catalyst pores. The use of salts can help avoid this as they give rise to gaseous decomposition products when heated, so do not bubble through the pores of the catalyst material in the same way as liquids. In general, zeolite catalysts, including ZSM-5, are known for their excellent tolerance to heat. Most zeolites can be used in temperatures up to 600°C, although this does decrease slightly with larger pore sizes and a higher aluminium content [132].

However, recent studies considering the conversion of triglycerides have used zeolites like ZSM-5 on their own and used modified zeolites demonstrated by the review provided earlier in Table 2-7. There are several examples where metals have been added to the catalyst. In literature, it is suggested that the addition of metals like these can enhance catalytic activity[109]. Other metals such as Pt, Re, Ga, Zn and Sn have also been utilised in studies considering the processing of triglyceride feedstocks.

In these studies, these metals were suggested to be catalytically active and may increase the proportion of aromatic hydrocarbons[149-151]. The metals Ni and Zn are both of particular significance as the literature suggests that nickel may increase the selectivity of benzene production. Both of these may increase the proportion of aromatic hydrocarbons[152].

In Table 2-7, section 2.3.2 regarding the decomposition of triglycerides, the table reviews several studies looking at the conversion of triglycerides ZSM-5, and other catalysts included the addition of metals such as NiMo, Ga, Al and Cu. In these studies, the aromatics, including BTX and their derivatives, were most abundant in the liquid products when triglycerides were processed using conditions akin to fast pyrolysis in the presence of a catalyst.

For example, in a study by Thanh-An Ngo et al., a soybean oil feedstock was processed in a fixed bed reactor with different catalysts. The key parameters of these studies are reviewed below in Table 2-9:

Table 2-9. Key parameters from fixed bed studies by Than-An Ngo

Catalyst	Major Products	Comment on Bio-oil & Aromatics Yield
ZSM-5 (Si/Al of 28, 40 and 180)	Primarily Aromatics	450 °C, ZSM-5 catalyst (Si/Al = 28). Bio-oil yield of 71.3 wt.% which 54.5% was aromatics including BTX
MCM-41 (2 wt.% Ga, Al, or Cu).	Mixture of alkanes, alkadienes, carboxylic acids and few aromatics	450 °C, Ga/MCM-41 (2 wt.% Ga) Bio-oil yield of 77.3 wt. %, proportion of aromatics not reported

The comparison of these studies highlights the more notable presence of aromatics when the feedstock is processed in the presence of a zeolite ZSM-5 catalyst rather than an MCM-41 catalyst. In addition, the application of ZSM-5 and its higher yield of aromatics compared to other types of catalysts is also observed by other authors including Viswanadham et al. 2014 and Sharma et al. 2014.

Another study with a canola oil feedstock by Prasad et al.,1985, using a ZSM-5 catalyst (Si/Al = ~28) in a fixed bed microreactor. Similarly, high rates of conversion were achieved but at lower temperatures of 370 °C to 375 °C. Within the products, up to 78 wt.% were aromatic hydrocarbons, but the coke yield was higher and in the range of 6-8 wt.%. The coke yield is of concern as a high amount of coke can cause a catalyst to become deactivated, making it ineffective [113].

Viswanadham and Sharma undertook a further two studies with Jatropha oil. Viswanadham et al. 2014 utilised a fixed bed downflow reactor operating at a temperature of 500 °C, and atmospheric pressure to process Jatropha oil. The four catalysts investigated included microcrystalline ZSM-5(MZ), nanocrystalline ZSM-5(NZ), Ultrastable Y (HY) and Beta (BEA). Of these catalysts, the NZ catalyst gave the highest liquid hydrocarbon selectivity of 77.4% in conjunction with the highest aromatics yield of all four catalysts of 45.5 wt.% [43]. Finally, Sharma et al. 2014 conducted investigations with ZSM-5 (Si/Al:35), ZSM-5/SiAl, and NiMo/SiAl catalysts at 375 °C in a batch reactor. The analysis of the liquid products indicated the presence of aromatics was highest with the ZSM-5 catalyst (45.9 wt.%) slightly more than the similar ZSM-5/SiAl catalyst (41.1 wt.%). In contrast, without a catalyst or with the NiMo/SiAl catalyst, the aromatics yields were very low at 1.02 wt.% and 6.0 wt.% respectively. This is of significance, as mentioned earlier in literature by Biswas et al., 2014 that it could potentially be of significance for contributing to the production of aromatics [45].

These catalysts with metal and ZSM-5 zeolite are often referred to as modified ZSM-5 catalysts can be prepared by methods such as ion exchange, solid-state ion-exchange or deposition of soluble or insoluble complexes or impregnation utilising metal salts. For example, the nickel can be deposited into the zeolite cavities; in this way, the desired metal is evenly dispersed on its high surface area support [132]. A summary of these methods, alongside the pros and cons, are discussed below.

When using the ion exchange method, the zeolite catalyst is suspended so that it is in an aqueous state. The solution consists of zeolite and soluble salt, which contains the cation that can transfer the ion, usually under elevated temperatures (90 °C) and stirring as these conditions favour mass transfer. Although this process is not complex, the disadvantages are that sometimes the hydrated cations are too bulky to enter the pores of the zeolite. It can also be problematic if the desired cation is not soluble in water or in its desired valence state.

An alternative process is solid-state ion exchange, where the zeolite is present typically in its H⁺ form and is heated in an inert stream of gas with a desired cation [137].

An alternative method is impregnation which is often applied when dealing with the preparation of multifunctional zeolites where a metal or metallic phase needs to be incorporated into a zeolite catalyst [15].

It is one of the most common and simplest ways to obtain a supported catalyst. The process involves the support being placed in contact with the metallic solution, i.e., nickel hexahydrate for the addition of nickel. The preparation of this solution lends its name to one of two method types: *incipient wetness impregnation* when the volume of water used is not more than the pore volume or *wet impregnation* when an excess of the solution is used. Owing to the simplicity of this method, there are several examples of wet impregnation methodologies throughout literature as reviewed in Table 2-10 below:

Table 2-10. Example conditions used for impregnation of metals in ZSM-5 zeolite catalysts

Impregnation Notes	Drying Conditions	Calcination Conditions	Ref*
Ni (NO ₃) ₂ Solutions with mass fraction ratio of Ni to ZSM of 1, 2, 3 wt. %, mixed for 4 hours at 35°C.	110 °C	4 hours at 550 °C	[153]
Ni (NO ₃) ₂ (ranging from 0.372 g to 1.487 g) mixed with 1 g of distilled water and ZSM-5 zeolite, mixed for 4 hours at ambient temperature	Dried overnight at ambient temperature and 12 hours at 110 °C	4 hours at 400°C in air, 5 hours at 500 °C in H ₂ with heating rate of 2 °C per min ¹	[154]
Ni (NO ₃) ₂ , 0.5 grams dissolved in 25ml water, mixed with 5g ZSM-5 catalyst. Solution stirred at 600rpm for 4 hours at 60 °C	Ambient temperature for 24 hours, 110 °C for 1 hour	6 hours at 600 °C	[138]
Ni (NO ₃) ₂ was dissolved in 5ml of deionised water to give a 10 wt.% Ni/ZSM-5 catalyst. Mixture was sonicated in a water bath at 45 kHz, 80°C for 3 hours.	Left overnight at 120 °C	4 h at 550 °C at a heating rate of 2 °Cmin ⁻¹	[155]
Ni (NO ₃) ₂ , 3.1 g of Ni was added to 100g of ZSM-5 to give 3.1 % Ni/ZSM-5.	3 hours at 110 °C	3 hours at 550 °C, at heating rate of 2 °C min ¹	[156]

*Reference

The resulting catalyst characteristics can depend upon conditions used during drying and calcination, i.e., heating rate, time, final temperature, atmosphere. These factors can affect how the new metal interacts with its support, so ultimately, how it will perform as a catalyst [157]. The resulting materials now possess a combination of Brønsted and Lewis acid sites alongside metallic centres that can interact in reaction systems in different ways to the zeolite catalyst on its own [15].

2.4. Summary and research objectives

From the review of varied literature sources, there are apparent gaps in the research considering the conversion of triglyceride feedstocks to higher-value chemicals, including aromatics. Though there is evidence from differing catalytic pyrolysis studies that ZSM-5 catalysts can improve yields of aromatics. Although nickel can improve aromatics yield, it does not appear to have been used with ZSM-5 alone but typically in the form of NiMo (nickel-molybdenum).

Furthermore, when it comes to the pyrolysis of triglycerides, there seemed to be no evidence of this in continuous fluidised bed systems but instead more commonly batch tubular and fixed bed reactors. Therefore, this work will address these issues by following the goals and objectives as defined in Chapter 1.0, section 1.2.

CHAPTER 3.0 EXPERIMENTAL METHODOLOGY

3.1. Introduction

In this research work, studies were undertaken in two main pyrolysis reaction systems, including a Pyroprobe 5200 pyrolyzer (CDS Analytical- <0.5 mg per sample) covered in section 3.2 and a bench-scale fast fluidised bed reactor (90 gh^{-1}) covered in section 3.3. These systems allowed to carry out experiments looking at both thermal and catalytic decomposition behaviour of selected feedstocks. Chapter 3.0 describes the materials and methods used to conduct the experimental work.

3.2. Pyroprobe Experiments

3.2.1. Materials and Catalyst Preparation for Pyroprobe Experiments

The materials sourced for the pyrolysis tests and preparation of the catalysts are discussed below. The feedstocks oleic acid and jatropha oil were used. The description of the ZSM-5 catalyst, the materials used in the preparation of the Ni/ZSM-5 catalysts (1 wt.%, 2wt.% ,5 wt.% and 1 wt.% Nickel), alongside additional materials used in for the analysis of liquid, solid, and gas products are also included in this section.

As highlighted in Chapter 2.0, section 2.1.3.3., on average 46 wt.% of Jatropha oil is the fatty acid compound oleic acid; second only to linoleic acid and palmitic acid which contribute 31.2 wt.% and 10.33 wt.%, respectively. Oleic acid was utilised in this work as a model compound, as it is the primary fatty acid found within jatropha oil. The purpose of this was to provide a less complex view and better understanding of the decomposition pathways of this major component into other potential products and serve in this way as a guideline for further jatropha oil examinations.

For the Pyroprobe 5000 pyrolyzer (CDS analytical) experiments, oleic acid from Alfa Aesar™ (99 % purity) was used. The jatropha oil feedstock, utilised in both the Pyroprobe 5000 pyrolzer and bench-scale fluidised bed reactor systems, was obtained from Matrix Biofuels Ltd., United Kingdom (2018). The oil was kept in a glass-sealed container and stored in a dry and cool cabinet.

As for the catalyst in this work, zeolite ZSM-5 ammonium (Si/Al 30, Alfa Aesar™) was utilised. The ZSM-5 catalyst was prepared for investigations by calcination at $500\text{ }^{\circ}\text{C}$ for 5 h under air atmosphere in a Carbolite furnace (of $5\text{ }^{\circ}\text{C min}^{-1}$ heating rate).

The same ZSM-5 catalyst was also modified by adding Nickel (II) Nitrate Hexahydrate ($\text{Ni}(\text{NO}_3)_2 \cdot 6\text{H}_2\text{O}$; Alfa Aesar™ Puratronic ®, 99.99 % purity). The series of modified nickel/ZSM-5 zeolites (Ni/ZSM-5) were prepared by the incipient wetness impregnation method to attain different nickel loadings of 1 wt.%, 2 wt.%, 5 wt.%, and 10 wt.%. This methodology was used as it is a simple and known method used for the preparation of multifunctional zeolites where a metal or metallic phase needs to be incorporated into a zeolite catalyst [15]. A variety of methods for the preparation of metallic-zeolite catalysts are available in literature i.e., Weikun Yao et al., Darui Wang et al., Widayat et al., Osman Ahmed et al. and Matthew Yung et al. The conditions used and reported in these methods were utilised to define the conditions and steps utilised in the preparation of catalyst in this work [153-156, 158].

The incipient wetness impregnation method involved mixing equal amounts of ZSM-5 zeolite and distilled water in a beaker with the appropriate amount of Nickel (II) Nitrate Hexahydrate ($\text{Ni}(\text{NO}_3)_2 \cdot 6\text{H}_2\text{O}$). The mixture was stirred using a magnetic stirrer at room temperature for 4 hours. The resulting solutions were left to air dry overnight after which they were placed in a drying oven at 110 °C for a period of 3 hours, in an air atmosphere. The Ni/ZSM-5 mixtures were all calcined in a Carbolite furnace at 500 °C for 5 h under air atmosphere, with a heating rate of 5 °Cmin⁻¹. The resulting catalysts were assigned as 1Ni/ZSM5, 2Ni/ZSM5, 5Ni/ZSM5, 10Ni/ZSM5, for the nickel loadings 1 wt.%, 2 wt.%, 5 wt.% and 10 wt.% respectively. All the catalysts were crushed and sieved to ensure a degree of uniformity and to obtain fine particles sizes between 25 µm and 53 µm. Before the catalytic pyrolysis tests, the catalysts were left to equilibrate with the atmosphere for a period of 12 hours, and their moisture content was determined via thermogravimetric analysis as described in section 3.3.2.1. The prepared catalysts were characterised via use of Thermogravimetric analysis, N₂ porosimetry and X-ray diffraction in order to ascertain their moisture content, surface area, pore volume, pore diameter and consider the catalyst surface structure.

3.2.2. Pyroprobe Experiment Methodology

Pyroprobe GM-MS (Py-GC-MS) systems are widely utilised within research relating to pyrolysis studies. In section 2.2.3.1 it was discussed that these systems have several advantages due including shorter times for analysis, sample preparation and reduced times for analysis to name a few[100]. The technique of Py-GC-MS differs from GC-MS itself as the method and way in which the sample is analysed in the two systems are different as with Py-GC-MS only a very small sample typically less than a milligram is analysed. For Py-GC-MS analysis the sample is heated in a quartz tube which is heated to a pre-set temperature for a given time period. This rapid heating causes the decomposition of the sample with the product containing a mixture of compounds then carried to the GC-MS system[159]. An example schematic of a typical Py-GC-MS system is shown in **Error! Reference source not found.** below.

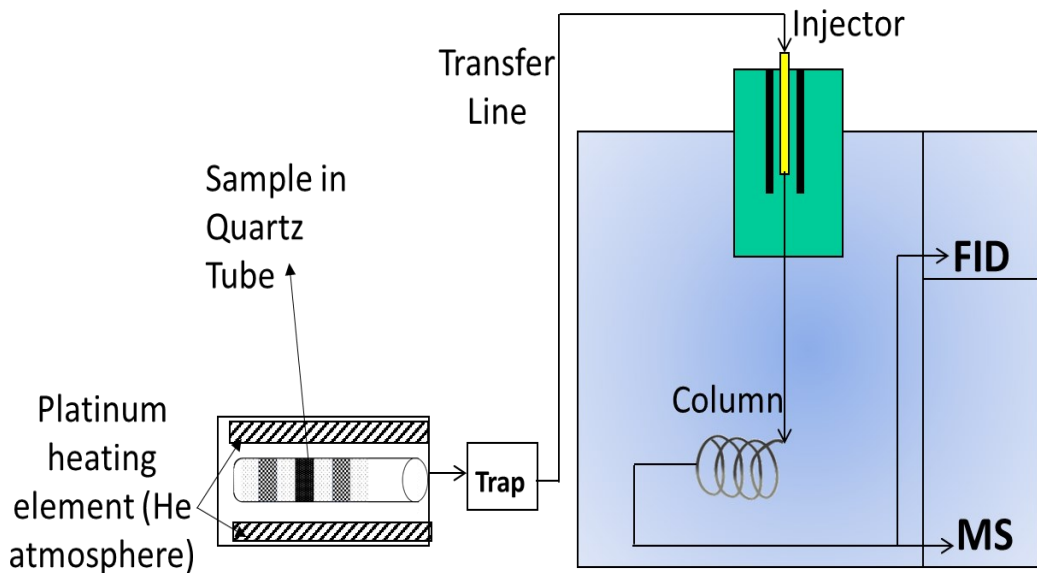


Figure 3-1. Schematic of a Pyroprobe GC-MS (Not to Scale)

A Pyroprobe 5000 pyrolyzer (CDS Analytical) was used to carry out small-scale fast pyrolysis experiments using two different feedstock samples: oleic acid and jatropha oil. A picture of the equipment used is shown below in **Error! Reference source not found..**



Figure 3-2. Pyroprobe 5000 pyrolyzer (CDS Analytical) system

The method of fast pyrolysis was selected on the basis that the desirable aromatic compounds are most prevalent in the liquid products. The samples were contained within open-ended quartz tubes (~2 mm diameter, 20 mm length), the tubes were loaded with 0.5 mg of feedstock and an appropriate mass of catalyst to maintain a catalyst to feed ratio close to 3:1, whilst accounting for the catalyst's moisture content. The catalyst amount was equally distributed on the two sides of the quartz tube. In non-catalytic runs, where no catalyst was used, the sample mass was reduced to 0.1 mg in order to avoid flooding the system with large amounts of unreacted oil. The layers of catalyst and samples were separated by small plugs of quartz wool to ensure that it was only oil vapours upon heating that came into contact with the catalyst bed. A schematic of a sample tube is shown in **Error! Reference source not found..**

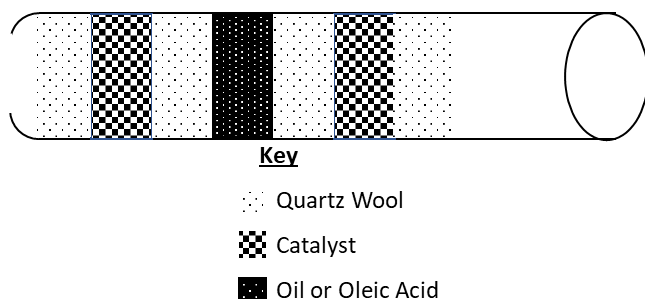


Figure 3-3. Cross section of Py-GC-MS quartz tube

All samples were pyrolyzed using a CDS 5200 pyrolyzer close-coupled to a PerkinElmer Clarus 680 gas chromatograph (GC) and Clarus 600S mass spectrometer (MS) with a flame ionization detector (FID) at a pyrolysis temperature of either 400 °C, 500 °C or 600 °C (20 °Cms⁻¹ heating rate, 30 s hold time). The compounds were immediately trapped on cold Tenax®-TA adsorbent trap (to avoid any additional secondary reactions) and the trap was then heated up to 350 °C with the pyrolysis products then transferred on to the GC column via a heated transfer line (300 °C) using an inert helium carrier gas (20 mLmin⁻¹). The pyrolysis products were separated using a 30 m Elite-1701 capillary separation column at a temperature of 350 °C, with the GC injection port kept at a temperature of 275 °C with a 1:125 split ratio. The FID detector was held at 275 °C with hydrogen–air combustion mixture (with constant flows of 45 mLmin⁻¹ and 450 mLmin⁻¹ for hydrogen and air respectively).

The chromatogram analysis was completed using OpenChrom data analysis system (2008) by LABLICATE peak efficiency in conjunction with the NIST11 mass spectra library(version 2.0) to identify compounds in the pyrolysis vapours using a match factor of 70% or higher. All the pyroprobe tests were completed in duplicate to ensure a degree of repeatability. As the chromatograms obtained were almost identical and there were no significant disagreements or anomalies completing duplicates catalytic investigations discussed in Chapter 5.0 were prioritised. The peak area values were then normalised to their weight as peak area per milligram of feedstock using Microsoft Excel, using several macro-enabled excel files created by Dr Stylianos Stefanidis. Therefore, any slight variations between the weight of feedstock used in each sample should not affect the overall results. This normalisation is apparent in the chromatogram presented throughout this work as the relative abundance is indicated as peak area per mg of feedstock. Some peaks remained unidentified due to a low match factor or were dismissed as they were deemed to be unfeasible compounds, e.g., chlorine or sulphur containing compounds.

3.2.3. Catalyst Characterisation

3.2.3.1.Thermogravimetric analysis (TGA)

TGA is a quantitative technique able to analyse small sample amounts, typically in the region of 1 mg to several grams. It utilises a furnace that can increase the temperature up to 1600 °C in a stable or changing flow of a desired carrier gas. This technique helps to derive the conversions, kinetics or mechanisms that occur when a change of mass is involved due to an increase in temperature. For example, in a reactive environment such as oxygen, the mass of the sample may increase as is the case with transition metals, but in an inert environment a sample containing a high proportion of volatiles when heated will decrease in mass[160]. This technique is useful as it can help to determine the moisture content in catalysts or solid content such as char in reacted solids.

A thermogravimetric analyser operates by utilising a precision micro balance connected to a sample pan which is contained within the furnace and connected to a temperature programmer and controller- thermo-balance. The starting weight of the sample is inputted into a programme interface at the start of the analyses and the micro balance determines any fluctuations in the mass of the sample throughout the desired temperature programme [160].

In this work, TGA analyses were carried out in a Mettler Toledo TGA/DSC 2 STA system using nitrogen as an inert atmosphere with a flow rate of 40 mLmin⁻¹ as shown in **Error! Reference source not found.** below.



Figure 3-4. Mettler Toledo TGA/DSC 2 STA system

Fresh and calcined catalyst samples as well as silica sand from the fluidised bed reactor was analysed. Prior to analysis, the catalyst samples were removed from

a desiccator and left open to the air 12 hours before analysis to equilibrate to room conditions. About 8 mg of fresh catalyst sample was placed in an alumina crucible (70 μL) and heated under air atmosphere from 25 °C up to 300 °C with 10 °C min⁻¹ heating rate and held for 30 minutes. The decreasing mass from room temperature to 300 °C was assumed to be the loss of water and therefore the moisture content of the catalyst [160]. After this, the temperature was further increased up to 700 °C at the same heating rate.

3.2.3.2. X-ray Diffraction (XRD)

XRD is a non-destructive technique used for the analysis of crystalline materials and heterogeneous catalysts including zeolites and metal oxides. XRD can provide information about the materials in terms of their structure, present phases, crystal orientations or texture alongside other structural parameters such as grain size and crystallinity. All these parameters are important to understand any structural changes after subjecting the catalyst to pyrolysis conditions [161, 162].

XRD relies upon the constructive interference of monochromatic x-rays and a crystalline material. The X-rays are created by a cathode ray tube, from which they are filtered producing a monochromatic source which is collimated to concentrate and direct them at the sample material. The interaction of these X-rays with the sample generates constructive interference and diffracted rays. These diffracted rays form the diffraction pattern with each reflection associated with a plane within a material, at a given angular position (θ), at a certain interplanar spacing at a given X-ray wavelength (λ). This can be represented visually by the schematic in **Error! Reference source not found.**:

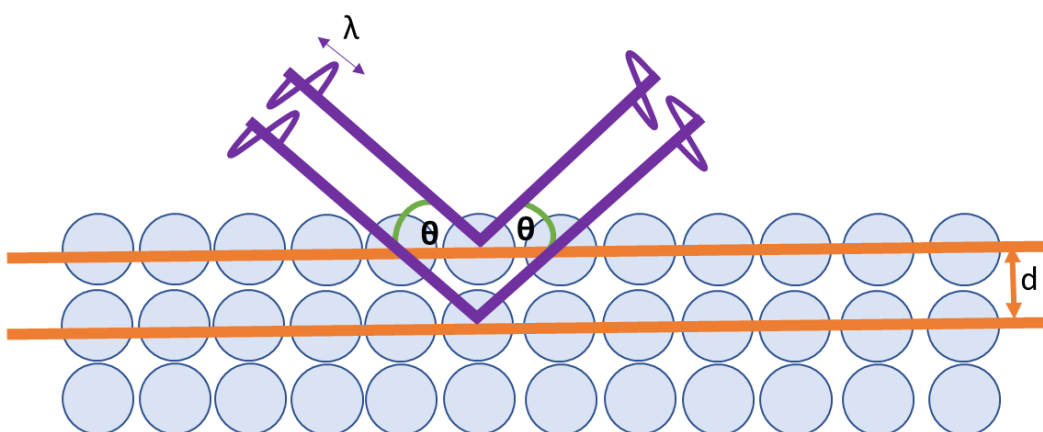


Figure 3-5. Schematic of X-ray diffraction

These parameters can be defined by Bragg's Law as shown in **Error! Reference source not found.** below, where n is an integer that denotes the order of reflection [161, 162].

Equation 3-1. Bragg's law

$$n\lambda = 2dsin\theta$$

This law relates the wavelength of the X-rays to both the diffraction angle and lattice spacing within the material. In order to ensure that the X-rays are monochromatic, the source can be filtered via the use of foils or a crystal monochromator with copper being the most common materials for single-crystal diffraction using CuK_α radiation with other metals such as Fe, Mo, and Cr also available. When these X-rays are collimated onto a sample and the sample and a detector are rotated, the detector records the intensity and processes the signal into a count rate. This signal can output to a computer program to form the diffraction pattern of any given material which can be analysed using the system database for observation and comparison[161, 162].

In this work, fresh samples of the catalyst used for the pyrolysis tests were analysed using a Bruker D8 Advance diffractometer in the Bragg Brentano mode.

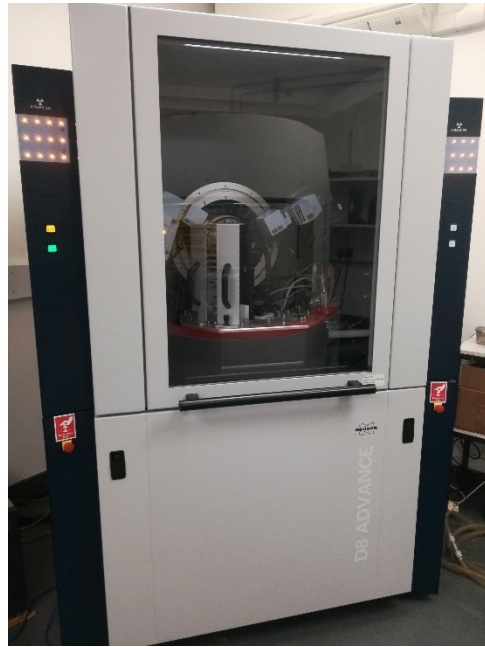


Figure 3-6. Bruker D8 advance diffractometer

For the analysis the diffractometer used a LYNXEYE PSD detector and a Cu K_{α1,2} radiation source operated at 40 kV and 40 mA. In order to ensure the X-ray source was as monochromatic as possible a 0.02mm Ni foil K_β filter was applied. The XRD scan was conducted between 10–80 ° 2θ range with step scans of

0.02 ° at 1 second per step. For analysis of the XRD patterns were analysed using the DIFFRAC.EVA 3.0 software by Bruker. As well as viewing the XRD patterns the software also allowed identification, comparison and determination of given peaks attributed to Nickel and their suggested crystallite size.

3.2.3.3.Brunauer–Emmett–Teller and Barret-Joyner-Halenda Analysis

The Brunauer-Emmett-Teller (BET) and Barret-Joyner-Halenda (BJH) analyses are common approaches used to assess the performance of materials including catalysts, as their performance depends on certain morphological characteristics. The application of these methods using gas adsorption allows quantification of parameters such as specific surface area, pore size (d_{pore}) and pore volume of given materials. The classification of pore sizes can fall into one of several categories, where those with $d_{pore} < 2$ nm are classified as micropores, between 2 nm and 50 nm mesopores and then macropores are where $d_{pore} > 50$ nm [163].

The BET method is based upon the amount of gas that is required to cover the external and internal surfaces of a solid with a single complete monolayer. The measurements are conducted by injecting nitrogen into a sample holder in successive steps at which the pressure is measured. The partial pressure is monitored typically over the range of 0 to 0.995 with the surface area being calculated using **Error! Reference source not found.** below[164]:

Equation 3-2. BET specific surface area

$$A_s = \frac{V_M}{V_m M_{sample}} S_{adsorbate} N_A$$

Where A_s (m^2/g) is the specific surface area of the solid, V_M (cm^3) is the volume of the adsorbed gas layer, $S_{Adsorbate}$ (m^2) is the area of the efficient section per adsorbate molecule, V_m is the volume of a molecular gram ($22414\ cm^3\ mol^{-1}$ at $P=1$ and $T=25\ ^\circ C$), M_{sample} (g) is the mass of the sample after degassing and N_A is the Avogadro's constant ($6.022 \times 10^{23}\ atoms\ mol^{-1}$)[164].

As for BJH analysis this method used for the calculate mesopore size distributions which is where pore sizes are less than 2 nm[165]. This method obtains the pore size distribution by calculating the nitrogen adsorption amount then the relative pressure is 0.99 using the following formula[166]:

Equation 3-3. BJH pore size

$$V_{pm} = \left(\frac{r_{pm}}{r_{kn} + \Delta t_n} \right)^2 (\Delta V_n - \Delta t_n \sum_{j=1}^{n-1} A_{cj})$$

Where V_{pm} is the pore volume, r_{pm} is the maximum pore radius, r_{kn} is the capillary radius, V_n is the capillary volume, t_n is the adsorbed nitrogen layer thickness and A_{cj} is the area after the emptying of the gas[166].

A Quantachrome NOVA 2200e series apparatus was used to determine the specific surface area and pore volume of fresh ZSM-5 and Ni-ZSM-5 catalysts (1 wt.%, 2 wt.%, 5 wt.% and 10 wt.%). Before sorption analysis the catalyst samples (~25 mg to ~40 mg) were degassed at a temperature of 120 °C overnight for a minimum of 12 hours. The instrument software used the BET method for calculation of the specific surface area and BJH method for the determination of the pore volume and diameter using **Error! Reference source not found.** and **Error! Reference source not found.** mentioned earlier.



Figure 3-7. Quantachrome NOVA 2200e series equipment

3.3. Fluidised Bed Reactor Experiments

The utilisation of fluidised bed systems for the processing of liquid triglyceride feedstock is not prevalent across existing literature as discussed in Chapter 2.0, section 2.2.3. Furthermore, it was identified that aromatic products including BTX which are a target product in this work were typically contained within the bio-oil product from varied conversion processes. It is known that fluidised bed reactors typically favour liquid products, therefore, the utilisation of such a system within this work is of novelty.

The concept of fluidised bed systems is well established with the earliest systems being utilised in the coal industry in the 1920's. The distinct advantages of fluidised bed systems are that they have superior heat transfer compared to other reactor types, move solids like a fluid and are able to process varied types of materials. Furthermore, for catalytic fluidised bed reactors fresh catalyst can be added without the requirement to shut down the reactor, with flexibility to have reactors couple together for the cycling of catalyst material so that it can easily be regenerated. The principle behind fluidised bed systems is that a bed material of a given particle size will fluidise when an upward flowing gas imparts a greater drag force that overcomes that of gravity. The point at which particles first become fluidised is known as the minimum fluidisation velocity and can be estimated by first calculating the Archimedes number as shown below in Equation 3-4:

Equation 3-4. Archimedes number for estimation of minimum fluidisation velocity[167]

$$Ar = \frac{\rho_g d_p^3 (\rho_p - \rho_g) g}{\mu^2}$$

Where Ar is the Archimedes number, ρ_g is the gas density, d_p is the Sauter mean particle size, ρ_p is the particle density, g is acceleration due to gravity and μ is the fluid viscosity. The Archimedes number can then be utilised in the well-established correlation by Wen and Yu, which also requires the calculation of the Reynolds number at minimum fluidisation velocity. The value for minimum fluidisation velocity is obtained by the rearrangement of Equation 3-5 and Equation 3-6 as defined below:

Equation 3-5. Wen and Yu correlation for minimum fluidisation[167]

$$Ar = 1,650 Re_{p,mf} + 24.5 Re_{p,mf}^2$$

Equation 3-6. Reynolds number at minimum fluidisation[167]

$$Re_{p,mf} = \frac{\rho_g u_{mf} d_p}{\mu}$$

Where $Re_{p,mf}$ is the Reynolds number at minimum fluidisation velocity and u_{mf} is the minimum fluidisation velocity. This minimum fluidisation velocity can be

influenced by many parameters but one of major significance is the bed material. This is typically a solid material such as silica sand which has a high thermal capacity. This allows for increased heat transfer to the feedstock and is also inert. A larger sand particle size will result in a higher minimum fluidization velocity. Furthermore, the velocity of the fluidising gas referred to as the carrier gas should be larger than the minimum fluidization velocity. This is to ensure that the mixing of the feedstock and material is maximised. On the other hand, if the carrier gas velocity is too high then sand can be entrained downstream and into the condensing system, which can be resolved by reducing the flow rate [168]. In this work the fast pyrolysis experiments were conducted within a continuous fluidised bed fast pyrolysis system situated in EBRI, Aston University. An early photograph of the system before some of the changes is shown in Figure 3-8. In addition, an initial and final process flow diagram (PFD) is shown in Figure 3-9 and Figure 3-10 reflecting all the changes and improvements after the reactor recommissioning.

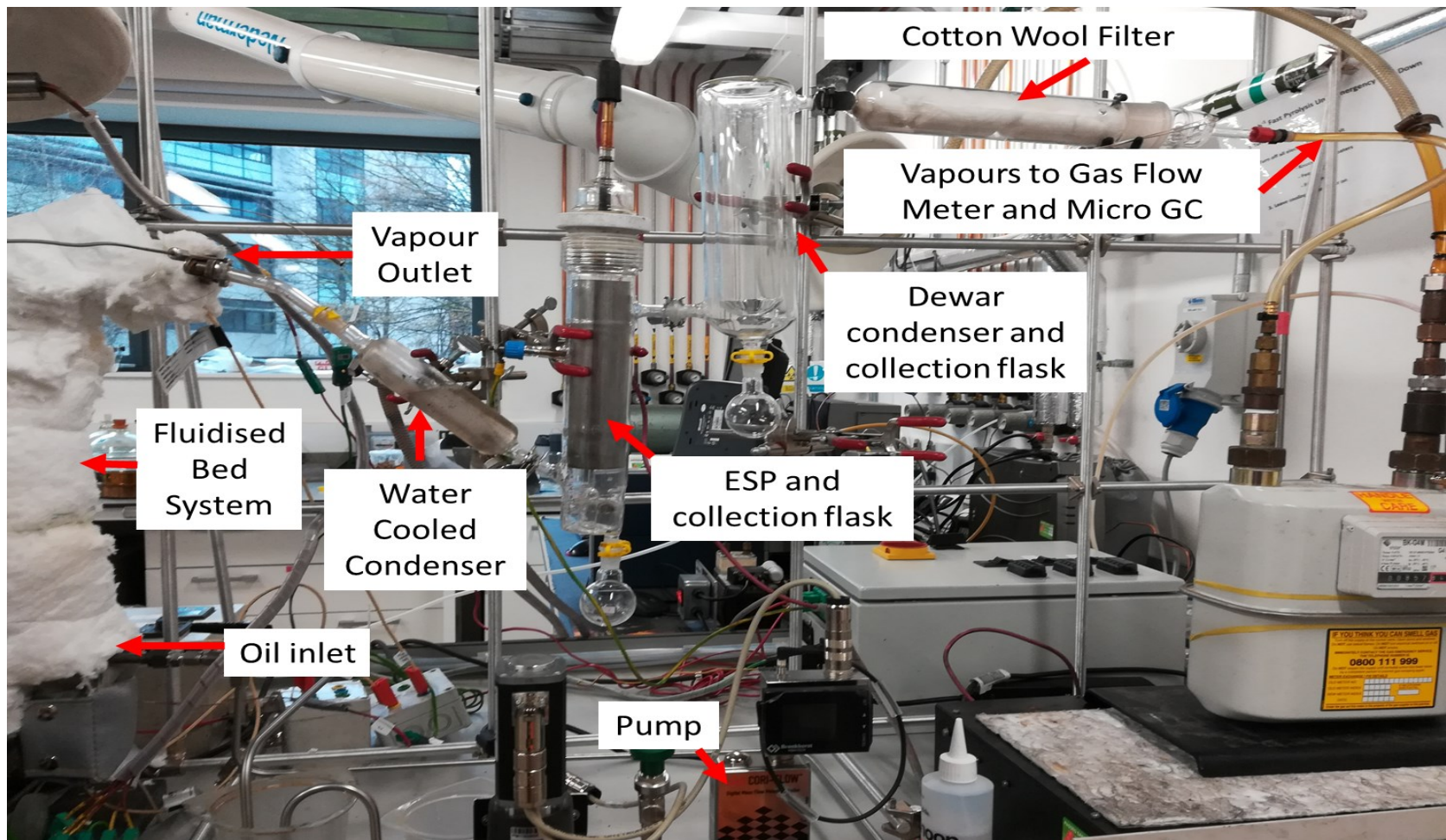
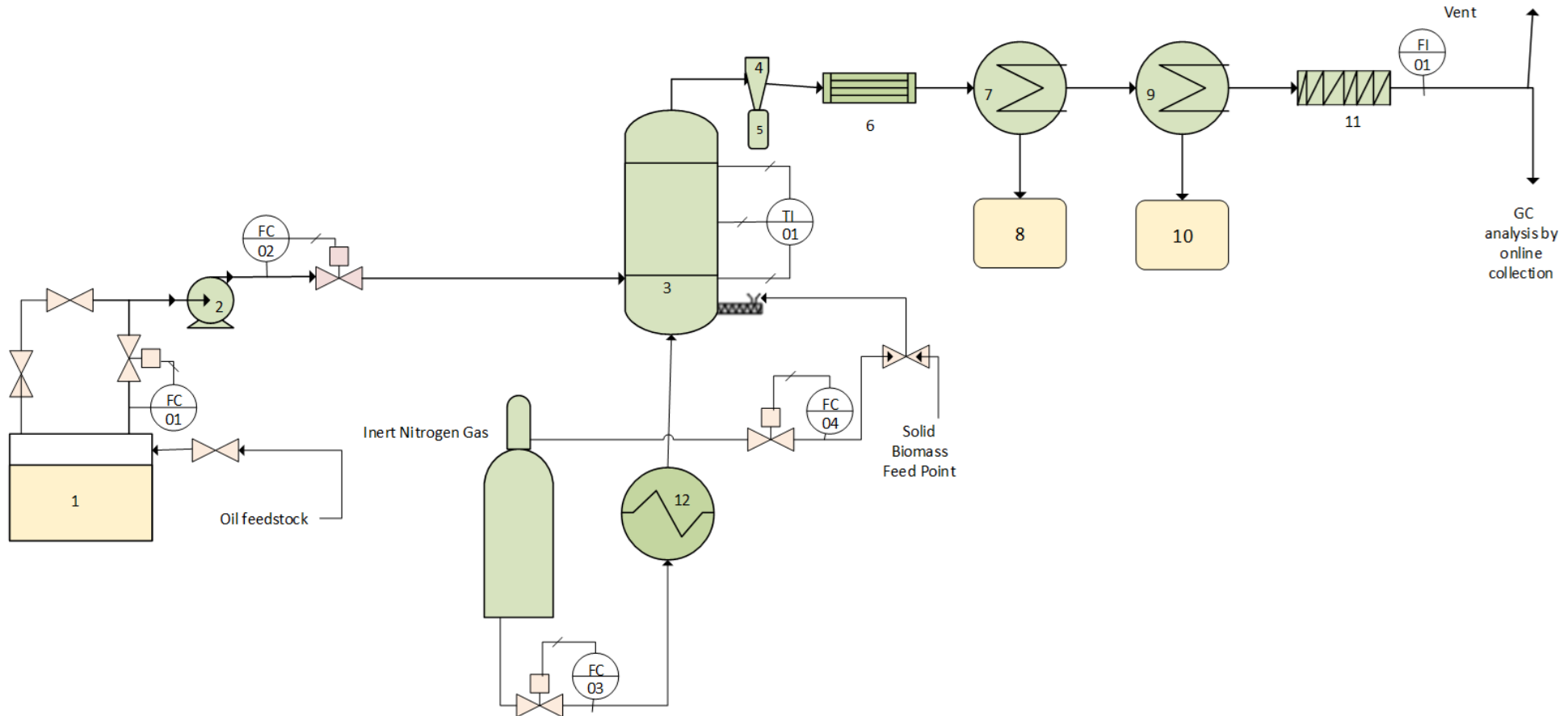
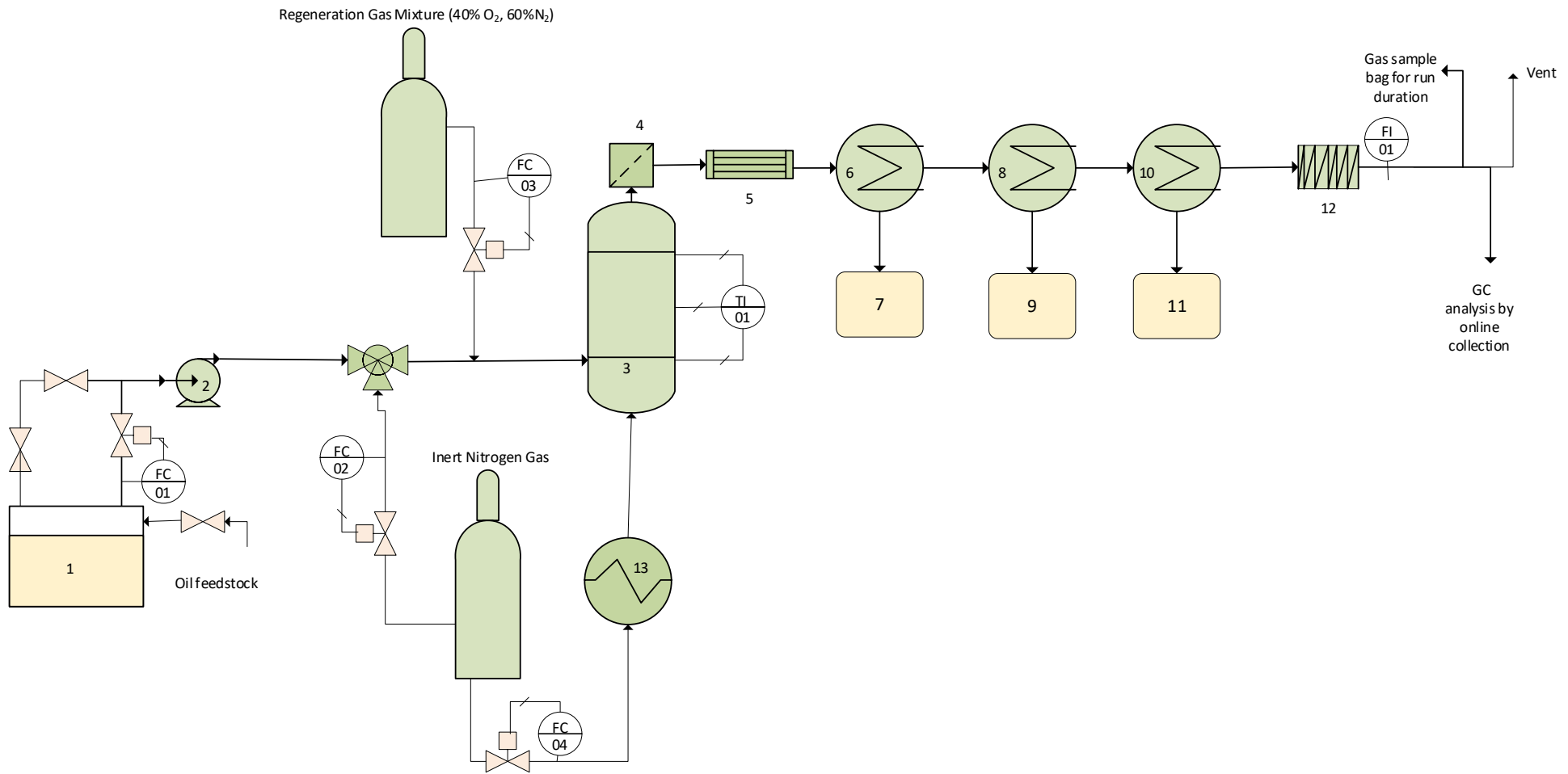


Figure 3-8. Descriptive photo of fast fluidised bed system



Item key: (1) Vegetable Oil Feedstock (2) Feed Pump to Reactor Inlet (3) Fluidised Bed Reactor (4) Cyclone (5) Char Pot (6) Water cooled condenser (7) Electrostatic Precipitator (8) Liquid Bio-oil collection 1 (9) Dewhal Dry Ice Condenser (10) Liquid Bio-oil collection 2 (11) Cotton Wool Filter (12) Fluidising Nitrogen Preheater

Figure 3-9. Process flow diagram fast fluidised bed reactor system process flow diagram initial set up



Item key: (1) Vegetable Oil Feedstock (2) Feed Pump to Reactor Inlet (3) Fluidised Bed Reactor (4) Filter (5) Water cooled condenser (6) Electrostatic Precipitator (7) Liquid Bio-oil collection point 1 (8) Dry Ice Condenser 1 (9) Liquid Bio-oil collection point 2 (10) Dry Ice Condenser 2 (11) Liquid Bio-oil collection point 3 (12) Cotton Wool Filter (13) Fluidising Nitrogen Preheater

Figure 3-10. Process flow diagram fluidised bed fast pyrolysis reactor system- final

The system consists of three major sections; feeding system, fluidised bed reactor and condensing train, which shall be described in turn in the following paragraphs:

The feeding system uses jatropha oil at a rate of 90 g h⁻¹ utilising a positive displacement pump (Tuthill) alongside a digital flow mass controller (Bronkhurst). The system uses a three-way-valve (ref to PFD) in a re-cycle loop to ensure that the feed is at a constant rate before entering the reactor. To ensure that the atmosphere within the reactor remained inert, a feed of nitrogen gas at a rate of 2 L min⁻¹ is mixed with the oil before it enters the fluidised bed system.

The fluidised bed system is a stainless-steel cylindrical reactor (height 35.1cm, diameter 6.69 cm) with two inlets and 1 outlet. The first inlet for the feed and second for the inert gas that fluidises the bed material, which is 300 g of silica sand (250-355 µm). The fluidizing gas enters at a rate of 8 L min⁻¹ and is preheated to 500 °C. The singular reaction vapours outlet allows the exit of reaction vapours and is fitted with a 5 µm filter to prevent deposition of solid particulates or entrainment of sand in the downstream condensing train. The temperature of the system is achieved via the use of a centrally placed electric furnace with heating tapes (Omega™ -STH051-040 (bottom) & STH101-040 (top)) to ensure even temperature distribution across the length of the reactor. These are controlled using Tempotron DTC410 Series temperature controllers. The system can operate up to a temperature of 520 °C, whilst under atmospheric pressure. In order to reduce heat lost to surroundings and maintain a uniform reactor temperature the external surfaces of the reactor are insulated. The main body of the reactor uses a ceramic fibre jacket, whilst the base, fluidising gas inlet and reaction vapours outlet are covered with ceramic fibre blanket and foil tape. The internal reactor temperature is monitored using 3 K-type thermocouples located vertically at even intervals within the fluidised bed. They are connected to an Omega RDXL4SD thermocouple reader for data collection using an integral SD card. As for the system pressure this is monitored, so that both leaks and blockages in the system can be detected.

The condensing train begins after a short transition pipe where the reaction vapours exit at the top of the reactor. The reaction vapours enter a water-ethylene glycol cooled condenser using Honeywell™ Ethylene Glycol (technical grade) and a Huber minichiller operating at a set point of -4 °C. This begins to cause condensation of the reaction gas vapours, which then flow into the Electrostatic Precipitator (ESP). From the ESP the vapours pass through two consecutive Dewar condensers with collection flasks. The condensers are filled with acetone in

addition to dry ice. Finally, any remaining vapours, were passed through a cotton wool filter before entering an Elster BK-G4M gas flow meter.

3.3.1. Reactor Re-Commissioning

The recommissioning of the reactor was required as it was using a feedstock different to that it was designed for. This involved conducting multiple runs to resolve issues as they arose during use. The issues along with the actions taken to prevent them in future experimental runs are summarised below. In total, eight runs were undertaken using the fluidised bed reactor and of these 3 were completed without major issues which allowed the collection of liquid products for analysis, as well as the completion of a mass balance. The issues encountered required correction to ensure that the equipment would operate reliably and accurately. The major issues rectified included:

- Glassware placement; prevent air bubbles in the water-cooled condenser and the ESP from shorting
- Overheating glassware; optimize settings of chiller and addition of glycol to chiller water (1:4) to achieve lower temperatures ($<0\text{ }^{\circ}\text{C}$)
- Liquid product collection: addition of secondary Dewar condenser to prevent condensation of products further downstream
- Entrainment of sand; addition of filter and sieving of sand to prevent the entrainment of fine sand particles downstream.
- Consistent heating: maintenance of reactor thermocouples to ensure reliable heat up and extra insulation to reduce heat loss to surroundings
- Nitrogen feed: addition of a nitrogen feed at reactor oil inlet to help prevent agglomeration of the sand
- Oil feed system: addition of pump and piping
- Regeneration of fluidised bed material; addition of a gas line containing an oxidising mixture (40% oxygen, 60% nitrogen) to regenerate fluidised bed without dismantling the whole reactor.

This meant that several alterations were required to be able to effectively utilise the system. These key stages and changes made to the system are highlighted in the photographic reactor commissioning steps timeline on the following page in Figure 3-11 and Figure 3-12 respectively. Figure 3-11 shows the major steps in reassembly, whilst Figure 3-12 shows the improvement and modifications for its use as a fluidised bed reactor for the processing of liquids.

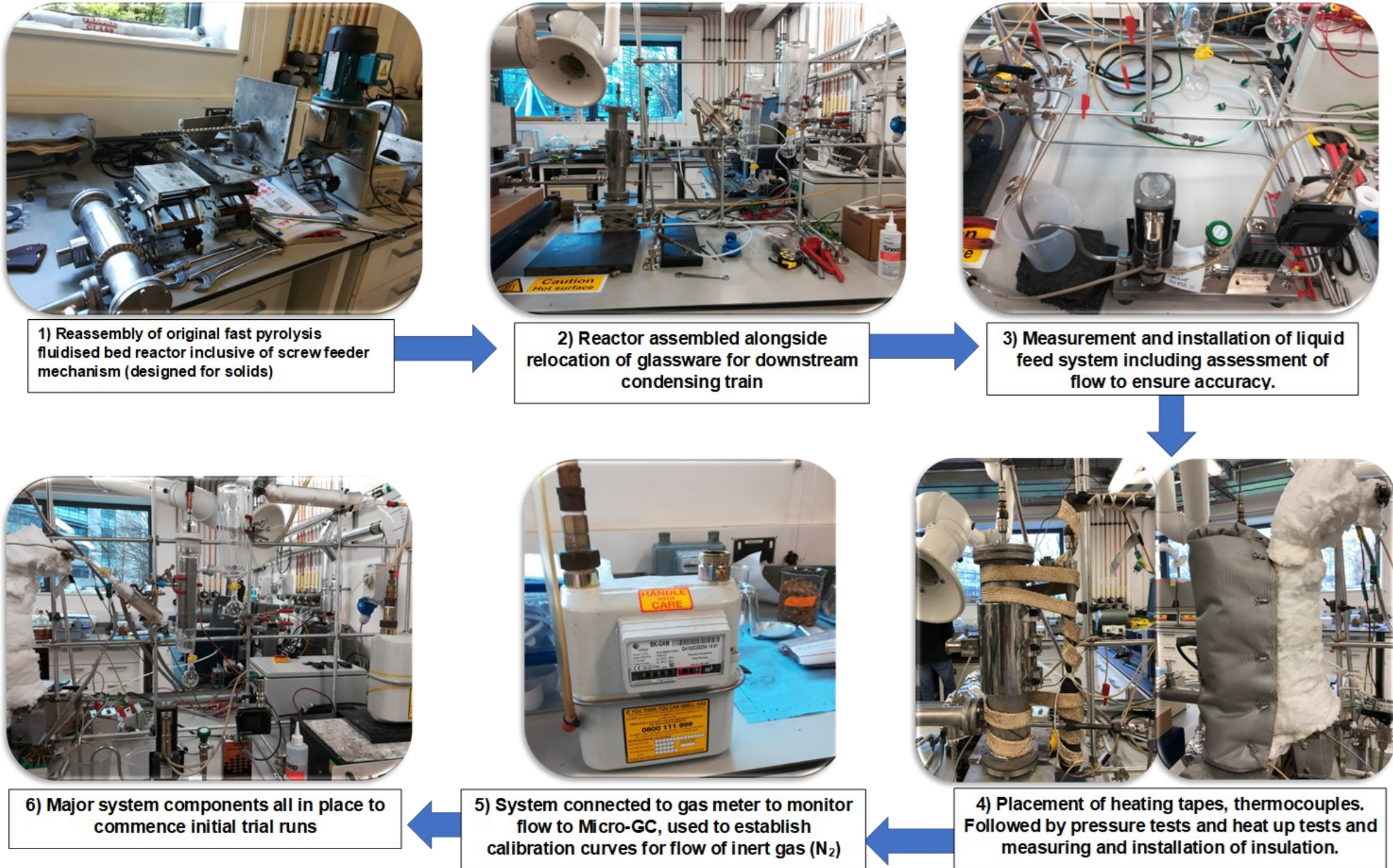


Figure 3-11. Initial reactor assembly major steps timeline

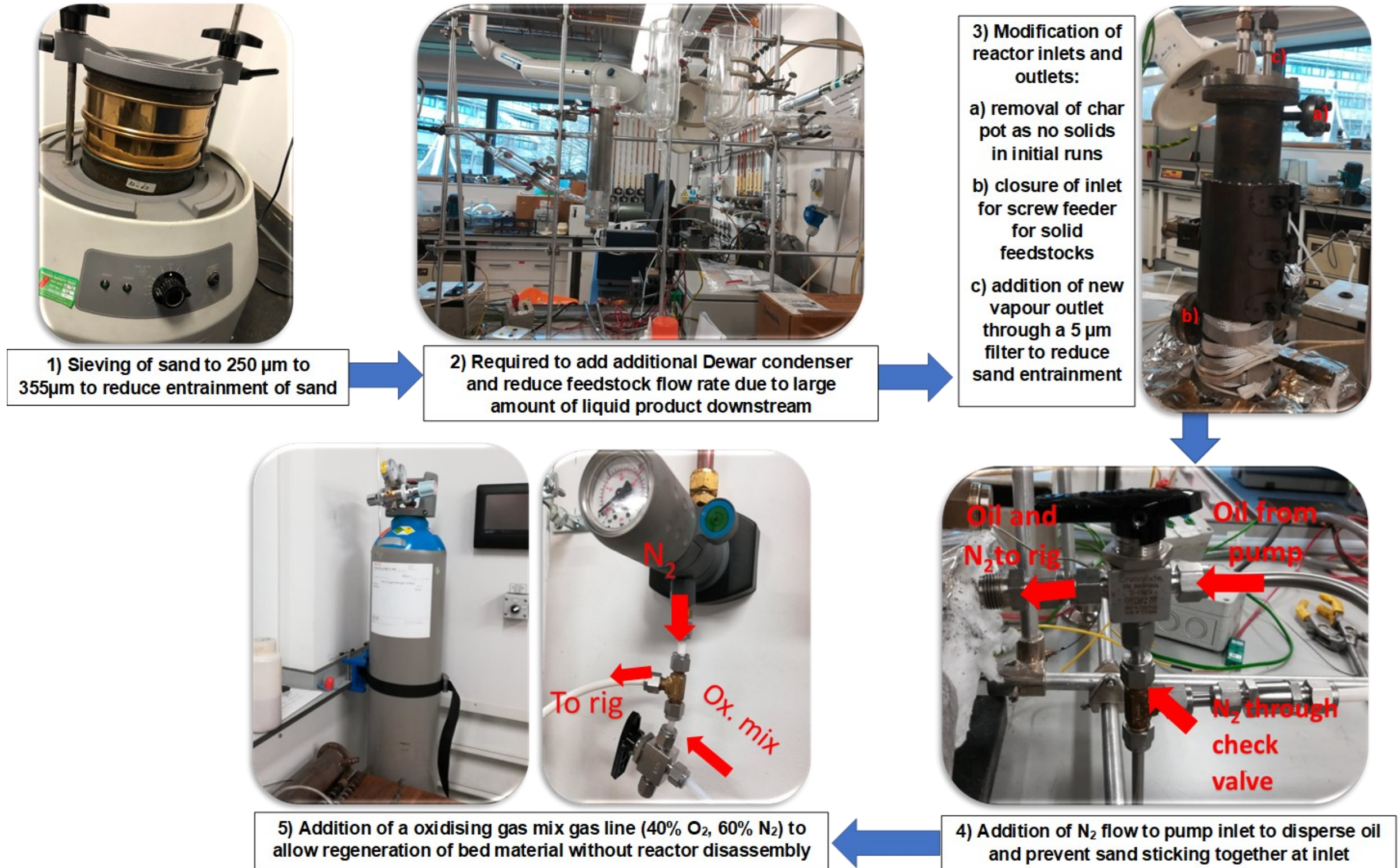


Figure 3-12. Reactor assembly modifications and improvements

3.3.2. Experimental Procedure

The general procedure used to complete a run in the fluidised bed system is summarised by the flow chart in Figure 3-13 **Error! Reference source not found..** Any data and information relevant to the experimental run was recorded on the experimental data sheet. This helped to ensure that relevant measurements were taken, and any issues observed during runs could be recorded and fixed in future runs.

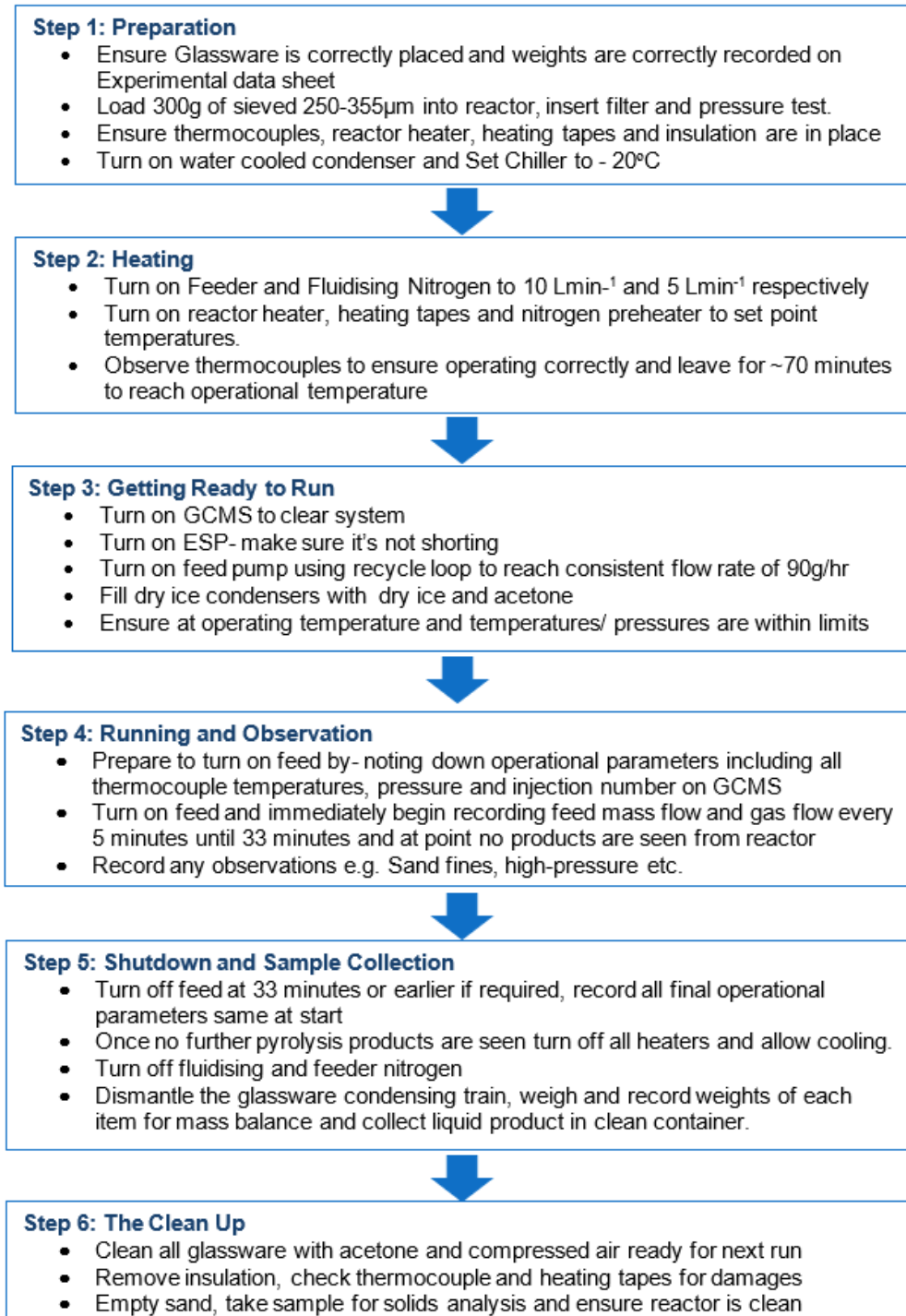


Figure 3-13. Fast fluidised bed reactor experimental procedure flow chart

3.3.3. Selection and Definition of Experimental Conditions

There are multiple parameters associated with the utilisation of the fluidised bed fast pyrolysis reactor in this work. These include the nitrogen flowrate, oil feed rate and operating temperature.

The nitrogen velocity is an important parameter that needs to be accurate to ensure that the minimum fluidisation of the bed material is achieved. Initially there were two nitrogen inlets, the fluidising nitrogen which entered from the bottom of the reactor and the feeder nitrogen. This entered through the inlet where the disused screw feeder was as shown in the initial reaction system in Figure 3-9. A flow from here was required in initial runs before modifications, to ensure that any sand or reaction products only exited from the top of the reactor as shown in the final reaction system as shown in Figure 3-10. The reported values were obtained using a gas mass flow meter (actual) and can be compared with the input values in Table 3-1 below.

Table 3-1. Calibration of fluidising nitrogen feeds and feeder nitrogen.

Fluidising Nitrogen			Feeder Nitrogen		
Input (L min ⁻¹)	Actual Flow (l/min)	Difference (%)	Input (l/min)	Actual Flow (l/min)	Difference (%)
5	5	+0.00	5	1.4	-72.00%
10	10.5	+5.00	10	3.3	-67.00%
15	15.8	+5.33	15	5.3	-64.67%
20	21.8	+9.00	20	7.5	-62.50%
25	27.9	+11.60	25	9.6	-61.60%

The information in Table 3-1 shows that the feeder nitrogen rate is actually significantly lower than the input rate. As for the fluidising nitrogen, this was fairly accurate at lower flow rates of 15 Lmin⁻¹ or less. The feeder nitrogen could have been changed to a more accurate controller but as this was left as this was no longer required after the modification to remove the screw feeder.

In terms of fluidising the bed material, initially a mass of 300 g of silica sand with a particle size of 550-650 µm was loaded into the reactor. The nitrogen flow was steadily increased but the sand was not moving at the maximum flow rate of 25 Lmin⁻¹. Therefore, a smaller particle size of 300-355 µm was selected and appeared to have a visible fluidisation velocity of 10 Lmin⁻¹ at room temperature. However, it is known that both temperature and pressure implicate the fluidisation velocity (see section 3.3.4.2 for information regarding the calculation of fluidisation velocity).

Consequently, the minimum fluidisation velocity has been estimated at room temperature and under operating conditions ($450\text{ }^{\circ}\text{C}$) to be 9.2 L min^{-1} and 4.47 L min^{-1} respectively. This was calculated using the Archimedes number as described above using Equation 3-5 and Equation 3-6 and detailed within Chapter 8.0, Appendix Two [169]. This difference in fluidisation velocity was anticipated as it is typical for the minimum fluidisation velocity to be lower under reaction conditions that are above room temperature.

In addition to an accurate and consistent nitrogen feed rate, the flow of the feedstock was also considered. The reactor selected was originally designed to fed solid feedstocks from a hopper into the reactor using a screw at a feed rate of 300 gh^{-1} . This was one of the major changes made in the initial assembly of the reaction system as highlighted in the reactor recommissioning section 3.3.4.2.1 and Figure 3-11. So, a liquid feedstock could be utilised, a new system using a pump from Tuthill in combination with a Bronkhurst digital mass flow meter and controller needed to be fitted to the feed system. During testing of the pump, it was established that it needed two to three minutes to reach a constant feed rate. Therefore, it was necessary for a three-way valve so that this could be established before oil feedstock would enter the reactor.

The final parameter of consideration is the reactor operating temperature. The studies discussed in Chapter 2.0, section 2.3.2 on the conversion of triglycerides to aromatics operated at temperatures within a range of $380\text{ }^{\circ}\text{C}$ to $550\text{ }^{\circ}\text{C}$. This range was too large to be consider for initial investigations and although an operating range would have been preferable, there was insufficient time to gather data at multiple temperatures. Therefore, the temperature of $450\text{ }^{\circ}\text{C}$ was selected as it was highlighted by Sadrameli et al. 2009 that liquid aromatics yields showed that temperatures $380\text{ }^{\circ}\text{C}$ to $450\text{ }^{\circ}\text{C}$ had provided the highest liquid aromatics yields. Furthermore, it also suggested that temperatures above $500\text{ }^{\circ}\text{C}$ would provide lower yields[112]. Finally, to ensure that uniform temperatures were consistently achieved in each experimental run the temperatures of the top, middle and bottom of the furnace were regularly monitored. In addition to this the profile of the reactor was assessed and recorded using an SD card within a digital thermocouple reader. This was utilised in both the initial blank runs as well as later runs that processed the jatropha oil feedstock.

3.4. Characterisation methods

In this section, the characterisation techniques and equipment used to analyse liquid, solid and gaseous samples and products is described.

3.4.1. Characterisation of liquids

In this section, liquid samples will include the main feedstock used for the pyrolysis tests (jatropha oil), as well as the pyrolysis liquid products. There are some techniques that were used for both set of samples and this is mentioned in the description of each technique.

The physiochemical properties and quality of conventional biofuels and vegetable oils can be assessed using several ASTM standards (American Society for Testing and Materials) [170-175]. These standards have been adopted and widely used as they provide parameters that allow the comparison of thermal, chemical, and physical properties of conventional fuels and biofuels.[3].

A summary of these characteristics, the relevant standards used to carry out the analyses, and the associated equipment used to obtain these values, is shown in Table 3-2.

Table 3-2. Oil characteristics, standard test methods, and equipment (expanded from [3])

No.	Characteristic	Associated Standard	Equipment/ Technique
1	Water Content	ASTM D 6304 07	Karl Fischer Titration [170]
2	Viscosity	ASTM D 445-06	Viscometer [174]
3	Higher Heating Value	ASTM D 2015	Adiabatic Bomb Calorimeter [175]
4	Acid Value	ASTM D 974	Titration equipment and Reagents :Potassium hydrogen phthalate ,Propanol (IPA) anhydrous, Toluene, H ₂ O [171]
5	Fatty Acid Composition	No specific standard*	Gas Chromatography with Mass Spectrometry
6	Iodine Value	ASTM D 1959	Titration equipment, Reagents: Thiosulfate Potassium Iodide solutions & Cyclohexane [173]
7	Density, 15°C, g·cc ⁻¹	ASTM D 1480	Pycnometer [172]
8	Molecular Weight	ASTM D 2503	Solvent, Thermistors, Closed Environment [172]
9	Pour Point, °C	ASTM D97/IP 15	Sample Jar, Water Bath and thermometers [176]

No.	Characteristic	Associated Standard	Equipment/ Technique
10	Elemental Analysis (wt.%, C, H, N, S & O by difference)	ASTM D 5291	Elemental Analyser [172]
11	Boiling Point Distribution (initial and final values)	ASTM D2887	Simulated Distillation [172]
12	Oil Decomposition Temperature	No specific standard (several methods used)	Thermogravimetric Analysis (TGA)

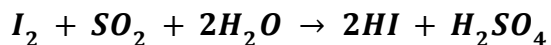
* Information in literature suggested various different dimension columns and carrier gases, almost all sources used Helium (He) as a carrier gas. [27, 43, 66, 116]

Out of the methods and parameters shown in Table 3-2, the following ones will be briefly described below including Karl-Fischer titration, viscosity, adiabatic bomb calorimeter and gas chromatography mass spectrometry. These methods were selected due to their accessibility as well as the relevance of the information provided. All these techniques and methods used are briefly described below.

3.4.1.1.Karl-Fischer Titration

Karl-Fischer (KF) titration is used to determine the water content of small amounts of liquid sample. The working principle of KF titration is based upon the redox reaction shown in Equation 3-7 below [177].

Equation 3-7. Redox reaction for Karl-Fischer titration



The water in the sample is consumed in this redox reaction, where the sulphur dioxide (SO_2) is both oxidised and consumed. The instrument used is a coulometric titrator where the iodine is produced electrochemically via anodic oxidation. The titrator consists of the generator electrode which acts as the cathode and contains the catholyte. The anode is a double platinum pin measuring electrode, which forms an electrolytic cell using the anolyte solution (titration flask). The current change is measured by the platinum electrode by the presence of iodine ions from the redox reaction. A general diagram of a KFT system is shown in Figure 3-14[177].

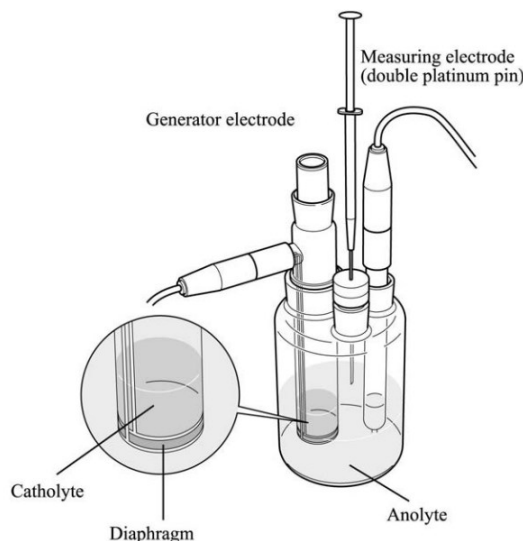


Figure 3-14. Mettler Toledo titration system [177]

In this work KF titration was used to measure the water content of jatropha oil and pyrolysis liquid product samples. The water content of these samples is of significance because any water contained within the feedstocks will form part of the pyrolysis liquid product along with any water created in the pyrolysis process [94, 178]. If the water content is in the range of 30 wt.% to 45 wt.% then this can cause phase separation and affect the stability of the liquid pyrolysis product [85, 93]. Although, the presence of water can reduce the viscosity, which can make it easier to pump and reduce costs[85].

Triglyceride feedstocks including Jatropha oil, typically contain near to no water (i.e. 0.2 wt.%) [72], which is desirable as an increased water content can reduce the heating value of the bio-oil [103].

The water content of jatropha oil and liquid pyrolysis product was determined using a Mettler Toledo V20 241 KF Titrator and a Sartorius analytical balance shown in Figure 3-15a, and 2b respectively.



Figure 3-15. Karl Fischer Titration equipment used for water content determination; (a) Mettler Toledo V20 Karl Fischer Titrator (b) Sartorius Analytical balance.

The working medium and titrant were Hydralan (R) K and Hydralan (R) Composite 5 K respectively (both from Honeywell Research Chemicals). A sample of about 5 mL was collected using a 10 mL syringe and weighed on the scale (Figure 3-15b). The sample was injected in the titration flask (Figure 3-15a). The mass of the injected sample was obtained by calculation of the weight difference before and after the sample was injected. The current change from the platinum electrode, together with the mass of the sample and titration time to reach the end point combined, allows the instrument to determine the sample's water content.

3.4.1.2.Viscometer

The viscosity parameter is a key factor in the design and application of pumping and piping systems. It is important as more viscous liquids require more power to pump and products with an inconsistent viscosity could cause blockages in the system. Furthermore, its measurement will indicate potential changes in the viscosity and consistency over a defined temperature range [179]. These issues are relevant as in this work the triglyceride feedstock will need to be pumped into a pyrolysis system in which the piping system will likely be above room temperature due to heat transfer. If the viscosity of the feedstock changes with temperature this could prove problematic, if it becomes too viscous or behaves inconsistently it may cause a blockage in the piping.

In this work, a Brookfield rotational viscometer; model DV-II+ Pro was utilised. In this viscometer, the amount of torque required to rotate a spindle immersed in the sample is measured. A schematic of a rotational viscometer is shown in Figure 3-16 [179]:

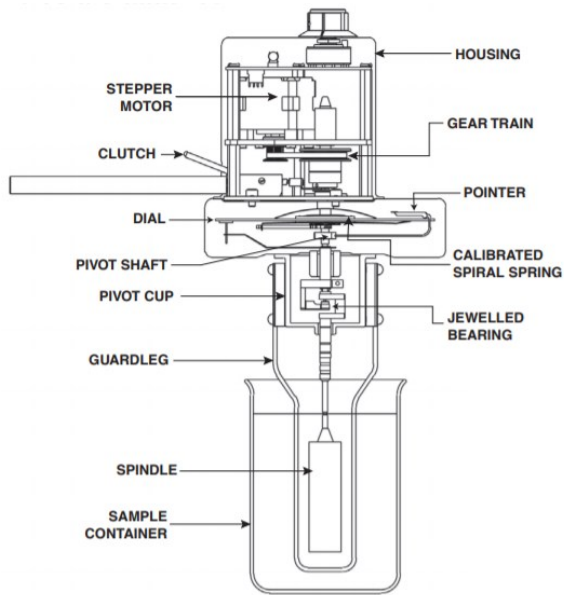


Figure 3-16. Brookfield rotational viscometer schematic[179]

A spindle is powered by a motor connected to the calibrated spiral spring, as the spindle moves through a fluid sample the deflection of the spring is indicated on the instrument interface. The spindle moves through the fluid at an increasing rotational speed and as such the resistance against the spindle also increases causing the spring to deflect. The greater the increase in deflection of the spring then the greater the increase in viscosity of the sample.

So that liquids over a wide range of viscosities can be measured spindles of differing geometry and size alongside differing rotational speeds can be utilised making the instrument highly versatile [179].

The viscosity of jatropha oil and the liquid pyrolysis product from fluidised bed investigations was assessed at room temperature in addition to samples of the bio-oil after conversion jatropha oil. Further analysis of the potential feedstock jatropha oil was carried out over a temperature range from ambient temperature to 90 °C. All viscosity analyses were carried out utilising a Brookfield rotational viscometer; model DV-II+ Pro as shown below in Figure 3-17.



Figure 3-17. Brookfield rotational viscometer model DV-II+ Pro

For all the analysis, the instrument was firstly calibrated using air via the instrument interface. An appropriate amount of sample was measured into the sample container depending on the spindle selected and the container returned to the instrument to attach the spindle. Using the apparatus software RheocalcT, the required parameters were inputted so the analysis could begin.

The analysis over a temperature range was conducted from the ambient room temperature (~23 °C) to 90 °C to ascertain if change of temperature would implicate the viscosity or consistency of the oil. The system software RheocalcT provided the value of the viscosity at each given temperature with data accessible for further review using Microsoft Excel.

3.4.1.3. Adiabatic Bomb Calorimeter

Adiabatic bomb calorimetry is used to determine the heating value of samples by measuring the enthalpy change between the reactants and products. Alternatively, the value can be obtained by calculation using information from the ultimate or proximate analysis of the feedstock [175]. The higher heating value (HHV) is the amount of heat released from the combustion of a sample with the water that is contained within the feedstock and generated in its combustion in a condensed state. It is of significance because it is an indicator of oxygen content with a small HHV often associated with a higher oxygen content. This can result in poor stability of the sample, which is problematic when producing both fuels and chemicals. Compounds such as esters, ketones, carboxylic acids and aldehydes are examples of oxygenated compounds that can contribute to a reduced heating value and reduced oil stability [2].

The working principle of an adiabatic bomb calorimeter is that the amount of heat released from a sample is compared to the heat obtained from a standard such as benzoic acid. When combusted benzoic acid releases heat it results in a temperature change in an absorbing medium such as water. Using the temperature change and specific heat capacity of the absorbing medium the heat of combustion of this standardised material can be calculated. The instrument can then compare the increase in temperature of a sample of unknown heating value to that of the standard and compute its heating value [180].

The HHV of jatropha oil and bio-oil from jatropha oil conversion, was determined by duplicate using a Parr 6100 Calorimeter shown in Figure 3-18a. For the analyses, 1.0 g to 1.5 g of the liquid samples were weighed in the crucible using a precision balance and placed on the sample holder as shown in Figure 3-18b.

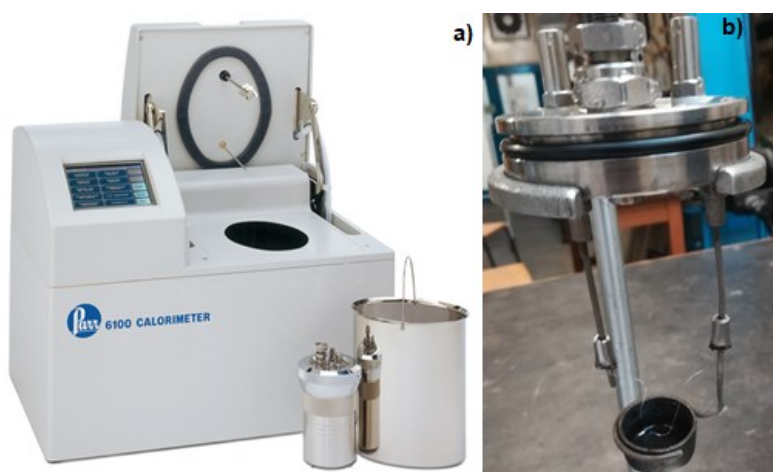


Figure 3-18. (a) Parr 6100 oxygen bomb calorimeter [181]; (b) sample holder and crucible

For the analysis of liquid samples, a 20 cm long fuse wire was placed between the two sides of the sample holder (Figure 3-18b) forming a loop of wire above the sample, whilst taking care to not directly touch the sample or crucible. The sample holder is placed in the bomb calorimeter vessel and screwed tightly; the vessel was filled with oxygen using a port on the lid. The bomb calorimeter vessel was placed in a water bucket containing 2000 g of distilled water and connected to the instrument using the banana wire connectors shown in Figure 3-19.

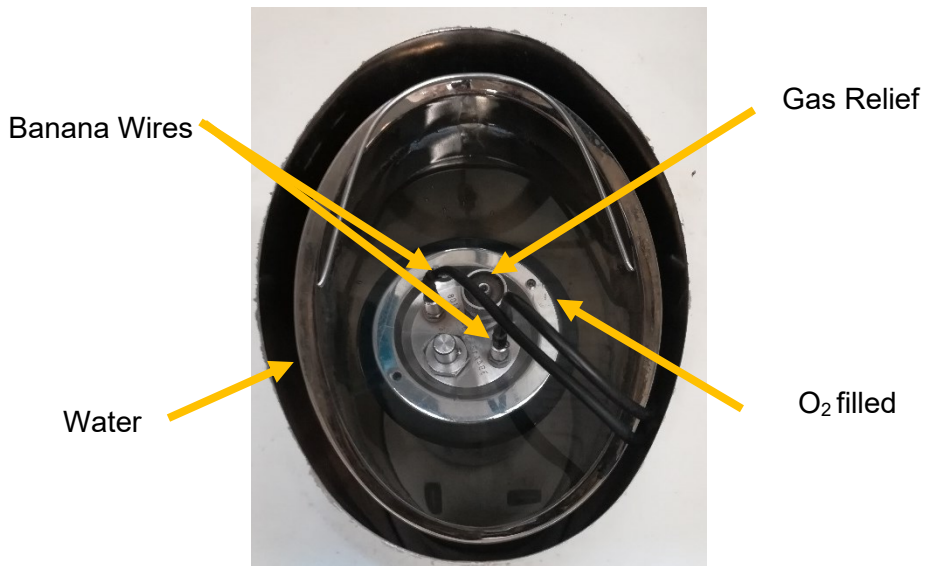


Figure 3-19. Bomb calorimeter vessel in-situ in Parr 6100 equipment

Any leaks present due to an improper seal were apparent by the formation of small bubbles around the vessel. In the event of this, the vessel was emptied, and reloaded. Finally, the sample weight and identification number were input in the computer's software, which displayed the heating value of the sample after a period of around twenty minutes.

3.4.1.4. Gas Chromatography- Mass Spectrometry (GC-MS) Analysis

Gas-Chromatography-Mass Spectrometry (GC-MS) is a highly versatile analytical technique used for the screening and identification of different types of compounds allowing the separation and identification of compounds within a sample even in very small amounts [182]. Typically, these systems are comprised of two independent parts the Gas Chromatograph (GC) and Mass Spectrometer (MS) that are coupled and work in succession. The GC contains a column in a temperature-controlled oven that is designed to heat and hold the temperature as defined by the system operator. Within the column separation of compounds occur, which can depend on factors including the types of compounds present, the column dimensions i.e., length, diameter, and film

thickness. A carrier gas such as hydrogen, helium or nitrogen move the vapours down the column with lighter compounds moving quickest until all vapours exit the column into the MS system.

MS systems typically include an ionization chamber, analyser, and ion detector. The molecules of the compounds are ionized and accelerated as they enter the MS. These ions then move to a mass analyser where they are further separated determined by their mass to charge ratio (m/z). These are detected by the mass analyser which records a signal which is interpreted by the data system and generates the mass spectrum. [182].

The analysis of these chromatograms can then give information about the sample injected, it may be compared to the chromatogram of a known desired compound or compared to a data base which can use a match factor to help determine what compound each peak is likely to represent.

In this work, the use of GC-MS allowed the identification of the fatty acids contained within the jatropha oil triglyceride feedstock, liquid pyrolysis products, and to identify newly formed compounds after processing such as smaller fatty acid chains, esters, aromatics and alcohols to name a few [183].

Jatropha oil and liquid products from the fluidised bed, were analysed using a Varian 450-GC with Varian 220-MS IT spectrometer with a Perkin Elmer Column Elite-1701 (30 m, 0.25 mm I.D., 0.25 μm film thickness). The system was set to use oven programme of 45 °C for 2 minutes, then ramped at 5 °C min^{-1} to 250 °C and held there for 3 minutes. The samples were prepared for analysis using a two-step filtration process followed by dilution with acetone. The filtration process used vacuum filtration with a 11 μm filter paper followed by syringe filtration using a 2 μm PTFE filter. The use of filtration was required to ensure that any particulates were removed to help with the preservation of column life and general equipment condition. Dilution was required in order to reduce the concentration of the analyte in order to prevent saturation of either the column or the detector [184]. For this reason, an initial sample size of 0.5 μl was injected and this was then increased to 2.0 μl if the chromatogram peaks were not sufficiently clear enough.

3.4.2.Characterisation of solid content on fluidised bed material

It was important to determine if any solid products had formed upon the surface of the sand i.e., char. This value was obtained either via use of thermogravimetric analysis as described in section 3.2.3.1 using the following methodology.

An ~8 mg of sand was placed in an alumina crucible (70 µL) and heated to a temperature of 700 °C for a period of 2 hours. These conditions ensured that any unreacted feedstocks will have been burnt off. Therefore, the only char remaining can be calculated by the difference in mass between the start and end weight of the sample. The value obtained from TGA analysis was compared with that obtained from analysis of the same sample using a muffle furnace as described in the following section 3.3.2.2.

A Muffle furnace is typically utilised in a laboratory setting due to their compact nature and ability to create high temperature atmospheres up to 900 °C. These furnaces are different as the heating chamber is externally heated. The walls of the furnace heat the contents of the chamber meaning that the samples are not in direct contact with a flame. The oven therefore heats via either conduction, convection or radiation to ensure the sample can be uniformly heated [185]. Owing to the operating temperature of this equipment it can be used in a similar way to Thermogravimetric analysis for the determination of the solids content of samples.

In this work an Carbolite AAF 1100 furnace was used to determine the proportion of solid products formed upon the silica sand from its use in the fluidised bed reactor. All of the sand was retrieved from the reactor (~300g) and placed on a metal tray. This was placed in the furnace at a temperature of 575 °C for a period of 24 hours. The cooled silica sand was weighed, and the change attributed to the solid products that had accumulated on the sand.

3.4.3.Characterisation of gases

The main gases analysed in this work were those produced from the pyrolysis of Jatropha oil in the fluidised bed system.

3.4.3.1. Micro gas chromatography

There are numerous types of gas analysers reported in the literature and used for the analysis of gases from experimental systems. One such example is the Micro Gas Chromatograph system which can provide rapid analysis of a number of complex chemical mixtures in a matter of minutes. The principles of micro-GC are very much like that of Gas Chromatography discussed earlier in section 3.3.1.5, with the main difference being that different components are miniaturized. This increases portability of the instrument, reduced power consumption and increases the speed of analyses[186]. In this work an on-line Varian CP 4900 Micro-GC, micro gas chromatograph with a thermal conductivity detector (TCD) with two columns (Varian CP-5A mol sieve and CP-PortaPLOT) was used as shown in Figure 3-20 below.



Figure 3-20. Varian CP 4900 Micro-GC, micro gas chromatograph with a thermal conductivity detector (TCD) with two columns (Varian CP-5A mol sieve and CP-PortaPLOT)

The analysis of the non-condensable gases from the pyrolysis of jatropha oil was conducted at intervals of 150 seconds. Any excess gases were vented to a fume hood. The data was collected using the instrument computer for analysis via the use of Microsoft excel. To ensure that gases are appropriately identified the equipment had been calibrated prior to use using standard samples of the relevant gases.

3.5. Summary

This Chapter 3.0 has discussed all the materials and methods utilised throughout this research. This includes two different types of reaction systems including a CDS Analytical 5200 Pyroprobe GCMS (Py-GCMS) unit alongside a fluidised bed fast pyrolysis reactor (90 gh^{-1}). In each case the characterisation of the feedstocks and products obtained from these investigations have been considered to evaluate changes that have occurred. The following Chapters 4.0, 5.0 and 6.0 will discuss the experimental data obtained. Firstly Chapter 4.0 will discuss results obtained from the non-catalytic pyrolysis of oleic acid and jatropha using the Py-GCMS. This will be followed by discussion of the catalytic pyrolysis of oleic acid and jatropha oil in the same system. Finally, the Chapter 6.0 will discuss the implementation of the fluidised bed fast pyrolysis system for the non-catalytic pyrolysis of jatropha oil.

CHAPTER 4.0 PYROLYSIS OF OLEIC ACID AND JATROPHA OIL

4.1. Introduction and aims

This chapter will assess the pyrolysis of oleic acid and jatropha oil in the absence of a catalyst at three different temperatures (400 °C, 500 °C and 600 °C). The temperature range was selected based on several studies concerning the conversion of various triglyceride feedstocks varying the pyrolysis temperatures between 375 °C and 650 °C (Chapter 2.0, section 2.3.2, Table 2-7)[2, 3, 43, 45, 109-117, 187]. The aim of these non-catalytic pyrolysis investigations is to:

- Investigate the decomposition of oleic acid as a model compound for jatropha oil via use of Pyroprobe-GCMS (Py-GCMS) allowing a less complex assessment of decomposition pathways.
- Evaluate and assess the decomposition products from the Py-GCMS of oleic acid and jatropha oil to identify components that affect the reaction mechanism or kinetics for the production of aromatics.
- For both feedstocks assess the impact of differing temperatures on the yield and distribution of aromatics including BTX as well as other major functional groups.

These investigations were conducted using a Pyroprobe CDS 5200 system as described earlier in section 3.3.4.1. This pyroprobe system was utilised due to several advantages including the small sample size requirements, time taken for analysis, and relative ease to repeat the tests at the exact same conditions. The sample size requirements were beneficial considering the relatively high cost of pure oleic acid. Regarding the analysis time, one pyroprobe sample can be prepared and analysed within 2.5 hours versus 2-3 days needed for a bench scale system like the fluidised bed reactor (see section 3.3.4.2).

Finally, the test conditions can be set in the system, allowing repeatability of the experiments to be assessed. In terms of the feedstocks the composition of jatropha oil is about 46 wt.% oleic acid, 31 wt.% to linoleic acid and 10 wt.% palmitic acid alongside smaller amounts of other fatty acids as described in section 2.1.3.2, Table 2-3[3, 5-10].

It is intended that studying the decomposition of this compound will allow the deduction and/or prediction of the major decomposition pathways. Furthermore, it may be indicative of the distribution and yields that might be obtained from the evaporation and pyrolysis of jatropha oil. From the literature review of fatty acid decomposition pathways in Chapter 2.0, section 2.3.3 three major paths appeared prominent.

These include a very early scheme by Chang et al. 1947, in addition to pathways suggested by Idem et al. 1996 and Schwab et al. 1998 [114, 119, 123].

In literature over the last several decades it was difficult to ascertain additional pathways due to the sporadic nature in which information on this topic seems to appear [121]. Furthermore, as highlighted in Chapter 2.0, section 2.3.2 difference between the pathways are highlighted demonstrating that existing pathways are not synonymous between authors. So, it is intended that this work will help both clarify and validate such pathways.

4.2.Pyroprobe GC-MS

The analysis of the results includes the chromatograms from single runs as an example at the given conditions. All graphs and tables presented utilise average values of peak areas obtained from the duplicate runs to analyse trends observed in the data. The peaks identified from the GC-MS coupled to the pyroprobe system were grouped into functional groups, which allow for easier identification of the major groups of products. These are important as when discussing decomposition pathways and the evolution of certain types of compounds, it will be easy to highlight the increase or decrease in a certain group of compounds. The designated functional groups and their abbreviations maybe used throughout the discussion are shown in Table 4-1 below.

Table 4-1. Functional group abbreviations for major products of pyroprobe GC-MS

Abbreviation	Functional Group
ALI	Aliphatics
AR	Aromatics
UN	Unknown
OxyPH	Oxygenated Polyaromatic Hydrocarbons
OxyAR	Oxygenated Aromatics
KET	Ketones
ALD	Aldehydes
ETH	Ethers
AL	Alcohols
EST	Esters
AC	Acids
PH	Phenols
PAH	Polyaromatic Hydrocarbons

4.2.1.Pyrolysis of oleic acid at different temperatures

Overall, from the pyrolysis of oleic acid in the absence of a catalyst at the different temperatures, it was observed that the major products were mostly acids alongside small proportions of aliphatics, aromatics, esters, alcohols, and aldehydes. The high proportion of acids was identified as a large peak. For oleic acid at 70.7 minutes in the chromatograms(Figure 4-1, Figure 4-2, Figure 4-3). All peaks were identified using the opensource software OpenChrom in conjunction with the NIST with the most appropriate peaks selected using a Microsoft Excel with a macro enabled workbook so that compounds with the highest match factors and probability could be selected. Other peaks have been labelled and identified on the chromatograms below to provide a visual representation of the compounds produced as some of these are later displayed in some of the decomposition pathway (Figure 4-1 Figure 4-2 and Figure 4-3). A summary of all the peaks associated with products from the decomposition of oleic acid in the absence of a catalyst, is shown in Table 4-2 below.

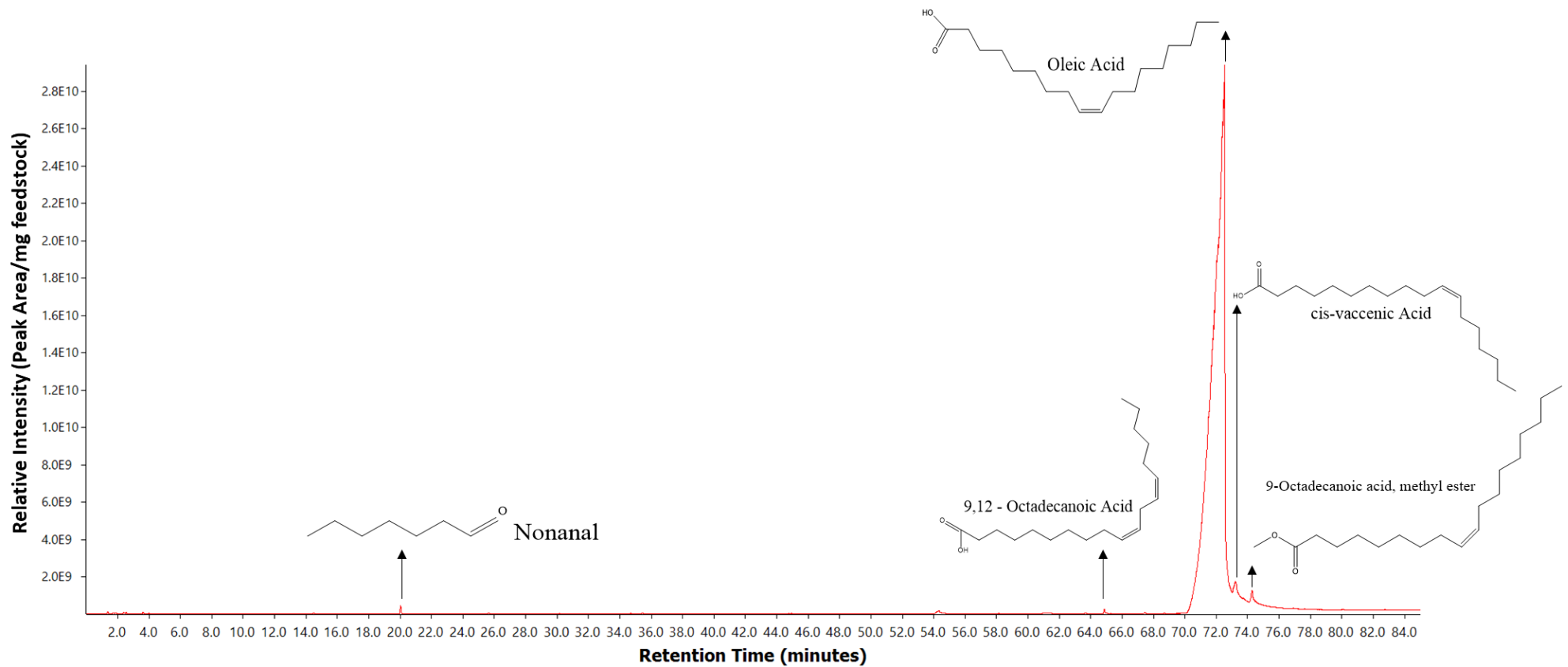


Figure 4-1. Pyrolysis of Oleic acid at 400 °C in the absence of a catalyst

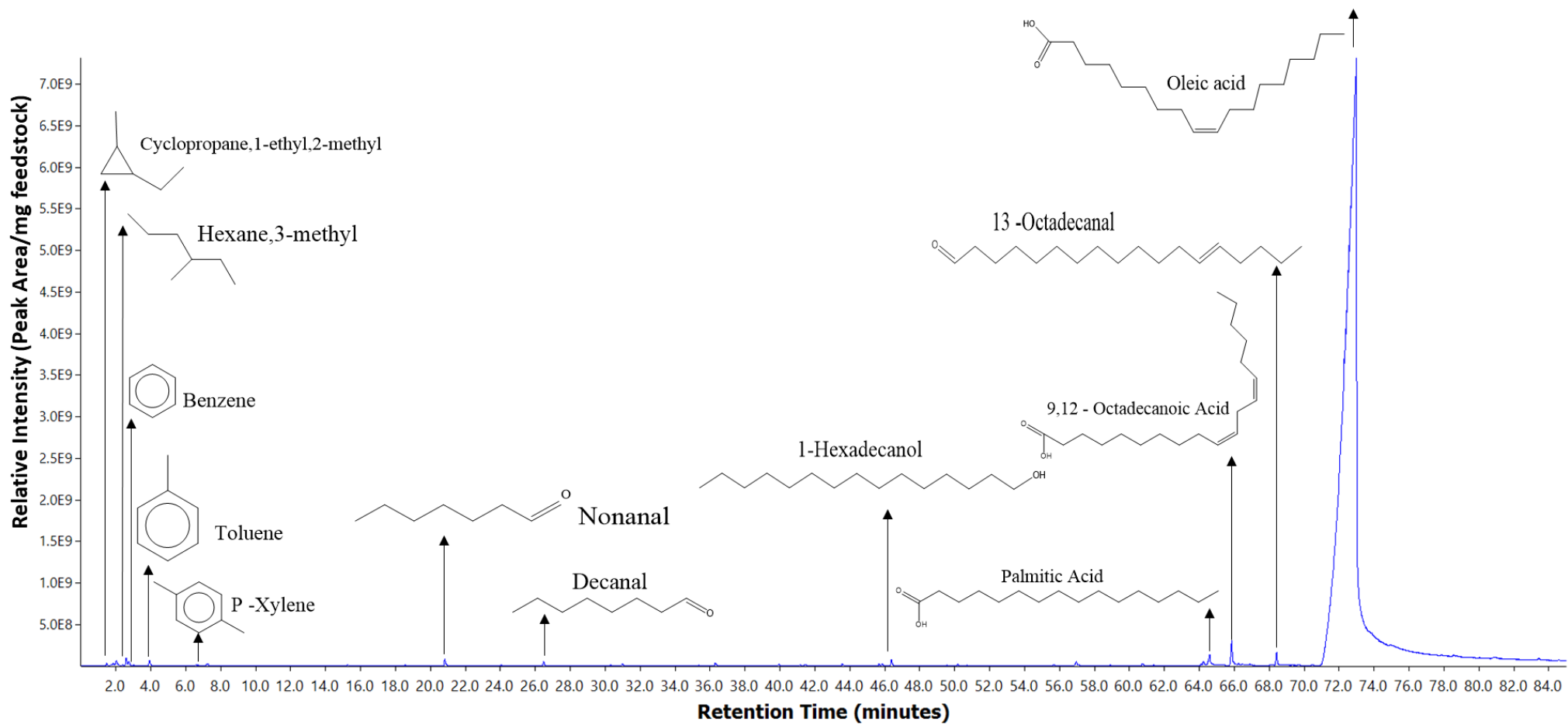


Figure 4-2. Pyrolysis of oleic acid at 500 °C in the absence of a catalyst

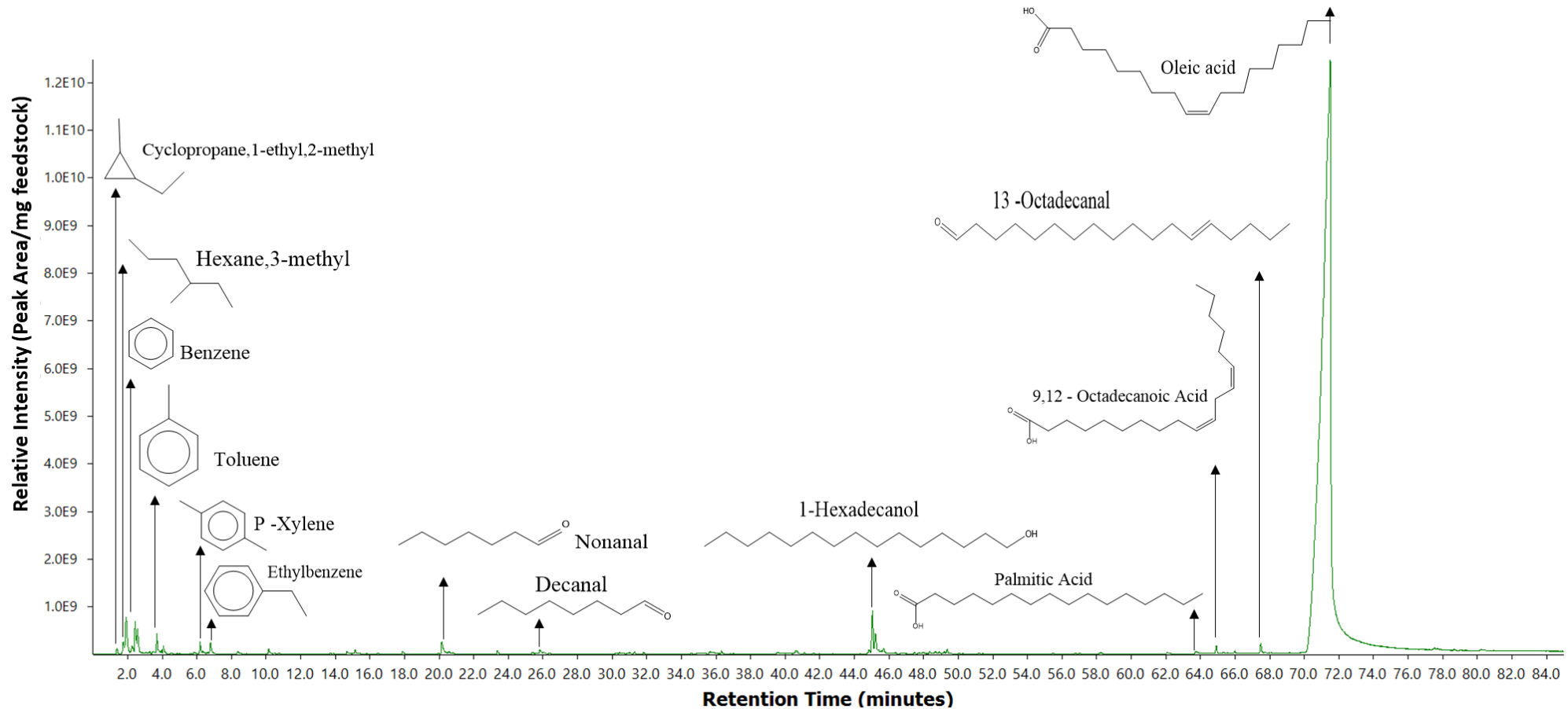
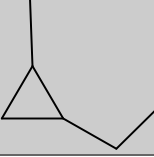
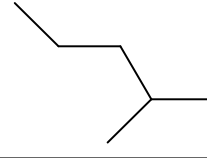
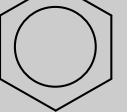
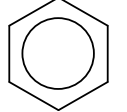
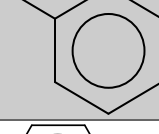
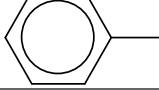
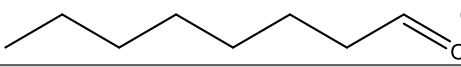
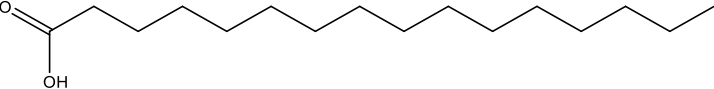
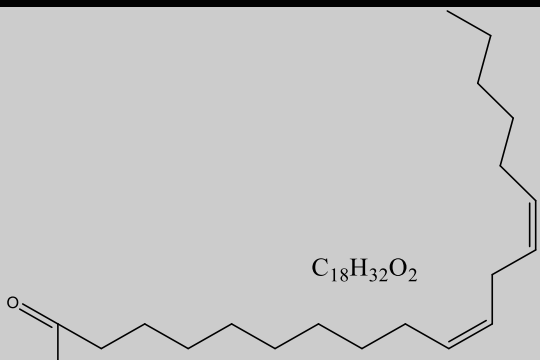
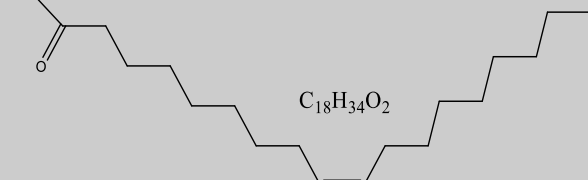
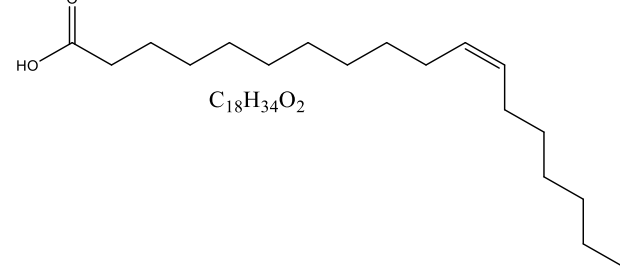
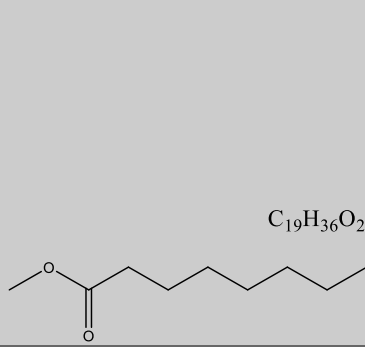


Figure 4-3. Pyrolysis of oleic acid at 600 °C in the absence of a catalyst

The most significant compounds identified in the chromatograms are summarised in Table 4-2 below with the skeletal formula and compound name placed above each peak where present in Figure 4-1, Figure 4-2 and Figure 4-3. The evolution of some of these compounds is discussed later in this section in various decomposition pathways.

Table 4-2. Notable peaks from pyrolysis of oleic acid at 400 °C, 500 °C and 600 °C

Retention Time (min)	Compound Name	Skeletal and Chemical Formulae
1.9	Cyclopropane, 1-ethyl, 2-methyl	 C ₆ H ₁₂
2.5	Hexane, 3-methyl	 C ₇ H ₁₆
2.6	Benzene	 C ₆ H ₆
4.1	Toluene	 C ₇ H ₈
6.5	P-Xylene	 C ₈ H ₁₀
6.9	Ethylbenzene	 C ₈ H ₁₀
20.1	Nonanal	 C ₉ H ₁₈ O
25.7	Decanal	 C ₁₀ H ₂₀ O
45.1	1-Hexadecanol	C ₁₆ H ₃₄ O 
64.5	Palmitic acid	 C ₁₆ H ₃₂ O ₂

Retention Time (min)	Compound Name	Skeletal and Chemical Formulae
66.0	9-12-Octadecanoic Acid	 $C_{18}H_{32}O_2$
68.0	13-Octadecanal	 $C_{18}H_{34}O$
70.7	Oleic Acid	 $C_{18}H_{34}O_2$
73.2	cis-vaccenic Acid	 $C_{18}H_{34}O_2$
74.3	9-Octadecanoic acid, methyl ester	 $C_{19}H_{36}O_2$

Considering the major peak at 70.7 minutes identified in Figure 4-1, Figure 4-2 and Figure 4-3 is oleic acid, it is clear that this is the predominant compound present at all three temperatures after thermal conversion as this peak has the largest peak area per milligram of feedstock. This is undesirable, as this shows that the oleic acid feedstock does not undergo conversion to other products at any of the temperatures in the absence of a catalyst. This means a proportion of the oleic acid must have just evaporated and condensed as part of the decomposition products.

As the temperature increased from 400 °C to 500 °C, the presence of other lower molecular weight products increased with mostly aliphatics (alkenes and alkanes), in addition to smaller amounts of alcohols, aromatics and aldehydes. The increased presence of these compounds at higher temperatures suggests that the decomposition of oleic acid into other products occurs more readily at the higher temperature of 600 °C rather than the lowest temperature of 400 °C that was considered in this work. This observation is consistent with findings reported by Kubátová et al. 2011, Asomaning et al. 2014 and Omidghane et al. 2017 who observed an increase in the presence of these lower molecular weight compounds as the pyrolysis temperature was increased [27, 80, 121, 188]. Given the trends observed it could be of interest to consider higher pyrolysis temperatures of 700 °C or 800 °C in future work.

For example, Kubátová et al. 2011, investigated the decomposition of soybean oil in a 1 L stainless steel autoclave with electric heater and stirrer at temperatures of 420 °C and 430 °C. It was concluded in prior optimization studies including Kubátová et al. that significant cracking of the triglyceride compounds in the oil does not occur below 420 °C [189]. This is of significance because soybean oil is typically around 25 wt.% oleic acid, alongside around 50 wt.% linoleic acid, an isomer of oleic acid [190].

Further agreement can be found in work by Asomaning et al. 2014. In their work they consider the decomposition of oleic acid. A 15 mL batch micro reactor was used for the pyrolysis tests at temperatures between 350 °C and 450 °C. During the identification of products in the pyrolysis liquids they reported that at lower temperatures (350 °C) there was lower feedstock to product conversion, while the conversion yielding lower molecular weight compounds was favoured at higher temperatures (450 °C).

Finally, Omidghane et al. 2017; used a 15 mL batch microreactor heated in a fluidised sand bath at temperatures of 390 °C, 430 °C and 450 °C for 2 hours in the absence of any catalyst. They highlighted that a higher degree of cracking can occur at higher temperatures up to around 420 °C after which the rate was consistent to temperatures up to 450 °C. Omidghane et al. later stated in their study that an increase in temperature to 430 °C resulted in the conversion of oleic acid to be near 100 %. This statement contradicts the observation in my work that at 600 °C a large proportion of the oleic acid feedstock is still present [80].

However, this inconsistency could be attributed to a number of factors including that this study uses a vastly different scale system using 1 g of oleic acid versus around the 0.4 µg used in this work. Furthermore, although both were batch systems the

reaction time was significantly longer at 2 h in work by Omidghane et al., whilst in the Pyroprobe GCMS the reaction time is just around 6-8 minutes depending on the reaction temperature.

In addition to considering the presence of specific groups of compounds it is also possible to compare the changing proportions of these compounds at different reaction temperatures. This data is presented using the graph in Figure 4-4 below, whilst abbreviations of the different groups of compounds are highlighted in Table 4-1 at the start of section 4.2.

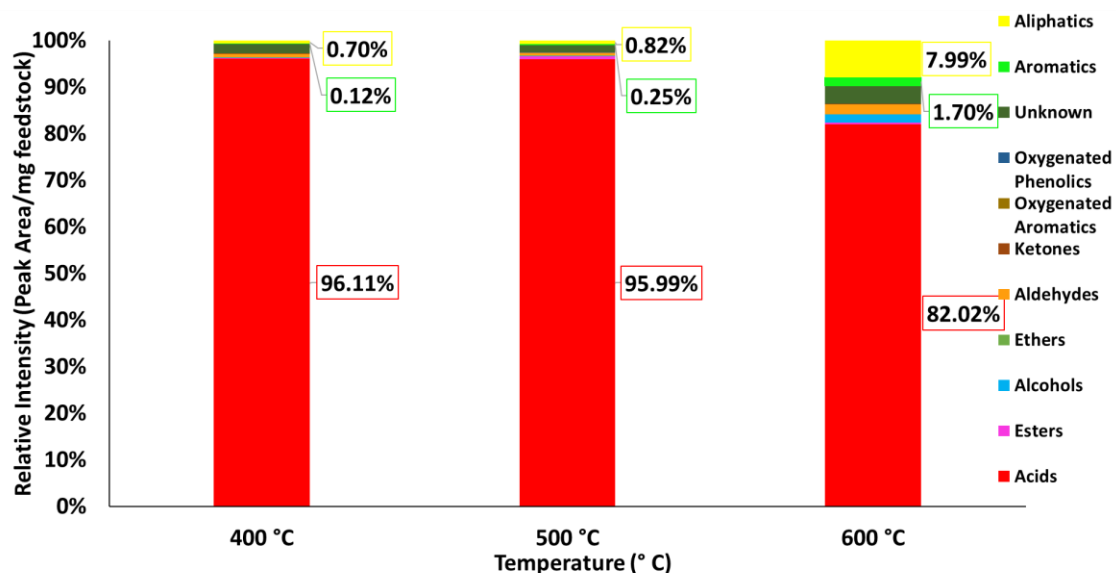


Figure 4-4. Products from the pyrolysis of oleic acid at different temperatures (average values from duplicated runs)

From Figure 4-4, it is observed that the most abundant functional group found for all the temperatures is the acid group, predominately oleic acid, with small amounts of linoleic acid. The product distribution in terms of functional groups for 400 °C and 500 °C were somewhat similar with slight variations in the proportion of acids, an increasing proportion of aliphatics and the largest increase at the highest temperature of 600 °C. This has previously been observed by Schwab et al. 1998, Chang et al. 1947, Alencar et al. 1983 and Idem et al. 1996, who have reported in their decomposition pathways that unsaturated fatty acids can yield these aliphatic compounds including alkenes and alkanes. A simplified version of the pathway from Schwab et al., 1998; is shown in Figure 2.11, previously in Chapter 2.0, section 2.3.3.

The Figure 2.11, the fatty acids yield compounds decompose forming aliphatics such as alkenes and alkanes via pathways B and C (cracking of the fatty acid chain). The fact that there are more of these aliphatics present at 600 °C (Figure 4-4) suggests that oleic acid decomposes more readily at higher temperatures. This increased formation of aliphatics has been associated with the increased cracking reactions at the higher pyrolysis temperature. This in turn is resulting in lower molecular weight compounds forming, such as cyclopropane, 1-ethyl-2-methyl as observed by Idem et al., 1996. In the reported work by Idem et al., a canola oil feedstock was thermally cracked using a down flow fixed bed reactor. The reaction runs were conducted over a temperature range of 300 °C to 500 °C with a flow rate of 5.11 gh^{-1} to 24.2 gh^{-1} [123]. The statement that more lower molecular weight compounds are produced at higher temperatures can be easily observed in this work. The chromatograms Figure 4-1, Figure 4-2 and Figure 4-3 show the decomposition of the oleic acid at increasing temperatures of 400 °C, 500 °C and 600 °C respectively and in each case additional and larger peaks are identified on the far-left hand side of the chromatogram.

A further observation is the increased presence of single aromatic ring compounds such as benzene and toluene together with other lower molecular weight compounds as temperature was increased from 500 °C (Figure 4-2) up to 600 °C (Figure 4-3). As this work is considering the production of aromatics, the peaks present at 2.6, 4.1, 6.5 and 6.9 minutes corresponding to benzene, toluene, p-xylene, and ethylbenzene respectively are of great significance. In the decomposition pathway shown earlier in Figure 2.11, it is clear that functional group of aliphatic compounds including alkenes and alkanes, are precursors to the highly desirable aromatic compounds. Therefore, these aromatic compounds are unobtainable unless the oleic acid decomposes to give reasonable amounts of alkenes and alkanes. This relationship is observable from Figure 4-4 as at 400 °C the aliphatics content is 0.7 % while the proportion of aromatics is just 0.12 %. Whereas at 600 °C, the aliphatics content was 7.99 % and the proportion of aromatics 1.7 %. Although this shows that as the amount of aliphatics increase so can the amount of aromatics the maximum proportion at 600 °C this increase is still very small. These trends are further validated by the graph below (Figure 4-5) below.

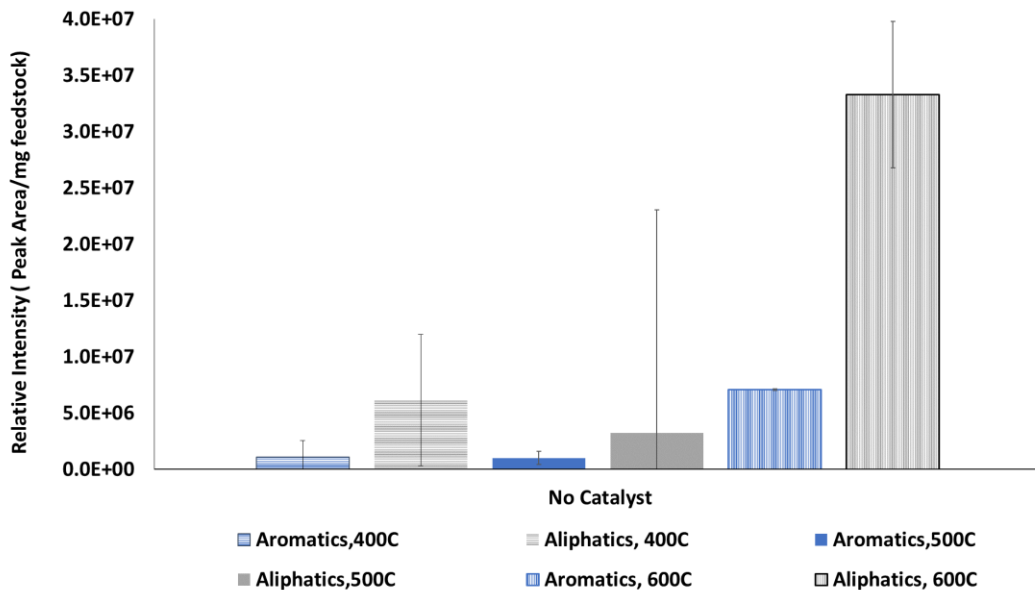


Figure 4-5. Yields of aromatics and aliphatics from the pyrolysis of oleic acid pyrolysis at different temperatures (average of duplicate runs, standard deviation given in error bars)

The graph in Figure 4-5 shows the peak area per mg of oleic acid at the different temperatures for the major group's aromatics and aliphatics. It can be observed that as the temperature increases from 400 °C to 600 °C there is a relationship between the aromatics content and aliphatics content with the highest yield of aromatics occurring alongside the highest yield of aliphatics at a temperature of 600 °C. This graph shows that significant increases in the aliphatics content are required to implicate the yields of aromatics.

Overall, when analysing the products distribution from the non-catalytic pyrolysis of oleic acid at the three different temperatures (400 °C, 500 °C and 600 °C), it was noted that the most prevalent functional group was acids. Among these, the most prevalent compound was the feedstock itself (oleic acid), meaning a relatively low decomposition from the original sample. A slightly higher oleic acid decomposition was observed at 600 °C resulting in a lower proportion of acids and increased proportion of aliphatics. This was possibly due to higher energy allowing the breakage of single and double carbon bonds from its original fatty acid structure. This thermal decomposition pathway for oleic acid shall be compared later in this Chapter 3.0 with the trends reported from jatropha oil decomposition at the same experimental conditions.

4.2.2.Pyrolysis of jatropha oil at different temperatures

It is anticipated that some of the trends observed in the decomposition of oleic acid will be visible in the decomposition analysis for jatropha oil, as oleic acid accounts for ~46 wt.% of the jatropha oil composition. If this is the case, then similar trends in the reduction of acids at the higher temperatures of 500 °C and 600 °C alongside an increase in aliphatics content can be expected. However, in addition to the oleic acid component consideration must be given to the two other major fatty acids linoleic and palmitic acid as well as glycerol that contribute to the makeup of jatropha oil. Therefore, jatropha oil decomposition might differ from oleic acid as these components might contribute to the formation of different functional groups.

The relevant peaks from the decomposition of jatropha oil at different temperatures of 400 °C, 500 °C and 600 °C have been labelled and identified on the chromatograms as shown in Figure 4-6, Figure 4-7 and Figure 4-8, respectively. The main peaks associated with the jatropha oil decomposition in the absence of catalyst is summarised in Table 4-3.

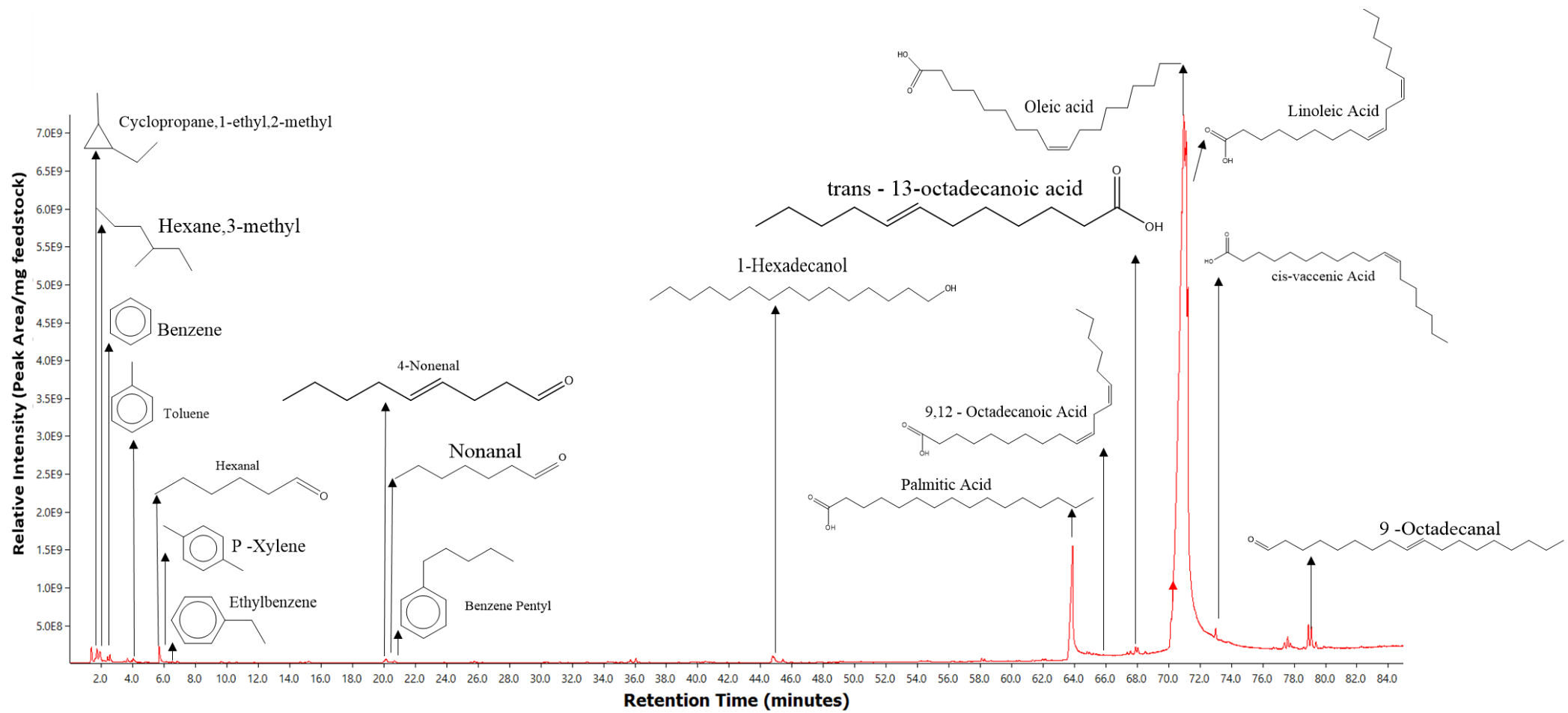


Figure 4-6. Jatropha oil pyrolysis at 400 °C in the absence of a catalyst

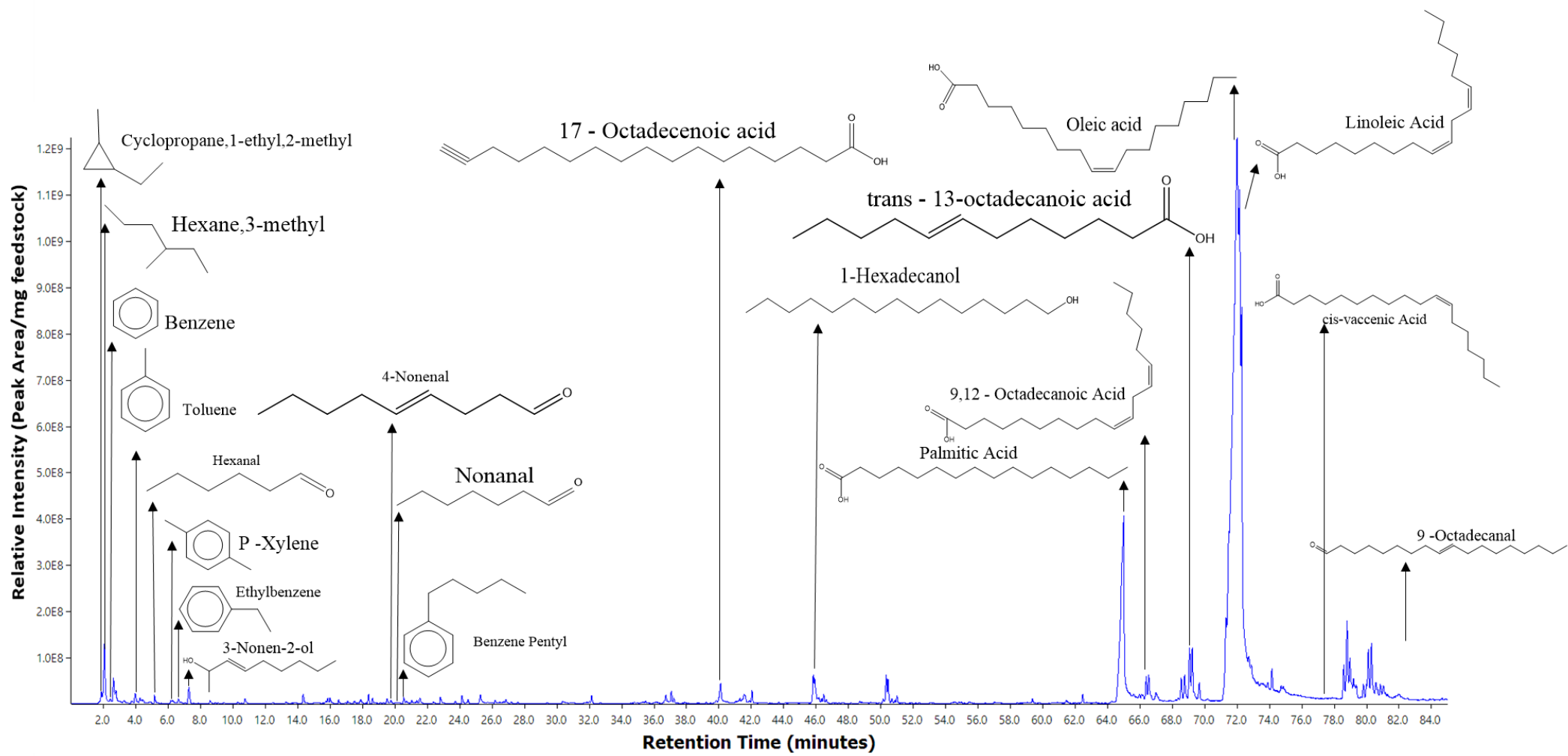


Figure 4-7.Jatropha oil pyrolysis at 500 °C in the absence of a catalyst

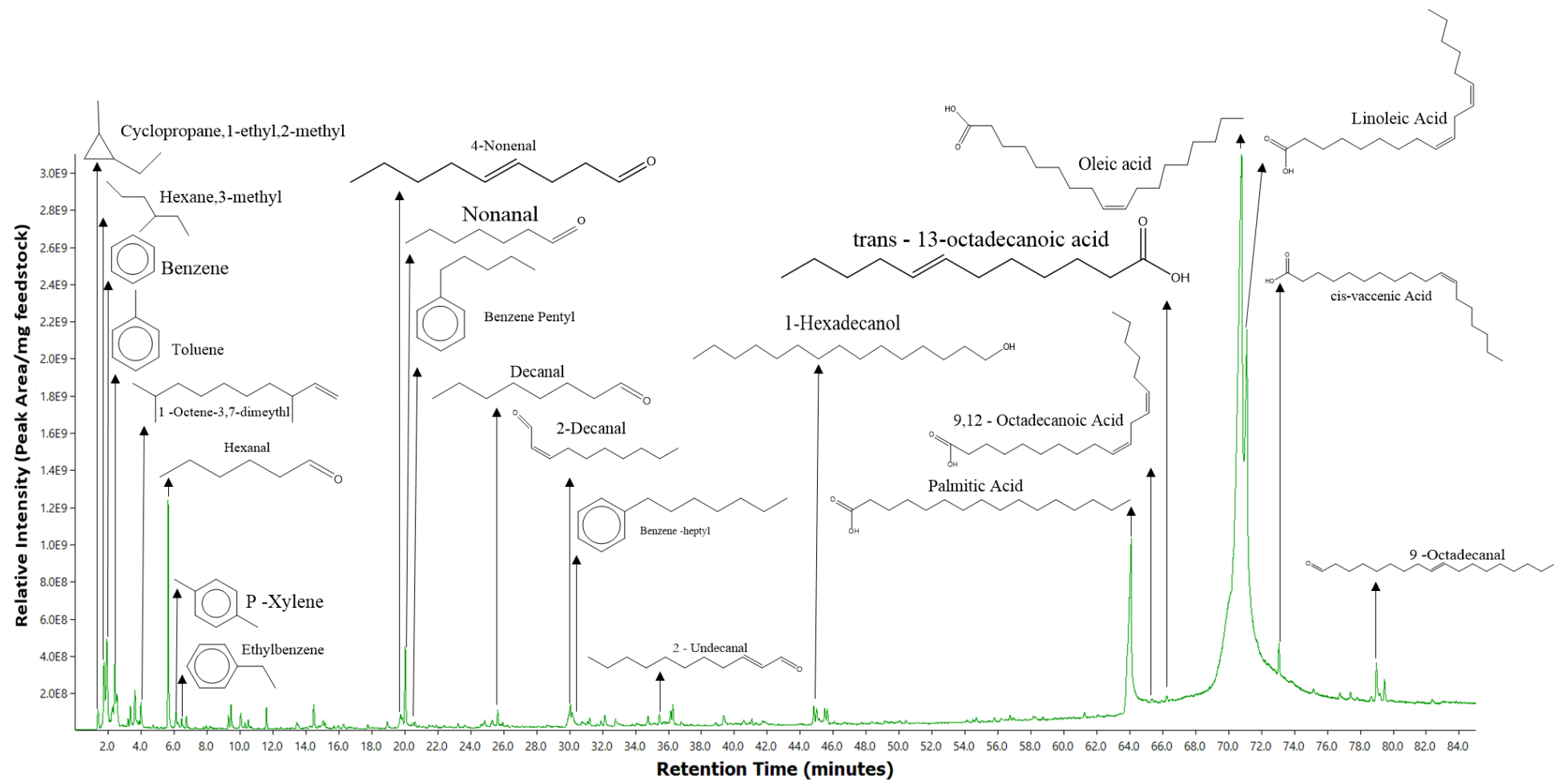
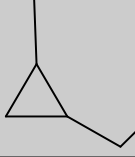
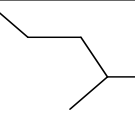
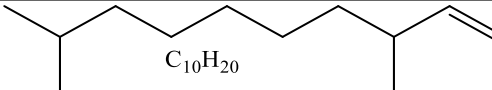
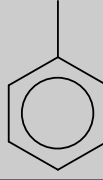
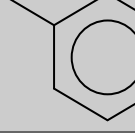
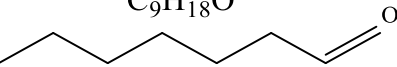
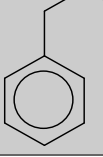
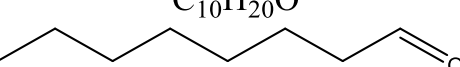
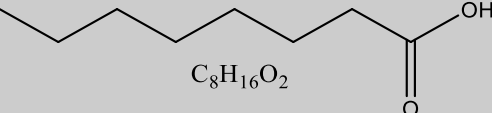
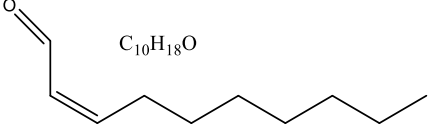
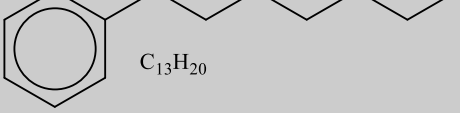
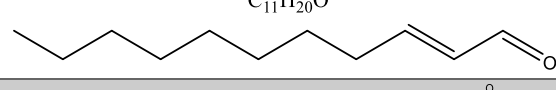
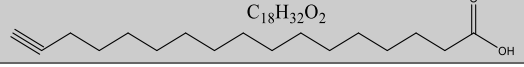
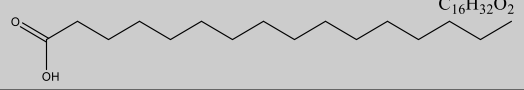
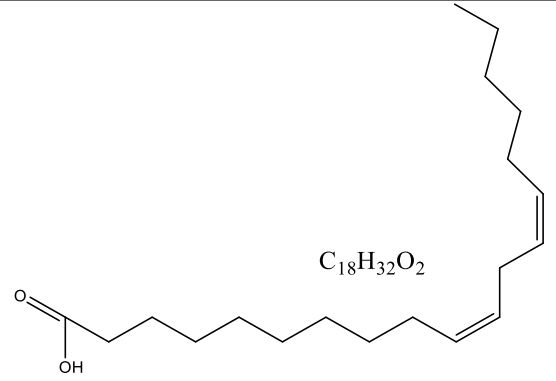
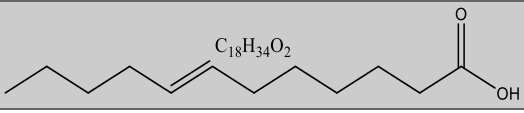
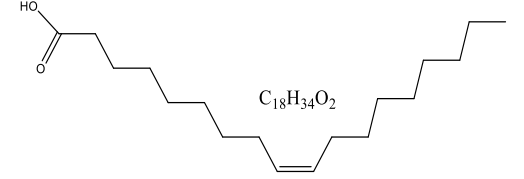
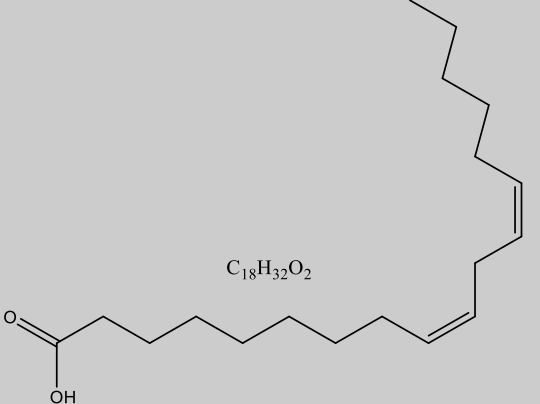
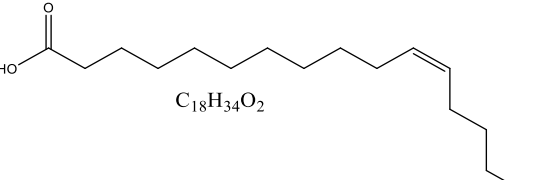
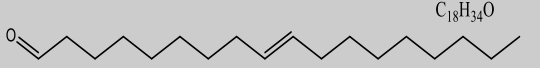


Figure 4-8. Jatropha oil pyrolysis at 600 °C in the absence of a catalyst

Table 4-3. Notable peaks from pyrolysis of jatropha Oil at 400 °C, 500 °C and 600 °C

ID	Retention Time (min)	Compound Name	Skeletal and Chemical Formulae
1	1.9	Cyclopropane,1-ethyl,2-methyl	 C ₆ H ₁₂
2	2.5	Hexane-3-methyl	 C ₇ H ₁₆
3	2.6	Benzene	 C ₆ H ₆
4	3.6	1-Octene, 3,7-dimethyl-	 C ₁₀ H ₂₀
5	4.1	Toluene	 C ₇ H ₈
6	5.7	Hexanal	 C ₆ H ₁₂ O
7	6.5	P-Xylene	 C ₈ H ₁₀
8	6.9	Ethylbenzene	 C ₈ H ₁₀
9	19.8	4-Nonenal	 C ₉ H ₁₆ O
10	20.1	Nonanal	 C ₉ H ₁₈ O
11	20.6	Benzene-Pentyl	 C ₁₁ H ₁₆
12	25.7	Decanal	 C ₁₀ H ₂₀ O
13	29.8	Octanoic acid	 C ₈ H ₁₆ O ₂

ID	Retention Time (min)	Compound Name	Skeletal and Chemical Formulae
14	30.1	2-Decanal	 C ₁₀ H ₁₈ O
15	31.7	Benzene-heptyl	 C ₁₃ H ₂₀
17	35.4	2-Undecanal	 C ₁₁ H ₂₀ O
18	40.0	17-Octadecenoic acid	 C ₁₈ H ₃₂ O ₂
19	45.1	1-Hexadecanol	 C ₁₆ H ₃₄ O
20	63.7	Palmitic acid	 C ₁₆ H ₃₂ O ₂
21	65.9	9-12 Octadecanoic acid	 C ₁₈ H ₃₂ O ₂
22	69.0	trans-13-Octadecanoic acid	 C ₁₈ H ₃₄ O ₂
23	70.7	Oleic Acid	 C ₁₈ H ₃₄ O ₂

ID	Retention Time (min)	Compound Name	Skeletal and Chemical Formulae
24	71.2	Linoleic Acid	 <p>C₁₈H₃₂O₂</p>
25	73.2	cis-vaccenic Acid	 <p>C₁₈H₃₄O₂</p>
26	78.9	9-Octadecanal	 <p>C₁₈H₃₄O</p>

Overall, the major products from the pyrolysis of jatropha oil in the Pyroprobe CDS 5200 system in the absence of a catalyst varied depending on the process temperature. At the lower temperatures of 400 °C and 500 °C (Figure 4-6 & Figure 4-7) the most prevalent group of products were acids with some aldehydes, alcohols, aliphatics and aromatics. At the higher temperature of 600 °C, although a large proportion of acids were still present it was about half the proportion than at lower temperatures. As for the proportion of aliphatics this was around three times higher at 600 °C than at 500 °C. This was in addition to greater fractions of major compound groups including aromatics, aldehydes and alcohols.

The three main three fatty acids of jatropha oil composition were identified in all the chromatograms (Figure 4-6, Figure 4-7 & Figure 4-8) at 70.7 minutes for oleic acid, 71.2 minutes for linoleic acid and 63.7 minutes for palmitic acid, for all of them. The number of other products from the decomposition of jatropha oil, considering the chromatograms (Figure 4-6, Figure 4-7 and Figure 4-8) and Table 4-3, is significantly more complex than that of oleic acid. The presence of greater fractions of other functional groups is highly desirable as this is indicative of triglyceride molecules in jatropha oil decomposing more readily than the oleic acid compound on its own.

This complexity was anticipated, so it is intended that data and observations from the oleic acid decomposition can be utilised in the analysis of the decomposition of the jatropha oil for comparison to reduce this complexity.

The most significant observation is the number of increased peaks on the left-hand side of the chromatograms which are due to the presence of a greater number of lower molecular weight compounds including aromatics. The increased complexity of jatropha oil compared to oleic acid is owed to the fact that whereas oleic acid is a single compound, jatropha oil comprises of triglyceride molecules with multiple different fatty acid chains alongside glycerol[3]. The increased variety of products is clearly presented in Figure 4-9 below which shows the proportions of different major groups of compounds present.

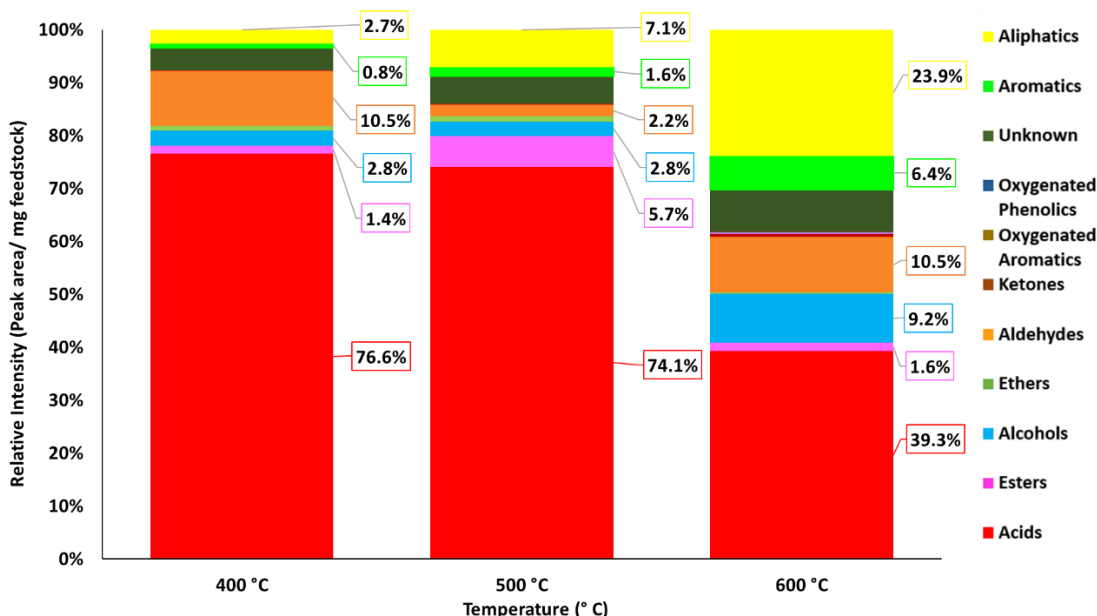


Figure 4-9. Product composition of jatropha oil pyrolysis at different temperatures *average values from duplicate runs

The graph shown in Figure 4-9 clearly shows the variety of products including aliphatics, ketones, aldehydes, alcohols, esters, and aromatics. With the largest proportion of other functional groups besides acids present at the higher temperature of 600 °C.

The first observation of interest is a trend similar to that was observed with oleic acid. It appears that in the case of jatropha oil the proportion of aliphatics also increases with temperature. At lower the lower temperature of 400 °C only 2.7 % of the peak area is attributed to aromatics, yet at the higher temperatures of 500 °C and 600 °C this increases to 7.1 % and a much increased 23.9 % respectively.

This supports the earlier statement when considering the decomposition of oleic acid that more aliphatics are obtained at the higher temperatures. A potential explanation for this could be owed to the fact that in jatropha oil, oleic acid is the most prevalent which is followed by linoleic and palmitic acid. Of these two other fatty acids linoleic has 2 carbon-carbon double bonds, whereas palmitic has none. With this in mind it could be inferred that at the lowest temperature of 400 °C the majority of the decomposition products will come from the decomposition of palmitic acid as this compound will more likely decompose at lower temperatures due to only having one single bond. Then at the higher temperatures of 500°C and 600 °C the palmitic acid would decompose even more readily. As for linoleic acid because it has two double bonds this would require the most energy in comparison to oleic and palmitic acid, as it is well known that double carbon bonds require more energy to break.

This is supported by a less significant reduction in acid contents at the lower temperatures of 400 °C and 500 °C. The decrease here is just noticeable from 76.6 % of the peak area to 74.1% of the peak area. Whereas at the higher temperature the decrease is more drastic from 74.1 % to just 39.3 % at 600 °C. Therefore, the substantial drop in the proportion of acids at the highest temperature of 600 °C is suggested to be because at this highest temperature there is enough energy to break more of the double bonds in both the oleic acid and linoleic acid than at the lower temperatures. This would be supported by the same decomposition mechanisms for the production of aliphatics from oleic acid. This includes the pathway suggested by Schwab et al. via pathways A, B and C (Figure 2.11) discussed earlier in the decomposition of the oleic acid in addition to the mechanism from Idem et al via pathways 1 and 4 (Figure 2.15,), as this supports the decomposition of both saturated and unsaturated triglycerides.

In the case of the proportion of aromatic compounds this increases from a very small 0.8 % of the peak area at 400 °C up to 1.6 % at 500 °C before increasing further to 6.4 % at 600 °C (Figure 4-9). This proportion of aromatics includes compounds such as benzene, toluene, p-xylene, and smaller amounts of ethylbenzene. The aromatics yields are greater than those obtained from oleic acid pyrolysis on its own at 1.7 % vs 6.4 % from the pyrolysis of jatropha oil both at the highest temperature of 600 °C. This could be attributed to the presence of additional fatty acids including linoleic and palmitic acid which are also decomposing to form aromatic compounds. For saturated fatty acids Chang et al., 1947 suggested that once alkanes are formed (part of the aliphatics group) aromatic cyclization of these alkanes can yield aromatics alongside hydrogen. However, this contradicts the pathway for saturated fatty acids proposed by

Alencar et al 1983 whom did not discuss the presence of aromatics. There has already been discussion suggesting that the palmitic acid decomposes at the lower temperature owing to having no double carbon bonds. If this is the case then then at the lower temperature of 400 °C where the palmitic acid should be breaking down, there should be a very small proportion of aromatics as is the case with just 2.7 % aliphatics and 0.8 % aromatics (Figure 4-9).

This in turn would mean that it is the unsaturated fatty acids oleic and linoleic acid that are contributing most significantly towards the aromatic group of compounds at the higher temperatures of 500 °C and 600 °C respectively. There is further evidence to support the decomposition of linoleic acid into aliphatics compounds as shown by Frankel et al. 1984, who proposed the following decomposition mechanism in Figure 4-10 below for linoleic acid.

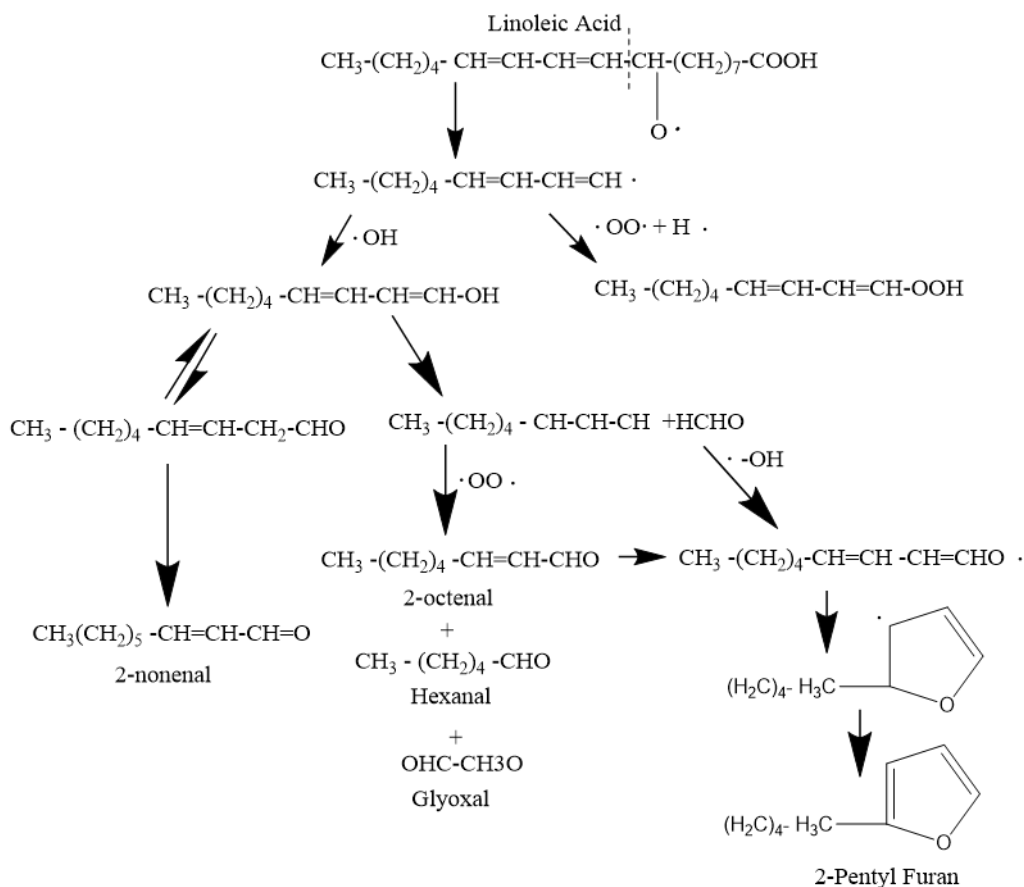


Figure 4-10. Decomposition of linoleic acid (Frankel et al 1984)[191]

In Figure 4-10 in addition to the presence of aliphatics there are also aldehyde products. This is of significance as in addition to an increase in aromatics and aliphatics at the higher temperature of 600 °C there is also a much larger proportion of aldehydes. The proportion of aldehydes varies and at the lowest temperature of 400 °C is 10.5 % of the peak area, which then drops to 2.5 % at 500 °C but increases once again at

600 °C to 10.5 %. When comparing the chromatograms for the three different temperatures besides the peaks of the fatty acids present one of the most significant peaks on the chromatogram at 600 °C (Figure 4-3) was observed at around 6 minutes, which was attributed to the aldehyde compound hexanal. The decomposition of hexanal is reported by multiple authors [191-194]. An example of one of these pathways from Shi et al. 1994, is shown in Figure 4-11 below:

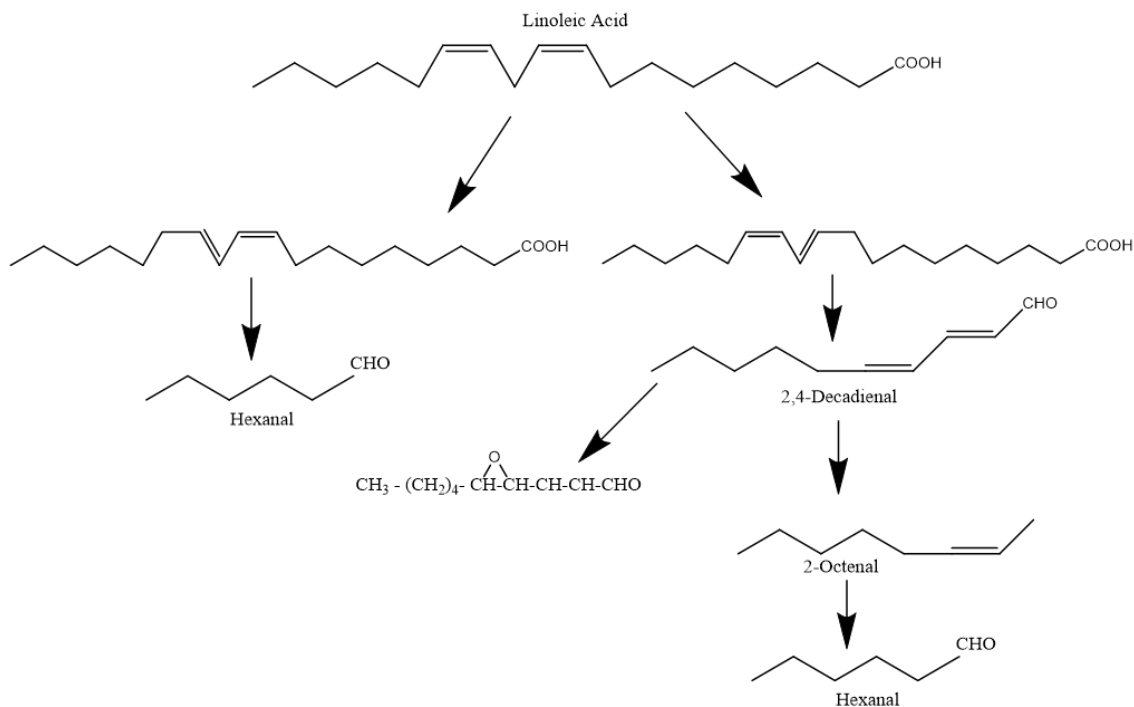


Figure 4-11. Decomposition of linoleic acid (Shi et al 1994, *adapted from graphic by Jayasena et al 2013)
[192](Shi et al 1994, *adapted from graphic by Jayasena et al 2013)

Here the decomposition of linoleic acid to hexanal is the final product of both the left- and right-hand side pathways, via left pathway (A) the linoleic acid decomposes into 13-hydroperoxy-octadecadienoic acid (HPODE) and subsequently into hexanal. Then via the right-hand side pathway (B), 9-hydroperoxy-octadecadienoic acid is formed followed by a succession of aldehyde compounds including 2,4-decadienal, 2-octenal and finally hexanal. As for the It can be observed on the right pathway that further aldehyde products such as 2,4-decadienal and 2-octenal are also produced. There are other aldehyde compounds are similar to others identified within the chromatograms in this work including nonanal at 20.1 minutes and decanal at 25.7 minutes in both the pyrolysis of oleic acid and jatropha oil. Therefore, oleic acid may also contribute to the production of some of these aldehyde compounds. This is supported by Cao et al. it was suggested that aldehyde compound nonanal was derived from the oleic acid compound rather than linoleic acid as shown by Figure 4-12 below [194]. .

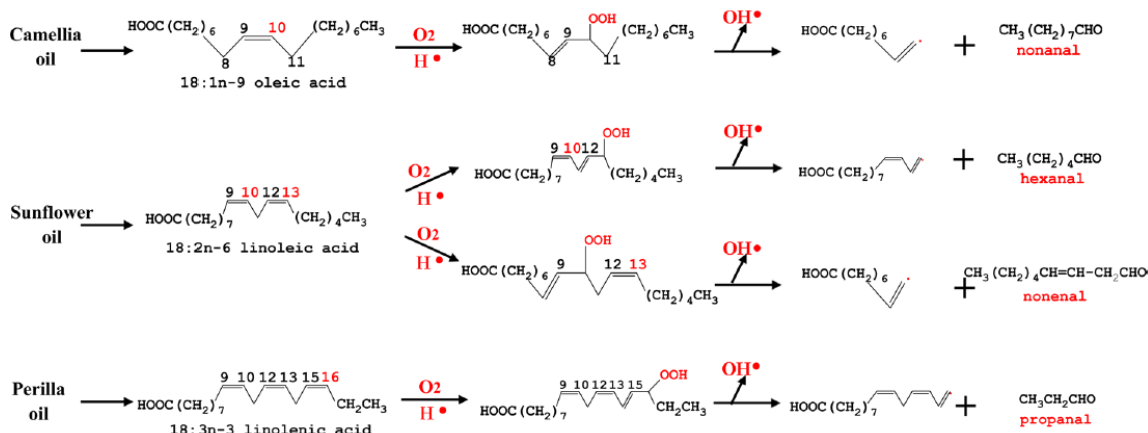


Figure 4-12. Decomposition of oleic and linoleic acid to aldehyde compounds[194]

This decomposition pathway in Figure 4-12 further supports hexanal being derived from linoleic acid as suggested by Shi et al. and Frankel et al. respectively. In addition to nonanal and hexanal being derived from linoleic acid. The pathway in Figure 4-12 also shows the product propanal but as this compound was not identified at any of the temperatures evaluated. This suggests the latter isomer of linoleic acid (18:3n-3 linoleic acid- Figure 4-12) was perhaps not present in the jatropha oil feedstock. Owing to the increased presence of aldehydes more so than aromatics at it appears that in the case of the non-catalytic decomposition of jatropha oil that the pathways producing aldehyde compounds are favoured.

This decomposition of unsaturated fatty acid into aldehydes is further supported by the mechanism suggested by Idem et al. (Figure 2.15). In their work canola oil was used as feedstock which shares similar major fatty acids to jatropha oil. For example, whilst jatropha oil is typically ~46 wt.% oleic acid, canola oil has between 50-65 wt.% [195]. From the decomposition scheme for a canola oil feedstock (Figure 2.15), aldehydes (RCHO) are considered a decomposition product via pathways 1 and 2, with these pathways also yielding carboxylic acids (RCOOH) and carboxylate esters (RCOOR). This is of significance as in this work, all these functional groups have been identified from the non-catalytic pyrolysis of jatropha oil with the exception of a large proportion of ketones at higher temperatures. However, this difference could be linked to the different type of feedstock used in their work (canola oil) and in this work (jatropha oil)[123]. The types of products observed by Idem et al. and in this work are also similar to those observed by Jiang et al. 2021 whom undertook the pyrolysis of oleic acid at 300 °C, 400 °C and 500 °C using a TG-FTIR system.

An overview of the decomposition of oleic acid compound, highlighting how its decomposition gives rise to certain products is shown below in Figure 4-13[196].

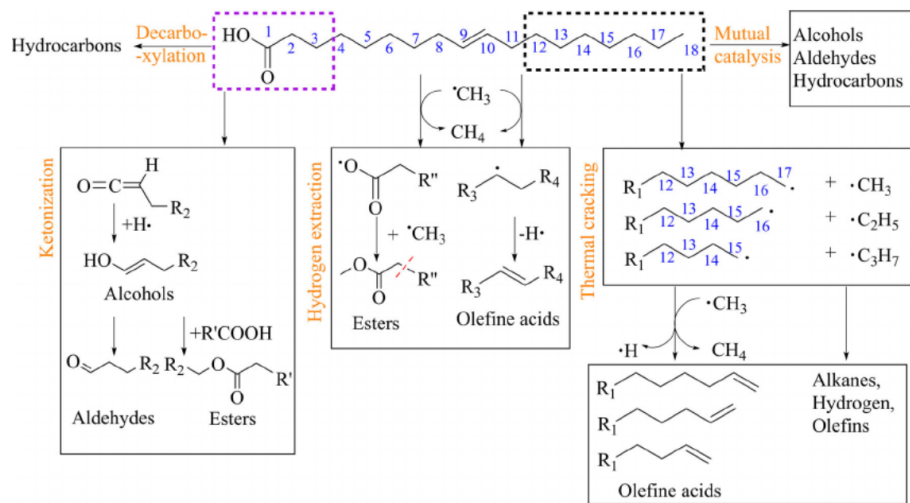


Figure 4-13. Degradation products of oleic acid from different parts of the fatty acid molecule [196]

In addition to the schematic in Figure 4-13, it can be noted that Jiang et al. also observed an increase in the hydrocarbons at higher temperatures, alongside a reduction in the acids content. As well as considering decomposition of the fatty acids within the jatropha oil, glycerol is another compound that contributes to the composition of this feedstock as part of the triglyceride molecules. In literature by Castello et al. 2014, focusing on the pyrolysis of glycerol concluded that glycerol's high thermal stability meant that even temperature above temperature of 600 °C there was little conversion of the feedstock even when in the presence of a catalyst[197].

This is of significance because this work has been conducted at temperatures of 400 °C, 500 °C and 600 °C. Therefore, it is unlikely that the decomposition of glycerol has implicated the product distribution at temperatures below 600 °C. As indicated previously in Figure 4-9 showing an overview of the proportions of major groups of compounds present from the pyrolysis of jatropha oil, it is clear that the increased temperature of 600 °C causes more significant changes in the distribution of the products than the temperature increases from 400 °C to 500 °C. So perhaps that it is at this higher temperature of 600 °C the glycerol component of the jatropha oil feedstock is decomposing. One of the most noticeable proportion changes at the highest temperature is the increased proportion of alcohols which contributes to 9.2 % of the peak area at 600 °C versus just 2.8 % of the peak area at the lower temperatures of 400 °C and 500 °C. The decomposition of glycerol into alcohols products has been observed in various literature sources[198-201].

The scheme in Figure 4-14 shows a range of alcohol and aldehyde products that glycerol can produce via several decomposition pathways.

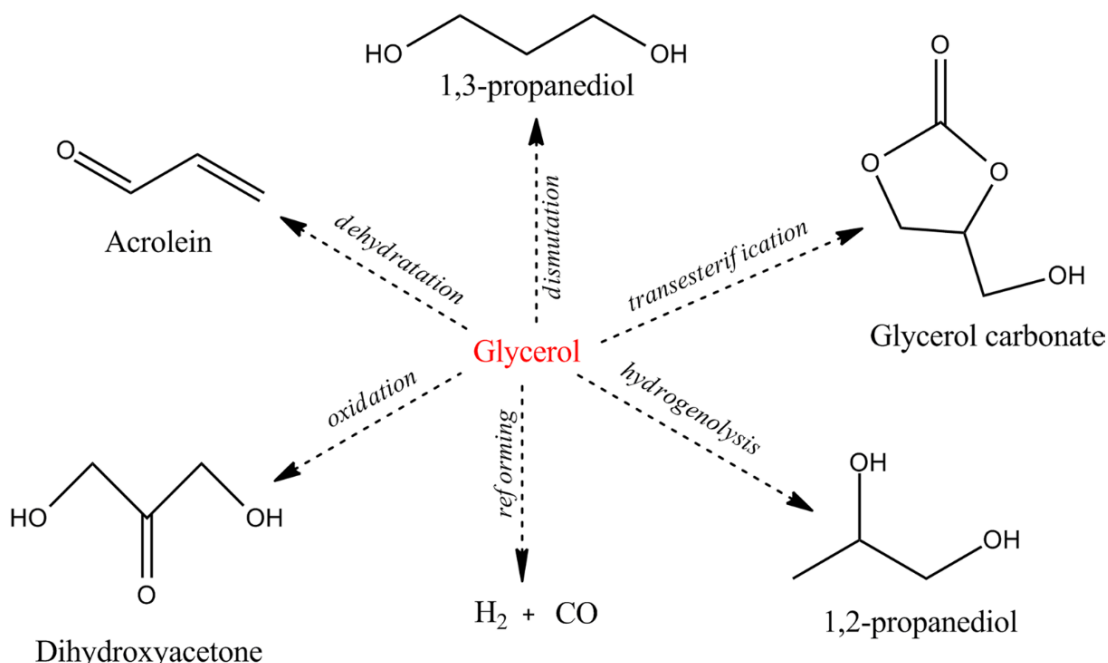


Figure 4-14. Glycerol decomposition products, Mitrea et al. 2017 [201]

In these non-catalytic experiments with jatropha oil there were no examples of products similar to those in Figure 4-14. This is likely attributed to the high thermal decomposition temperature of glycerol (600 °C), which means that in this work there has been no significant decomposition of this compound and therefore none of the compounds shown in Figure 4-14 were observed due to the maximum investigation temperature being 600 °C. The main alcohol peak at any of the temperatures was 1-hexadecanol at 45.1 minutes. Owing to long hydrocarbon chain it is believed that this alcohol compound is derived from one of the fatty acid compounds.

4.3.Comparing decomposition pathways for oleic acid and jatropha oil

The most obvious similarity between the decomposition of oleic acid and jatropha oil was the trend with the increasing aliphatics content due to the presence of alkene and alkane compounds as the temperature increased from 400 °C to 600 °C. The production of alkane and alkene compounds appear to be a shared initial decomposition step with the most aliphatics being produced at the higher temperature of 600 °C in the case of both feedstocks. This is associated with the enhanced breakage of carbon-double bonds of oleic and linoleic acid at the higher reaction temperature of 600 °C. If even higher temperatures were used then there may well be a further increase in the proportion of aliphatics and in turn proportions of other compounds including aromatics and aldehydes. However, it is questionable how much a further increase in temperature will implicate the proportions of compounds as there although there was noticeable difference between the temperatures of 400 °C and 500 °C they were fairly similar. If this were to be the case for the temperatures of 600 °C and 700 °C then increasing the temperature would provide little benefit and would ultimately just make the process more costly.

The major difference between the two feedstocks decomposition is the number of pyrolysis products, with jatropha oil giving rise to more owing to its increased complexity being a mixture of triglyceride molecules rather than a singular fatty acid compound. This included a more varied range of hydrocarbons in particular aldehydes, esters and alcohols which were only seen in very small or negligible amounts with the decomposition of oleic acid. It was determined that the alcohol products are most likely from the further decomposition of one of the fatty acids within the jatropha oil such as linoleic or palmitic acid owing to the fact that the same increase in alcohol content was not observed with oleic acid. This was supported by the fact that the alcohol compounds associated with the decomposition of glycerol and this was most likely due to the high decomposition temperature of the compound.

4.4. Conclusions

It was possible to conclude based on experimental results concerning the non-catalytic pyrolysis of oleic acid and jatropha oil at the temperatures of 400 °C, 500 °C and 600 °C that a high proportion of the feedstock is still present as acid compounds. This is attributed to the presence of the double bonds in the oleic and linoleic fatty acid compounds which are difficult to break at the lower reaction conditions investigated (400 °C & 500 °C). It was observed that as the reaction temperature increased the proportion of aliphatic compounds increased marginally at the lower temperatures (400 °C & 500 °C) and then more significantly at the highest reaction temperature (600°C) from accounting for 0.70 % to 0.82 % to 7.99% of the peak area at 400 °C, 500 °C and 600 °C respectively. This occurred alongside an increase in the proportion of aromatic compounds. However, in both cases the proportion of aromatics compounds remained small, with the maximum proportion obtained at just 6.4% of the peak area from Jatropha oil at a temperature of 600 °C.

By considering the pyrolysis of both oleic acid and jatropha oil it was possible to ascertain that it is highly likely a proportion of the aldehyde compounds such as nonanal was obtained from its decomposition of oleic acid. Therefore, investigating the decomposition of the fatty acid compound on its own has helped to establish the decomposition pathways of Jatropha oil. With the low proportion of aromatics, it appears that their decomposition to aliphatic and aldehyde products is favoured in the non-catalytic decomposition of these feedstocks. In the following chapter the catalytic decomposition of these feedstocks will be considered under the same reaction conditions. It is anticipated that the addition of a catalyst will enhance the formation of the higher value aromatic compounds, formed via the Diels-alder pathway which could increase the proportion of aromatic products.

CHAPTER 5.0 CATALYTIC DECOMPOSITION OF OLEIC ACID AND JATROPHA OIL

5.1. Introduction and aims

This chapter will assess the pyrolysis of oleic acid and jatropha oil in the presence of a selection of catalysts at three different temperatures (400 °C, 500 °C and 600 °C). It is intended the pyrolysis tests will ascertain if the utilisation of differing temperatures, in addition to using different catalysts will have an impact upon the yield and distribution of aromatics compounds such as Benzene, Toluene and Xylenes (BTX) alongside other products of the feedstock decomposition. As stated in Chapter 4.0 The temperature range was selected based on a range of studies concerning the conversion of various triglyceride feedstocks varying the pyrolysis temperatures between 375 °C and 650 °C (Chapter 2.0, section 2.3.2, Table 8).

These investigations were conducted in a Pyroprobe CDS 5200 system couple to a GCMS as described earlier in section 3.3.4.1. This Pyroprobe system was utilised due to several advantages which were discussed earlier in Chapter 4.0 regarding the thermal decomposition of oleic acid and jatropha oil. The small sample size of feedstock and catalyst required for these investigations was of very useful in this work as this meant the catalysts used for the experiments could be made in one batch with the same being used throughout the investigations allowing for greater continuity.

It is intended this work will evaluate what effect the utilisation of the catalyst has on the decomposition of oleic acid and jatropha oil. It is anticipated that the application of these catalyst will allow production of higher value compounds including aromatics. With the information obtained from this work the intention is to be able to recommend the best combination of catalyst and process temperature for the conversion of a jatropha oil feedstock in the bench scale fluidised bed reactor discussed in Chapter 6.0 of this work. This recommendation will be supported by a comparison of data obtained from non-catalytic investigations in both of the Pyroprobe CDS5200 system and fluidised bed reactor.

5.2. Catalyst characterisation

Several investigations to characterise the catalysts utilised in this work were conducted on samples of the commercially available ZSM-5 (Si/Al 30, Alfa Aesar™) and the four prepared Ni/ZSM-5 catalysts, 1Ni/ZSM-5, 2Ni/ZSM-5, 5Ni/ZSM-5 and 10Ni/Ni/ZSM-5. It is intended that information gathered from these analyses will be useful in analysis of the catalytic decomposition results and assist with the explanation of preferred pathways or products.

5.2.1.Thermogravimetric analysis (TGA)

In this work fresh samples of the catalysts investigated in this work (ZSM-5, 1Ni/ZSM-5, 2Ni/ZSM-5, 5Ni/ZSM-5 and 10Ni/ZSM-5) were assessed for their moisture content. It was necessary to determine this parameter owing to the very small proportions of catalyst being utilised in the pyroprobe analysis and as such small amounts of moisture would implicate the catalyst to feed ratio.

It is known that changes in mass at given temperatures can be indicative of the loss of certain compounds i.e., loss of moisture will be most noticeable around the temperature of 100 °C as this is the boiling point of water. Typically, mass lost due to the presence of moisture will firstly occur as the temperature rises to 150 °C due to the presence of physiosorbed water, followed by secondary mass lost between 150 °C and 250 °C due to the presence of chemisorbed water[160]. Over this temperature range low molecular weight volatile compounds, solvents, trapped gases may also evolve [160]. As for determining the presence of volatiles and fixed carbon content then temperatures up to 700 °C and 950 °C maybe utilised respectively[202]. The values obtained are surmised below in Table 5-1

Table 5-1. Catalyst moisture content

Catalyst	Moisture Content (wt.%)
ZSM-5	3.33%
1Ni/ZSM-5	2.45%
2Ni/ZSM-5	6.45%
5Ni/ZSM-5	6.38%
10Ni/ZSM-5	6.00%

The difference in the values observed in Table 5-1 for the 1Ni/ZSM-5 and other Ni/ZSM-5 catalysts could be attributed to the fact they were prepared and tested on different days. This could mean that in the preparation and testing of 1Ni/ZSM-5 it was less humid conditions or there were discrepancies in the process used to prepare the catalyst. The ZSM-5 was commercially prepared so that was anticipated to be different.

5.2.2. N₂ porosimetry

Fresh samples of the catalysts used in this work (ZSM-5, 1Ni/ZSM-5, 2Ni/ZSM-5, 5Ni/ZSM-5 and 10Ni/ZSM-5) were analysed to determine their surface area and porous properties. The analyses were carried out in triplicate to ensure data was repeatable. It was reported in literature that errors associated with this type of gas adsorption analysis are related to both instrumental error as well as sample preparation. The results can be implicated when there are variations in degassing

conditions such as time and temperature[163]. This catalyst surface area (S_{BET}) was determined via the BET method in addition to the pore volume (V_p) and pore diameter (D_p) via the BJH method. The N_2 adsorption- desorption isotherms for the catalysts investigated are shown below in

Figure 5-1.

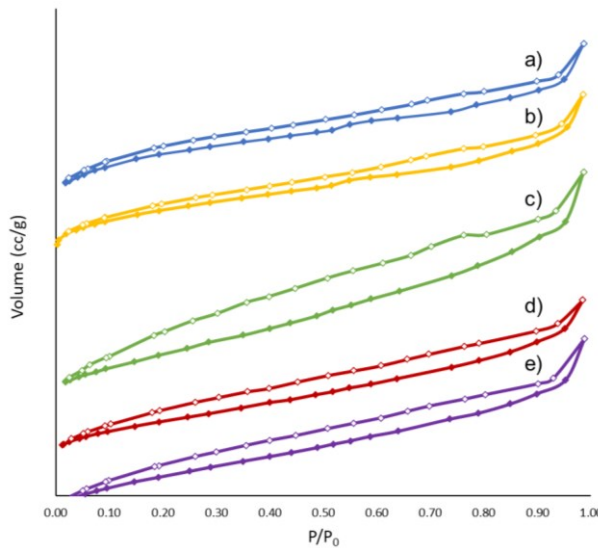


Figure 5-1. N_2 adsorption-desorption isotherms (a) ZSM-5, (b) 1Ni/ZSM-5, (c) 2Ni/ZSM-5, (d) 5Ni/ZSM-5, (e) 10Ni/ZSM-5

The five isotherms are fairly similar in terms of adsorption and also desorption with the exception of a difference in the desorption isotherm for the 2Ni/ZSM-5 catalyst. When considering the IUPAC (International Union of Pure and Applied Chemistry) it is possible to identify these isotherms as a Type IV isotherm from Figure 5-2 below.

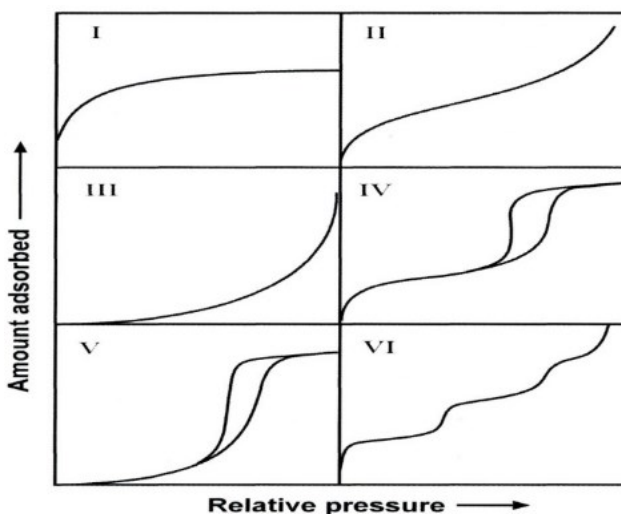


Figure 5-2. IUPAC adsorption-desorption isotherms[203]

This isotherm type is typically associated with mesoporous materials. A further feature of Type IV isotherms as seen in Figure 5-2 is the hysteresis loop which can present

itself in different ways as shown by Figure 5-3 below. This is of significance as the different shapes in this hysteresis loop are indicative of the pore size distribution and shape of the catalyst pores[132, 140, 203].

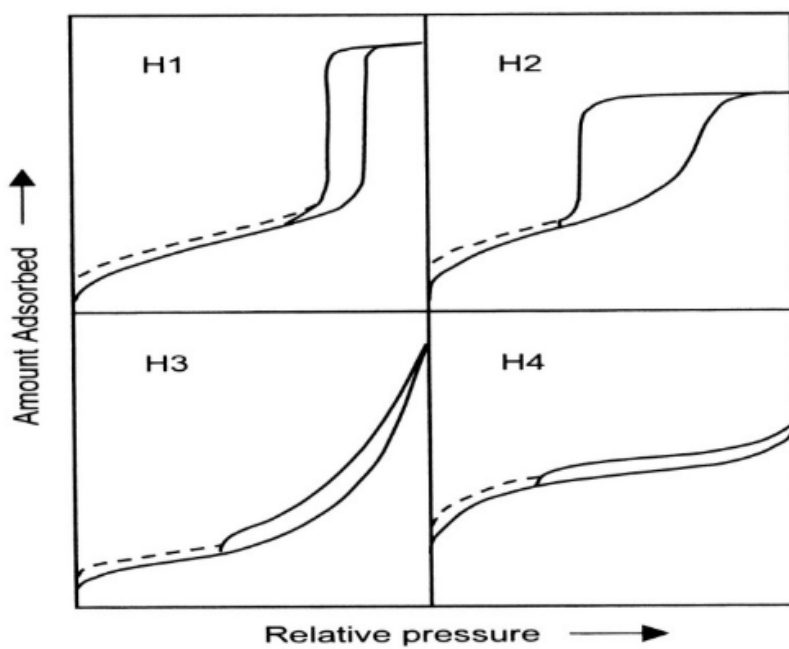


Figure 5-3. Hysteresis loops in type IV and type V isotherms[203]

From Figure 5-3 the hysteresis loop observed from the isotherms obtained in this work when compared to

Figure 5-1 is quite broad and match best with the H4 hysteresis loop. This type of loop is associated with narrow slit like pores. These results are similar to those presented by several authors including Sakar 2012 et al., Teh et al. 2015, Hoan et al. 2019 and Wei et al. 2020, whom all observed similar type IV isotherms with a hysteresis loop[204-207]. The main difference in these results is the 2Ni/ZSM-5 desorption isotherm does not seem to follow completely the same trend. At lower pressures unlike the other catalysts there is near to no overlap in the adsorption and desorption curves. Wei et al. 2020 suggests the overlap of these branches suggests the presence of both microporous and mesoporous structure. As type IV isotherms are associated with mesoporous materials it suggests that perhaps the 2Ni/ZSM-5 has different pore structure to the other catalysts.

This can be evaluated by considering the pore diameter and pore volume values obtained from the N₂ physisorption analysis which are presented alongside the surface area in Table 5-2 below. The presented values are averages of two or more data points.

Table 5-2. Properties of Ni/ZSM-5 catalysts

	V_p (cc/g)	D_p (nm)	S_{BET} (m ² /g)
ZSM-5	0.195 ±0.001	1.505 ±0.064	383.0 ±9.6
1Ni/ZSM-5	0.197 ±0.012	1.528 ± 0.012	370.0 ±8.7
2Ni/ZSM-5	0.234 ±0.027	2.021 ± 0.011	332.2 ±64.3
5Ni/ZSM-5	0.186 ±0.014	1.606 ± 0.350	347.6 ±21.5
10Ni/ZSM-5	0.144 ±0.072	1.555 ± 0.016	317.4 ±3.2

From the data presented in Table 5-2 the pore volume and pore diameter appear to increase with Nickel loading to a point and then decrease again at higher loadings. For both the pore volume and pore diameter maximum values are obtained from the 2Ni/ZSM-5 of 0.234 cc/g and 2.021 nm respectively. When considering pore diameter it is of significance to note that materials 2-10 nm are considered mesoporous materials[137]. Therefore, the earlier assumption that the 2Ni/ZSM-5 catalyst may have larger pores due to less overlap in the adsorption and desorption isotherms was correct.

Furthermore, it can be observed for the most part that as the nickel loading of the catalyst is increased the surface area of the catalyst is decreasing. This is with the exception of the value obtained for 2Ni/ZSM-5. Although, the surface area of the 2Ni/ZSM-5 catalyst is slightly lower than anticipated at 332.2 ±64.3 m²/g it was only possible to obtain 2 data points for this value and as such the standard error is fairly significant, therefore the actual surface area of the catalyst could still follow this trend. This would be also be supported by literature as the reduction in BET surface area of the catalysts with increasing nickel loading was expected and has been observed by others including Dewajani et al. 2016, Sriatun 2019 and Wei et al. 2020 [152, 207, 208]. These authors highlight that the reduction in surface area is attributed to the distribution of the nickel metal across the ZSM-5 surface, the nickel metal is accumulated either at the mouth of the pore or is unevenly distributed across the surface of the ZSM-5.

5.2.3. X-ray diffraction (XRD)

XRD analyses were carried out on fresh catalyst samples (ZSM-5, 1Ni/ZSM-5, 2Ni/ZSM-5, 5Ni/ZSM-5 & 10Ni/ZSM-5) in order to identify the crystalline phases present. The analysis was completed using a Bruker D8 Advance diffractometer in Bragg Brentano mode using parameters earlier defined in Chapter 3.0, experimental methodology, section 3.3.2.3. The data obtained from the analyses by the DIFFRAC EVA 3.0 software is presented below in Figure 5-4.

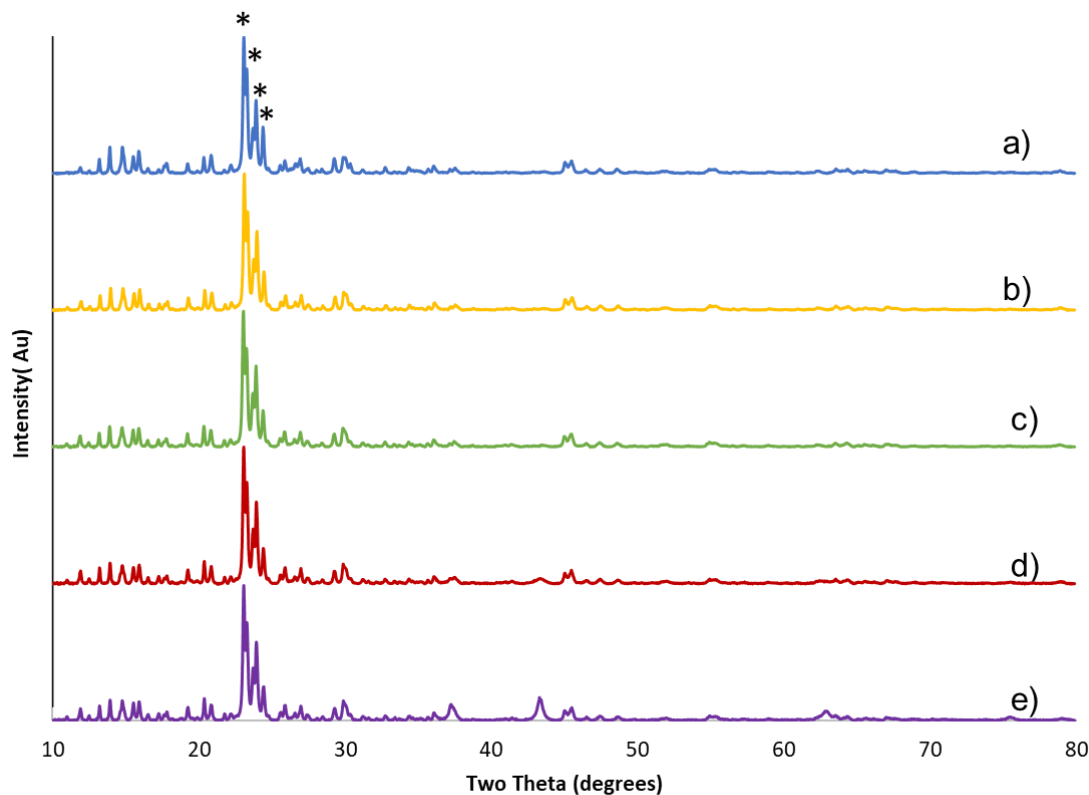


Figure 5-4. XRD Diffraction Pattern for a) ZSM-5 b) 1Ni/ZSM-5 c) 2Ni/ZSM-5 d) 5Ni/ZSM-5 e) 10Ni/ZSM-5

The XRD pattern in Figure 5-4 shows various peaks some of which are attributed to the ZSM-5, whilst others are associated with the differing amounts of nickel on each of the catalysts. The main peaks associated with the ZSM-5 catalyst were visible in the range 23 ° to 25 ° as denoted by the asterisks. This agrees with results reported in the literature [46, 71, 111], which also indicates that the preparation method used has not altered the ZSM-5 zeolite's structure. The next peaks to consider, that are of most significance is those associated with the nickel addition. The DIFFRAC EVA database was used to analyse the diffraction patterns to ascertain what peaks were suggested to be associated with the nickel metal. It highlighted several peaks for both nickel and nickel oxide in two different searches which appear as peak lists.

The identified peaks all of which were determined to be nickel oxide. The peaks were observed at $2\theta = 37.2^\circ$, 43.3° , 62.9° and 75.2° . These peaks correspond to the (111), (200), (220) and (311) crystal faces respectively [209, 210]. These peaks are shown in closer detail in Figure 5-5a , b, c and d below. It can be observed that almost of these peaks are fairly broad perhaps with the exception of the 37.5° and 43.3° peak for 10Ni/ZSM-5.

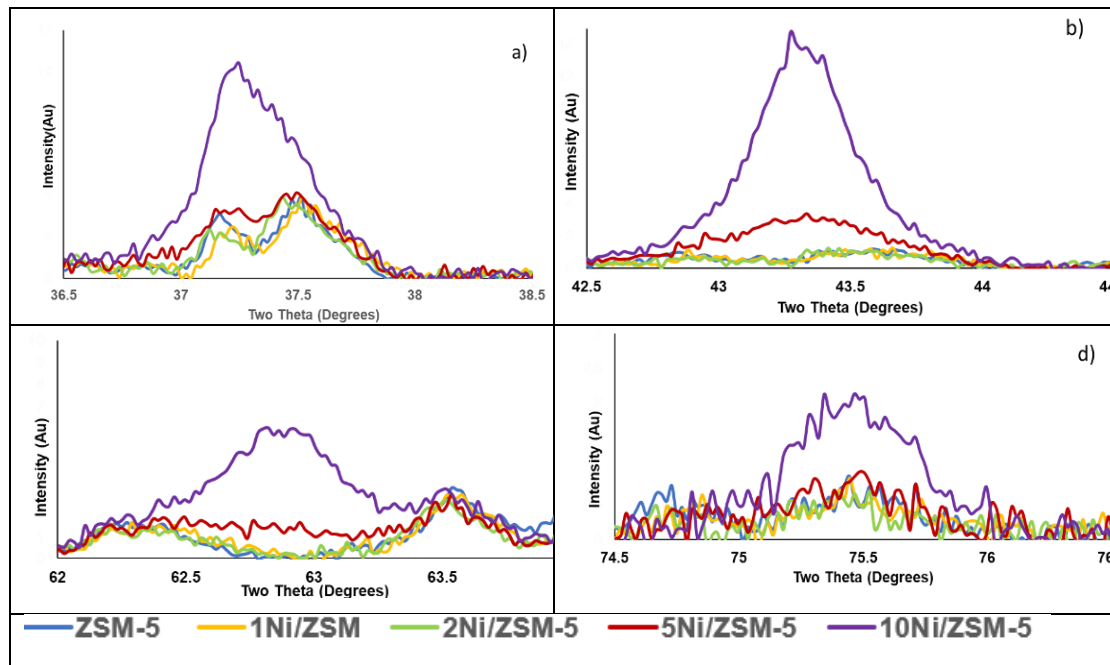


Figure 5-5. XRD NiO peaks at 2θ , a) 37.2° b) 43.3° c) 62.9° d) 75.2°

The peaks observed in Figure 5-5 are also identified by multiple other studies who obtained similar peaks with nickel modified catalysts [57, 117, 155, 209, 210]. From these images (Figure 5-5 a-d) it is clear that these are broad peaks which can be indicative of poor crystallinity [209]. It is suggested in literature that poorer crystallinity catalysts maybe able to yield higher proportions of liquid products because that structure maybe more accessible for larger molecules[49]. This is desirable as it was indicated in section 2.3 that aromatic compounds including BTX are typically contained within the liquid products.

5.3.Catalytic decomposition using a pyroprobe GCMS

5.3.1.Introduction and aims

This section will assess the products from the pyrolysis of oleic acid and jatropha oil in the presence of a catalyst (ZSM-5, 1Ni/ZSM-5, 2Ni/ZSM-5, 5Ni/ZSM-5 & 10Ni/ZSM-5) at three different temperatures (400 °C, 500 °C, and 600 °C). The pyrolysis tests will ascertain if the utilisation of different temperatures in conjunction with a catalyst has an impact upon the yield and distribution of aromatics including BTX as well as other major functional groups.

These investigations were conducted in a Pyroprobe CDS 5200 system as described in section 3.3.4.1. The advantages of using this system i.e., small sample size, short analysis time etc., were highlighted earlier in section 4.1., concerning the non-catalytic decomposition of oleic acid and jatropha oil. In these investigations, the preparation steps and analysis as in section 4.2 concerning the non-catalytic pyrolysis of oleic acid and jatropha oil.

It is intended that studying the catalytic decomposition of both oleic acid and jatropha oil will allow the deduction of the decomposition pathways, focusing on the production of high value aromatic compounds such as benzene, toluene, and xylenes. From literature there are some catalytic decomposition pathways of triglycerides as well as those that consider the production of aromatics from triglycerides components i.e., glycerol [120]. The data obtained in these investigations will be utilised in future work to optimise the investigations in the fast pyrolysis fluidised bed system for the production of aromatics. This will require the selection of the catalyst and temperature that favours the production and yield of the most desirable aromatic compounds.

5.3.2.Catalytic pyrolysis of oleic acid at different temperatures

A variable distribution of products from the catalytic pyrolysis of oleic acid (ZSM-5, 1Ni/ZSM-5, 2Ni/ZSM-5, 5Ni/ZSM-5 & 10Ni/ZSM-5), at different temperatures (400 °C, 500 °C and 600 °C) was observed. Overall, it was noted that at 400 °C for any of the catalysts tested, the acid functional group was the major group in the products, with between 48.4% and 69.7%. This contribution was reduced to around 26.8 % to 48.4% by increasing the temperature to 500 °C, leading to the formation of aromatics in the range of 33.5 % to 44.4%, for any of the catalysts tested as shown later in Figure 5-7. Finally, at 600 °C it was observed that the predominant group of compounds was heavily dependent upon the catalyst used. For example, in the presence of the ZSM-5, 1Ni/ZSM-5 and 10Ni/ZSM-5, acids remained as the dominant product, whilst in the presence of the 2Ni/ZSM-5 and 5Ni/ZSM-5, aromatics were the predominant compound.

The predominant functional identified at all three temperatures included acids, aliphatics and smaller amounts of alcohols which were similar to those from the non-catalytic pyrolysis of oleic acid (Chapter 4.0, section 4.2.1). However, there was also the addition of a much larger proportion of aromatics alongside the groups above, although their distribution was significantly different in the presence of the catalysts.

A comparison between the GC-MS chromatograms obtained from the non-catalytic and catalytic (ZSM-5) pyrolysis of oleic acid at 400 °C is shown below in Figure 5-6.

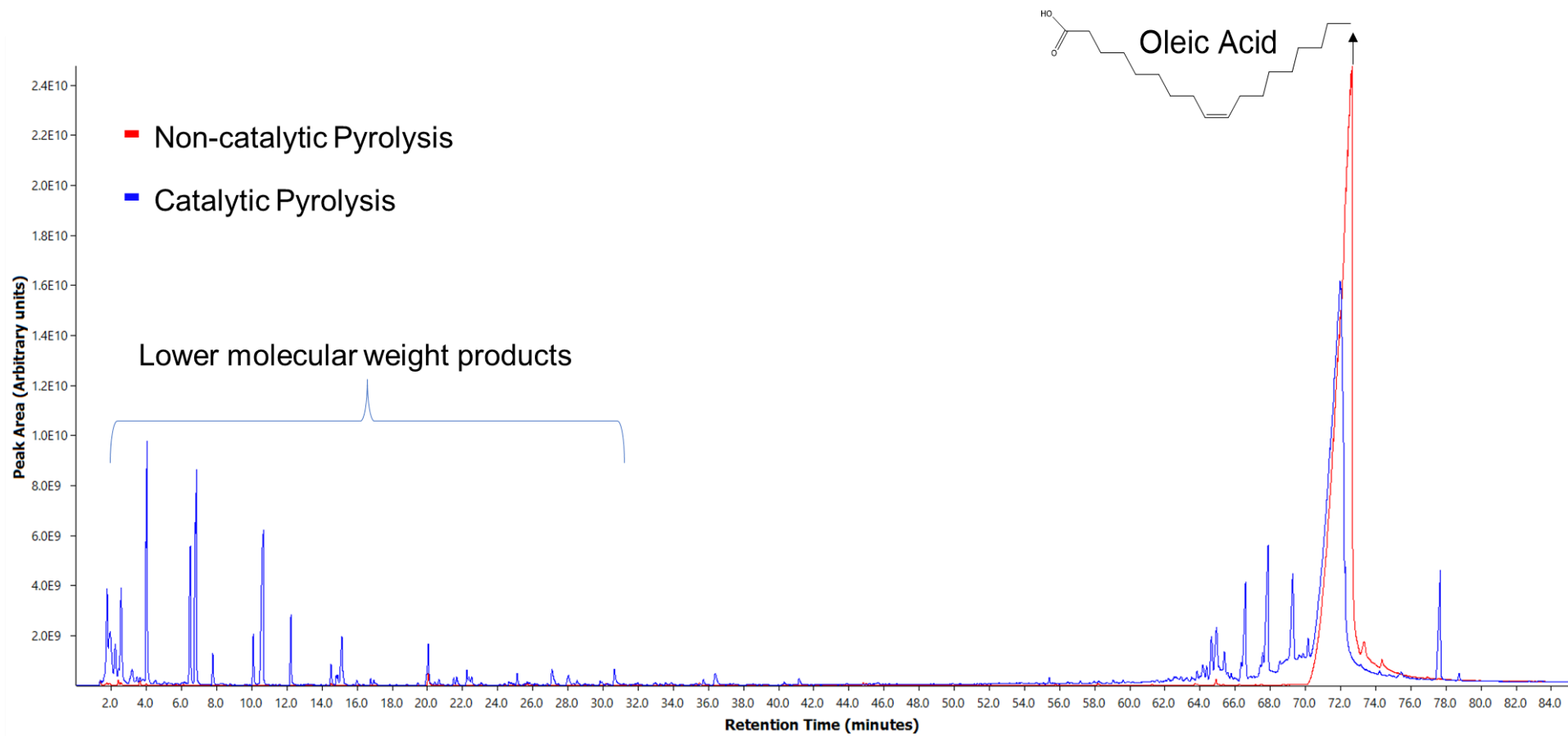


Figure 5-6. Py-GCMS chromatogram for the pyrolysis of oleic acid at 400 °C: without catalyst (red); and with ZSM-5 (blue).

From Figure 5-6 above the peaks at around 70.7 minutes are attributed to the feedstock oleic acid as identified in the non-catalytic pyrolysis of oleic acid using OpenChrom and NIST in Chapter 4.0, section 4.2.1. In the presence of the ZSM-5 catalyst (Figure 5-6, blue peaks) the oleic acid peak is significantly smaller than for the non-catalytic test. About 0.1 μL were used for non-catalytic investigations, whilst 0.5 μL were used for those with a catalyst, nevertheless the larger sample still shows a much smaller peak for the oleic acid (~70.7 min), which demonstrates the efficiency of the ZSM-5 catalyst to break down the initial oleic acid structure into other products.

The decomposition of the oleic acid feedstock to a wider range of lower molecular weight products is reflected in the number and intensity of the peaks on the left-hand side of the chromatogram (Figure 5-6, blue peaks). These products include aliphatics (cyclopropane 1-2, dimethyl (1.7 minutes), 1-petene, 3-methyl (1.9 minutes) and aromatics (benzene (2.6 minutes), toluene (4.1 minutes), p- xylene (6.5minutes), benzene,1 -ethyl, 4 -methyl (10.6 minutes) and mesitylene (12.2 minutes). As for peaks on the right-hand side of the chromatogram these still make up most of the products with oleic acid at 70.7 minutes as discussed earlier in addition to other compound such as 6-octadecenoic acid, methyl ester at 64.6 minutes, 9-12-octadecanoic acid at 66.0 minutes and 13-octadecanal at 68.0 minutes. The increased prominence of the lower molecular compound peaks is desirable as it indicates that the feedstock has been broken down into more compounds due to the presence of the catalyst.

The difference in the distribution of the major products can be observed in the graphs below at the different investigation temperatures (Figure 5-7). This shows the proportions of the different functional groups present such as acids, aromatics, aliphatics etc. at each of the process temperatures with each catalyst.

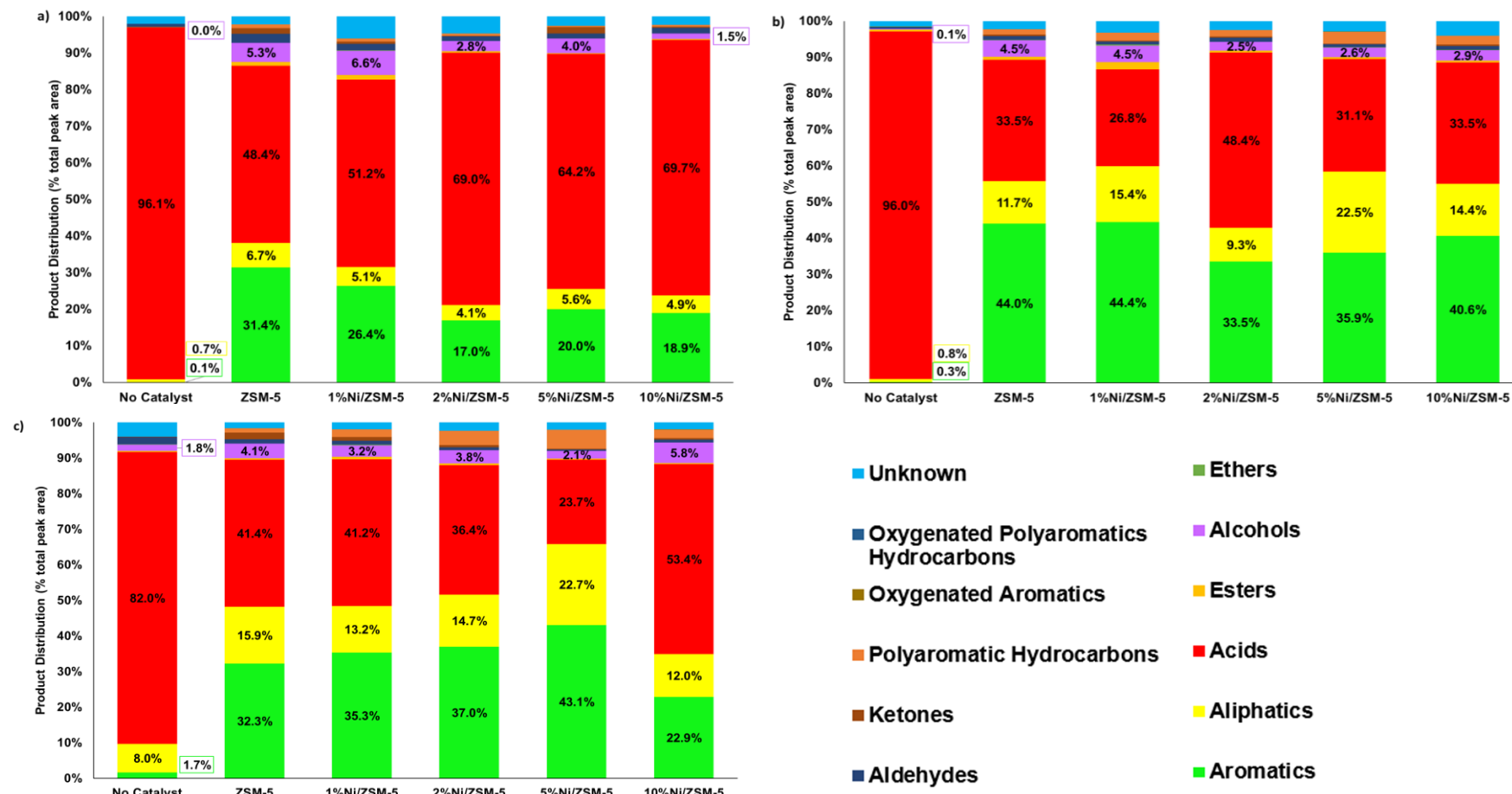


Figure 5-7. Functional groups products from the pyrolysis of oleic acid with and without catalysts at: (a) 400 °C; (b) 500 °C; (c) 600 °C

From Figure 5-7, it is clear that acid compounds (red colour) are a prominent functional group for all the pyrolysis tests. For the three temperatures tested (Figure 5-7), a major reduction of this group of compounds is observed when adding ZSM-5 and Ni/ZSM-5 catalysts. At 400 °C (Figure 5-7a), the acids content dropped from 96.1% to 48.4% and 51.2% upon addition of ZSM-5 and 1NiZSM-5 respectively. Whilst at higher nickel loadings (2Ni/ZSM-5, 5Ni/ZSM-5 and 10Ni/ZSM-5), the lowest proportion of acids was 64.2% with the 5Ni/ZSM-5 catalyst. At 500 °C, similar observations were made with the presence of acids being lowest for the 1Ni/ZSM-5 catalyst (26.8%), with similar proportions present using the 5Ni/ZSM-5 catalyst (31.1%). However, at the final reaction temperature the proportion of acids was lowest in the presence of the 5Ni/ZSM-5 catalyst which is different to all the other reaction temperatures.

A reduction of acid compounds in the presence of catalyst was anticipated as it was expected a catalytic cracking of oleic acid components will be favoured. When considering the catalyst characterisation data provided in Table 5-2 it is possible that the slightly increased pore diameters of the 1Ni/ZSM-5 and 5Ni/ZSM-5 catalysts of 1.528 nm and 1.606 nm versus 1.505 nm of the ZSM-5 have allowed these catalysts to be more effective. This is due to a report in literature by Weber et al. 2021 suggesting that larger pore ZSM-5 catalysts can give greater selectivity to aromatic products[211]. Although the 2Ni/ZSM-5 catalyst was identified to have the largest pore diameter at 2.021nm it also had the smallest surface area at 332.2 m²/g whilst the 1Ni/ZSM-5 and 5Ni/ZSM-5 had the increased pore diameters alongside a less significant reduction in surface area to just 370.0 m²/g and 347.6 m²/g respectively.

In addition to the acid compounds the second most prevalent groups of compounds were aromatics alongside smaller amounts of alcohols, polyaromatic hydrocarbons, aldehydes and esters. Considering Figure 5-7 it can be observed at all three-reaction temperatures there was a clear increase in the presence of aromatics when utilising a catalyst alongside the reduction in the proportion of the acids. The highest proportion of aromatics is obtained at 500 °C with the 1Ni/ZSM-5 catalyst. In this case the proportion of aromatic compounds is 44.4 % and acids 26.8 % compared to 0.3 % aromatics and 96 % acids in the absence of a catalyst. This increase in aromatic compounds is highly desirable as it is aromatic compounds that are the focus of this work. It is of even greater significance because BTX compounds were identified in this group of aromatic compounds.

The higher proportion of aromatics under these conditions (1Ni/ZSM-5 and 500 °C) could be associated with the catalyst characteristics mentioned earlier, with the 1Ni/ZSM-5 catalyst having a slightly increased pore diameter alongside its surface area being most similar to the parent ZSM-5 catalyst, as a higher catalyst surface area will allow for more catalytic reactions to occur. Furthermore, the temperature of 500 °C could be influencing the proportion of aromatics as when considering the proportions of aliphatic compounds present in Figure 5-7b and c (~9 % to ~20 %) versus those in Figure 5-7a (~4 % to 6 %). This is of significance as it was identified that aliphatic compounds are precursors to aromatics in the decomposition pathway that is proposed by Schwab et al., 1998 (Chapter 4.0, section 4.2.1, Figure 2.11)[119]. Overall, this increased proportions of aromatics suggests that the presence of the ZSM-5 or Ni/ZSM-5 is favouring the decomposition of the fatty acids to these compounds via this pathway.

In addition to the proportions of aromatics compounds present it is also important to consider their yield (peak area per mg of feedstock). As although they may contribute the most to the overall composition it doesn't convey which catalyst and temperature combination may provide the highest yield of aromatics but rather the selectivity towards different groups of compounds. Therefore, the yields (peak area per mg of feedstock) of the groups that are of most significance including the acids, aliphatics and aromatics are presented in Figure 5-8 below.

It can be observed in Figure 5-8 that the aromatics content is highest at a temperature of 500 °C, the same temperature at which the highest proportion of aromatics was also obtained. The fact that aromatics yields were typically highest at this temperature irrespective of the catalyst utilised suggests that this temperature is preferable for the formation of aromatic compounds.

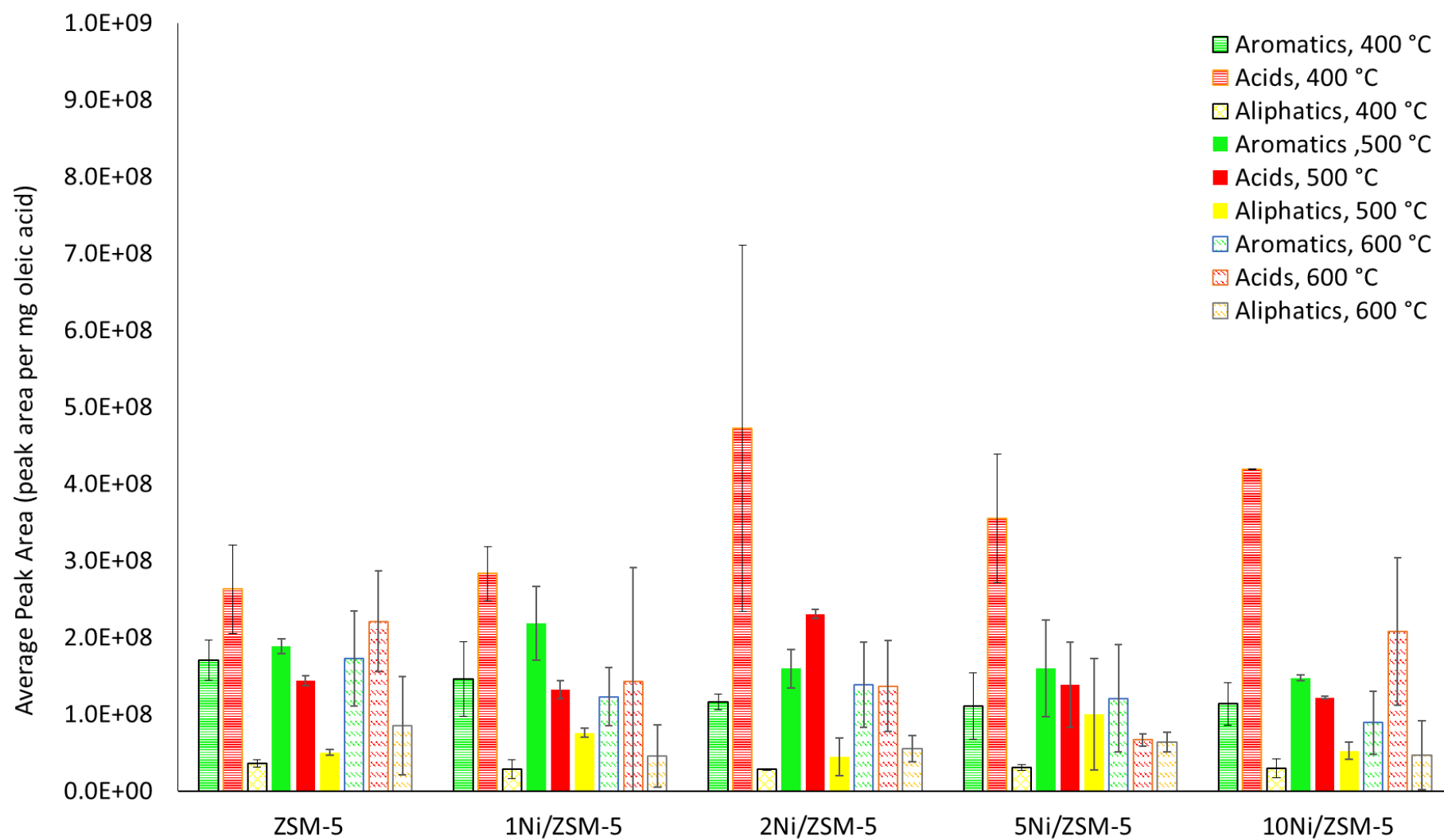


Figure 5-8. Yield of major compound groups in the catalytic pyrolysis of oleic acid (average values from duplicate runs)

The preference to temperatures of 500 °C for the production of aromatics is likely associated with the fact literature suggests pyrolysis of triglycerides at temperatures of 400 °C to 500 °C results in cracking with the formation of short chain hydrocarbons [103]. It is these short chain hydrocarbons that are initial decomposition products which is observed in the decomposition mechanism Figure 5-9 below forming aromatics as well as that by Schwab et al. in the non-catalytic decomposition of oleic acid(Chapter 4.0, section 4.2.1, Figure 4.5)[119].

Furthermore, according to Fréty et al. 2014 at temperatures of 400 °C to 500 °C hydrocarbons are able to reduce nickel oxide to metallic nickel, which may also have a role in the formation of aromatic compounds[117]. The presence of nickel is reported in literature to promote the conversion of oxygenated and nitrogen compounds to aliphatics and aromatics. Its presence is believed to favour the production of carbon dioxide and reduce presence of water so that more hydrogen can be incorporated into the products[212]. Therefore, as the cracking and reduction of the nickel occur in the same temperature range it is possible that it is the combination of these two factors that are giving the improved yields of aromatics at the temperature of 500 °C.

The preference to this pathway in the catalytic decomposition of oleic acid is supported by the fact that the proportions of the other groups of compounds such as alcohols, aldehydes and polycyclic aromatic hydrocarbons have not increased in the same way and remain in similar proportions to investigations that did not utilise a catalyst. Furthermore, the evolution of aromatics specifically from the decomposition of oleic acid with ZSM-5 catalyst can be further supported by Benson et al., 2008. Benson et al. proposed the decomposition in Figure 5-9 for the conversion of oleic acid to aromatic compounds in the presence of a H-ZSM-5 catalyst at 400 °C using a Quatra C reaction device with GC-TCD and MS.

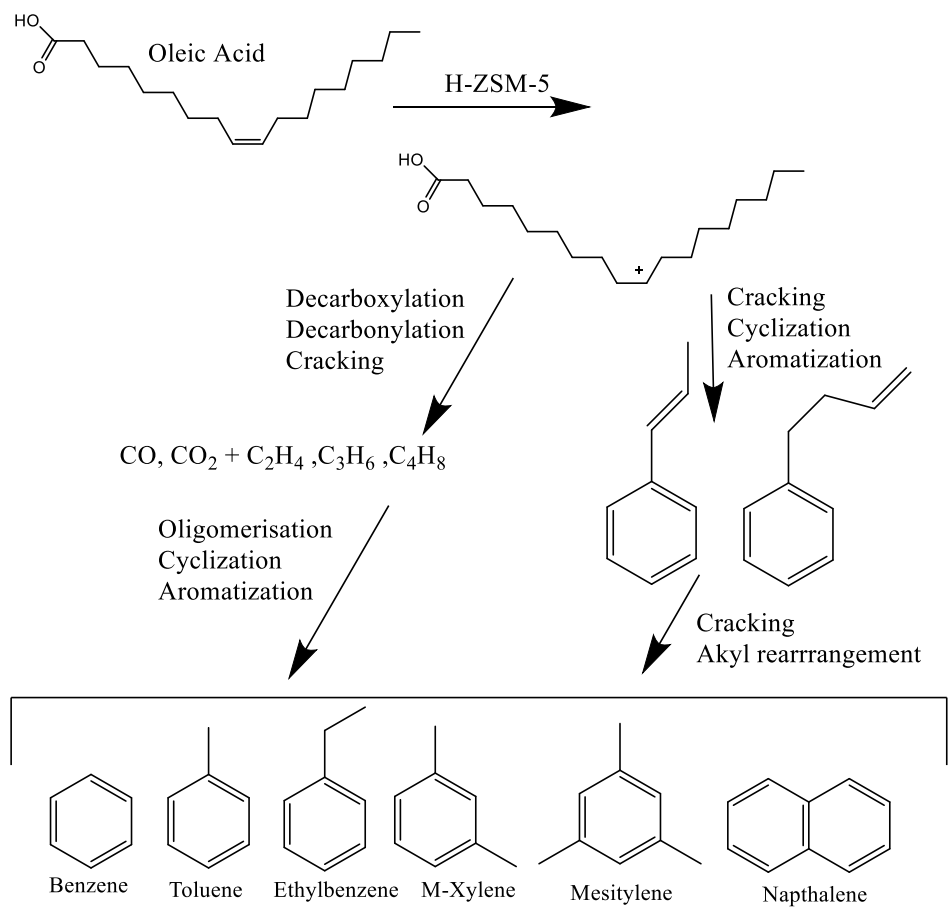


Figure 5-9. Decomposition of oleic acid to aromatics in the presence of H-ZSM-5 catalyst, Benson et al. 2008[213]

Other studies in addition to Benson et al. that considered the decomposition of oleic acid or feedstocks that contained oleic acid also observed several compounds from Figure 5-9 [214, 215]. The compounds benzene, toluene, xylenes in addition to other benzene derivatives have been identified in this work. Although Benson et al. observed other aromatic compounds such as naphthalene, m-xylene and mesitylene which were not identified in this work differences in product composition could be attributed to factors including different types of reactor system, different scale systems, or the catalyst preparation methods.

In Figure 5-8 the catalyst with the highest peak area contributing towards aromatic compounds was the 1Ni/ZSM-5 catalyst at a temperature of 500 °C, the same conditions and catalyst that was also identified to have the highest proportion of aromatics. With the more highly weighted nickel catalysts (2Ni/ZSM-5, 5Ni/ZSM-5 and 10Ni/ZSM-5) all having a lower yield of aromatics at any of the reaction temperatures. The second highest peak area was associated with the unmodified ZSM-5 catalyst at the same temperature.

This suggests that the addition of nickel may only be enhancing the decomposition of the oleic acid to aromatic products when present in smaller amounts. However, this is desirable as the lower the amount of nickel the less costly it is to manufacture the catalyst at same time it is potentially increasing the value of the products.

In terms of the aromatic compounds themselves, those of interest include the benzene, toluene, and xylenes due to being high value compounds. The presence of these compounds alongside ethylbenzene in addition to other benzene derivatives were identified in all of the catalytic runs at all three reaction temperatures. In addition to the yields or these aromatics shown in Figure 5-8, it is of importance to consider what proportions of these aromatic compounds are present as some have more uses than others and therefore of even higher value.

For example considering Chapter 2.0, section 2.3.1 evaluating the significance of aromatic compounds it is highlighted in Figure 2.9 that when it comes to toluene, 28 % of it is used to make benzene and 30 % of it used to make xylenes, suggesting that these two other chemicals have more value than toluene[108]. Although Toluene may have fewer uses the fact that it can be used in the manufacture of some of the other high value products may mean that the product is more versatile. In order to compare the effect of temperature and the use of different catalysts on the presence of different high value compounds the graphs (Figure 5-10, Figure 5-11 and Figure 5-12) below show what proportion of benzene, toluene, ethylbenzene, xylenes (BTEX) and other aromatics are present in each run.

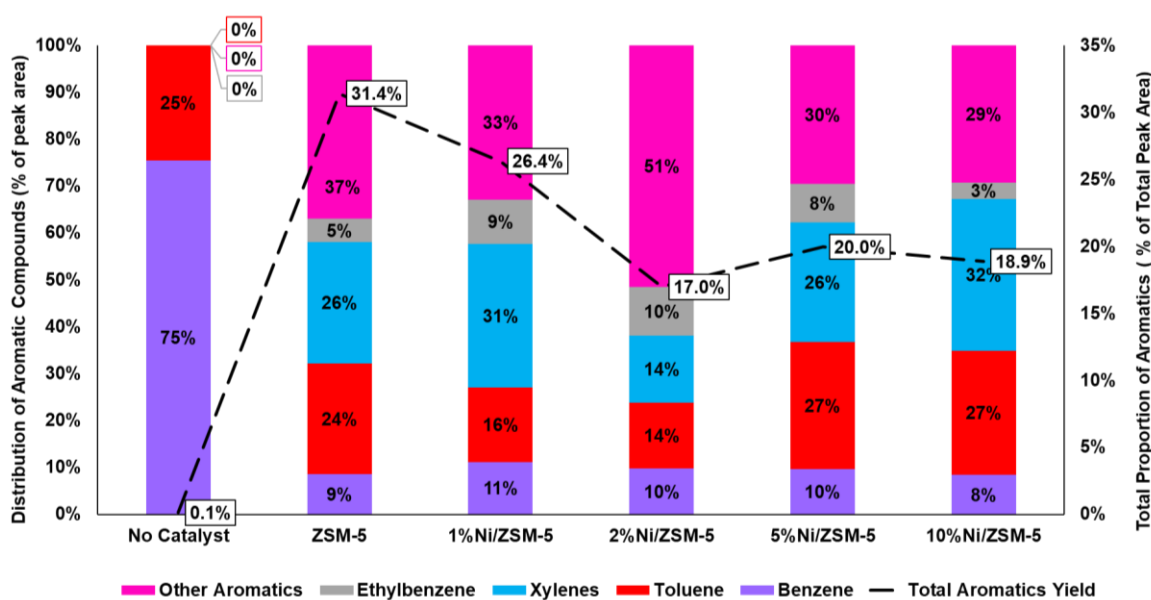


Figure 5-10. Proportions of aromatics from pyrolysis of oleic acid at 400 °C

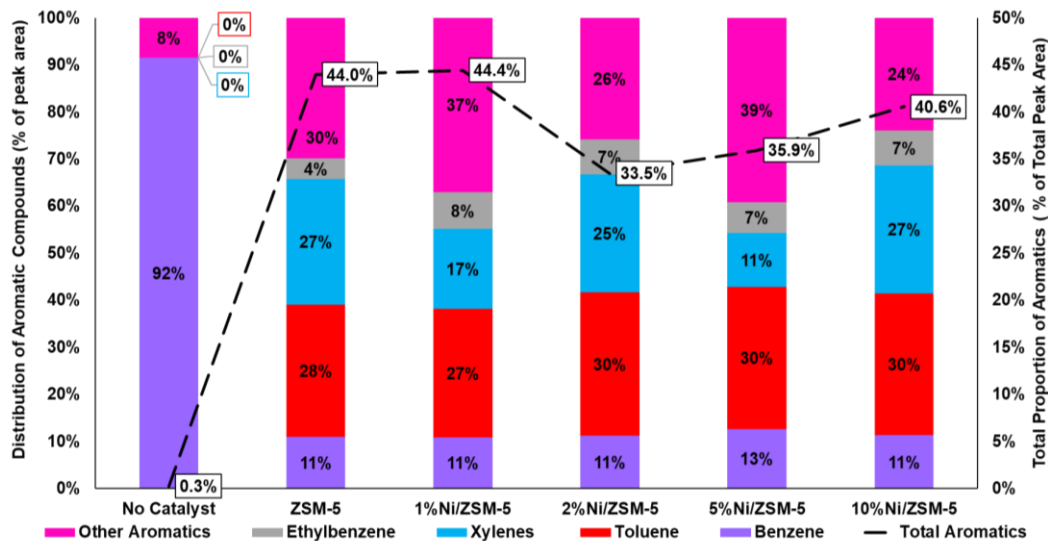


Figure 5-11. Proportions of aromatics from pyrolysis of oleic acid at 500 °C

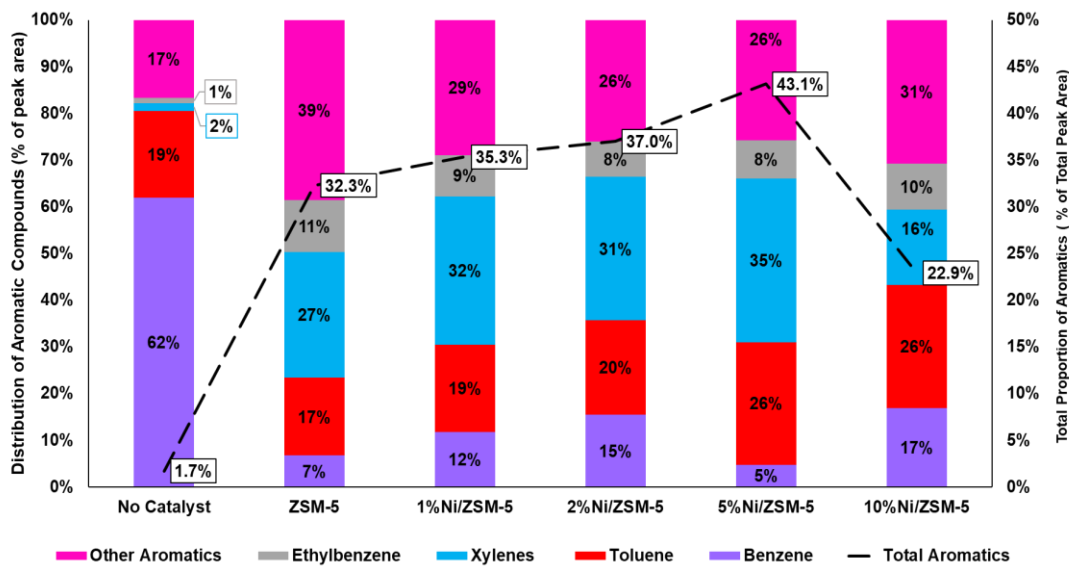


Figure 5-12. Proportions of aromatics from pyrolysis of oleic acid at 600 °C

From Figure 5-10, Figure 5-11 and Figure 5-12 multiple observations and comparisons can be considered about the effect of the temperature and different weighted nickel ZSM-5 catalyst on the proportions of the BTEX present and the overall proportion of aromatics yielded. It is known that the BTEX aromatic compounds can easily diffuse through the pores of the ZSM-5 catalyst and show shape selectivity a catalyst phenomenon described in Chapter 2.0, section 2.3.3.3. The shape selectivity of catalyst can be related to catalyst characteristics such as the pore diameter as if this is reduced it can mean that certain compounds can make it more difficult for the compounds to diffuse through the pores of the catalyst as easily or at all [1, 216].

The pore diameter for the catalysts used in this work was reported in section 5.2.2, Table 5-2. A slight increase in pore diameter was observed between the ZSM-5 and the 2Ni/ZSM-5 catalyst from 1.505 ± 0.064 nm to 2.021 ± 0.011 nm, although values were also marginally higher for the other Ni/ZSM-5 catalysts (1/Ni/ZSM-5, 2Ni/ZSM-5 and 10Ni/ZSM-5) the increases there were deemed negligible. Alongside the increased pore diameter an increase in pore volume was observed from 0.195 ± 0.001 cc/g (ZSM-5) versus 0.234 ± 0.027 cc/g(2Ni/ZSM-5). This was in conjunction with a reduced surface area of 332.0 ± 64.3 m²/g down from 383.0 ± 9.6 m²/g for the 2Ni/ZSM-5 and ZSM-5 catalysts respectively. This reduction was associated with deposition of the Nickel at the mouth of pores of the catalyst reducing its overall surface area (section 5.2.2). These changes in catalyst characteristics could be associated with the drop in yields of aromatics from the 2Ni/ZSM-5 catalyst as at 400 °C and 500 °C at just 17.0 % and 33.5 % respectively.

However, the same trend was not observed at the highest temperature of 600 °C where the aromatics yields for the ZSM-5, 1Ni/ZSM-5 and 2Ni/ZSM-5 are all fairly similar at 32.3 %, 35.35 % and 37.0 % respectively. This could perhaps be due to that fact that at the highest temperature of 600 °C more reactions are promoting the formation of coke which is known to cause issues with deactivation of catalysts like ZSM-5[217].

Overall, it was determined that aromatic compounds including BTEX can be obtained from the catalytic pyrolysis of oleic acid. It was concluded that the presence of the ZSM-5 catalyst increased the presence of the aromatic compounds due to a greater catalytic decomposition of the oleic acid from aliphatics to aromatics as shown by the pathway in Figure 2.11. It is possible that small amounts were produced by thermal cracking also or that the thermal cracking of the oil and producing aliphatics contributed towards producing some of the aromatic compounds. It was determined that a temperature of 500 °C was most favourable for yielding aromatic compounds with the 1Ni/ZSM-5 catalyst with a proportion of 44.4 % aromatics. However, similar proportions were also obtained of 44.0 % also at the temperature of 500 °C and with the ZSM-5 catalyst. Therefore, although the presence of Nickel may have influence on the production of aromatic compounds it was observed from Figure 5-11 that more xylenes are produced from the ZSM-5 catalyst alone at 500 °C so in this processes application it will be important to decide if whether a higher presence of a specific aromatic compound or overall presence of aromatics is desired.

5.3.3.Catalytic pyrolysis of jatropha oil at different temperatures

The decomposition products of jatropha oil in the presence of different catalysts (ZSM-5, 1Ni/ZSM-5, 2Ni/ZSM-5, 5Ni/ZSM-5 & 10Ni/ZSM-5), and at different temperatures (400 °C, 500 °C and 600 °C) were variable. The groups were identical to the major functional groups that were identified in the non-catalytic pyrolysis of jatropha in Chapter 4.0, section 4.2.2., although their distribution appears significantly different in the presence of the catalysts. At all 3 temperatures in the presence of the catalysts, aromatic compounds were the most prevalent contributing between 51.5 % to 80.0 % of the total peak area. In each case other groups of compounds were also present including acids and smaller amounts of aliphatics, polyaromatic hydrocarbons and alcohols. In Figure 5-13 below the chromatograms for the decomposition of jatropha oil in the absence of a catalyst at the lowest temperature of 400 °C, alongside its decomposition at the same temperature in the presence of the commercially available ZSM-5 zeolite catalyst can be compared.

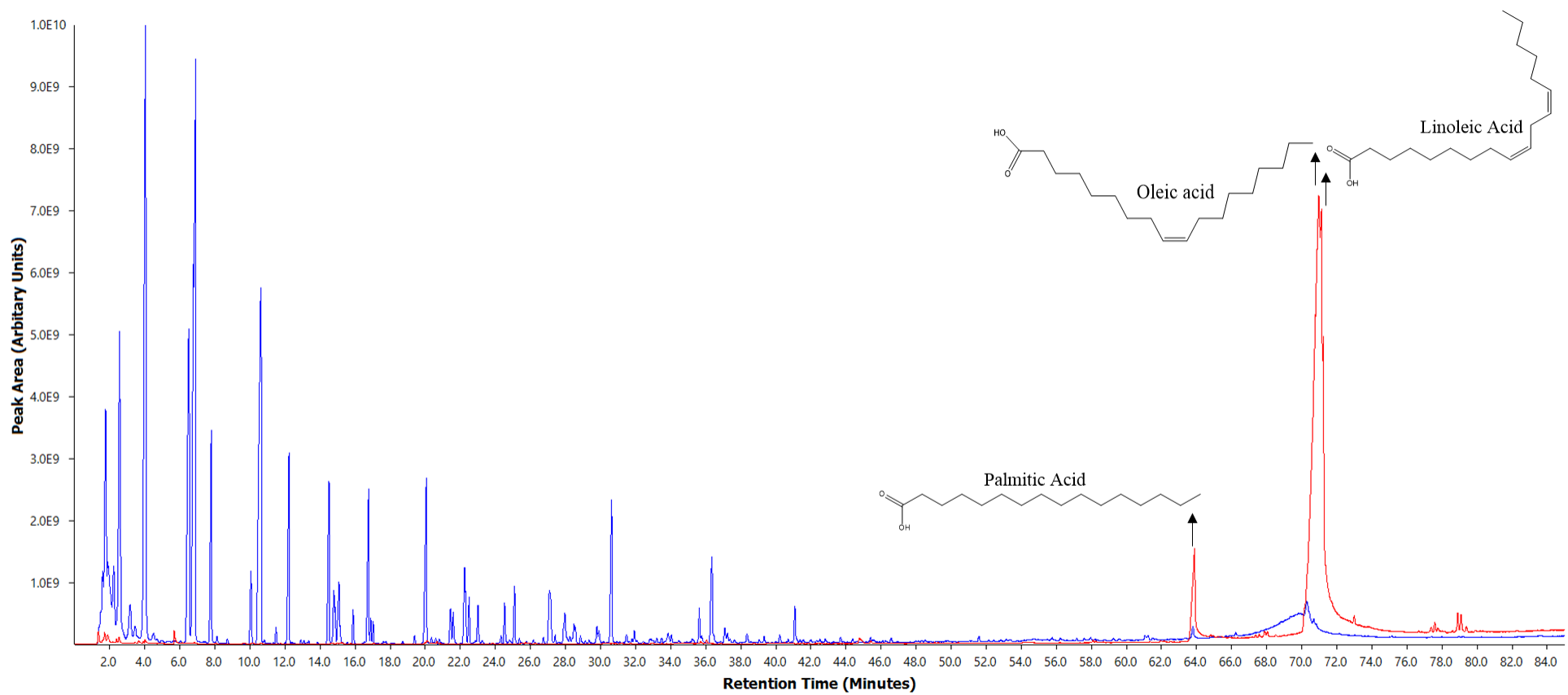


Figure 5-13. Py-GCMS Chromatogram showing decomposition of jatropha oil in absence of catalyst at 400 °C (red) & decomposition of jatropha oil in the presence of a ZSM-5 catalyst at 400 °C (blue).

Similarly, to the catalytic decomposition of oleic acid as seen in section 5.3.1, Figure 5-6, there is an increased presence and intensity of peaks from numerous lower molecular weight products on the left-hand side of the blue chromatogram observed in Figure 5-13 . This observation indicates that the catalytic decomposition of jatropha oil is affected by the addition of the ZSM-5 catalyst. Furthermore, the peaks on the blue catalytic chromatogram at 64.5 minutes, 70.7 minutes and 71.2 minutes that are attributed to palmitic, oleic and linoleic acid respectively are significantly smaller than the same peak from the red non-catalytic chromatogram. This once again is despite the difference in sample size for catalytic and non-catalytic experiments, as just 0.1 μ L were used for non-catalytic investigations, whilst 0.5 μ L were used for those with a catalyst. Although an increase in the number of lower molecular weight products was observed in the non-catalytic investigations their presence here with the ZSM-5 catalyst is vastly more prominent with the blue peaks in Figure 5-13 being larger and more frequent. The proportion of acid compounds alone at 400 °C (mostly attributed to the major fatty acids oleic, linoleic, and palmitic acid) dropped from 76.6 % of the peak area when pyrolyzed in the absence of a catalyst to 10.5% of the peak area with the ZSM-5 catalyst. This can be observed below in Figure 5-14a alongside additional graphs showing the distribution of the products present from the catalytic pyrolysis of jatropha oil at 400 °C, 500 °C and 600 °C.

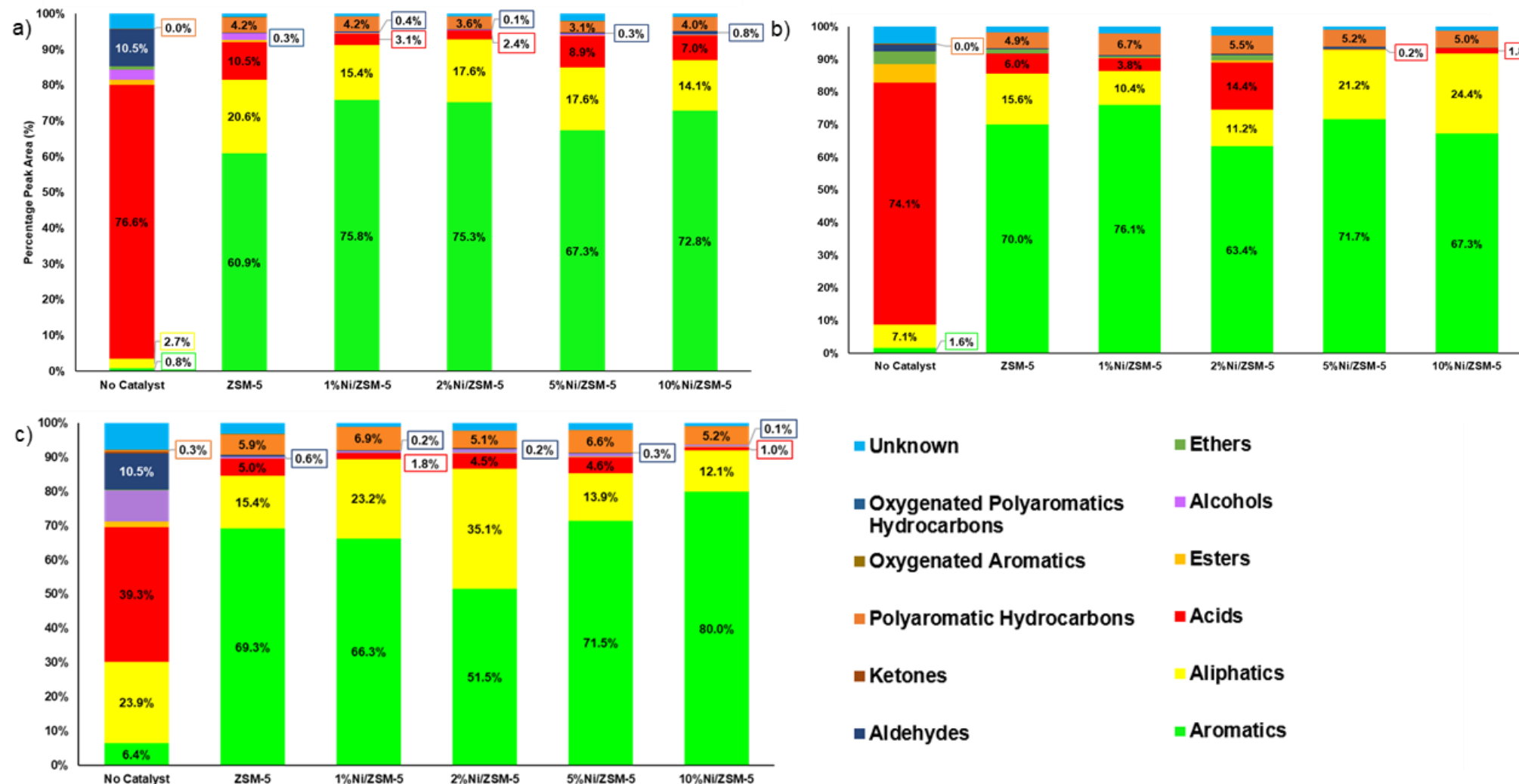


Figure 5-14. Functional groups products from the pyrolysis of jatropha oil with and without catalysts at: (a) 400 °C; (b) 500 °C; (c) 600 °C

It can be observed from Figure 5-14a that the reduction in the proportion of acids is most significant in the presence of the 1Ni/ZSM-5 and 2Ni/ZSM-5 catalysts unlike oleic acid where the proportion of acids were lowest with the ZSM-5 catalyst. The major catalytic products were aromatics alongside some aliphatics in addition to small amounts of polyaromatics and aldehydes. The implication of utilising a catalyst on the distribution of products at different reaction temperature was also considered with the product distribution for at 500 °C and 600 °C shown in Figure 5-14b and Figure 5-14c.

When considering the above data from Figure 5-14a-c together it is apparent that in the presence of the catalysts, (ZSM-5 and differently weighted Ni/ZSM-5) aromatics form the majority of the products. The highest proportions of aromatics at 76.1 %, 75.8% and 75.5% were obtained at 500 °C with a 1Ni/ZSM-5 catalyst and then 400 °C with the ZSM-5 and 1Ni/ZSM-5 catalyst respectively. Similarly, the highest proportion of aromatics at 44.4% from the catalytic decomposition of oleic acid was also obtained at 500 °C with the 1Ni/ZSM-5. This is different to the non-catalytic experiments where the highest aromatics yields were obtained at the highest temperature of 600 °C.

As with the catalytic decomposition of oleic acid BTX compounds were also identified in the catalytic pyrolysis of jatropha oil in varying proportions. It is dependent on the temperature and catalyst utilised but the presence of aromatics and BTX in the products is greater than that of any of the catalytic decomposition of oleic acid investigations. In Chapter 4.0, section 4.2.2 in addition to the decomposition of the fatty acid components the decomposition of glycerol was also discussed. Glycerol is present in triglyceride molecules with its decomposition to aromatics being covered in various resources. There are several examples of different pathways of significance including those by Mitrea 2017 et al. as well as several reviewed by Zakira et al. 2013 which include those by Corma et al. 2008 and Hoang et al. 2007[120, 198, 201, 218]. The pathway by Hoang et al. 2007 (Figure 2.12) shows the decomposition of glycerol to C₆+ aromatics in the presence of a ZSM-5 catalyst similar to the one utilised in this work, although reactions were conducted under different conditions (300 °C- 400 °C & 2.1MPa).

Similary, it can be observed from the pathway by Corma et al. 2008 shown below in Figure 5-15, that aromatics alongside other groups of compounds such as alcohols were also considered a decompositision product. In this work glycerol was converted at temperatures of 500 °C to 700 °C in the presence of an N₂ flow in a micro activity reactor[198].

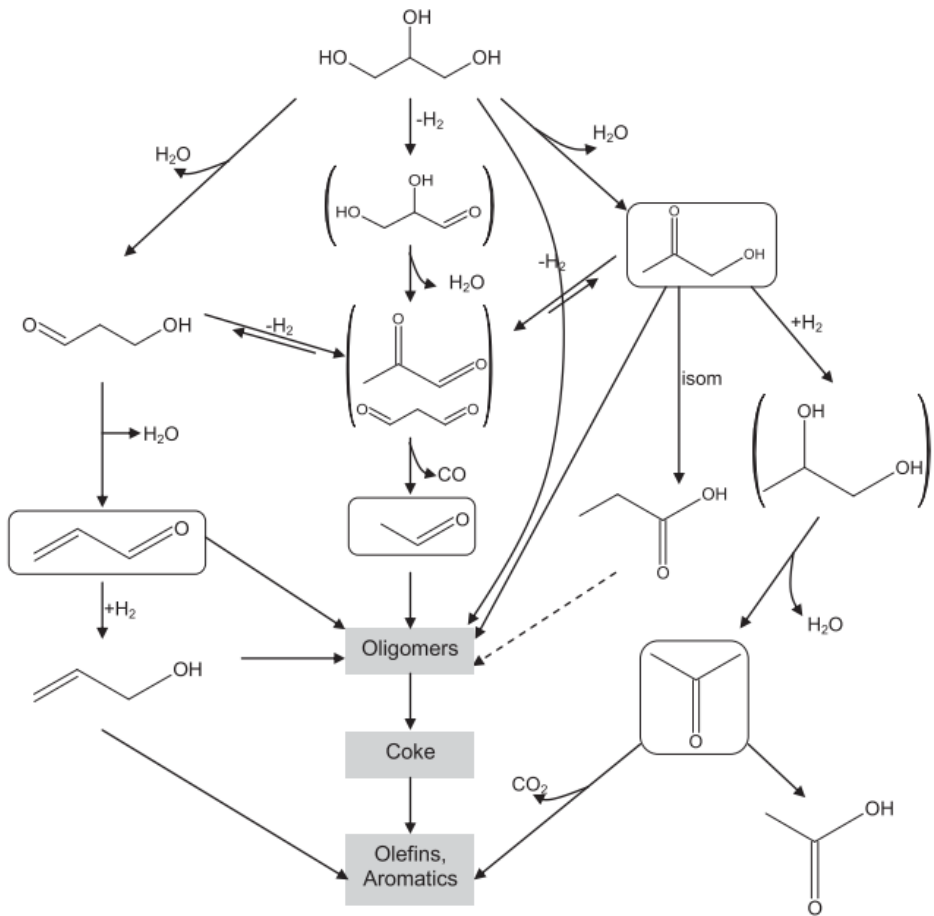


Figure 5-15. Decomposition of glycerol, Corma et al. 2008 [198]

In either the case of Hoang et al. or Corma et al. the first steps in both pathways are similar with C₃ oxygenates by Hoang et al. referring to C₃ aldehydes and alcohols agreeing with the work by Corma et al. These decomposition mechanisms (Figure 2.12 and Figure 5-15) demonstrate how the glycerol maybe contributing to the much higher aromatics content alongside the fatty acid compounds such as oleic acid, linoleic acid, and palmitic acid. Whilst the fatty acids within jatropha oil could use similar pathways to those discussed in section 5.3.2 including the pathway by Benson et al. as shown in. Further mechanisms that consider the decomposition of fatty acids such as linoleic or palmitic acid in the presence of ZSM-5 catalysts include the below mechanism proposed in Figure 5-16 by Fischer et al. 2015, considering the decomposition of palmitic acid to aromatic compounds[215].

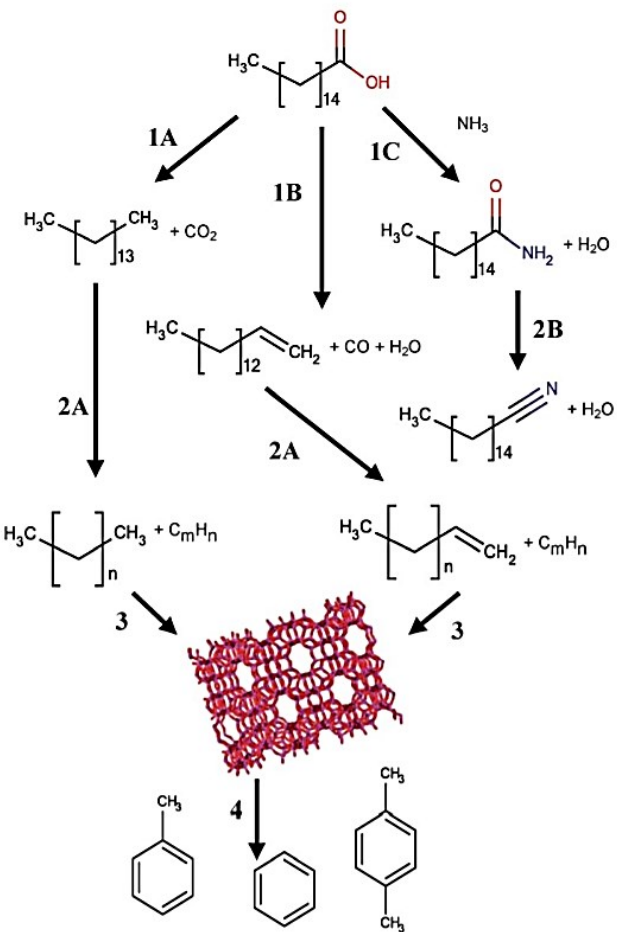


Figure 5-16. Decomposition of palmitic acid to aromatic compounds, (1A) decarboxylation, (1B) decarbonylation, (1C) ammonia substitution, (2A) thermal cracking, (2B) amine pyrolysis, (3) catalytic cracking, (4) oligomerization, cyclization, and aromatization, Fisher et al. 2015[215]

Similar work to Fischer et al. concerning the decomposition of palmitic acid in the presence of ZSM-5 has been carried out by Shi et al. 2017, whom suggested that the ZSM-5 catalyst favoured the decarbonylation pathway as shown in Figure 5-16. Here path 1B gives rise to carbon monoxide and water and then hydrocarbon product 1-pentadecene whilst decarboxylation gives rise to pentadecane.

These two aliphatic compounds were not identified in the catalytic pyrolysis of jatropha oil in this work. However, this could just mean that all they were converted to aromatics as they are the precursor to the aromatic compounds when considering the pathway in Figure 5-16. The evolution of aliphatic compounds is of significance because this is the second largest group of compounds present in from the catalytic decomposition of jatropha oil as observed in the graphs shown in Figure 5-14a-c. In Chapter 4.0, section 4.2.2 it was identified in the non-catalytic pyrolysis of jatropha oil these aliphatic compounds are precursors to aromatics. The aliphatic compound in the absence of a catalyst were identified as thermal decomposition products of the fatty acid compounds

in pathways by authors including Schwab et al., Idem et al. and Frankel et al. (Chapter 4.0, Figure 4.5, Figure 4.11, and Figure 4.12)[119, 123, 191].

Whilst in the presence of a catalyst these compounds can evolve as a result of thermal or catalytic cracking. A primary example of this is the pathway above in Figure 5-16 showing the decomposition of palmitic acid where the initial decomposition products which are aliphatics are formed using thermal cracking but then go onto form aromatics in the presence of a catalyst. This means when the proportion of acids are low it is expected more aliphatics and in turn more aromatics maybe produced. The yields of each of these groups of compounds present from the catalytic decomposition of jatropha oil are presented in the graph Figure 5-17 using the same format utilised earlier for oleic acid in Figure 5-8 in section 5.3.1.

It can be observed from Figure 5-17 below that the catalyst with the highest peak area contributing towards aromatic compounds was the 1Ni/ZSM- catalyst at a temperature of 500 °C, the same conditions and catalyst that was also identified to have the highest proportion of aromatics at 76.1% of the peak area in Figure 5-11. With the more highly weighted nickel catalysts (2Ni/ZSM-5, 5Ni/ZSM-5 and 10Ni/ZSM-5) all having a lower yield of aromatics at any of the reaction temperatures. The second highest peak area was associated with the unmodified ZSM-5 catalyst at the same temperature.

This suggests that the addition of nickel may be enhancing the decomposition of the jatropha oil to aromatic products when present in smaller amounts. The observations from Figure 5-17 regarding the yields of aromatics from the catalytic decomposition of jatropha oil are identical to those deduced from Figure 5-8 considering the catalytic decomposition of oleic acid in section 5.3.1. Such similarities in the decomposition of jatropha oil to oleic acid were anticipated owing to the fact that the oil is ~46 wt.% oleic acid and the second major compound linoleic acid is also a similar compound.

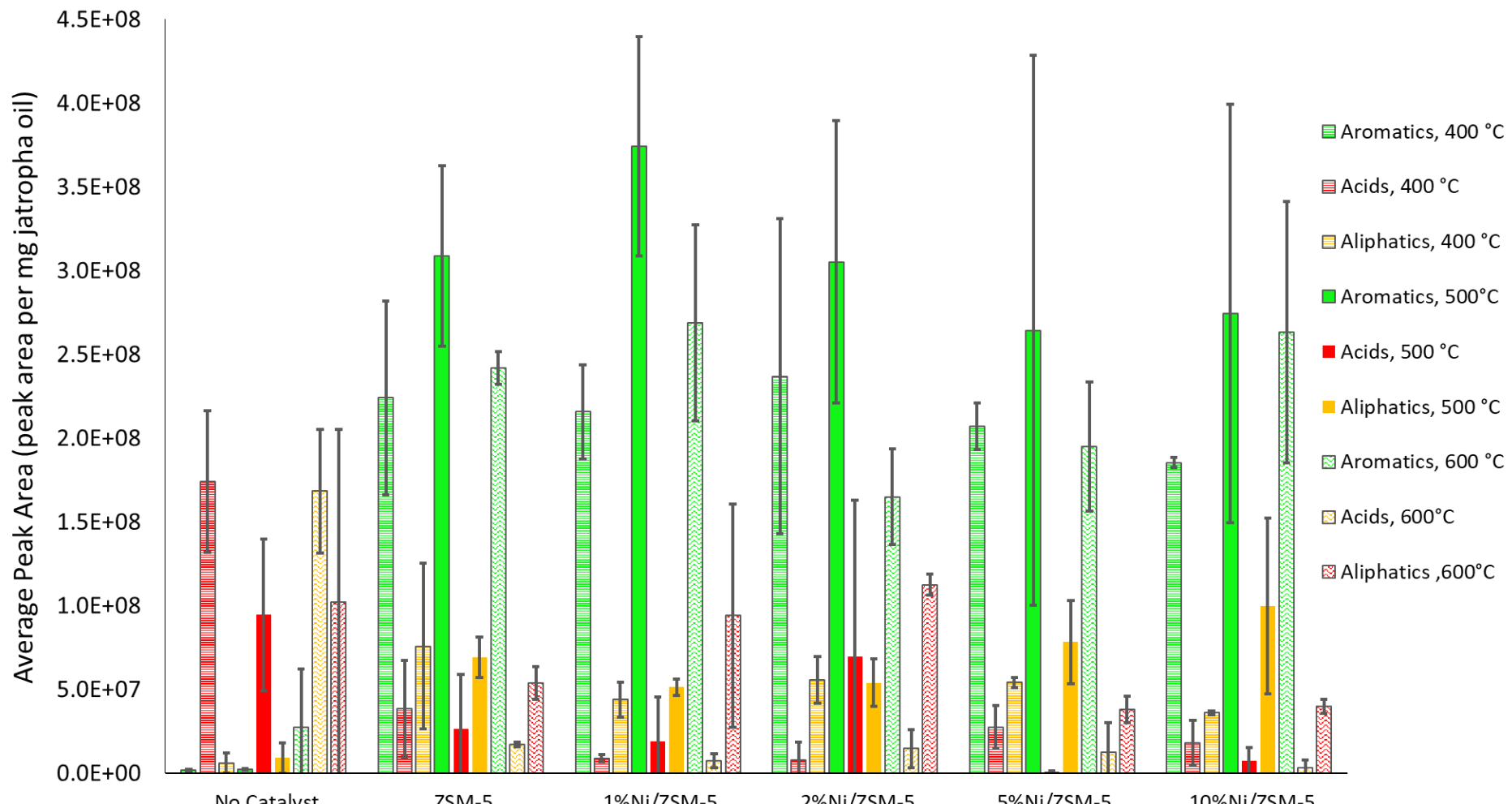


Figure 5-17. Yield of major compound groups in the catalytic pyrolysis of jatropha oil (average values from duplicate runs)

In addition to the yields of aromatics shown above in Figure 5-17, consideration should also be given to the types of aromatic compound present. This is because of the fact that it is the higher value aromatic compound BTX that are of most significance in this work. The proportions of these aromatic compound alongside the overall proportion of the peak area they cover are presented in the graphs Figure 5-18, Figure 5-19 and Figure 5-20 below.

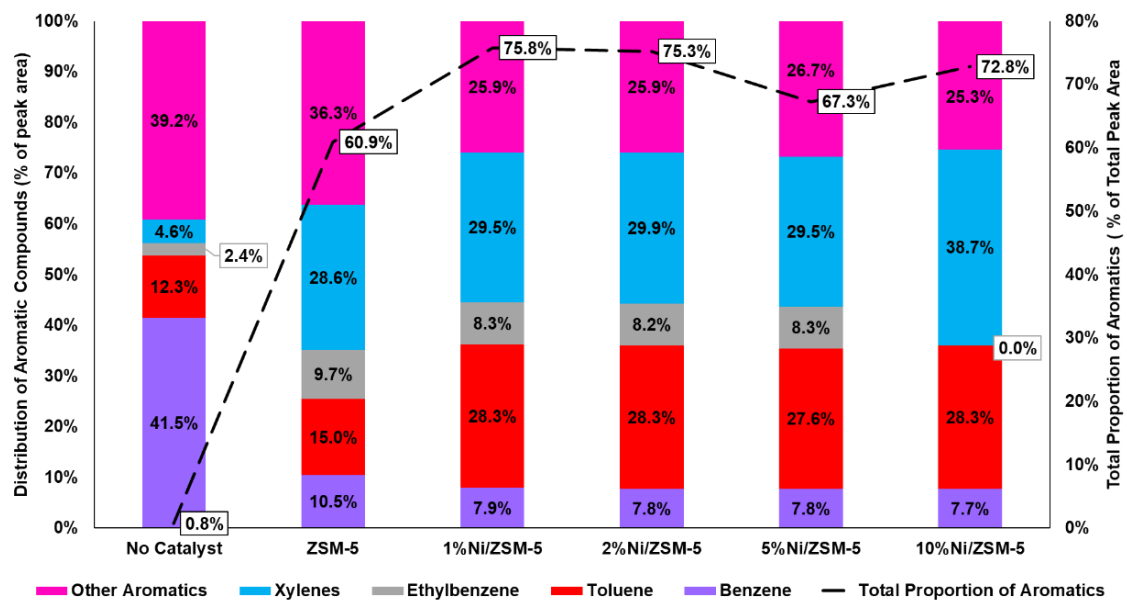


Figure 5-18. Proportions of aromatics from pyrolysis of jatropha oil at 400 °C

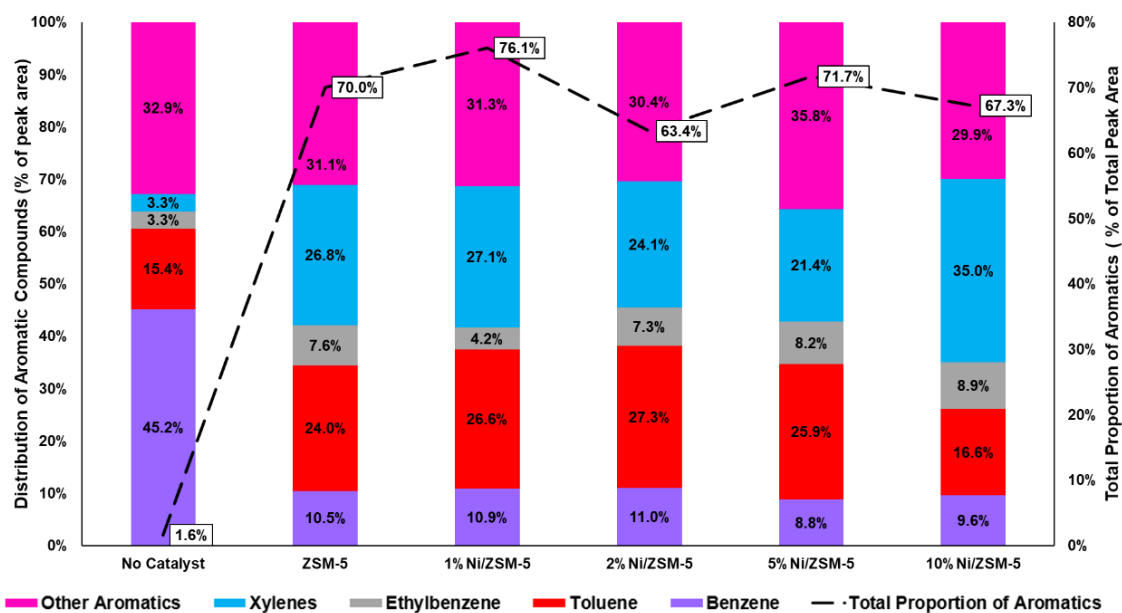


Figure 5-19. Proportions of aromatics from pyrolysis of jatropha oil at 500 °C

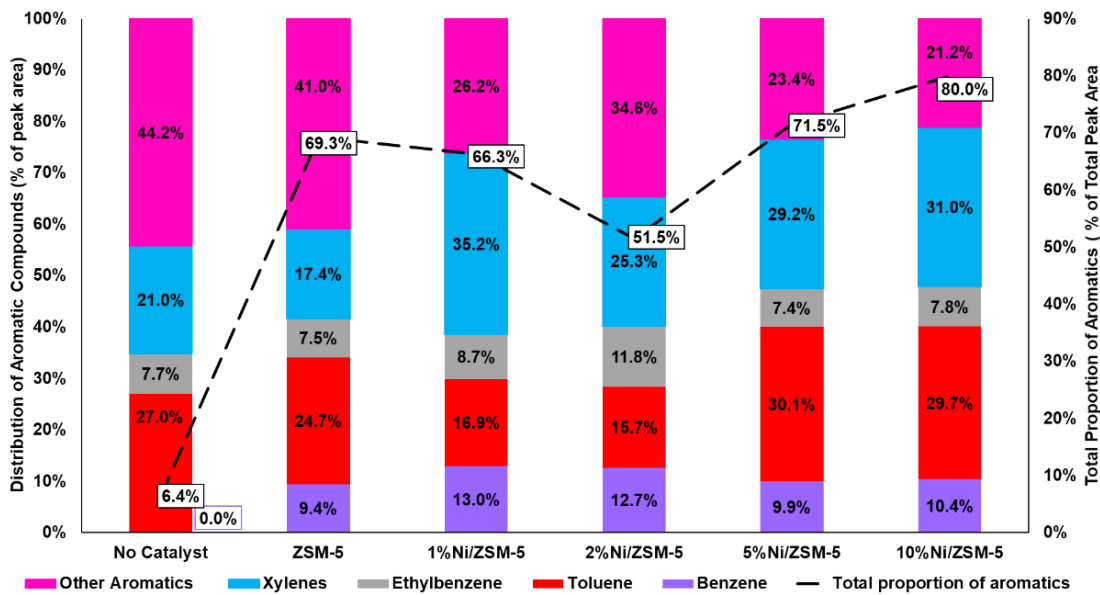


Figure 5-20. Proportions of aromatics from pyrolysis of jatropha oil at 600 °C

From Figure 5-18, Figure 5-19 and Figure 5-20 multiple observations and comparisons can be considered about the effect of the temperature and different weighted nickel ZSM-5 catalyst on the proportions of the BTEX present and the overall proportion of aromatics yielded. It was mentioned earlier in section 5.3.1 how the characteristics of the different catalysts may implicate the presence of different aromatics. The overall yields of aromatics for Jatropha oil with the highest still at a temperature of 500 °C and in the presence of a 1 Ni/ZSM-5 at 76.1%, the cumulative proportion of BTEX was similar to that of the other catalysts at the same temperature.

Similar proportions of aromatics at 75.8 %, just 0.3 % less were obtained using the same catalyst but a temperature of 100 °C less. This is of significance as the BTEX products are also present in similar distributions which means it could be possible to achieve similar results at the lower temperature. In general, lower process temperatures are desirable as they make them more economically viable as less power is required. However, in this case the yield of the aromatics at this temperature is significantly lower when you compare 1Ni/ZSM-5 aromatics at 400 °C and 500 °C in Figure 5-17.

Overall, it was determined that aromatic compounds including BTEX can be obtained from the catalytic pyrolysis of jatropha oil. The presence of the ZSM-5 catalyst as seen in the case of the oleic acid increases the presence of the aromatic compounds due to the catalytic decomposition of the fatty acids and in the case of jatropha oil perhaps also the glycerol that is part of the triglyceride molecules.

It has been concluded the aromatics present were obtained via the decomposition pathways shown in Figure 2.12, Figure 5-15 and Figure 5-16 respectively. In addition to obtaining these compounds from catalytic decomposition it is also feasible that small amounts of aromatics along with the other groups of compounds present were produced by thermal cracking utilising the pathways discussed in Chapter 4.0, by Schwab et al and Idem et al (Figure 2.11, Figure 2.15). It was determined that a temperature of 500 °C, with the 1Ni/ZSM-5 catalyst was most favourable to achieve both the highest yield (Figure 5-17) and proportion of aromatics (76.1 %,Figure 5-14).

5.4. Comparing catalytic decomposition of oleic acid and jatropha oil

The most obvious similarity between the catalytic decomposition of oleic acid and jatropha oil was the increased presence of aromatic compounds and reduction in acids with the ZSM-5 and Ni/ZSM-5 catalysts present. It is apparent that the increase in aromatics seen in the products from the conversion of jatropha oil is a lot more than that from oleic acid. The maximum proportion of aromatics obtained from oleic acid was just 44.4 % with the 1Ni/ZSM-5 catalyst at a temperature of 500 °C, whilst proportions of 76.1 % were achieved from the conversion of jatropha oil with the same catalyst and temperature. Such difference in the increased presence of aromatics from jatropha oil compared to oleic acid is potentially attributed to the other components in jatropha oil such as glycerol as well as other fatty acids such as linoleic and palmitic acid. The decomposition of these components could have contributed more to the formation of aromatics due to the fact that they could have assisted in the production of aromatics via either catalytic or thermal decomposition mechanisms discussed in this chapter. The jatropha oil components would have undergone catalytic decomposition via the pathways Figure 5-9,Figure 2.12 ,Figure 5-15 and Figure 5-16. In addition, the fatty acids could decompose via thermal pathways discussed in Chapter 2.0 such as Figure 2.11 and Figure 2.15 with the initial decomposition such as aliphatics and then follow the catalytic pathways to form aromatics more readily. This would make sense as aliphatics were identified as precursors to aromatic compounds in Chapter 4.0.

In terms of differences between the products from the catalytic pyrolysis of oleic acid and jatropha oil small proportions of alcohols (2 % to 5 %,Figure 5-7) had been observed from oleic acid at all temperatures whilst the proportions from jatropha oil were closer to negligible (0.5 % to 2 %,Figure 5-14).

Given that the polyaromatic hydrocarbons would have been formed using similar paths to the aromatics it makes sense that in the case of jatropha oil where there is a more significant presence of aromatics there is also a more significant presence of polyaromatics. It is possible that the production of these polyaromatics can be associated with the lower alcohol content from jatropha oil pyrolysis in the presence of a catalyst. This is supported by the decomposition pathway in Figure 5-15 which shows alcohols are a precursor to aromatics in the decomposition of glycerol.

5.5. Conclusions

It was possible to conclude from the catalytic pyrolysis of oleic acid and jatropha oil at the temperatures of 400 °C, 500 °C and 600 °C that in the presence of a catalyst the proportion of aromatics is substantially increased, and acids decreased. For oleic acid the proportion of acids dropped from a range of 96.0 % to 82.0 % in the absence of a catalyst to 69.7 % to 23.7 % in the presence of ZSM-5 and Ni/ZSM-5 catalysts (Figure 5-7). Whilst the aromatics content rose from within the range of 0.1 % to 1.7 % to 17.0 % to a maximum of 44.4 % which was achieved at a temperature of 500 °C, with the 1Ni/ZSM-5 catalyst (Figure 5-7). At this maximum aromatic proportion, the compound benzene, toluene, xylenes, and ethylbenzene were identified to account for 11 %, 27 %, 17 % and 8 % of the total aromatic compounds present whilst the remaining 37 % were defined as other aromatics (Figure 5-11). As for jatropha oil the proportion of acids dropped from a range of 76.6 % to 39.3 % in the absence of a catalyst, to 14.4 % to 1.0 % in the presence of ZSM-5 and Ni/ZSM-5 catalysts (Figure 5-14). Whilst the aromatic content rose from within a range of 0.8 % to 6.4 % to 51.5 % to a maximum of 76.1 % which was achieved at 500 °C with the 1Ni/ZSM-5 the same as with oleic acid. At this maximum proportion, the compounds benzene, toluene, ethylbenzene, and xylene were identified to account for 10.9 %, 26.6 %, 4.2 % and 27.1 % of the total aromatic compounds present whilst the remaining 31.3 % was defined as other aromatics (Figure 5-19).

With both feedstocks (oleic acid and jatropha oil) the yield and proportion of aromatics was highest in the presence of the 1Ni/ZSM-5 catalyst (oleic acid- Figure 5-8 and Figure 5-11, jatropha oil- Figure 5-17 and Figure 5-19). The proportion of aromatics was 6% greater than using the ZSM-5 catalyst in the case of jatropha oil. This is of significance as such as increase for a small addition of nickel is of great benefit. The small increase in the presence of the 1Ni/ZSM-5 catalyst was attributed to its slightly larger pore volume and diameter established as part of the catalyst characterisation summarised in Table 5-2.

Overall, looking back to Chapter 2.0, section 2.4 where the research objectives were discussed it is possible to state that from the data presented in this chapter that BTX compounds are obtainable from the catalytic Py-GCMS of jatropha oil and that the utilisation of the 1Ni/ZSM-5 at a temperature of 500 °C provides the highest yield and proportion of aromatic products. A lower Nickel loading gives the slight increase in aromatics due to higher pore diameter and volume whilst almost maintaining the surface area of its parent ZSM-5 catalyst. The use of the oleic acid feedstock in conjunction with the jatropha oil has helped highlight different pathways and that aromatics and other compounds present in the jatropha oil will come from other compounds within the oil including the other fatty acids and glycerol.

CHAPTER 6.0 FLUIDISED BED FAST PYROLYSIS OF JATROPHA OIL

6.1. Introduction and aims

This chapter will consider the investigations completed for the thermal conversion of jatropha oil using the fluidised bed fast pyrolysis reactor system as described in section 3.3.4.2.

A process flow diagram of the fluidised bed reactor for the pyrolysis of inedible vegetable oils is provided in Chapter 3.0, section 3.3.4.2. These two process flow diagrams show the changes implemented to make the system more effective and reliable. The system was re-commissioned from a reactor previously used for the pyrolysis of solid feedstocks. A summary of the operational and design parameters used for the fluidised bed fast pyrolysis investigations is summarised in Table 6-1. These include values utilised to calculate parameters such as the fluidisation velocity, with complete calculations available in Chapter 8.0, Appendix Two.

Table 6-1. Summary of fluidised bed fast pyrolysis reactor parameters

Parameter	Value
Feed Rate	90 g h ⁻¹
Reactor Diameter	6.69 cm
Reactor Height	35.1 cm
Average sand particle size	300 µm
Mass of Sand	300 g
Minimum fluidisation velocity at operating temperature	4.47 L min ⁻¹
Nitrogen Pre- heater temperature	500 °C
Furnace temperature	470 °C
Heating Tape temperatures (Top, Bottom)	520 °C, 450 °C
Chiller Temperature	-4 °C
Overall Reactor Operating Temperature	450 °C

The purpose of these investigations was to ascertain if it was possible to undertake fluidised bed pyrolysis of a liquid triglyceride feedstock. The selection of reactor type was novel because no prior literature indicated this type of continuous reactor had been used to process this type of feedstock either thermally or catalytically. Furthermore, it was intended to analyse the effect of thermal processing on jatropha

oil feedstock and determine if it yielded similar results to those from the Pyroprobe GCMS investigations. This would allow clarification if similar decomposition products could be observed from both systems and determine how representative is the data obtained from the Pyroprobe GCMS investigations. It is highly beneficial to understand how similar data obtained from the reactor is to that of the pyroprobe because of the massively reduced time for the preparation and running of a Pyroprobe GCMS sample versus a couple of days for investigation in the fluidised bed fast pyrolysis reactor.

6.2.Feedstock characterisation

This section covers the characterisation of the fresh jatropha oil feedstock utilised in the fluidised bed fast pyrolysis reactor. The relevant results for the feedstock's heating value, viscosity, fatty acid composition and water content are presented in sections 6.3.1 to 6.3.4 below. The use of elemental analysis to investigate the CHNOS content, in addition to thermogravimetric analysis to assess the feedstock's thermal behaviour, was considered but was not possible due to a combination of equipment availability and concerns about potential damage to the analysis equipment. However, the data collected from these analyses will be compared against liquid product characteristics from the fluidised bed fast pyrolysis investigations to assess the changes.

6.2.1.Heating value

The higher heating value of fresh jatropha oil was obtained in duplicate using the Parr 6100 Calorimeter as per the method described in Chapter 3.0, section 3.3.1.3. The values obtained were duplicated, giving an average value of $39.73\text{ MJ/kg} \pm 0.19$. Compared to literature, this is within the range of 37.46 MJ/kg - 46.91 MJ/kg suggested by various sources [45, 47, 48, 65, 70, 71]. Furthermore, the values are similar to those obtained by Omran 2017 (39.74 , 39.47 and 39.18 MJ/kg), who used the same equipment to determine the higher heating value of jatropha oil from the same source [219].

6.2.2.Viscosity

The viscosity of jatropha oil was assessed using a Brookfield rotational viscometer; model DV-II+ Pro. The oil's viscosity was first assessed at room temperature and then from room temperature to $90\text{ }^{\circ}\text{C}$. The full methodology is explained within Chapter 3.0, section 3.3.1.2.

The viscosity of jatropha oil at room temperature (22.3 °C) was reasonably consistent 56.4 mPa.s, similar to the value of 55 mPa.s found in the literature[63]. Owing to the need to pump the oil, low viscosity and consistency are preferable for the feedstock.

To assess if there could be any implications on the viscosity when being heated, the change in its viscosity was monitored from room temperature to 90 °C. At the increased temperature, the viscosity of the jatropha oil reduced from 52.40 mPa.s and 56.92 mPa.s to 8.17 mPa.s and 8.10 mPa.s in Run 1 and Run 2, respectively. This makes the viscosity seven times lower at temperatures near 90 °C than that at room temperature. Although the reactor's operating temperature is significantly higher than this (450 °C), the reduction in viscosity is preferable as it means that the oil is unlikely to cause a blockage in the pump or reactor inlet when heated.

6.2.3.Fatty acid composition via GCMS

The fatty acid composition of jatropha oil was determined via GC-MS as per the method denoted in Chapter 3.0, section 3.3.1.5, which included the filtration and dilution of the jatropha oil sample. However, the chromatogram was not clear enough using a dilution of 3 parts acetone to 1-part jatropha oil, so this ratio was reduced to 2:1, with the analysis being duplicated to ensure consistency. The chromatogram for acetone: jatropha (2:1) is shown below in Figure 6-1 shows a closer view of the peaks of interest (X, Y, and Z), corresponding to palmitic acid, oleic acid, and linoleic acid, respectively.

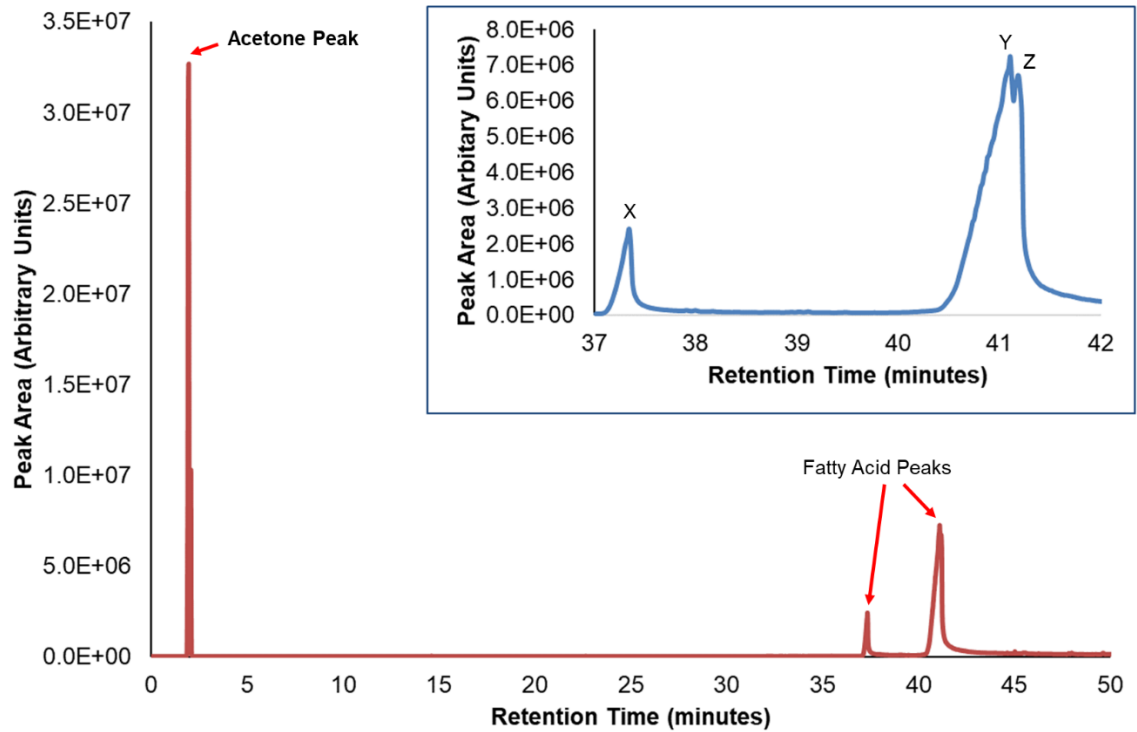


Figure 6-1. GCMS chromatogram of acetone with jatropha oil and peak identification (2:1)

The analysis of the chromatograms was completed using NIST and OpenChrom alongside considering the fatty acid composition of jatropha oil as discussed in Chapter 2.0, section 3.3.1.5. A summary of the relevant peaks identified from the chromatogram in Figure 6-1 is presented below in Table 6-2.

Table 6-2. Fatty acids identified in GCMS of jatropha oil

Peak	Time (min)	Identified Compound	Formula
X	37.2	n-Hexadecenoic acid (Palmitic Acid)	
Y	41.1	9-Octadecenoic Acid	
Z	41.2	9,12-Octadecenoic Acid	

From the literature, it was expected that these fatty acids would be identified as they make up the most significant proportion of jatropha oil (~87.3%) [3, 6, 8]. Although these results are quantitative, the area of the peak on the chromatogram is indicative of the abundance of each compound. The first peak (X) is the most minor and is palmitic acid (~10.3% of jatropha oil), whereas the more significant peaks Y and Z are oleic (~46% of jatropha oil) and linoleic acid (~31% of jatropha oil) respectively. These two peaks overlap one another and merge because oleic and linoleic acid are isomers of one another. The chromatogram obtained (Figure 6-1) will be compared with those obtained from the liquid pyrolysis product to determine how fluidised bed fast pyrolysis affects the jatropha oil feedstocks.

6.2.4. Water content via Karl-Fischer titration

The water content was determined using a Mettler Toledo V20 241 Karl Fischer (KF) titrator in triplicate using the methodology specified in Chapter 3.0 section 3.3.1.1. The values obtained are presented below in Table 6-3 alongside an average value and the standard deviation.

Table 6-3. Water content (%) of jatropha and neem oil by KF titration

Feedstock	Water Content (wt. %)			
	1	2	3	Average
Jatropha Oil	0.024	0.043	0.042	0.036 ± 0.009

From Table 6-3, the results show that the average water content of jatropha oil is near to negligible. This was anticipated due to the immiscible nature of triglyceride feedstocks and is supported by several literature sources that suggest it is typical for jatropha oil to have a water content of ~0.2 wt.%[72]. This is highly desirable for a pyrolysis feedstock as typically water contained within the feedstock will also be present in the product, reducing the higher heating value and reducing the stability of the liquid bio-oil products.

6.3. Non – catalytic fluidised bed fast pyrolysis

The jatropha oil feedstock was processed in the fluidised bed fast pyrolysis reactor without a catalyst at a temperature of 450 °C. A total of eight investigations were conducted in developing and altering the fluidised bed fast pyrolysis system to obtain sufficient data to complete a mass balance and characterising the liquid, gas, and solid products. The characterisation of the liquid, gas and solid pyrolysis products is presented in section 6.3.1. In addition, three of the eight runs provided the data to complete a mass balance which is presented in section 6.3.2 and reported as Run 1, Run 2, and Run 3. The triplicate values allow the calculation of an average composition with a standard deviation.

6.3.1. Fluidised bed fast pyrolysis products and characterisation

The fluidised bed reactor products have been investigated, specifically the liquid product whose viscosity, heating value, water content, and composition can be compared against the fresh jatropha oil feedstock. In addition, the composition of the gaseous products has been assessed using data obtained from the micro-GC and

solids content determined using either thermogravimetric analysis or the muffle furnace.

6.3.1.1. Liquid products

The gases from the fluidised bed reactor were cooled in a downstream condensing train with three collection points for liquid products, as shown in Chapter 3.0, section 3.3.4.2, Figure 3.17. These liquid products were collected after each investigation once the glassware of the condensing system had cooled. The liquid product's appearance differed from fresh jatropha oil feedstock, as shown in Figure 6-2.



Figure 6-2. Visual comparison of fresh jatropha oil (left) and fluidised bed fast pyrolysis liquid product (right)

In addition to the visual changes, there were minor differences in the characteristics of the liquid product, including water content, heating value and viscosity. These are presented below in Table 6-4 alongside the fresh jatropha oil characteristics for comparison.

Table 6-4. Characteristics of liquid fluidised bed fast pyrolysis product and jatropha oil feedstock

Run	Water Content (wt. %)	HHV (MJ/kg)	Viscosity at Room Temperature (mPa.s)
1	0.0525	40.64	20.50
2	0.0425	40.83	22.00
3	0.0403	40.76	20.50
average liquid pyrolysis product	0.0451 ± 0.01	40.74 ± 0.1	21.00 ± 0.87
jatropha oil	0.036 ± 0.009	39.73 ± 0.19	56.40

From Table 6-4 it is apparent that the increase in the higher heating value (HHV) and water content in the liquid pyrolysis products, compared to those of fresh jatropha oil, are of little significance, particularly the very low water content. As for the viscosity of the fresh jatropha oil, it had decreased from a value of 56.40 mPa.s to 21.00 mPa.s ± 0.087 . Similar changes were observed by Wang et al. 2016 who considered the thermal decomposition of jatropha oil at a temperature of 410 °C with the jatropha oils'

kinematic viscosity decreasing from $33.56 \text{ mm}^2 \text{s}^{-1}$ to $1.76 \text{ mm}^2 \text{s}^{-1}$ [47]. Wang et al., 2016 attributed the changes in viscosity to the formation of short-chain hydrocarbons and fatty acid compounds, also observed in this work. The product's viscosity is significant because high viscosities can make its transportation and storage more challenging and costly[220]. It is of significance to note that the liquid product had a very low viscosity in this work. This was despite its low water content as typically high-water content feedstocks have low viscosities and vice versa. It is shown in work by Nolte et al. 2010 in Figure 6-3 the implication of these characteristics have on a variety of biomass feedstocks[221].

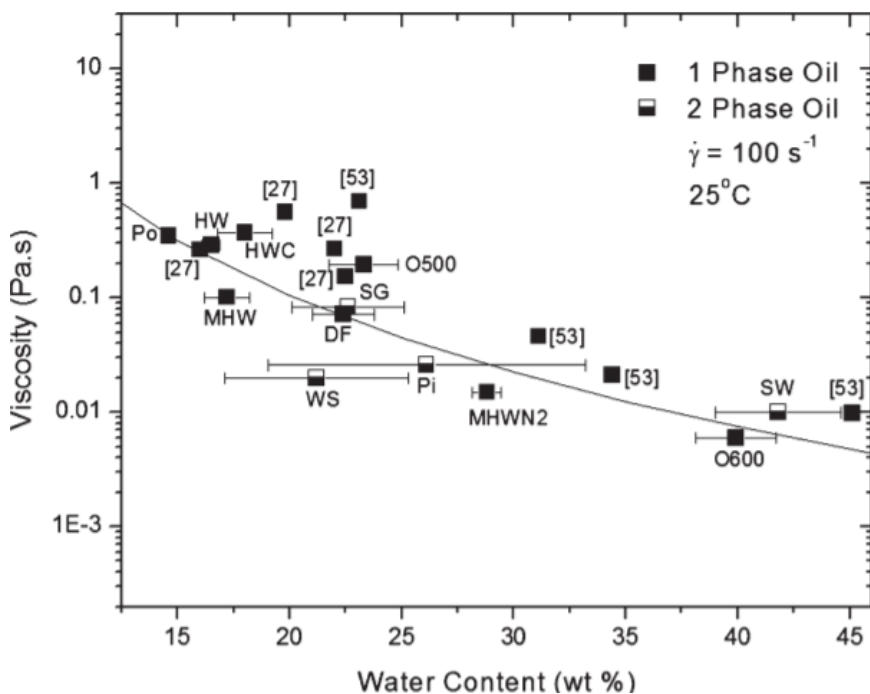


Figure 6-3. Relationship between water content and viscosity of pyrolysis bio-oils, Nolte et al. 2010 [221]

In addition to the characteristics of the liquid product, its composition was also considered, with the analysis of the liquid product being carried out in duplicate and using the same method as described in section 3.3.1.5. All samples were $0.5 \mu\text{l}$ and used a ratio of three parts of acetone.

The graphs shown below (Figure 6-4, Figure 6-5 &) are the chromatograms from the first runs. The duplicates were almost identical and did not show any anomalies of significance.

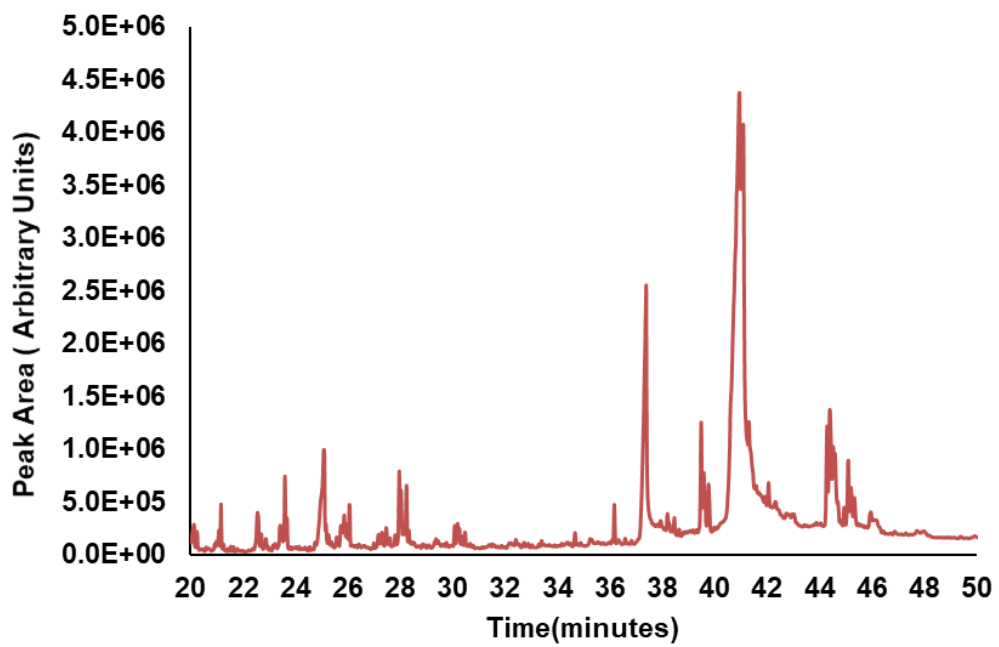


Figure 6-4. GCMS chromatogram acetone: liquid pyrolysis product (3:1) from run 1

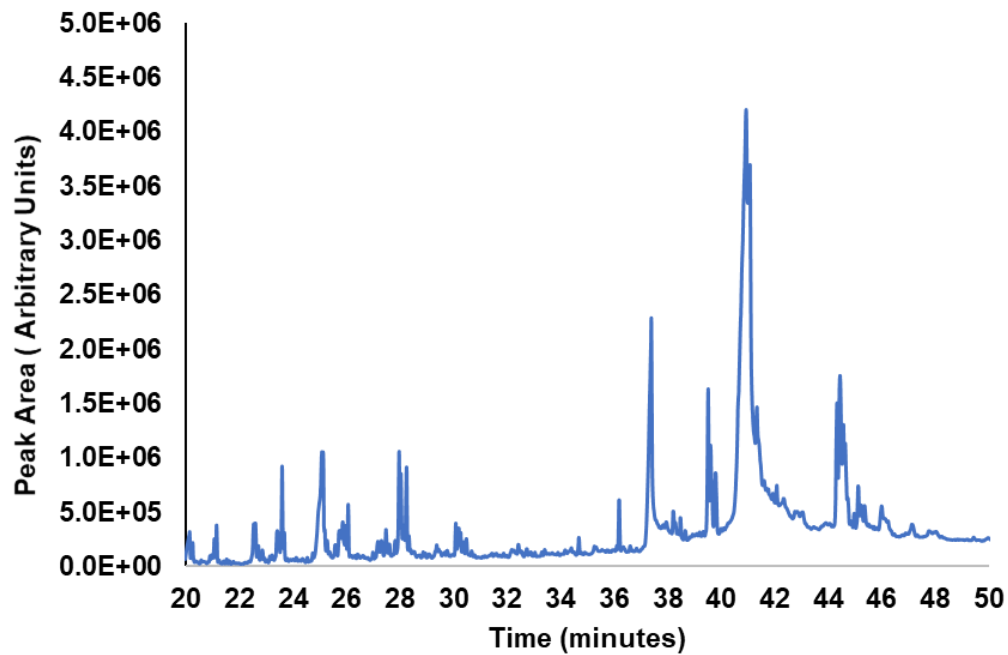
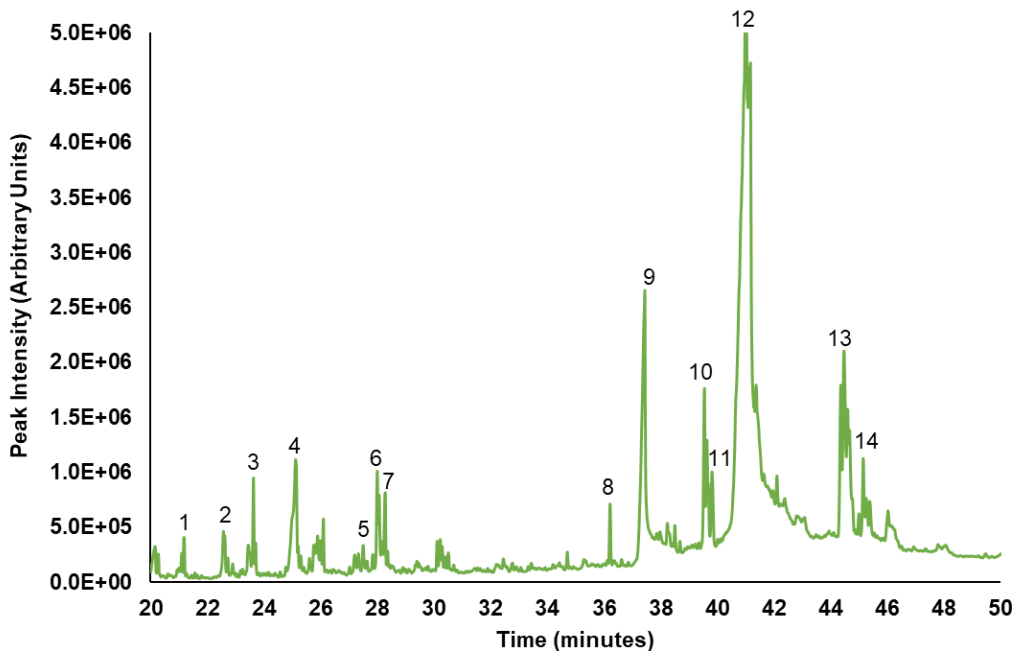


Figure 6-5. GCMS chromatogram acetone: liquid pyrolysis product (3:1) from run 2



Figure

6-6. GCMS chromatogram acetone: liquid pyrolysis product (3:1) from run 3

The GCMS data shown in the chromatograms (Figure 6-4, Figure 6-5 & Figure 6-6 above) are very consistent compared to one another. The duplicate chromatograms further verify these. Overall, 14 key peaks were identified using OpenChrom and NIST. The potential compounds labelled in Figure 6-6 have each been matched to a retention time, with the key peaks being summarised in

Table 6-5 below:

Table 6-5. Summary of key peaks from GCMS of liquid pyrolysis product

Peak#	Retention Time	Suggested Compound	Comments/ Formulae
1	21.2	7-Tetradecene	Aliphatic, C ₁₄ H ₂₈
2	22.6	17-Octadecenoic acid	Acid, C ₁₈ H ₃₂ O ₂
3	23.6	Oxirane-Tetradecyl	Ether, C ₁₆ H ₃₂ O
4	25.1	Unidentified	Unidentified
5	26.1	13-Octadecenal	Aldehyde, C ₁₈ H ₃₄ O
6	27.98	cis-9-Hexadecanal	Aldehyde, C ₁₈ H ₃₀ O
7	28.26	Aspidospermidin-17-ol, 1-acetyl-19,21-epoxy-15,16-dimethoxy-	Nitrogen compound- C ₂₃ H ₃₀ N ₂ O ₅
8	36.12	cis-13-Eicosenoic acid	Fatty Acid- C ₂₀ H ₃₈ O ₂
9	37.40	i-Propyl 14-methyl-pentadecanoate	Ester, C ₁₉ H ₃₈ O ₂
10	39.50	Ethanol,2-(9-octadecenloxy)-, (Z)	Ether, C ₂₀ H ₄₀ O ₂
11	39.78	E, E, Z-1,3,12-Nonadecatriene-5,14-diol	Alcohol- C ₁₉ H ₃₄ O ₂
12	40.97	i-Propyl 11-octadecenoate	Ester, C ₂₁ H ₄₀ O ₂
13	44.32	Linoleic acid ethyl ester	Ester, C ₂₀ H ₃₆ O ₂
14	45.12	Oleic anhydride	Fatty acid anhydride- C ₃₆ H ₆₆ O ₃

From the chromatograms (Figure 6-4, Figure 6-5 and Figure 6-6) alongside

Table 6-5, it can be observed that the most prevalent compounds are peaks 9 and 12, corresponding to the ester compounds i-Propyl 14-methyl-pentadecanoate and i-Propyl 11-octadecenoate at 37.40 minutes and 39.78 minutes, respectively. The abundance of these ester compounds and others is very noticeable in Figure 6-7 below. This graph shows the percentage of the peak area of the major groups of compounds present in the liquid product of the products from each of the runs.

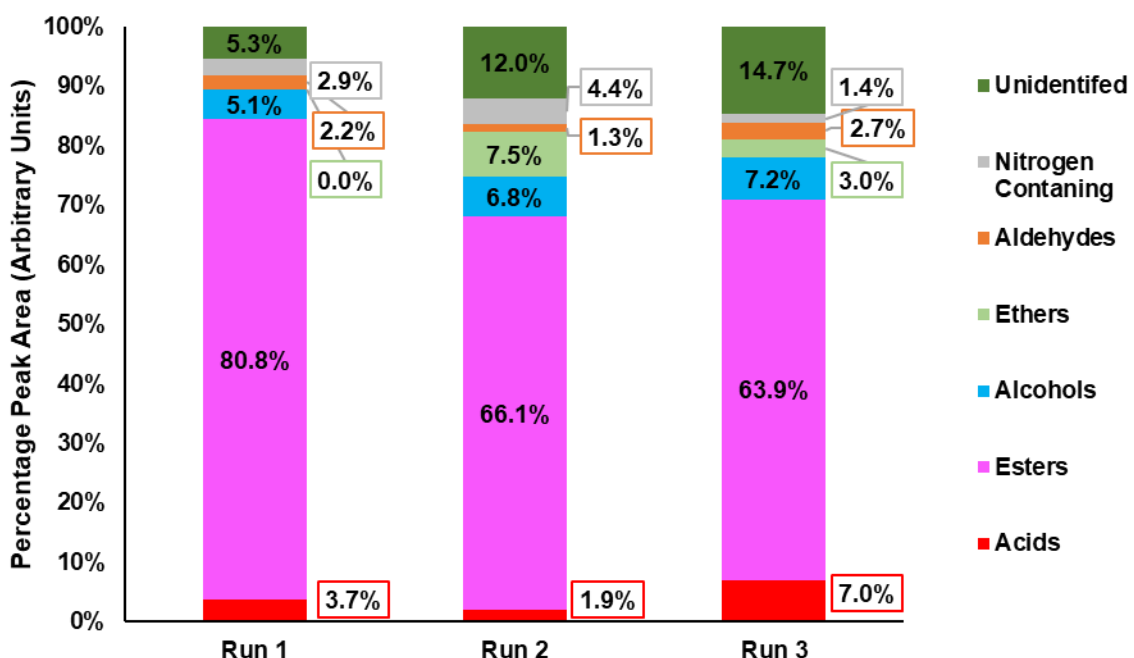


Figure 6-7. Pyrolysis liquid products from jatropha oil in a fluidised bed reactor at 450 °C

From both Figure 6-7 and

Table 6-5, it is clear that the liquid pyrolysis product composition is more complex than the jatropha oil feedstock owing to the presence of a much greater number of peaks than observed in the analysis of the feedstock (Figure 6-1). The presence of the compound i-Propyl 11-octadecenoate makes sense as this is an ester (EST) of Oleic acid which contributes to ~46 wt.% to the jatropha oil composition. Oliveira et al. 2013 report that esters of the fatty acids, including Oleic acid ethyl ester and Palmitic ethyl ester, have a heating value in the region of 41 to 41.5MJ/kg[222]. The evolution of ester compounds from triglyceride feedstocks, including oleic, linoleic, and palmitic acid, found in jatropha oil, was discussed in work by Idem et al. earlier in Chapter 4.0, section 4.2.1 and 4.2.2. It was suggested by Idem et al. that the production of these

esters is a result of the initial decomposition of the triglyceride molecule alongside other compounds such as aldehydes, alcohols, and smaller fatty acids.

Therefore, the presence of such fatty acid esters could be the reason for the marginal increase in the heating value of the liquid product, as reported from 39.73MJ/kg to 40.74MJ/kg.

When focusing on esters, Idem et al. suggest their formation usually occurs at the lower temperatures between 240 °C and 300 °C[123]. In light of this temperature range and the smaller proportions of aldehydes and alcohols, it could be concluded that the residence time was too short or the oil was not exposed to high enough temperatures to decompose it further. As the internal reactor temperature was monitored and observed to go above 450 °C, it must be that the residence time is too short. This would result in the vapours exiting the downstream condensing train too quickly for further decomposition reactions.

Other compounds identified in the liquid products included acids, ether, alcohol, and aldehyde compounds (Figure 6-7). These included the fatty acid compounds, oleic acid and linoleic acid, which were identified in Table 6-2, discussing the composition of the jatropha oil feedstock prior to the conversion of the feedstock in the fluidised bed fast pyrolysis system. Following conversion in the fluidised bed reactor, only a small amount of acids are present at a maximum of 7.0% and a minimum of 1.6% of the peak area, as shown in Figure 6-6. This was attributed to the presence of cis-13-Eicosenoic acid, which must have been formed from the decomposition of the triglyceride compounds as this fatty acid is not present in jatropha oil.

As for the ether and alcohol compounds in the literature, it is suggested by Wang et al. that these compounds can be produced from the deoxygenation of fatty acids, with the decomposition scheme for Oleic acid shown below in Figure 6-8 [223].

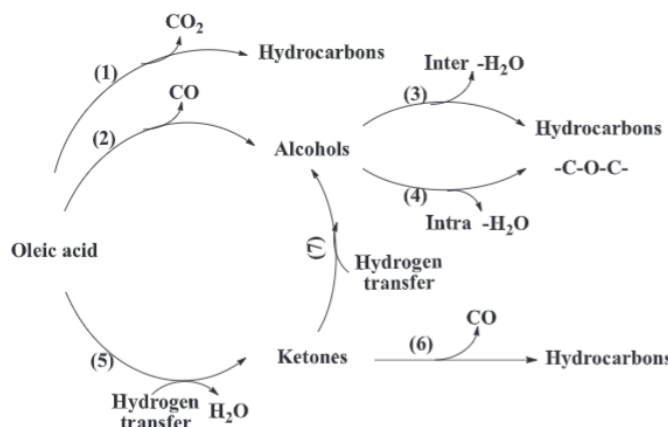


Figure 6-8. Decomposition scheme for oleic acid to alcohols and ethers, Wang et al. [223]

Considering the scheme in Figure 6-8 and considering fatty acids such as palmitic and the cis-13-eicosenoic acid decomposing in the same way then this could give rise to some of the compounds listed in

Table 6-5. It is possible that the ether compound Oxirane- Tetradecyl (23.6 minutes) was produced from Palmitic acid by following pathways 2 and 3 or 5, 7 and 4. Then the alcohol compound Ethanol,2-(9-octadecenloxy)-, (Z) (39.5 minutes) from cis-13-eicosenoic acid via pathways 2 or 5 and 7.

As for the small amount of aldehyde products visible in Figure 6-7, these only contribute 2.2 %, 1.6% and 2.7% of the peak area in run 1, run 2 and run 3. It is anticipated that these were produced via similar pathways to those observed in the non-catalytic pyrolysis of jatropha oil in the Py-GCMS system. The relevant pathways for the production of aldehydes in Chapter 4.0 include those by Frankel et al. and Shi et al. as per Figure 4.12 and Figure 4.13 from section 4.2.2. The major aldehyde compound was cis-9-hexadecanal, was identified in Figure 6-6 and

Table 6-5 as peak 6.

Finally, the last peak of the chromatograms (Figure 6-4, Figure 6-5 and Figure 6-6) was attributed to the compound Oleic anhydride. Similar anhydride compounds were observed by Gosselink et al., 2013, who investigated Stearic acid decomposition [75]. In contrast to Gosselink, no ketones and negligible amounts of aliphatics, including the straight-chain alkenes and alkanes, were observed in this work. This observation suggests that the pathways for the production of ester compounds were most definitely favoured in this work. This preference towards esters agrees with the earlier statement that perhaps the high proportion of esters arises from the initial decomposition of the triglyceride occurring at the lower temperatures of 240 °C and 300 °C[123]

6.3.1.2. Gaseous products

The gaseous products from the fluidised bed fast pyrolysis reactor were analysed by an online Micro GC system described in section 3.3.3. The system analysed the pyrolysis gases at regular intervals of 150 seconds throughout each run. The gas composition was variable between the three completed investigations. Therefore, the total mass of gaseous products has been calculated as part of the mass balance in the following section (6.3.2).

The gas composition was measured throughout the investigation from the heating up of the reactor and throughout the initial reactor cool down when oil had been stopped

being fed into the reactor. For evaluating the gas composition, an average has been calculated using values from the Micro GC during the reaction period. The average proportion of gases present throughout the reaction period are presented in Table 6-6 below. The calculations assumed that all Nitrogen in the gaseous product is from its use as the inert fluidising and carrier gas, and the reaction period is assumed to be from the point at which the oil feed was started until no visible vapour products were observed after the oil feed was turned off.

Table 6-6. Average gas products composition from the pyrolysis of jatropha oil

Gases	Run 1 (vol. %)	Run 2 (vol.%)	Run 3 (vol.%)
CO	24.5	0.0	0.0
CO₂	33.0	26.4	48.4
CH₄	0.0	2.4	7.6
C₂=	14.1	4.3	14.9
C₂	7.7	3.2	9.5
C₃=	11.3	58.9	12.6
C₃	4.8	4.7	7.1
C₄=	3.2	0.0	0.0
C₄	1.4	0.0	0.0
H₂	0.1	0.0	0.0

From Table 6-6, it can be seen that the product gases include CO, CO₂ and a range of hydrocarbons, including CH₄, C₂, C₃ and C₄ alkenes and alkenes and in the case of Run 1, also a small amount of hydrogen. The first observation is the absence of CO in the second and third run, which was identified as an issue with the equipment recording this proportion of gas. A comparison of the different gases present is shown below in graph Figure 6-9.

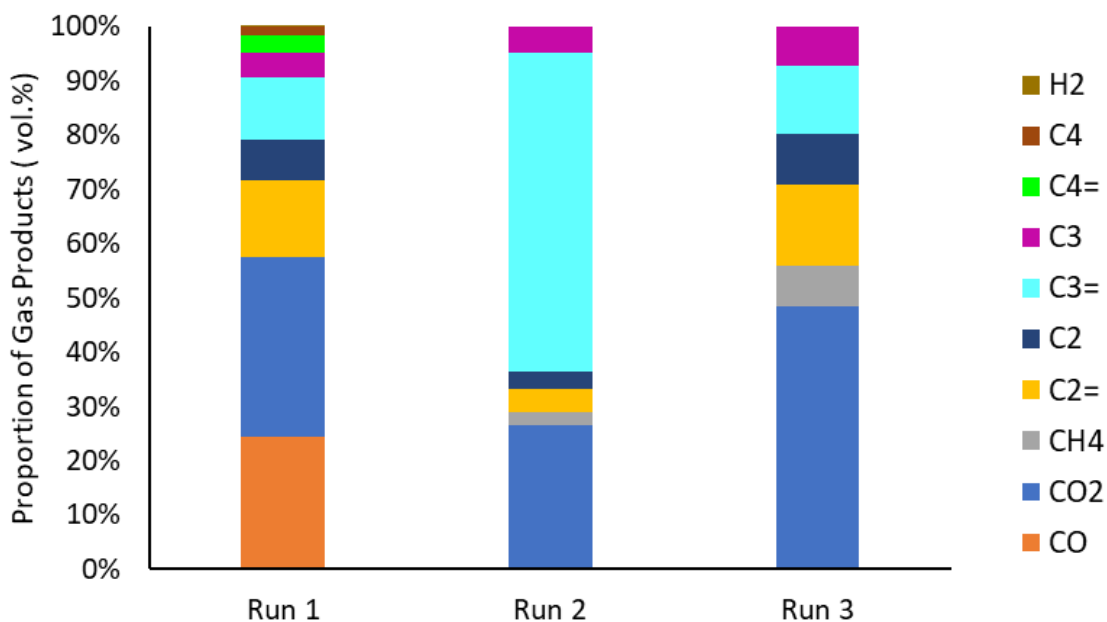


Figure 6-9. Comparison of the composition of gaseous products from the pyrolysis of jatropha oil

A comparison of the overall composition from Figure 6-9, as anticipated, shows that there are some similarities with each run sharing CO₂ and almost all of the light hydrocarbon gases (C₂= to C₃) as common products. The absence of CO from the second and third run was attributed to an error within the Micro-GC, which meant that it was impossible to identify this product in the gas stream, making the overall gas composition of Run 2 in particular vastly different. The composition from Run 1 and Run 3 was the most similar, with them sharing similar proportions of the light hydrocarbon gases including C₂= (14 vol.% and 15 vol.%), C₂ (8 vol.% and 9 vol.%), C₃= (11 vol.% and 13 vol.) and C₃ (5 vol.% and 7 vol.%).

The identified gas composition in this work was anticipated, as other studies considering the pyrolysis of triglycerides have shown the production of similar gas components [2, 48]. For example, Beims et al., 2018; the pyrolysis of mixtures consisting of different proportions of soyabean oil and hydrogenated fat were investigated. The feedstocks were processed in a plug flow reactor at 525 °C. Their reported gas composition is shown in Figure 6-10 below.

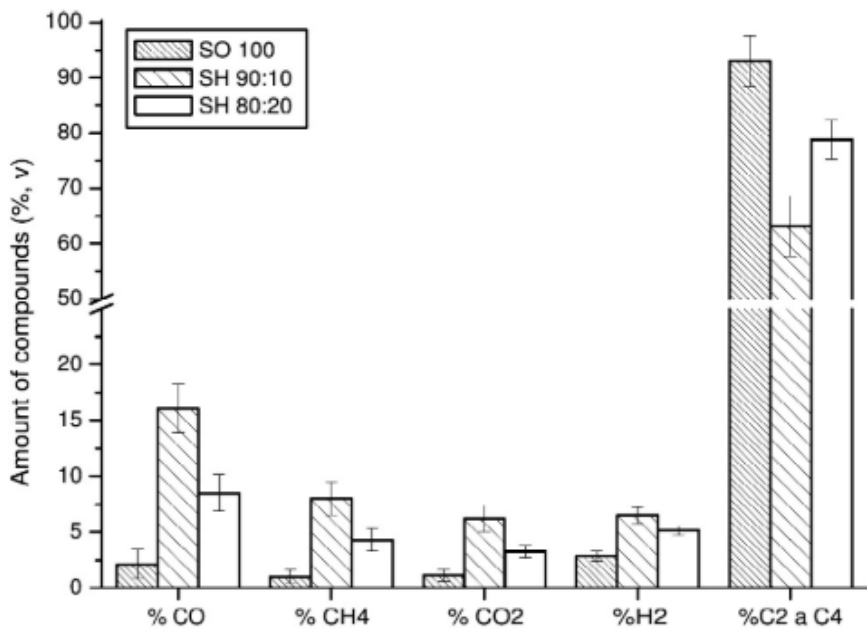


Figure 6-10. Beims et al., 2018, Composition of gaseous fractions produced in thermal cracking of soybean oil(SO) and soybean oil:hydrogenated fat mixtures (SH)[2]

From Figure 6-10, although similar gases to those produced in this work are observed, the amounts of the different gases present are very different. For example, in work by Beims et al., the light hydrocarbon gases (C_2 to C_4 hydrocarbons), as shown in graph Figure 6-10, made up most gas products in the range of 60 vol% to 90 vol%. However, in this work, as shown by Figure 6-9 Run 1 and 3, these products attributed for just ~42.5 vol.% and 44 vol.% of the light hydrocarbon gases, respectively. Furthermore, a large difference was observed in the amounts of CO_2 and hydrogen present with Beims et al. observing ~2 vol.% to ~7 vol.% CO_2 and ~3 vol.% to ~7 vol.% hydrogen compared to values of 33.0 vol.% and 48.4% vol.% The similarities in terms of the different gases present are potentially attributed to the soybean oil used by Beims et al. containing similar fatty acids to jatropha oil, including oleic and palmitic acid. However, the large differences in the proportions present in the light hydrocarbons, CO_2 and hydrogen could be attributed to multiple factors, including the different type of reactor system, utilisation of an argon carrier gas instead of nitrogen as well as the feedstock containing different proportions of these similar fatty acids [2].

6.3.1.3. Solid Products

The mass of solids from the non-catalytic fast pyrolysis of jatropha oil was determined by thermogravimetric analysis for Run 2 and using a muffle furnace for Run 3 (section 3.3.2). It was not possible to calculate this value for Run 1; so, for mass balance purposes, a value of 0.1% was assumed as determined by the thermogravimetric analysis has been used as this is the more precise methodology. This gave an average solids content near to negligible at just 0.72 wt.% \pm 0.27. These methods were utilised due to time restraints and equipment availability.

The low proportion of solid products was very apparent in the initial investigations. In addition, it showed there was no requirement for a char pot, unlike when the system was previously utilised to process solid feedstocks like the lignocellulosic feedstocks discussed earlier in section 2.1.2. This absence of char is likely attributed to the composition of the feedstock as jatropha oil.

In a work by Biswas et al. 2013, the thermal cracking of jatropha oil was undertaken in a batch reactor at temperatures of 300 °C, 350 °C and 375 °C at atmospheric pressure with an inert nitrogen atmosphere for different lengths of time. No solid products were observed at the lowest temperature, only gases and liquids alongside some unreacted feedstock. As for the higher temperatures, 350 °C and 375 °C, the char yields were dependent upon the reaction time. At around 2 minutes, the char accounted for ~25% or 20% at a temperature of 350 °C and 375 °C. This dropped significantly at a reaction time of 4 minutes to values of ~5% and near 0% at a temperature of 350 °C and 375 °C, respectively. Beyond this reaction time at 350 °C, the amount of char was near to 0% up till around 10 minutes, whilst at the higher temperature of 375 °C, it to be 0% from around 5 minutes. This indicates that higher temperatures may reduce char yields, so at a temperature of 450 °C, as in this work, similar negligible solids yields may be observed[71].

6.3.2. Mass balance

A mass balance has been conducted for the fluidised bed fast pyrolysis of jatropha oil. In the process of completing the mass balance, the following assumptions have been made:

- No solid product was collected in the char pot, so the only solid products were assumed to be present in the sand. Therefore, the content value for Run 1 was assumed to be the same as Run 3 as determined by TGA at a value of 0.1%.
- For the gas product, the average percentage composition from the micro-GC data was utilised. The ideal gas law was used to calculate the mass of the gas by using an average relative molecular mass (M_r) of the gas.
- The liquid fed in was assumed to be that measured by the flow meter. The liquid products out were calculated by the mass difference between the glassware in the condensing train before and after the run.

The yields of the major products, including solids, liquids, and gases, in addition to the losses, are presented below in Figure 6-11.

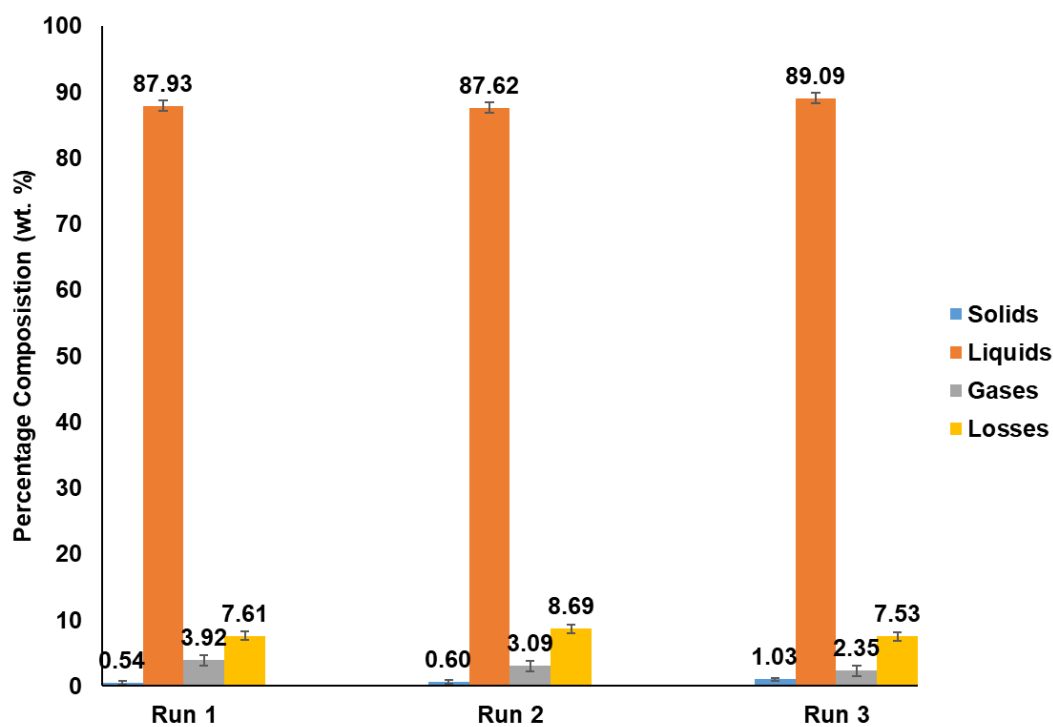


Figure 6-11. Mass balance, composition of products for fluidised fast bed pyrolysis of jatropha oil

From Figure 6-11, it can be observed that the distribution of the products from jatropha oil pyrolysis is relatively consistent. The amount of liquids was the highest in each run, with an average of 88.21 wt.% \pm 0.77. As for the solids and gases, their average values were 0.72 wt.% \pm 0.27 and 3.12 wt.% \pm 0.78, respectively. The slightly increased variation in the mass of solids for Run 3 could be because the solids content for the final run was determined using the muffle furnace, which is not as accurate as the thermogravimetric analysis used in Run 2. Overall, an average of 92.06 wt.% \pm 1.83 of the products was accounted for. The losses have been attributed to small glassware leaks and a culmination of the errors associated with determining the proportion of liquids, solids, and gases. In literature by M. S. Landis et al. 2012 values of 80% to 120% are quoted as acceptable[224].

6.4.Comparison of fluidised bed and pyroprobe systems

This section will compare the data obtained from the non-catalytic conversion of jatropha oil in the fluidised bed fast pyrolysis reactor and the Pyroprobe (Py-GCMS). This comparison aims to assess the similarities or differences in the yield and distribution of the products. The comparison will be used to ascertain if data obtained from the pyroprobe could be used as a reference point to predict what is obtainable utilising the fluidised bed reactor.

The analysis will include a comparison of the jatropha oil decomposition pathways for both systems and highlight major product compounds identified. This comparison is of significance as shorter times (sample preparation, analysis, and data processing) are needed when using the Py-GCMS system (~4 to ~6 hours); versus the times needed to operate the fluidised bed fast pyrolysis system (3 to 4 days).

The pyrolysis products distribution for both systems were compared at similar processing temperatures, including 400 °C and 500 °C for the Py-GCMS and 450 °C for the fluidised bed. The major functional groups from both the Py-GCMS system (400 °C and 500 °C) and the fluidised bed (450 °C) are shown in Figure 6-12 below.

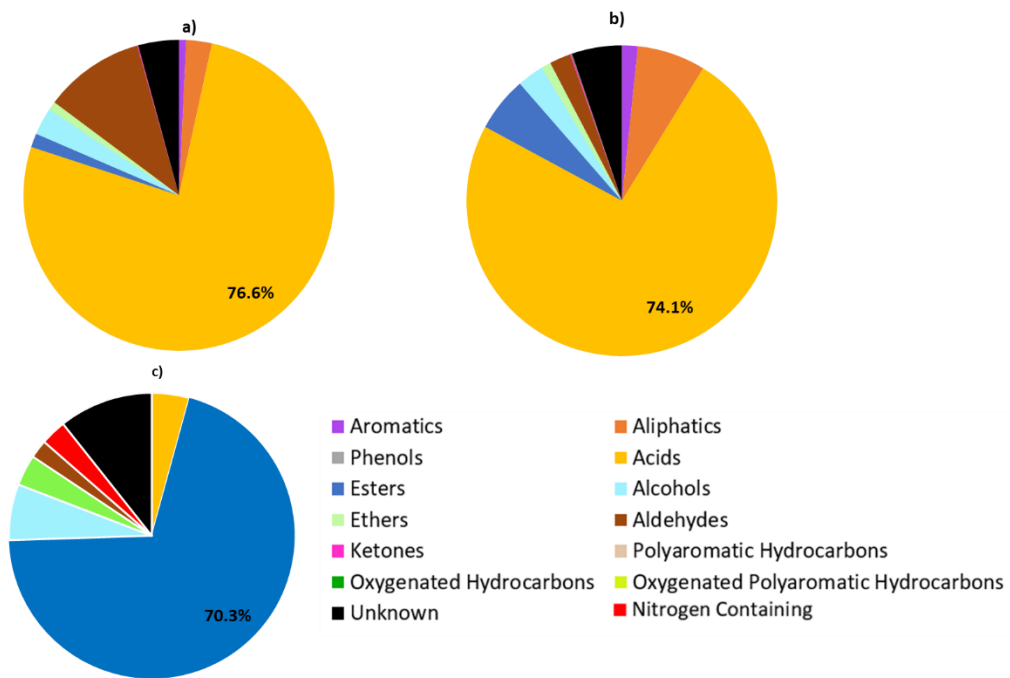


Figure 6-12. Product distribution from non-catalytic pyrolysis of jatropha oil: a) Py-GCMS at 400 °C, b) Py-GCMS at 500 °C; and c) fluidised bed at 450 °C.

When comparing the yield and distribution of the various products from the pyroprobe (Figure 6-12a-b) and fluidised bed (Figure 6-12c) systems, the product distribution differences can be attributed to how these systems process the feedstock. In literature, Bressler et al. 2007, state that the results of pyrolyzing triglyceride feedstocks can be dependent on factors such as the reactor type, residence time, reaction temperature, and the procedures and analysis used for the assessment of reaction products [103]. Nevertheless, although the results are likely to have differences, there is still potential for identifying similarities in the data, which is of great benefit owing to the reduced time required for Py-GCMS analysis compared to investigations in the fluidised bed fast pyrolysis reactor.

From the Py-GCMS results (Figure 6-12a-b), it is observed that changing the temperature between 400 °C and 500 °C does not drastically alter the distribution of the product, so it can be assumed that a similar product distribution for Py-GCMS test at 450 °C would be obtained. However, major differences in terms of product distribution are observed when comparing the Py-GCMS (Figure 6-12a-b) against the fluidised bed fast pyrolysis system (Figure 6-12c). For example, while the jatropha oil conversion in the pyroprobe results mainly in acids (~78%), the main products from the jatropha oil conversion in the fluidised bed are esters (70.3%).

With the major product from Py-GCMS being acids and aliphatics versus esters from the fluidised bed fast pyrolysis reactor, it is apparent that the two systems favour different major decomposition pathways.

In addition, to the presence of acids and esters, a small number of functional groups were identified in both systems, including alcohols, aldehydes, and ethers. As well as these compounds, nitrogen-containing compounds were identified in the fluidised bed products, whilst in the Py-GCMS products, small amounts of aromatics and aliphatics were present. The aliphatics and aromatics identified in the Py-GCMS investigations included the higher value compounds BTX as discussed in Chapter 4.0, section 4.2.1.

The non-catalytic pyrolysis of jatropha oil (Py-GCMS) identified a preference for the decomposition of fatty acid compounds into aliphatics. Whilst the acid compounds present were simply unconverted fatty acid compounds from the jatropha oil feedstock. These aliphatic compounds were identified as precursors of aromatic compounds in the decomposition pathway by Schwab et al. 1998 (see Chapter 4.0, section 4.2.1, Figure 4.5). Comparatively, in the fluidised bed (Chapter 6.0, section 6.3.3.1), a preference was shown for the decomposition of jatropha oil to ester compounds.

The difference in preference could be attributed to several factors, with one of those being residence time. The literature by Idem et al. 1996 stated that a low space velocity and a long residence time are required to decompose triglyceride compounds into intermediate products [123]. This means shorter residence times like those in the Pyroprobe leads to the lack of conversion of acids initially present in the feedstock (jatropha oil). This was supported by the proportion of acids shown in Figures 12a-b (~75%). In comparison, longer residence times comparable to the fluidised bed resulted in further feedstock conversion into other products such as esters (Figure 6-12c). When comparing this to the fluidised bed reactor (Figure 6-12c), a significantly lower proportion of acids are present (~2.7%), demonstrating how the more extended time has allowed for greater feedstock conversion to other products.

The evolution of ester compounds in the fluidised bed fast reactor is of significance as similar observations were made in work by Biswas et al. A jatropha oil feedstock was heated to 375 °C in a fixed bed tubular batch reactor in the absence and presence of a ZSM-5 catalyst with the esters only present in the catalyst's absence. [45]. This is of interest as the observations from Biswas et al. and Idem et al. in Figure 4.11 Chapter 4.0, section 4.2.2, suggest that esters can further decompose into aromatics via pathways 1,2,17 and 23.

Although the conversion of jatropha oil in the fluidised bed reactor (450°C) showed no aromatics production (Figure 6-12c), the high proportion of ester compounds identified are relevant. It is feasible that these could be further converted into aromatics by adding ZSM-5 catalysts as suggested by the two decomposition mechanisms below from Habibi et al., 2018 (Figure 6-13 and Figure 6-14).

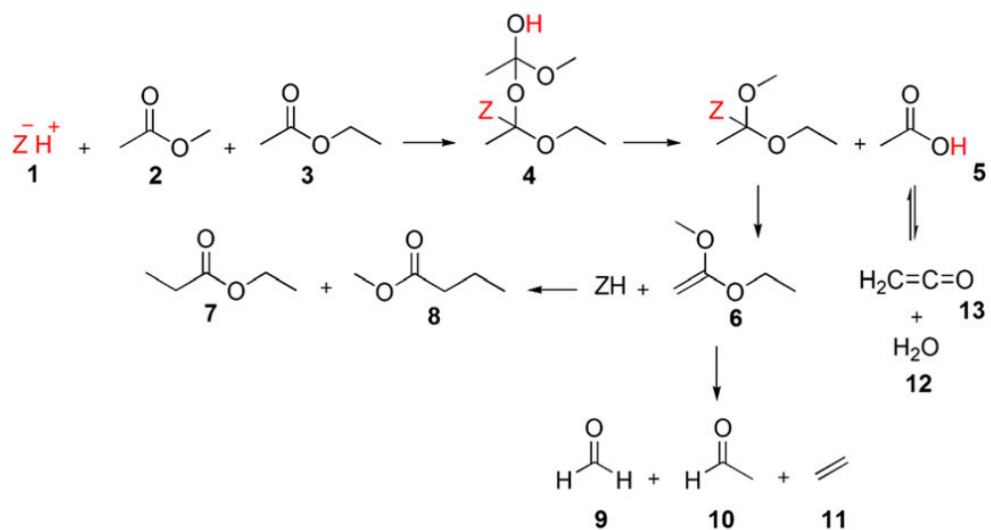


Figure 6-13. Part one- conversion of esters to aromatics in the presence of a ZSM-5 catalyst, Habibi et al., 2018 [22]

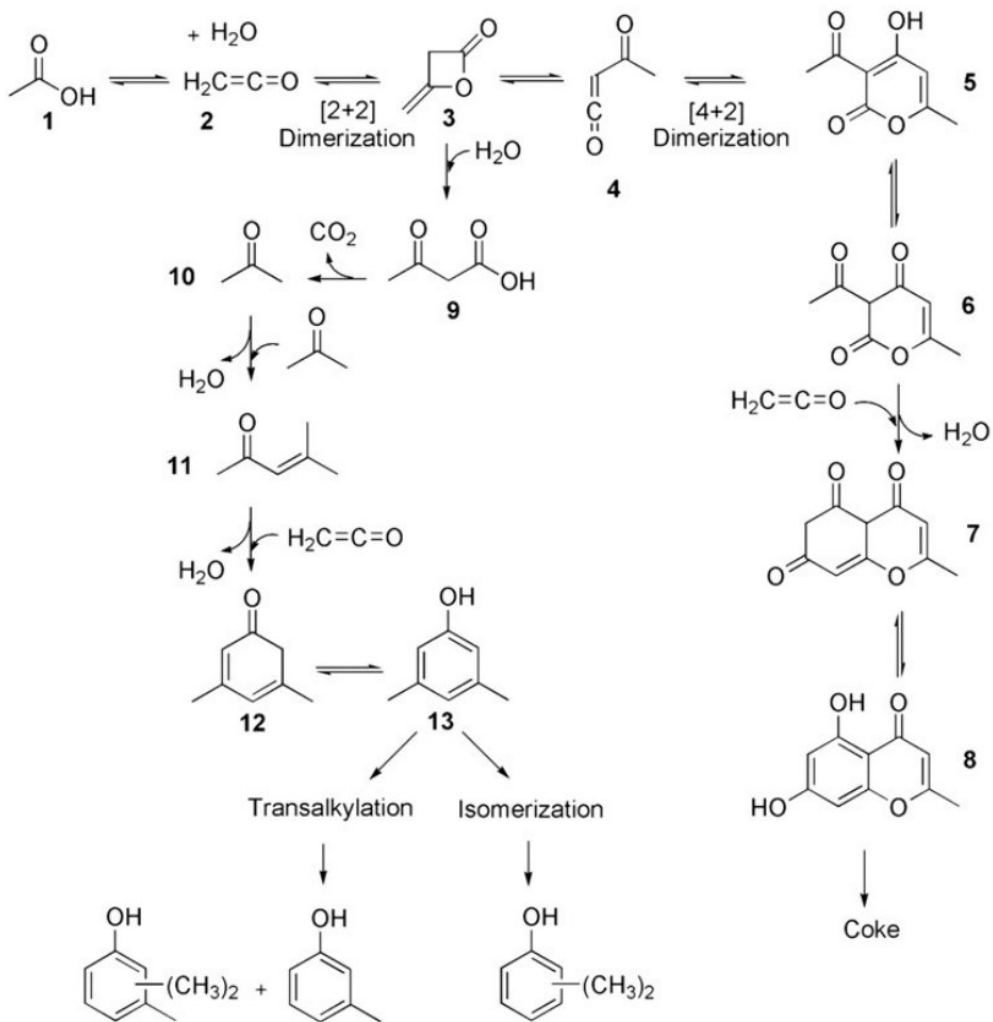


Figure 6-14. Part two- conversion of esters to aromatics in the presence of a ZSM-5 catalyst, Habibi et al., 2018 [225]

From Figure 6-14, it can be observed that aromatics are produced via reactions such as dimerization, transalkylation and isomerisation reactions. This means that although the non-catalytic decomposition of the jatropha oil in the fluidised bed fast pyrolysis reactor shows no evidence of aromatic compounds (Figure 6-12c) and has a different distribution of the major compounds, it still could be feasible for aromatics to be produced in the presence of a catalyst.

Similar observations have been made by Singh et al. 2021 in work considering the decomposition of the ester of steric acid (methyl octadecadienoate) being converted to aromatics over ZSM-5 and ZnCo/ZSM-5 catalysts [226].

Some similar compounds have been identified in this work in Table 6-5 including i-Propyl 14-methyl-pentadecanoate, i-Propyl 11-octadecenoate and Linoleic acid ethyl ester, which may decompose using the same decomposition pathway as proposed by Singh et al. 2021 shown below in Figure 6-15.

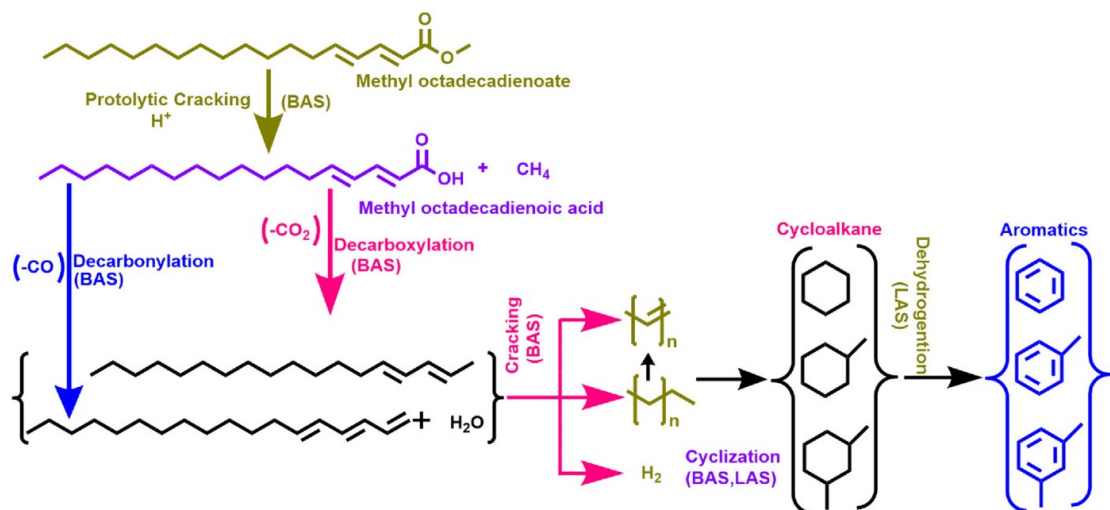


Figure 6-15. Decomposition of esters BTX aromatics, Singh et al., 2021[226]

In the context of this work, this mechanism suggested by Singh et al., 2021 (Figure 6-15) is of great significance. The mechanism shows the decomposition of ester compounds into aromatics in the presence of a ZSM-5 catalyst via various reaction steps, including cracking, decarbonylation or decarboxylation followed by cracking, cyclization, and dehydrogenation. The evolution of aromatics from jatropha oil in the presence of a catalyst could also arise from other components present in the feedstock, such as glycerol. It was discussed in Chapter 5.0, section 5.3.3 that the decomposition of glycerol to aromatics can occur in the presence of a ZSM-5 catalyst with the pathway proposed by Hoang et al., 2017 in Figure 5-19[218]. When considering the pathways presented by Habibi et al., Singh et al. and Hoang et al. together, it indicates that aromatics, particularly BTX, may still be obtainable from the fluidised bed fast pyrolysis of jatropha oil in the presence of a catalyst. However, it will be difficult to assess the most appropriate temperature and catalyst combination to yield the most aromatics in the fluidised bed system when using the Py-GCMS data. This is owing to the two systems seemingly favouring two differing decomposition pathways (Py-GCMS acids prefer to decompose to aliphatics versus Fluidised Bed where acids decompose to esters).

Overall, it can be concluded that the product distribution from non-catalytic pyrolysis of jatropha in a Py-GCMS system do differ from those in a fluidised bed fast pyrolysis system due to different decomposition pathways being favoured in each of the systems. It has been concluded that these differences arise due to a preference for different decomposition pathways, which is mainly influenced by the residence time of the feed in each system. The data shows that smaller amounts of the jatropha oil decompose to aliphatics in the Py-GCMS system with larger proportions of acid compounds present in the products. Most of the jatropha oil decomposes to esters in the fluidised bed system, with small proportions of acid compounds remaining in the products.

Considering this difference, it is not possible to recommend that the Py-GCMS be used to predict the products from the fluidised bed fast pyrolysis system. This means data from the catalytic pyrolysis of jatropha in the Py-GCMS may not be suited to decide the most appropriate catalyst and temperature combination for aromatics production in the fluidised bed fast pyrolysis reactor. However, it has been suggested by a culmination of decomposition pathways from Habibi et al. and Singh et al. that ester compounds produced from the thermal decomposition of jatropha oil in the fluidised bed could yield aromatics in the presence of a catalyst such as ZSM-5. This could be in addition to the aromatics from the glycerol component of the jatropha oil as discussed in Chapter 5.0, section 5.3.3, Figure 5-19. Therefore, in future work utilising a catalyst, it could still be feasible to obtain aromatic compounds, including BTX, from the fluidised bed fast pyrolysis system.

6.5.Further recommendations

Several avenues could have been explored to further investigate the fluidised bed fast pyrolysis reactor.

The first was to consider the use of catalytic pyrolysis of jatropha oil within the fluidised bed fast pyrolysis system. The implementation of this may have allowed further comparison of the Py-GCMS as the presence of a catalyst may influence the decomposition pathways and fluidised bed system. However, it not possible to undertake this due to successive delays in prior training and experimental work, which were primarily attributed to lab closures and ongoing restrictions with the COVID-19 pandemic.

A catalyst was intended to be selected based on the Pyroprobe GCMS data prioritising the yield and distribution of aromatic products. Its use in the fluidised bed reactor would allow comparison of the same catalyst and temperature combination used in the Py-GCMS investigations, i.e., 400 °C, 500 °C and 600 °C with the ZSM-5 1Ni/ZSM-5, 2Ni/ZSM-5, 5Ni/ZSM-5 and 10Ni/ZSM-5. The utilisation of a catalyst would have involved the incorporation of the catalyst into the fluidised bed as an example of an in-situ system. Alternatively, an ex-situ system could be developed to contain the catalyst at the reactor outlet for the reaction vapours to pass through before they are carried into the downstream condensing train. The use of a catalyst in this system would allow for a huge range of studies considering the catalyst: feed ratio as well as the catalyst lifetime

In addition to the above, other system improvements were also considered. These included replacing the rotameters used to measure the flow of nitrogen for the original solid feedstock feeder. The accuracy of these meters was highlighted in Chapter 3.0, section 3.3.4.2.3. Their replacement would also involve an additional O₂ line so the gas could be directly mixed with N₂ in the fluidised bed instead of having an external cylinder of an oxidising gas (40% O₂, 60%N₂) for the regeneration of the fluidised bed. An effective system for the regeneration of the fluidised bed is required even in non-catalytic runs to ensure fresh sand. It requires the disassembly of the top part of the reactor. This was incredibly time-consuming, taking around 2 days' work to disassemble and put back together after cleaning.

CHAPTER 7.0 CONCLUSIONS, RECOMMENDATIONS AND FURTHER WORK

7.1. Conclusions

From work conducted in the preceding chapters, the aims defined in the summary and research objectives in Chapter 2.0, section 2.4 have been addressed.

A route for converting a triglyceride feedstock to yield higher value aromatic compounds has been achieved via the catalytic fast pyrolysis of the inedible oil feedstock jatropha oil in a Py-GCMS system. The inedible oil feedstock was processed with ZSM-5 and Ni/ZSM-5 catalysts (1wt.%, 2 wt.%, 5wt.% and 10 wt.%) at temperatures of 400 °C, 500 °C and 600 °C. This was in order to determine the effect of different temperatures and the utilisation of a Nickel weighted catalyst upon the yield and distribution of the pyrolysis products. The main product of interest was aromatic compounds including benzene, toluene, and xylenes (BTX). It was noted that the small addition of nickel (1wt.% Ni/ZSM-5) increased the aromatics yield by ~6% at 500 °C with the jatropha oil feedstock to the maximum aromatic proportion observed at 76.1% when compared with the ZSM-5 catalyst.

The higher aromatics content in the presence of Nickel was attributed to a slight increase in pore diameter (1.505nm for ZSM-5 and 1.528nm for 1Ni/ZSM-5) alongside the low amount of nickel, not drastically decreasing the catalyst surface area (383.0 m²/g for ZSM-5 and 370.0 m²/g for 1Ni/ZSM-5). These findings demonstrate that the temperature of 500 °C and 1Ni/ZSM-5 catalyst is most favourable in this type of system for the decomposition of jatropha oil to aromatics, including BTX.

In addition to jatropha oil, oleic acid was used as a model compound and pyrolyzed in the same Py-GCMS system to help establish the potential decomposition pathways of the jatropha oil as a whole. In the absence of catalyst, acids formed a significant proportion of the products from the pyrolysis of both oleic acid and jatropha oil, min.82.0%, 600 °C and min. 39.3%, 600 °C, jatropha oil respectively.

These acid compounds were identified as unconverted fatty acids from the feedstock, whilst the common decomposition product was identified as aliphatics. The proportion of aliphatics was observed to increase with temperature. The proportions of aliphatics from oleic acid rose from 0.7% to 0.8% then 1.7% at temperatures of 400 °C, 500 °C and 600 °C, with similar observations made for jatropha oil with 2.7%, 7.1% and 23.9% aliphatics at 400 °C, 500 °C and 600 °C respectively.

This increase was in line with a rising aromatics content in the case of both feedstocks. Therefore, in conjunction with the literature, it was concluded that aliphatic compounds, including alkenes and alkanes, are precursors to aromatic compounds.

Furthermore, this work has demonstrated that a fluidised bed fast pyrolysis reactor can be utilised to convert jatropha oil. This reactor type was not observed in past literature, with most studies utilising fixed bed reactors or tubular reactors. Conversion of jatropha oil at 450 °C and flow rate of 90 ghr⁻¹ produced, on average, 88.21 wt.% ±0.77 liquid products, 3.12 wt.% ±0.78 gases and negligible solids at 0.72 wt.% ±0.27.

On average, the liquid product obtained from these investigations was predominantly made of esters at around 70.3% of the product, with minimal amounts of acid compounds remaining at just 4.2%. Therefore, it was concluded that esters were formed as initial decomposition products due to the residence time being too short for the components in the oil to decompose further to other products.

Finally, this work has compared the small scale Py-GCMS system and the bench-scale fluidised bed fast pyrolysis system. In addition, the data obtained from the non-catalytic conversion of jatropha oil in the fluidised bed fast pyrolysis reactor was compared with the Py-GCMS data obtained at 400 °C and 500 °C. It was apparent that the predominant compounds from each were very different with the Py-GCMS product mainly consisting of acids (76.6% at 400 °C, 74.1% at 500 °C) with smaller amounts of aliphatics (2.7% at 400 °C, 7.1 at 500 °C) and negligible amounts of aromatics (0.8 % at 400 °C, 1.6% at 500 °C) whilst the fluidised bed fast pyrolysis system product was mostly esters (70.3%) with a small proportion of acids (4.2%).

This difference in composition was attributed to systems having a preference for differing decomposition pathways associated with the systems residence times. It was also concluded that in the future, aromatics could still be obtained from the fluidised bed system if a catalyst was utilised based on evidence of esters being converted to aromatics in several literature sources.

7.2. Recommendations and future work

This section covers recommendations and further work. The suggestions focus on the two different reaction systems utilised in this work

7.2.1. Py-GCMS Studies

The recommendation for further Py-GCMS studies would be to investigate other predominant compounds within jatropha oil to ascertain if they decompose in the same manner as oleic acid. The compounds of most interest would be linoleic acid due to being so similar to oleic acid and the second most prevalent fatty acid in jatropha oil at 31.2 wt.% of the oil. This would be alongside the compound's palmitic acid (10.33 wt.% jatropha oil) and glycerol in triglyceride feedstocks with the fatty acid chains. The investigation into these compounds, in the same manner, would help to validate further the pathways suggested in Chapters 4.0 and 5.0. In addition, it would confirm the potential involvement of the glycerol compound in the catalytic decomposition as it was suggested this compound was attributed to the more significant increase in aromatics content seen with catalytic pyrolysis of jatropha oil versus the catalytic pyrolysis of oleic acid. In addition to considering alternative feedstocks, other metal modified ZSM-5 catalysts or other promising zeolite catalysts could be considered beyond ZSM-5, favourably influencing the aromatics yield or selectivity. Other potential metals discussed in the literature review within Chapter 2.0, section 2.3.4.2 include Platinum, Rhenium, Gallium, Zinc and Tin.

7.2.2. Fluidised bed studies

In addition to the non-catalytic conversion of jatropha oil in the fluidised bed, it would be desirable to conduct catalytic investigations using the catalysts from this work. It would be desirable to compare the catalytic data from the Py-GCMS to that from the fluidised bed reactor to ascertain: if the two systems still favour different decomposition pathways, as well as if aromatics are indeed yielded from the ester compounds as suggested by the decomposition mechanisms suggested in Chapter 6.0, section 6.4. In order to conduct these catalytic investigations, either an in-situ or ex-situ system must be defined and commissioned for its use. Further studies about the use of the catalyst in the fluidised bed fast pyrolysis system could include those into the catalyst lifetime to assess causes of catalyst deactivation and the effect of the catalyst to feed ratio on the yield and proportions of aromatic products.

CHAPTER 8.0 - APPENDICES

8.1.Appendix One- Reaction descriptors for the thermal cracking of canola oil

The following table gives reaction descriptors for the decomposition pathway shown in Chapter 2.0, section 2.2.3, Figure 2.15, in further detail. The letters I and II denote residual oil and organic liquid products, respectively.

Table 8-1. Descriptors of reactions occurring in the proposed reaction scheme for the thermal cracking of canola oil

Number	Reaction Information
1	Initial cracking of canola oil
2	C-C bond cleavage of unsaturated oxygenated hydrocarbons
3	Decarbonylation of saturated oxygenated hydrocarbons
4	Decarbonylation of saturated oxygenated hydrocarbons
5	Decarboxylation of short-chain oxygenated hydrocarbons
6	Decarbonylation of short-chain oxygenated hydrocarbons
7	Bimolecular dehydration of alcohols
8	Dehydration of ether
9	Bimolecular dehydration of short-chain alcohols to form short-chain ether
10	Dehydration of short-chain ether
11	
12	
13	Ethylene elimination, isomerization, and hydrogen transfer reactions
14	
15	Cyclization to from C ₃ to C ₅ cycloolefins
16	Cyclization to form C ₃ to C ₅ cycloparaffins
17	Diels- Alder addition of dienes to olefins to form C ₆₊ cycloolefins
18	Dehydrogenation of C ₃ to C ₅ cycloparaffins to form C ₃ to C ₅ cycloolefins
19	Hydrogenation of C ₃ to C ₅ cycloolefins to form C ₃ to C ₅ cycloparaffins
20	Dehydrogenation of C ₆₊ cycloparaffins to form C ₆₊ cycloolefins
21	Hydrogenation of C ₆₊ cycloolefins to form C ₆₊ cycloparaffins
22	Polymerization/Dehydrogenation of olefins, to from dienes, acetylenes and polyolefins
23	Aromatization of C ₆₊ cycloolefins to form C ₆₊ aromatics
24	Polymerisation of aromatics form polyaromatics
25	Coking from polyaromatics
26	Coking by polycondensation of oxygenated hydrocarbons
27	Coking by polycondensation of canola oil
28	Splitting of long-chain hydrocarbons into its elements and ultimately hydrocarbons
29	Polymerization of olefins to form coke
30	Direct route for C1 to C5 hydrocarbon formation from the triglyceride molecule

8.2.Appendix Two- Estimation of nitrogen fluidisation velocity

8.2.1. Calculation of fluidisation velocity at room temperature

$$Ar = \left[\frac{150(1 - \varepsilon_{mf})}{\psi^2 \varepsilon_{mf}^2} \right] R + \left[1.75 \times \frac{R^2}{(\psi \varepsilon_{mf}^3)} \right]$$

(Equation 1)

$$Ar = \frac{\rho_f (\rho_p - \rho_f) g d_p^3}{\mu_f^2}$$

(Equation 2)

$$\psi = Sphericity = 0.94 [227]$$

$$\rho_p = \text{density of the sand} = 2830 \text{ kg m}^{-3} [92]$$

$$\rho_f = \text{density of the Nitrogen gas at } 20^\circ\text{C} = 1.165 \text{ kg m}^{-3} [228]$$

$$d_p = \text{diameter of the sand particles} = 3 \times 10^{-4} \text{ m}$$

$$\mu_f = \text{absolute viscosity of Nitrogen gas at } 20^\circ\text{C} = 1.76 \times 10^{-5} \text{ Pas} [229]$$

$$\varepsilon_{mf} = \text{Porosity of bed} = 0.52 [230]$$

R= bed expansion ratio

Combining equations 1 and 2 gives a quadratic equation to solve in the form of:

$$\left[\frac{150(1 - \varepsilon_{mf})}{\psi^2 \varepsilon_{mf}^2} \right] R + \left[1.75 \times \frac{R^2}{(\psi \varepsilon_{mf}^3)} \right] - \frac{\rho_f (\rho_p - \rho_f) g d_p^3}{\mu_f^2} = 0$$

The first term to be calculated is (c)

$$\frac{\rho_f (\rho_p - \rho_f) g d_p^3}{\mu_f^2} = \frac{1.165 \times (2830 - 1.165) \times 9.81 \times (3.0 \times 10^{-4})^3}{(1.76 \times 10^{-5})^2} = 2847.99993$$

$$C = 2847.99993$$

The next term is (b),

$$\left[\frac{150 \times (1 - \varepsilon_{mf})}{\psi^2 \varepsilon_{mf}^3} \right] = \left[\frac{150 \times (1 - 0.52)}{0.94^2 0.52^3} \right] = 579.51777$$

$$B = 579.51777$$

Finally, the (a) term:

$$1.75 \times \frac{R^2}{(\emptyset \varepsilon_{mf}^3)} = \frac{1.75}{0.94 \times 0.52^3} = 13.24037$$

Using the quadratic equation, the value the Bed expansion ratio R is given, $R= 5.572007299$

Therefore, rearranging equation 6, the u_{mf} can be calculated:

$$u_{mf} = \frac{Ru_f}{d_p \rho_f} = \frac{5.572007299 \times 1.76 \times 10^{-5}}{3 \times 10^{-4} \times 1.165} = 0.28059 \text{ ms}^{-1}$$

0.28059 ms^{-1} As a flow rate in the fluidization column

Diameter of column is 6.69cm = 0.0669m

$$\text{Volumetric flow of } N_2 = \frac{\pi}{4} \times D_c \times u_{mf} = \frac{\pi}{4} \times 0.0669 \times 0.28059 = 0.000153383 \text{ m}^3\text{s}^{-1}$$

m^3s^{-1} to m^3hr^{-1} by multiplying by 3600 $\rightarrow 0.552177602 \text{ m}^3\text{hr}^{-1}$

Finally, to L/min as that is the units of the flowmeter, m^3hr^{-1} to Lmin^{-1} by multiplying by

$$16.6667 \rightarrow \mathbf{9.20 \text{ L min}^{-1}}$$

8.2.2.Calculations at reactor operating temperature

$$Ar = \left[\frac{150(1 - \varepsilon_{mf})}{\psi^2 \varepsilon_{mf}^2} \right] R + [1.75 \times \frac{R^2}{(\psi \varepsilon_{mf}^3)}]$$

(Equation 1)

$$Ar = \frac{\rho_f (\rho_p - \rho_f) g d_p^3}{\mu_f^2}$$

(Equation 2)

$$\psi = Sphericity = 0.94 [227]$$

$$\rho_p = \text{density of the sand} = 2830 \text{ kg m}^{-3}$$

$$\rho_f = \text{density of the Nitrogen gas at } 20^\circ\text{C} = 0.469 \text{ kg m}^{-3} [92]$$

$$d_p = \text{diameter of the sand particles} = 3 \times 10^{-4} \text{ m}$$

$$\mu_f = \text{absolute viscosity of Nitrogen gas at } 20^\circ\text{C} = 3.28 \times 10^{-5} \text{ Pas} [228]$$

$$\varepsilon_{mf} = \text{Porosity of bed} = 0.6 [230]$$

R= bed expansion ratio

Combining equations 1 and 2 gives a quadratic equation to solve in the form of:

$$\left[\frac{150(1 - \varepsilon_{mf})}{\psi^2 \varepsilon_{mf}^2} \right] R + \left[1.75 \times \frac{R^2}{(\psi \varepsilon_{mf}^3)} \right] - \frac{\rho_f (\rho_p - \rho_f) g d_p^3}{\mu_f^2} = 0$$

The first term to be calculated is (c)

$$\frac{\rho_f (\rho_p - \rho_f) g d_p^3}{\mu_f^2} = \frac{0.469 \times (0.469) \times 9.81 \times (3.0 \times 10^{-4})^3}{(3.28 \times 10^{-5})^2} = 326.71749$$

$$C = 326.71749$$

The next term is (b),

$$\left[\frac{150 \times (1 - \varepsilon_{mf})}{\psi^2 \varepsilon_{mf}^3} \right] = \left[\frac{150 \times (1 - 0.6)}{0.94^2 0.6^3} \right] = 314.37050$$

$$B = 314.37050$$

Finally, the (a) term:

$$1.75 \times \frac{R^2}{(\emptyset \varepsilon_{mf}^3)} = \frac{1.75}{0.94 \times 0.6^3} = 8.61899$$

Using the quadratic equation, the value the Bed expansion ratio R is given, R= 1.070706045

By rearranging, the u_{mf} can be calculated:

$$u_{mf} = \frac{Ru_f}{d_p \rho_f} = \frac{1.070706045 \times 3.28 \times 10^{-5}}{3 \times 10^{-4} \times 0.469} = ms^{-1}$$

$0.13638ms^{-1}$ As a flow rate in the fluidization column

Diameter of column is 6.69cm = 0.0669m

$$\text{Volumetric flow of } N_2 = \frac{\pi}{4} \times D_c \times u_{mf} = \frac{\pi}{4} \times 0.0669 \times 0.13638 = 7.455 \times 10^{-5} m^3 s^{-1}$$

$m^3 s^{-1}$ to $m^3 hr^{-1}$ by multiplying by 3600 → $0.26838015 m^3 hr^{-1}$

Finally, to L/min as that is the units of the flowmeter, $m^3 hr^{-1}$ to $L min^{-1}$ by multiplying by 16.6667 → **4.47 L min⁻¹**

8.3. References

1. Perego, C., *Encyclopedia of Hydrocarbons, Refining and Petrochemicals, Bulk Products and Production Lines in the Chemical Industry*. 2005.
2. R.F. Beims, V.B., L. Endera, D.R. Scharfb, E.L. Simionattob, H.F. Meiera and V.R. Wiggers, *Effect of Degree of Triglyceride Unsaturation on Aromatics Content in Bio-oil*. Fuel, 2018. **217**: p. 175-184.
3. Bhatia Subhash, N.T., *Catalytic Cracking Of Edible And Non-Edible Oils For The Production Of Biofuels*. 2011. **Energy and Environmental Science(4)**.
4. Lee Eng Oi, M.-Y.C., Hwei Voon Lee, Noorsaadah Abdul Rahman, Joon Ching Juan, *Chapter 9 - Mesoporous And Other Types Of Catalysts For Conversion Of Non-Edible Oil To Biogasoline Via Deoxygenation*, in *Sustainable Bioenergy, Advances and Impacts*. 2019. p. 257-281.
5. Swarup Kumar Nayak, P.C.M., Ankit Kumar, Gyana Ranjan Behera & Biswajeet Nayak *Experimental Investigation On Property Analysis Of Karanja Oil Methyl Ester For Vehicular Usage*. Energy Sources Part a-Recovery Utilization and Environmental Effects, 2017. **Part A: Recovery, Utilization, and Environmental Effects**.
6. J. K. Satyarthi, T.C., D. T. Gokak and P. S. Viswanathan, *An Overview of Catalytic Conversion of Vegetable oils/fats into Middle Distillates*. Catal. Sci. Technol, 2013. **3**: p. 70-80.
7. Lekha Charan Meher, S.N.N., Malaya Kumar Naik, and Ajay Kumar Dalai, *Biodiesel Production Using Karanja (Pongamia pinnata) and Jatropha (Jatropha curcas) Seed Oil*. 2006.
8. Yee Kang Ong, S.B., *The Current Status and Perspectives of Biofuel Production via Catalytic Cracking of Edible and Non-edible Oils*. Energy 2010 **35** p. 111–119.
9. K.V.Radha, G.M., *Novel Production Of Biofuels From Neem Oil*, in *World Renewable Energy Congress 2011*: Linköping, Sweden
10. Sergio Muñoz-Valenzuela, A.A.I.-L., Luis Mariano Rubio-Silva, Humberto ValdezDávila, and Jesús Borboa-Flores, *Neem Tree Morphology and Oil Content*. Issues in new crops and new uses. , 2007.
11. Center for Sustainable Systems, U.o.M., *Greenhouse Gases Factsheet*. 2017.
12. Julia Tomei, R.H., *Food versus fuel? Going beyond biofuels*. Land Use Policy, 2016. **56**
13. R. Zanzi , X.B., P.Capdevila and E. Bjornbom. *Pyrolysis of Biomass in the Presence of Steam for Preparation of Activated Carbon, Liquid and Gaseous Products*. . in *6th World Congress of Chemical Engineering*. 2001. Melbourne, Australia
14. David Martin Alonso, J.Q.B.a.J.A.D., *Catalytic Conversion of Biomass to Biofuels*. Green Chem., 2010. **12**: p. 1493–1513
15. David P. Serrano, J.A.M., Gabriel Morales, Jose Iglesias and Patricia Pizzaro, *Progress in the Design of Zeolite Catalysts for Biomass Conversion into Biofuels and Bio-based Chemicals*. 2017. **Catalysis Reviews(60)**: p. 1-70.
16. Burcu, B., *Pyrolysis: A Sustainable Way from Waste to Energy*. 2012: Anadolu University, Faculty of Engineering, Department of Chemical Engineering UZUN.
17. Andreas Niebel (KIT), H.B.A.-C., Thomas Reisch (AVA-CO2), Angelos Lappas (CERTH), Chrysa Michailof (CERTH), *Biomass Based Energy Intermediates Boosting Biofuel Production, Feedstock Selection, Characterisation and Preparation*. 2012, KIT, AVA-CO2 & CERTH.
18. Juan Antonio Melero, J.I.a.A.G., *Biomass As Renewable Feedstock in Standard Refinery Units. Feasibility, Opportunities and Challenges*. Energy Environ. Sci., 2012. **5**.
19. Chen, W.-H., *Pretreatment of Biomass Processes and Technologies*, in *Chapter 10 - Torrefaction*. 2015: Department of Aeronautics and Astronautics, National Cheng Kung University, Tainan, Taiwan, Republic of China. p. Pages 173-192.

20. Mohammad I. Jahirul , M.G.R., Ashfaque Ahmed Chowdhury and Nanjappa Ashwath, *Biofuels Production Through Biomass Pyrolysis —A Technological Review*. Energies 2012. **5**: p. 4952-5001.
21. Crocker, M., Andrews, Rodney, *Chapter 1 The Rationale for Biofuels*, in *Thermochemical Conversion of Biomass to Liquid Fuels and Chemicals*. 2010, The Royal Society of Chemistry. p. 1-25.
22. Tadeusz Zajac , A.K.-K., Anna Lorenc-Kozik, Karolina Ratajczak, *Analysis of yield and plant traits of oilseed rape (Brassica napus L.) cultivated in temperate region in light of the possibilities of sowing in arid areas*. Acta Agrobot, 2016. **69**(4).
23. Herbst, M.C., *Fact Sheet on Canola Oil*, C.A.o.S.A. (CANSA), Editor. 2014.
24. Mohd Esa Norhaizan, S.H., Surendiran Gangadaran, Sin Tien Lee, Fatemeh Ramezani Kapourchali and Mohammed H. Moghadasian, *Palm oil: Features and applications*. Lipid Technology 2013 **25** (2): p. 39-42.
25. Ogan I. Mba, M.-J.e.D., Michael Ngadi, *Palm oil: Processing, characterization and utilization in the food industry – A review*. Food Bioscience 2015 **10**: p. 26 –41.
26. Bhatia, P.T.a.S., *Catalytic Cracking of Palm Oil for the Production of Biofuels: Optimization Studies*. Bioresource Technology 2007. **98** p. 3593–3601.
27. J. W. Alencar, P.B.A., and A. A. Craveiro, *Pyrolysis of Tropical Vegetable Oils*. Journal of Agricultural and Food Chemistry, 1983. **31**: p. 1268-1270.
28. Aditya Pratap, S.K.G., Jitendra Kumar, Suhel Mehandi, Vankat R. Pandey, *Chapter 12: Soyabean*, in *Breeding Oilseed for Sustainable Production: Opportunities and Constraints*, S.K.G. Sher-e-Kashmir, Editor. 2016, Elsevier: University of Agricultural Sciences & Technology Chatha, Jammu (J&K), India.
29. Dinesh K. Agarwal, P.S., Mukta Chakrabarty, A J Shaikh, S G Gayal, *Cottonseed Oil Quality, Utilization and Processing* M.Sabesh, Editor. 2003, Central Institute for Cotton Research Nagpur.
30. Vinay R. Patel, g.g.d., Lakshmi C. Kasi Viswanath, Randall Maples and Bryan John J. subong, *Castor Oil: Properties, Uses, and Optimization of Processing Parameters in Commercial Production*. Lipid Insights, 2016. **9** p. 1–12.
31. Rakshit K. Devappa , H.P.S.M.a.K.B., *Jatropha Toxicity—A Review*. Journal of Toxicology and Environmental Health, 2010. **Part B**(13:6): p. 476-507.
32. B.K. Barnwal, M.P.S., *Prospects of Biodiesel Production from Vegetable Oils in India*. Renewable and Sustainable Energy Reviews, 2005. **9** p. 363–378.
33. Joon Ching Juan , D.A.K., Ta Yeong Wub and Taufiq-Yap Yun Hin *Biodiesel Production From Jatropha Oil by Catalytic and Non-Catalytic Approaches: An Overview*. Bioresource Technology, 2011. **102**: p. 452–460.
34. Alam, R., *Studies on the Properties of Karanja Oil For Probable Industrial Application* in *Department of Chemistry*. 2011, National Institute of Technology Rourkela, Orissa.
35. Jessinta D/O Sandanasamy, A.H.N., Saiful Nizam Bin Tajuddin and Abdurahman Hamid Nour, *Fatty Acid Composition and Antibacterial Activity of Neem (Azadirachta indica) Seed Oil*. The Open Conference Proceedings Journal, , 2013. **4**(Suppl-2 M11): p. 43-48.
36. Verma, A.R.a.N.K., *A brief study on neem (Azadirachta indica A.) and its application-A review*. Research Journal of Phytomedicine, 2015. **1**.
37. Farha Tinwala, P.M., Snehal Parmar, Anant Patel and Kamal K. Pant, *Intermediate Pyrolysis of Agro-industrial Biomasses in Bench Scale Pyrolyser: Product yields and its Characterization* 2014, Sardar Patel Renewable Energy Research Institute (SPRERI): Gujarat.
38. Rosillo-Calle, F., *Food versus Fuel: Toward a New Paradigm—The Need for a Holistic Approach*. FrankRosillo-Calle, ISRN Renewable Energy 2012. **ID 954180**.

39. Thompson, P.B., *The Agricultural Ethics of Biofuels: The Food vs. Fuel Debate*. Agriculture 2012. **2**: p. 339–358.
40. Ayhan Demirbas, A.B., Waqar Ahmad and Manzoor Sheikh, *Biodiesel production from non-edible plant oils*. Energy Exploration & Exploitation 2016. **34**(2): p. 290–318.
41. Liv S. Severino, D.L.A., Marco Baldanzi, Magno J. D. Cândido, Grace Chen, William Crosby, Tan D., Xiaohua He, P. Lakshamma, C. Lavanya, Olga L. T. Machado, Thomas Mielke, Máira Milani, Travis D. Miller, J. B. Morris, Stephen. A. Morse, Alejandro A. Navas, Dartanhã J. Soares, Valdinei Sofi atti, Ming L. Wang, Maurício D. Zanotto, and Helge Zieler, *A Review on the Challenges for Increased Production of Castor*. Agronomy Journal 2012. **104**(4): p. 853–880.
42. National Commodity & Derivatives Exchange Ltd. *National Commodity & Derivatives Exchange*. 2003-2018; Available from: <https://www.ncdex.com/MarketData/FuturePrices.aspx>.
43. Viswanadham, S.K.S.a.N., *Selective Production of Green Gasoline by Catalytic Conversion of Jatropha Oil*. Fuel Processing Technology 2014. **119**: p. 158–165.
44. Rui Wang , M.A.H., Wan-Wei Zhou , Pinaki S. Bhadury , Qi Chen , Bao-An Song, Song Yang *Production and Selected Fuel Properties of Biodiesel From Promising Non-edible Oils: Euphorbia lathyris L., Sapium sebiferum L. and Jatropha curcas L.* Bioresource Technology 2011. **102**: p. 1194–1199.
45. Shelly Biswas, D.K.S., *Effect of Different Catalysts on the Cracking of Jatropha Oil*. Journal of Analytical and Applied Pyrolysis, 2014. **110** p. 346–352.
46. G. Ramya, R.S., J. Amala Infant Joice, R. Ramakrishnan and T. Sivakumar, *Liquid Hydrocarbon Fuels From Jatropha Oil Through Catalytic Cracking Technology Using AIMCM-41/ZSM-5 Composite Catalysts*. Applied Catalysis A: General, 2012 **433–434**: p. 170–178.
47. Yi-Yu Wang, C.-C.C., Ching-Yuan Chang, Yi-Hung Chen , Je-Lueng Shie , Min-Hao Yuan , Yen-Hau Chen , Li-Xuan Huang , Cesar Augusto Andrade-Tacca , Do Van Manh , Min-Yi Tsai and Michael Huang, *Thermal Cracking of Jatropha Oil with Hydrogen to Produce Bio-Fuel Oil*. Energies, 2016: p. 9.
48. Shelly Biswas , P.M.a.D.K.S., *Studies on Co-cracking of Jatropha Oil with Bagasse to Obtain Liquid, Gaseous Product and Char*. Renewable Energy 2014. **63**: p. 308-316.
49. Hao Chen, Q.W., Xiangwen Zhang, and Li Wang, *Hydroconversion of Jatropha Oil to Alternative Fuel over Hierarchical ZSM-5*. Ind. Eng. Chem. Res. , 2014. **53**: p. 19916–19924.
50. Abul K. Hossain, D.I.S., Philip A. Davies, *Effects of Engine Cooling Water Temperature on Performance and Emission Characteristics of a CI Engine Operated with Biofuel Blend*. Journal of Sustainable Development of Energy, Water and Environment Systems, 2017. **5**((1)): p. 46–57.
51. A.K. Hossain, P.A.D., *Performance, emission and combustion characteristics of an indirect injection (IDI) multi-cylinder compression ignition (CI) engine operating on neat jatropha and karanj oils preheated by jacket water*. Biomass and Bioenergy, 2012. **46**: p. 332-342.
52. Wouter MJ Achten and Erik Mathijs, L.V., Virendra P Singh, Raf Aerts and Bart Muys, *Jatropha biodiesel fueling sustainability?* Society of Chemical Industry and John Wiley & Sons, Ltd, 2007: p. 284-291.
53. Gebresilassie Asnake Ewunie a, John Morken a, Odd Ivar Lekang a, Zerihun Demrew Yigezu *Factors affecting the potential of Jatropha curcas for sustainable biodiesel production: A critical review*. Renewable and Sustainable Energy Reviews (2021) **137** (110500).
54. Samodini S. Nevase , S.R.G., A.K. Dubey and B.D. Kadu, *Economics of biodiesel production from Jatropha oil*. Journal of Agricultural Technology, 2012. **8**(2): p. 657-662
55. Avinash Kumar Agarwal , K.R., *Experimental investigations of performance and emissions of Karanja oil and its blends in a single cylinder agricultural diesel engine*. Applied Energy 2009. **86** p. 106–112.

56. B. Deepanraj, M.S., N. Arun, G. Sankaranarayanan & P. Abdul Salam, *Comparison of jatropha and karanja biofuels on their combustion characteristics*. International Journal of Green Energy, 2017. **14:15** p. 1231-1237
57. Sudhakara Reddy Yenumala, S.K.M.a.D.S., *Hydrodeoxygenation of karanja oil over supported nickel catalysts: influence of support and nickel loading*. Catal. Sci. Technol., 2016. **6**.
58. Amir Abadi, H.M., Ni Luh Arpiwi, Colin Stucley , John Bartle, Rick Giles, *Economics of Oil Production from Pongamia (Millettia pinnata) for Biofuel in Australia*. Bioenerg. Res. , 2016. **9**: p. 874–883.
59. Budi Leksono , S.M., Syed Ajijur Rahman , Deki A Purbaya , Yusuf B Samsudin , Agus M Maulana, Jaya Wohono , Himlal Baral, *Pongamia (Pongamia pinnata): A Sustainable Alternative for Biofuel Production and Land Restoration in Indonesia*. 2018, Center for Forest Biotechnology and Tree Improvement (BIOTIFOR), The Forestry and Environmental Research, Development and Innovation Agency (FOERDIA).
60. P. Bhandarea, G.R.N., *Functional properties of neem oil as potential feedstock for biodiesel production*. International Letters of Natural Sciences, 2015. **7** p. 7-14
61. Xin Tinghui, M.W., Michael O'Shea, Ma Deling, *World Distribution and Trade in Neem Products with Reference to their Potential in China*, in *AARES conference of Australian Agricultural and Resource Economics Society*, . 2001: Adelaide,.
62. Baboo, P., *Neem Oil and Neem Coated Urea*. 2014.
63. Carolin Nuortila *, R.H., Katriina Sirviö, Helena Suopanki, Sonja Heikkilä and Seppo Niemi, *Selected Fuel Properties of Alcohol and Rapeseed Oil Blends*. Energies, 2020. **13**(3821).
64. Nayan, N.K., *Experimental Studies On Extraction Of Valuable Fuels From Karanja And Neem Seed By Pyrolysis*, in *Department Of Chemical Engineering*. 2011, National Institute of Technology: Rourkela.
65. Anil Kumar Dubey, R.M.S.a.A.R., *Characterization of Processed Jatropha Oil for use as Engine Fuel*. Current World Environment 2011. **6**(1): p. 101-107
66. Diedhiou Djibril, Faye Mamadou, Vilarem Gérard, Mar-Diop Codou Geuye, Sock Oumar and Rigal Luc, *Physical characteristics, Chemical composition and Distribution of constituents of the Neem seeds (Azadirachta indica A. Juss) collected in Senegal*. Research Journal of Chemical Sciences, 2015. **5**(7): p. 52-58.
67. Avinash Kumar Agarwal, D.A., *Novel Methodology to Utilise Neem (Azadirachta Indica) Oil in a Direct Injection Compression Ignition Engine: Performance and Emissions Characterization*, S. International, Editor. 2009.
68. Harshob Singh, C.D.S., Sunil Mahla, Pali Rosha, *Preparation of Biodiesel from Crude Karanja Oil by Using KOH Catalyst*. International Journal of Emerging Technologies in Computational and Applied Sciences (IJETCAS), 2015. **15**(447): p. 302-305.
69. Vasanthakumar SathySelvabala , T.K.V., Dinesh Kirupha Selvaraj ,Vijayalakshmi Ponnusamy , Sivanesan Subramanian *Removal of free fatty acid in Azadirachta indica (Neem) seed oil using phosphoric acid modified mordenite for biodiesel production*. Bioresource Technology 2010. **101** p. 5897–5902.
70. Shelly Biswas, D.K.S., *Co-cracking of Jatropha Oil, Vacuum Residue and HDPE and Characterization of Liquid, Gaseous and Char Products Obtained*. Journal of Analytical and Applied Pyrolysis, 2013. **101**: p. 17–27.
71. Shelly Biswas, D.K.S., *Studies on cracking of Jatropha oil*. Journal of Analytical and Applied Pyrolysis 2013. **99** p. 122–129.
72. C. Silva, T.A.S.C., E. A. Silva, V. F. Cabral, J. V. Oliveira and L. Cardozo-Filho, *Continuous catalyst-free production of esters from Jatropha curcas L. oil under supercritical ethanol*. 2014. **31**(03): p. 727 - 735.

73. Abdul Munir Hidayat Syah Lubisa, B.A., Mustafar Bin Sudind, *Investigation on oxidation and thermal stability of jatropha oil*. A. M. H. S. Lubis, Bambang & Mustafar / Jurnal Teknologi (Sciences & Engineering), 2015. **77**(21): p. 79–83
74. M. H. Mosarof, M.A.K., H. H. Masjuki, A. Arslan, I. M. Monirul, A. M. Ruhul, S. A. Shahir and L. S. Khuong, *Analysis of thermal stability and lubrication characteristics of Millettia pinnata oil*. RSC Adv., 2016, . **6**: p. 81414–81425.
75. Robert W. Gosselink, S.A.W.H., Shu-Wei Chang, Jacco van Haveren, Krijn P. de Jong, Johannes H. Bitter and Daan S. van Es, *Reaction Pathways for the Deoxygenation of Vegetable Oils and Related Model Compounds*. ChemSusChem 2013. **6**: p. 1576 – 1594.
76. Mathias Snåre, I.K.k., Pa1ivi Ma1ki-Arvela, Kari Era1nen, and Dmitry Yu. Murzin*, *Heterogeneous Catalytic Deoxygenation of Stearic Acid for Production of Biodiesel*. Ind. Eng. Chem. Res., 2006. **45**: p. 5708-5715.
77. Robert W. Gosselink, a. and b.S.-W.C. Stefan A. W. Hollak, [a] Jacco van Haveren,[b] Krijn P. de Jong,[a] Johannes H. Bitter,*[a] and Daan S. van Es*[b], *Reaction Pathways for the Deoxygenation of Vegetable Oils and Related Model Compounds*. ChemSusChem 2013. **6** p. 1576 – 1594.
78. Marilia R. Santosa, S.A., Jose F. Padilhab,d, Maria Clara N. Carneirob,d, Emerson Andrade Salesb,c, Jose Geraldo A. Pachecoa,* Roger Frétyb,c, *Catalytic cracking of palmitic and oleic acids pre-adsorbed on γ-alumina*. Catalysis Today, 2019.
79. Roger Fréty, a Maria da Graça C. da Rocha,a Soraia T. Brandão,a Luiz A. M. Pontes,b Jose F. Padilha,b and L.E.P.B.a.W.A. Gonzalezc, *Cracking and Hydrocracking of Triglycerides for Renewable Liquid Fuels: Alternative Processes to Transesterification*. J. Braz. Chem. Soc., 2011. **Vol. 22**,(No. 7): p. 1206-1220.,.
80. Mehdi Omidghane, E.J., Michael Chae, and David C. Bressler*, *Production of Renewable Hydrocarbons by Thermal Cracking of Oleic Acid in the Presence of Water*. Energy Fuels 2017. **31**: p. 9446–9454.
81. Faisal Abnisa, W.M.A.W.D., *A review on co-pyrolysis of biomass: An optional technique to obtain a high-grade pyrolysis oil*. Energy Conversion and Management, 2014. **87** p. 71–85.
82. Brownsort, P., *Biomass Pyrolysis Processes: Review of Scope, Control and Variability*. Uk Biochar Research Centre Working Papers, 2009.
83. Management, F.R., *Advanced Thermal Treatment of Municipal Solid Waste*. 2012, Frith Resource Management (FRM).
84. Pratyasha Tripathy Bhubaneswar, A.P., Chinmoy Kumar Panigrahi. *A Review on Pyrolysis of Biomass Feedstocks*. in *International Conference on Emerging Technological Trends*. 2016.
85. Bridgwater, A., *Upgrading Fast Pyrolysis Liquids: Blends of Biodiesel and Pyrolysis Oil*. 2012.
86. S. Czernikand, A.V.B., *Overview of Applications of Biomass Fast Pyrolysis Oil*. Energy& Fuels 2004. **18**: p. 590-598.
87. Nicholas Canabarro, J.F.S., Chayene G Ancheta, Camila S Kelling and Marcio A Mazutti, *Thermochemical Processes for Biofuels Production from Biomass*. 2013, Sustainable Chemical Processes.
88. Hornung, A. *BioEnergy IV: Innovations in Biomass Conversion for Heat, Power, Fuels and Chemicals*. 2013. Petten: Engineering Conferences International, ECI Digital Archives.
89. Viktor J. Bruckman, J.L., Başak B. Uzun and Esin Apaydın Varol, *Biochar: A Regional Supply Chain Approach in View of Climate Mitigation*. 2016: Cambridge Univeristy Press.
90. Haiping Yang , R.Y., Hanping Chen, Dong Ho Lee and Chuguang Zheng *Characteristics of Hemicellulose, Cellulose and Lignin Pyrolysis*. Fuel 2007. **Fuel** (86).
91. R. Michel, N.M., B. Azambre , G. Finqueneisel, J. Machnikowski, P. Rutkowski, T. Zimny and J. V. Weber, *Miscanthus × Giganteus Straw and Pellets as Sustainable Fuels and Raw Material for Activated Carbon*. Environmental Chemistry Letters, 2006. **4**: p. 185–189.

92. Johnny Matta, *Biomass Fast Pyrolysis Fluidized Bed Reactor: Modelling and Experimental Validation*, in *Department of Chemical and Biological Engineering*. 2016, University of Ottawa.
93. R.H. Venderbosch, W.P., *Fast Pyrolysis Technology Development*. Biofuels, Bioproducts and Biorefining, 2010. **4**: p.:178-208.
94. A.J. (Sandy) Marshall, P.E., *Commercial Application of Pyrolysis Technology in Agriculture*. 2013 Ontario Federation of Agriculture p. thermal technolgies overview, bio oil applications, pyrolysis products
95. Qingang Xiong, S.A., and Song-Charng Kong, *Modeling Effects of Operating Conditions on Biomass Fast Pyrolysis in Bubbling Fluidized Bed Reactors*. Energy Fuels 2013. **27**: p. 5948–5956.
96. Najaf Ali, M.S., Khurram Shahzad, Sadiq Hussain and Arshad Chughtai, *Effect of Operating Parameters on Production of Bio-oil From Fast Pyrolysis of Maize Stalk in Bubbling Fluidized Bed Reactor*. Polish Journal of Chemical Technology, , 2016. **18**, (3,): p. 88—96.
97. Joseph Eke , J.A.O., Anthony V. Bridgwater, *Influence of Moisture Contents on the Fast Pyrolysis of Trommel Fines in a Bubbling Fluidized Bed Reactor*. Waste and Biomass Valorization, 2020. **11**: p. 3711–3722.
98. Scott W. Banks, D.J.N., and Anthony V. Bridgwater, *Impact of Potassium and Phosphorus in Biomass on the Properties of Fast Pyrolysis Bio-oil*. Energy Fuels 2016. **30**: p. 8009–8018.
99. Xiaodong Huoa, J.X., *, Min Songa, Li Zhub, *Comparison between in-situ and ex-situ catalytic pyrolysis of sawdust for gas production*. Journal of Analytical and Applied Pyrolysis 2018. **135** p. 189–198.
100. Montalbani, S., *Pyrolysis-Gas Chromatographymass Spectrometry And Chemometric Analysis For The Characterization Of Complex Matrices*, in *Department Of Chemistry*. 2012, Alma Mater Studiorum-University Of Bologna
101. Shubin Wu, G.L.a.R.L., *Applications of Chromatography Hyphenated Techniques in the Field of Lignin Pyrolysis*. South China University of Technology, China.
102. Bakhshi, Y.S.P.a.N.N., *Effect of Pretreatment of HZSM-5 Catalyst on its Performance in Canola Oil Upgrading* Applied Catalysis, 1985. **18**: p. 71-85.
103. Bressler, K.D.M.a.D.C., *Pyrolysis of Triglyceride Materials for the Production of Renewable Fuels and Chemicals*. Bioresource Technology 2007. **98**: p. 2351–2368.
104. Publications, I., *World Energy Outlook 2018*. 2018.
105. BP, *BP Statistical Review of World Energy*. 2019.
106. D.X.Hu. *Synthetic Methods, Industrial Feedstock Chemicals*. [Powerpoint Presentation] 2013.
107. Cullen, P.G.L.a.J.M., *Mapping Global Flows of Chemicals: From Fossil Fuel Feedstocks to Chemical Products* Environ. Sci. Technol. , 2018. **52**: p. 1725–1734.
108. Bender, M. *Global Aromatics Supply - Today and Tomorrow*. in *New Technologies and Alternative Feedstocks in Petrochemistry and Refining*. 2013. DGMK Conference , Dresden, Germany.
109. Xiaosong Yang, J.L., Kai Fan and Long Rong, *Hydrocracking of Jatropha Oil over non-sulfided PTA-NiMo/ZSM-5 Catalyst*. 2017.
110. Thanh-An Ngo , J.K., Sun Kuk Kim and Seung-Soo Kim, *Pyrolysis of Soybean Oil with H-ZSM5 (Proton-exchange of Zeolite Socony Mobil #5) and MCM41 (Mobil Composition of Matter No. 41) Catalysts in a Fixed-bed Reactor*. Energy, 2010. **35** p. 2723–2728.
111. Hao Chena, Q.W., Xiangwen Zhang and Li Wang, *Quantitative Conversion of Triglycerides to Hydrocarbons Over Hierarchical ZSM-5 Catalyst*. Applied Catalysis B: Environmental 2015. **166–167**: p. 327–334.

112. S.M. Sadrameli, A.E.S.G.a.W.S., *Modeling Representations of Canola Oil Catalytic Cracking for the Production of Renewable Aromatic Hydrocarbons*. J. Anal. Appl. Pyrolysis 2009. **86** p. 1–7.
113. Bakhshi, Y.S.P.a.N.N., *Catalytic Conversion of Canola Oil to Fuels and Chemical Feedstocks Part I. Effect of Process Conditions on the Performance of HZSM-5 Catalyst*. The Canadian Journal of Chemical Engineering 1986. **64**.
114. Chia-Chu Chang And Shfa-Vi L Vi An, C.V.O.C., Shanghai, China's Motor Fuels from Tung Oil. Industrial and Engineering Chemistry 1947. **39**(12): p. 1543-1548.
115. Hong Li, P.Y., Benxian Shen *, *Biofuel potential production from cottonseed oil: A comparison of non-catalytic and catalytic pyrolysis on fixed-fluidized bed reactor*. Fuel Processing Technology (2009) **90** p. 1087–1092.
116. Savage, N.M.a.P.E., *Hydrothermal Catalytic Cracking of Fatty Acids with HZSM-5*. ACS Sustainable Chemistry & Engineering, 2014. **2**: p. 88-94.
117. Roger Fréty, a.M.R.S., a Renan F. Sales,a Antonio O. S. Silva,b Celmy B. M. Barbosa a and a. and Jose G. A. Pacheco*, *Flash Pyrolysis of Oleic Acid as a Model Compound Adsorbed on Supported Nickel Catalysts for Biofuel Production*. J. Braz. Chem. Soc., 2014. **Vol. 25**: p. 2433-2443.
118. Jun Zhang, Z.W., Xun Li, Yu Zhang, Zhenghong Bao, Lei Bai, and Fei Wang, *Catalytic Cracking of Inedible Oils for the Production of Drop-In Biofuels over a SO₄²⁻/TiO₂-ZrO₂ Catalyst*. Energy Fuels, 2020: p. 14204–14214.
119. A.W. Schwab, G.J.D., E. Selkea , S.C. Sorensonb and E.H. Pryde, *Diesel Fuel from Thermal Decomposition of Soybean Oil*. JAOCS, 1988 **65**.
120. Zaki Y. Zakaria a, N.A.S.A.a., *, Juha Linnekoski b, *A perspective on catalytic conversion of glycerol to olefins*. biomass and bioenergy, 2013. **55**: p. 370-385.
121. Alena Kubátová a, b., Yan Luo a,c, Jana Št'ávová a,b, S.M. Sadrameli d, Ted Aulich e, Evgenii Kozliak a,b, Wayne Seames *New path in the thermal cracking of triacylglycerols (canola and soybean oil)*. Fuel 90 (2011): p. 2598–2608.
122. B. S. Greensfelder, H.V., And G. M. Good *Catalytic And Thermal Cracking Of Pure Hydrocarbons, Mechanisms Of Reaction*. Industrial and Engineering Chemistry, 1949. **41**(11): p. 2573-2584.
123. Raphael O. Idem, S.P.R.K., and Narendra N. Bakhshi, *Thermal Cracking of Canola Oil: Reaction Products in the Presence and Absence of Steam*. Energy & Fuels 1996. **10**; p. 1150-1162.
124. Paul B. Weisz, W.O.H., Paul G. Rodewald, *Catalytic Production of High-Grade Fuel (Gasoline) from Biomass Compounds by Shape-Selective Catalysis*. Science, 1979. **206**: p. 57-58.
125. Y. S. PRASAD and N. N. BAKHSHI , J.F.M., *Catalytic Conversion of Canola Oil to Fuels and Chemical Feedstocks, Part I1 Effect of Co-feeding Steam on the Performance of HZSM-5 Catalyst* THE CANADIAN JOURNAL OF CHEMICAL ENGINEERING., 1986. **64**: p. 285-292.
126. Sai P. R. Katikaneni, J.D.A., and Narendra N. Bakhshi*, *Catalytic Conversion of Canola Oil to Fuels and Chemicals over Various Cracking Catalysts*. The Canadian Journal of Chemical Engineering, 1995. **73**: p. 484-497.
127. Sai P. R. Katikaneni, J.D.A., and Narendra N. Bakhshi*, *Studies on the Catalytic Conversion of Canola Oil to Hydrocarbons: Influence of Hybrid Catalysts and Steam Energy & Fuels*, 1995. **9**.
128. Milne, T.A.E., R. J.; Filly, J. In, *Research in Thermochemical Biomass Conversions*; ed. A.V. Bridgewater, Kuester, J. L., Eds.;. 1988, London, : Elsevier Applied Science: .
129. Nelson, G.E.a.E.F., *Cracking Alaskan Fur-Seal Oil*. Industrial and Engineering Chemistry, 1933. **25**: p. 386-387.

130. Morrell, G.E.a.J.C., *The Cracking of Cottonseed Oil* Industrial and Engineering Chemistry, 1932. **24**: p. 1426-1427.
131. Hudson, A.C.T.D.H.B.J.F., *The effect of heat on pure triglycerides*. Journal of the American Oil Chemists Society, 1962 **39**(1).
132. Edited by G. Ertl, H.K., J. Weitkamp, *Handbook of Heterogeneous Catalysis*, ed. D.M. Bar. 1997: VCH Verlagsgesellschaft mbH, Weinheim (Federal Republic of Germany).
133. Mark E. Davis, R.J.D., *Fundamentals of Chemical Reaction Engineering*. 2003: McGraw-Hill Chemical Engineering Series.
134. J. K. Satyarthi, T.C., D. T. Gokak and P. S. Viswanathan, *An Overview of Catalytic Conversion of Vegetable Oils/fats Into Middle Distillates*. Catalyst Science Technology, 2013,. **3**: p. 70- 80.
135. Rhodes, C.J., *Properties and Applications of Zeolites*. Science Progress 2010. **93**(3): p. 1–63
136. Abdul M. Ziyath, P.M., Ashantha Goonetilleke, Moses O. Adebajo, Serge Kokot, Adekunle Oloyede, *Influence of Physical and Chemical Parameters on the Treatment of Heavy Metals in Polluted Stormwater Using Zeolite-A Review*. Journal of Water Resource and Protection, 2011 **3**: p. 758-767
137. Weitkamp, J., *Zeolites and Catalysis*. Solid State Ionics 2000 **131** p. 175-188.
138. Annisa, W.W.a.A.N. *Synthesis and Characterization of ZSM-5 Catalyst at Different Temperatures*. in *2nd Materials Research Society of Indonesia Meeting*. 2017,. IOP Publishing.
139. Material, A.C.S., *ZSM-5- Zeolite Socony Mobil-5*. 2019.
140. Jiří Čejka, A.C., and Stacey Zones, *Zeolites and Catalysis-Synthesis, Reactions and Applications*. 2010 WILEY-VCH Verlag GmbH & Co. KGaA, Weinheim.
141. S.S. Deo, F.I., S. Ansari, R.D. Utane, *ZEOLITICAL CHEMISTRY: A REVIEW*. International Journal of Researchers in Biosciences, Agriculture and Technology 2015. **6**.
142. Peskov, M. *Tutorial- Zeolites*. 2006 [18/12/2018]; Available from: <http://asdn.net/asdn/chemistry/zeolites.php>.
143. E.G. Derouane , J.C.V., R. Ramos Pinto, P.M. Borges ,L. Costa , M.A.N.D.A. Lemos , F. Lemos a & F. Ramôa Ribeiro *The Acidity of Zeolites: Concepts, Measurements and Relation to Catalysis: A Review on Experimental and Theoretical Methods for the Study of Zeolite Acidity* Catalysis Reviews: Science and Engineering, 2013. **55**:4: p. 454-515.
144. Bryan R. Goldsmith, B.P., J. Karl Johnson, Bruce C. Gates and Susannah L. Scott, *Beyond Ordered Materials: Understanding Catalytic Sites on Amorphous Solids*. ACS Catal. , 2017. **7**.
145. IUPAC, P.C.D.o.S.C.I.C.S.o.C.C., *Manual on Catalyst Characterisation*. Pure & App/. Chem., 1991. **63**(9): p. 1227-1246.
146. A. Maghfirah a, M.M.I.a., A.T.N. Fajar b, G.T.M. Kadja a, c, d, *, *A review on the green synthesis of hierarchically porous zeolite*. Materials Today Chemistry 2020. **17**.
147. Roduner, E., *Understanding Catalysis*. Chem. Soc. Rev, 2014. **43**: p. 8226.
148. Gilson, M.G.J.-P., *Zeolites for Cleaner Technologies*, ed. S.E.G.J. Hutchings. Vol. CATALYTIC SCIENCE SERIES — VOL. 3. 2005.
149. Kazuhisa Murata, Y.L., Megumu Inaba, and Isao Takahara, *Production of Synthetic Diesel by Hydrotreatment of Jatropha Oils Using Pt-Re/H-ZSM-5 Catalyst*. Energy Fuels 2010, . **24**, : p. 2404–2409
150. Rubén Ramos, A.G., † Juan A. Botas,† and David P. Serrano, *Enhanced Production of Aromatic Hydrocarbons by Rapeseed Oil Conversion over Ga and Zn Modified ZSM-5 Catalysts*. Ind. Eng. Chem. Res. , 2016, . **55**, : p. 12723–12732.
151. Suarez, R.L.Q.Æ.A.P.T.Æ.A.n.C.P.Æ.J.C.R.Æ.P.A.Z., *Studying the Influence of Alumina Catalysts Doped with Tin and Zinc Oxides in the Soybean Oil Pyrolysis Reaction*. J Am Oil Chem Soc 2009 **86**: p. 167–172.

152. Sriatun, e.a., *Characteristic of ZSM-5 catalyst supported by nickel and molybdenum*, in IOP Conf. Ser.: , M.S. Eng., Editor. 2019
153. Weikun Yao, a.J.L., a Yu Feng,a Wei Wang,a Xianlong Zhang,b Qun Chen,c Sridhar Komarnenid and Yujue Wang*a, *Thermally stable phosphorus and nickel modified ZSM-5 zeolites for catalytic co-pyrolysis of biomass and plastics*. RSC Adv., 2015. **5**.
154. Darui Wang, B.M., Bo Wang, Chen Zhao* and Peng Wu, *One-Pot Synthesized Hierarchical Zeolites Supported Metal Nanoparticles for Highly Efficient Biomass Conversion*. Chemical Communications, 2015(82).
155. Ahmed I. Osmana, b., Jonathan Meudalc, Fathima Laffird, Jillian Thompsona,* , David Rooney, *Enhanced catalytic activity of Ni on $\square\text{-Al}_2\text{O}_3$ and ZSM-5 on addition of ceria zirconia for the partial oxidation of methane*. Applied Catalysis B:: Environmental 2017. **212** p. 68–79.
156. Matthew M. Yung, A.K.S., Calvin Mukarakate, Allison M. Crow, Marissa A. Leshnov, and Kimberly A. Magrini, *Biomass Catalytic Pyrolysis on Ni/ZSM-5: Effects of Nickel Pretreatment and Loading* Energy Fuels 2016,. **30**, : p. 5259–5268.
157. Busca, G., *Preparation of Solid Catalysts: A Short Summary*. 2014, Elsevier.
158. Annisa, W.W.a.A.N., *Synthesis and Characterization of ZSM-5 Catalyst at Different Temperatures*. IOP Conf. Ser.: Mater. Sci. Eng. , 2017. **214**.
159. Shubin Wu, G.L.a.R.L., *Applications of Chromatography Hyphenated Techniques in the Field of Lignin Pyrolysis*, in *Applications of Gas Chromatography*, R.D.a.M. Jafarkhani, Editor. 2012.
160. Chaouki, N.S.A.C.G.S.A.P.L.M.L.S.S.G.S.P.J., *Experimental methods in chemical engineering: Thermogravimetric analysis—TGA*. The Canadian Journal of Chemical Engineering, 2019. **98**: p. 34–43.
161. Perego, G., *Characterization of heterogeneous catalysts by X-ray diffraction techniques*. Catalysis Today, 1998 **41** p. 251±259.
162. Andrei A. Bunaciu, E.g.U.H.Y.A.-E., *X-Ray Diffraction: Instrumentation and Applications*. Critical Reviews in Analytical Chemistry, 2015 **45**: p. 289-299.
163. Raoof Bardestani, G.S.P., Serge Kaliaguine, *Experimental methods in chemical engineering: specific surface area and pore size distribution measurements—BET, BJH, and DFT*. Can J Chem Eng., 2019;. **97**: p. 2781–2791.
164. al., C.Y.e., *SI -1 Specific Surface Area Measurement*. 2017.
165. Sebastian Storck, H.B., Wilhelm F. Maier, *Characterization of micro- and mesoporous solids by physisorption methods and pore-size analysis* Applied Catalysis A: General 1998. **174** p. 137±146.
166. Xiaohong Li , Z.G., Siyi Fang , Chao Ren , Kun Yang and Fuyong Wang *Fractal Characterization of Nanopore Structure in Shale, Tight Sandstone and Mudstone from the Ordos Basin of China Using Nitrogen Adsorption*. Energies, 2019. **12**.
167. Knowlton, R.C.S.B.R.K.T., *Introduction to Fluidization*, in *Back to Basics*, A.I.o.C.E. (AIChE), Editor. 2014: AIChE.
168. Salman Jalalifara, R.A., Vikram Garaniyaa, Kelly Hawboldtc, Mohammadmahdi Ghijid, *Parametric Analysis of Pyrolysis Process on the Product Yields in a Bubbling Fluidized Bed Reactor*. Fuel 234, 2018. **234**
p. 616–625.
169. Knowlton, R.C.S.B.R.K.T., *Introduction to Fluidization*. 2014, American Institute of Chemical Engineers (AIChE).
170. ASTM International, *ASTM D 6304 – 07 Standard Test Method for Determination of Water in Petroleum Products, Lubricating Oils, and Additives by Coulometric Karl Fischer Titration*. 2007: 100 Barr Harbor Drive, PO Box C700, West Conshohocken, PA 19428-2959,United States.

171. Metrohm, *Determination of the total acid number in petroleum products*, in *Application Bulletin AB-404_1_EN*. 2016.
172. Nadikarni, R.A.K., *Guide to ASTM Test Methods for the Analysis of Petroleum Products and Lubricants* Millennium Analytics, Inc., East Brunswick NJ, 2000.
173. P. Bondioli, L.D.B., A. Gallonzelli, *The evaluation of Iodine Value in biodiesel samples. A comparison between volumetric and gascromatographic techniques*. La Rivista Italiana Delle Sostanze Grasse, 2011. **88**.
174. International, A., *Standard Test Method for Kinematic Viscosity of Transparent and Opaque Liquids (and Calculation of Dynamic Viscosity)1*. 2009: 100 Barr Harbor Drive, PO Box C700, West Conshohocken, PA 19428-2959, United States.
175. Sukru Acar*, A.A., *Determination of higher heating values (HHVs) of biomass fuels*. Energy Education Science and Technology Part A: Energy Science and Research 2012 **2**(28): p. 749-758.
176. International, A., *ASTM D 97 / IP15 Standard Test Method for Pour Point of Petroleum Products*. 2005: 100 Barr Harbor Drive, PO Box C700, West Conshohocken, PA 19428-2959, United States.
177. Mettler-Toledo AG, A., *Karl Fischer Titration - Good Titration Practice Brochure*. 2011.
178. Brownsort, P.A., *Biomass Pyrolysis Processes:Review of Scope, Control and Variability*. 2009,.
179. AMTEK, B., *More Solutions to Sticky Problems, A Guide to Getting More from your Brookfield Viscometer and Rheometer*, I.a.S.C. Divsion, Editor. 2017.
180. Company, P.I., *Introduction to Bomb Calorimetry*. 2007.
181. Company., P.I. *Oxygen Bomb Calorimeter 6100 Compensated Calorimeter*. [cited 2021 12/01]; Available from: <https://www.parrinst.com/products/oxygen-bomb-calorimeters/6100-compensated-jacket-calorimeter/#:~:text=The%206100%20Calorimeter%20is%20a,used%20in%20the%206200%20Calorimeter>.
182. N. Thajuddin, T.S.K., D. Dhanasekaran ***Biological Techniques a Laboratory Manual***. 2016, Bharathidasan University.
183. Kusch, P., *Gas Chromatography, Derivatization, Sample Preparation, Application*, in *Introductory Chapter: Gas Chromatography- The Most Versatile Analytical Technique*. 2019: IntechOpen.
184. Technologies, A., *Sample Preparation Fundamentals for Chromatography* 2013.
185. Hussain, G., *Muffle Parts Construction*. 2015.
186. Agah, B.P.R.a.M., *Micro Gas Chromatography: An Overview of Critical Components and Their Integration*. Anal. Chem, 2018,. **90**: p. 13133–13150.
187. Juan A. Melero, M.M.C., Guillermo Calleja, Alicia Garcí'a Ruben Miravalles, and Tamara Galindo, *Production of Biofuels via the Catalytic Cracking of Mixtures of Crude Vegetable Oils and Nonedible Animal Fats with Vacuum Gas Oil*. Energy Fuels 2010. **24** , : p. 707–717 : .
188. Justice Asomaning, P.M., David C. Bressler* *Thermal deoxygenation and pyrolysis of oleic acid*. Journal of Analytical and Applied Pyrolysis (2014). **105** p. 1–7.
189. Yan Luo a, I.A.b., Alena Kubálová c, Jana Šťávová c, Ted Aulich d, S.M. Sadrameli e, W.S. Seames, *The thermal cracking of soybean/canola oils and their methyl esters*. Fuel Processing Technology 2010. **91** p. 613–617.
190. Gregory, J.A., *Thermal Conversion of Triglycerides of Vegetable Oil for Production of Renewable Lamp Fuel*. 2015, The University of Western Ontario.
191. FRANKEL, E.N., Progress in Lipid Research, 1984. **23**(4): p. 197-221.
192. Dinesh D. Jayasena, D.U.A., Ki Chang Nam2 and Cheorun Jo*, *Flavour Chemistry of Chicken Meat: A Review* Asian Australas. J. Anim. Sci., 2013. **Vol. 26** , : p. 732-742

193. Diaz, J.M.R., *Use of amaranth, quinoa and kañiwa in extruded corn snacks*, in *Food Sciences / Food Bioprocessing track*. 2011: Helsinki
194. Jun Cao, L.D., Xue-Mei Zhu, Yawei Fan,* Jiang-Ning Hu, Jing Li, and Ze-Yuan Deng, *Novel Approach To Evaluate the Oxidation State of Vegetable Oils Using Characteristic Oxidation Indicators*. J. Agric. Food Chem., 2014. **62**: p. 12545–12552.
195. Ruchira Nandasiri, N.A.M.E., Peter Eck, UshaThiyam-Höllander., *Chapter 8 - Application of green technology on extraction of phenolic compounds in oilseeds (Canola)*, in *Green Technology, Bioactive Compounds, Functionality, and Applications*, M.F. Ramadan, Editor. 2020. p. 81-96.
196. Yang, D.J.C.Y.X.C.S.W.H.L.X., *Study on the pyrolysis mechanism of unsaturated fatty acid: A combined density functional theory and experimental study*. Int J Energy Res. , 2021: p. 1–12.
197. Margarida L. Castelló1, Jo Dweck1, Donato A. G. Aranda1, Rosana C. L. Pereira3, Manoel J. R. Guimarães Neto3, *ZSM5 as a Potential Catalyst for Glycerol Pyrolysi*. Journal of Sustainable Bioenergy Systems, 2014. **4**: p. . . .
198. Avelino Corma a, George W. Huber a,1, Laurent Sauvanaud a, Paul O'Connor a,b, *Biomass to chemicals: Catalytic conversion of glycerol/water mixtures into acrolein, reaction network*. Journal of Catalysis 2008. **257**: p. 163–171.
199. Pushan Sharma a, C.T.A.a., ↑, Jordan D. Brunson a, Wing Tsang, *Decomposition by film boiling heat transfer of glycerol*. International Journal of Heat and Mass Transfer 2019. **139** p. 873–880.
200. Marulanda, V.F. *Glycerol and methylesters decomposition in the supercritical production of biodiesel: Potential alternative to improve fuel characteristics and yield*. in *International Conference on Energy Systems and Technologies 2011*. Cario, Egypt: Universidad de La Salle, Bogotá, Colombia.
201. Laura Mitrea, M.T., Adriana-Florinela Cătoi and Dan-Cristian Vodnar, *Utilization of biodiesel derived-glycerol for 1,3-PD and citric acid production* Microb Cell Fact, 2017. **16**.
202. Crespi1, L.D.M.T.M.S., *New approach for proximate analysis by thermogravimetry using CO₂ atmosphere Validation and application to different biomasses*. J Therm Anal Calorim (2017) **128**: p. 1–14
203. Alothman, Z.A., *A Review: Fundamental Aspects of Silicate Mesoporous Materials*. Materials Today Chemistry, 2012. **5**,: p. 2874-2902.
204. Bipul Sarkar, R.T., Rajib Kumar Singha, Shashank Suman, Shilpi Ghosh, Shankha Shubhra Acharyya, Kshudiram Mantri, L.N. Sivakumar Konathala, Chandrashekhar Pendem, Rajaram Bal, *Reforming of methane with CO₂ over Ni nanoparticle supported on mesoporous ZSM-5*. Indian Journal of Chemistry - Section A Inorganic, Physical, Theoretical and Analytical Chemistry., 2012. **51** : p. 1348-1353..
205. L. P. Teh, S.T., * A. A. Jalil, C. R. Mamat, S. M. Sidik,d N. A. A. Fatah, R. R. Muktie and T. Shishido, *Nickel-promoted mesoporous ZSM5 for carbon monoxide methanation*. RSC Adv., 2015. **5**: p. 64651.
206. Armbruster, X.H.V.a.U., *Designing Hierarchical ZSM-5 Materials for Improved Production of LPG Olefins in the Catalytic Cracking of Triglycerides*. Advances in Materials Science and Engineering Volume 2019, . Article ID 3198421.
207. Wei Qiang, Z.P., Liu Xiaodong, Huang Wenbin, Fan Xiayun, Yan Yitong, Zhang Rongxun, Wang Lin, Zhou Yasong, *Synthesis of Ni-Modified ZSM-5 Zeolites and Their Catalytic Performance in n-Octane Hydroconversion*. Frontiers in Chemistry, 2020. **8**: p. 1167.
208. Heny Dewajani, R., Suryo Purwono, and Arief Budiman. *Effect of Modification ZSM-5 Catalyst in Upgrading Quality of Organic Liquid Product Derived from Catalytic Cracking of Indonesian Nyamplung Oil (*Calophyllum inophyllum*)*. in *Advances of Science and Technology for Society*. 2016. AIP Publishing.

209. Jiangwei Li, P.L., Jiangbing Li , Zhiqun Tian and Feng Yu, *Highly-Dispersed Ni-NiO Nanoparticles Anchored on an SiO₂ Support for an Enhanced CO Methanation Performance*. Catalysts 2019. **9**.
210. Adawiya J. Haidera, Riyad Al- Anbarib, Hiba M. Samib, Mohammed J. Haider, *Photocatalytic Activity of Nickel Oxide*. Journal of Materials and Research Technology 2019. **8**: p. 2802-2808.
211. J.L. Weber a, D.M.d.M.b., R. Beerthuis a, J. Dufour b,c, C. Martos b, K.P. de Jong a, P. E. de Jongh a, *Conversion of synthesis gas to aromatics at medium temperature with a fischer tropsch and ZSM-5 dual catalyst bed*. Catalysis Today 2021. **369** p. 175–183.
212. Ya-Long Ding1, H.-Q.W., Mei Xiang2, *The Effect of Ni-ZSM-5 Catalysts on Catalytic Pyrolysis and Hydro-Pyrolysis of Biomass* Front. Chem. , 2020. **8**: p. 790.
213. Thompson3, T.J.B.R.H.M.G.W.W.T.F.E.E.A.W.E.H.B., *Heterogeneous Cracking of an Unsaturated Fatty Acid and Reaction Intermediates on H⁺* ZSM-5 Catalyst. Clean 2008, . **36**: p. 652–656.
214. Songbo He, F.G.H.K., Thomas Sjouke Kramer, Anshu Chandel, Zhuorigebatu Tegudeer, Andre Heeres, and Hero Jan Heeres* *Catalytic Conversion of Free Fatty Acids to Bio-Based Aromatics: A Model Investigation Using Oleic Acid and an H-ZSM-5/Al₂O₃ Catalyst*. ACS Sustainable Chem. Eng., 2021. **9**: p. 1128–1141.
215. Ari Fischer, S.D., ‡ Julia A. Valla and George M. Bollas*, *The effect of temperature, heating rate, and ZSM-5 catalyst on the product selectivity of the fast pyrolysis of spent coffee grounds*. RSC Adv., 2015. **5**: p. 29252.
216. Nishu, R.L., Md. Maksudur Rahman, Manobendro Sarker, Meiyun Chai, Chong Li, Junmeng Cai, *A review on the catalytic pyrolysis of biomass for the bio-oil production with ZSM-5: Focus on structure*. Fuel Processing Technology, (2020). **199** p. 106301.
217. J.A. Botasa, D.P. Serranoa,b, A. Garcíac, R. Ramosa.
218. Hoang T, D.T., Lobban LL, Resasco DE, Mallinson RG. , *Catalytic conversion of glycerol to fuel*; . 2007.
219. Omran, A., *Sustainable Biofuels for Electricity generation in Sudan*, in *Mechanical Engineering* 2017, Aston University
220. Liberatore, M.W.N.a.M.W., *Viscosity of Biomass Pyrolysis Oils from Various Feedstocks*. Energy Fuels, 2010. **24**: p. 6601–6608
221. Liberatore*, M.W.N.a.M.W., *Viscosity of Biomass Pyrolysis Oils from Various Feedstocks*. Energy Fuels, 2010, . **24**, : p. 6601–6608.
222. Oliveira L. E.1, D.S.M.L.C.P. *Comparative study of calorific value of rapeseed, soybean, jatropha curcas and crambe biodiesel*. in *International Conference on Renewable Energies and Power Quality (ICREPQ'13)*. 2013 Bilbao (Spain), .
223. Hui Wang, H.L., Ying Zhenga,,*, Siauw Ng, Hilary Brown, Yu Xia, *Kaolin-based catalyst as a triglyceride FCC upgrading catalyst with high deoxygenation, mild cracking, and low dehydrogenation performances*. Catalysis Today, 2019. **319** p. 164–171.
224. M.S.Landis*J.P.Pancras†J.R.Graney‡R.K.Stevens§K.E.Percy¶S.Krupall, Chapter 18 - *Receptor Modeling of Epiphytic Lichens to Elucidate the Sources and Spatial Distribution of Inorganic Air Pollution in the Athabasca Oil Sands Region*, in *Developments in Environmental Science* 2012. p. 427-467.
225. Habibi, N., *Mechanism study of the conversion of esters to high-octanenumber aromatics over HZSM-5*. Appl Organometal Chem., 2019. **33**.
226. Omvir Singh a, b., Ankit Agrawal a, b, Neha Dhiman a, b, Bhanu Prasad Vempatapu c, Ken Chiang d, Shailendra Tripathi a, Bipul Sarkar, *Production of renewable aromatics from jatropha oil over multifunctional ZnCo/ZSM-5 catalysts*. Renewable Energy, 2021. **179** p. 2124 to 2135.

227. Andri Cahyo Kumoro , D.A.N., Adi Cifriadi , Aprilina Purbasari and Asron Ferdian Falaah, *A New Correlation For The Prediction of Minimum Fluidization of Sand And Irregularly Shape Biomass Mixtures In A Bubbling Fluidized Bed*. International Journal of Applied Engineering Research, 2014. **9** (23): p. 21561-21573.
228. Toolbox, E. *Nitrogen - Density and Specific Weight Online Calculator* [cited 2019 February]; Available from: https://www.engineeringtoolbox.com/nitrogen-N2-density-specific-weight-temperature-pressure-d_2039.html.
229. Toolbox, E. *Nitrogen - Dynamic and Kinematic Viscosity Online Calculator*. [cited 2019 February]; Available from: https://www.engineeringtoolbox.com/nitrogen-N2-dynamic-kinematic-viscosity-temperature-pressure-d_2067.html.
230. Gurmen, H.S.F.a.M.N., *Elements of Chemical Reaction Engineering* ed. 4th Edition. Vol. Chapter 12:Diffusion and Reaction in Porous Catalysts. 2008.